UNIVERSITY OF
BIRMINGHAM

Hydrogen release and absorption in mixed anion lithium amide/lithium ternary nitride systems

by

Trang Thi Thu Nguyen

Supervisor: Dr Paul A. Anderson

A thesis submitted to The University of Birmingham for
the degree of Doctor of Philosophy

The School of Chemistry
College of Engineering and Physical Sciences
The University of Birmingham
November 2015

Abstract

In this work, reactions of either lithium borohydride, zinc chloride or zinc nitride with lithium amide have been studied.

The presence of CoO catalyst was found to affect significantly the products and hydrogen release on heating mixtures of xLiBH$_4$-yLiNH$_2$. In products from a mixture of LiBH$_4$-*2*LiNH$_2$ increasing amounts of the $I4_1/amd$ polymorph of Li_3BN_2 were observed with a greater amount of CoO, and transformation from the $I4_1/amd$ to the $P2_1/c$ polymorph occurred under hydrogen pressure. On addition of CoO, at all ratios of the xLiBH$_4$-yLiNH$_2$ systems studied the temperature of hydrogen release was greatly reduced, starting from 100°C and peaking around 250°C, much lower than 240°C and 330°C without catalyst. Ball-milling helped to improve the amounts of hydrogen desorbed from these ratios from 3–4 wt% up to greater than 10 wt%.

In the reactions of $ZnCl_2$ + nLiNH$_2$ (where n = 2–6), LiCl and two nitrides Zn_3N_2 and LiZnN were obtained in the reaction products. Ammonia was the main gas released from these reactions at around 300°C. The addition of LiH was found to change the main gaseous product from NH_3 to H_2, which was released at a low temperature beginning around 90°C, much lower than in the absence of LiH. A mixture of LiZnN and LiCl obtained from this reaction was partly rehydrogenated to form Li_2NH and Zn.

The reaction of Zn_3N_2 and LiNH$_2$ in the presence or absence of LiH was found to produce pure LiZnN without LiCl. NH_3 was the main gas released from mixtures of Zn_3N_2 and LiNH$_2$, but again this was converted into H_2 on addition of LiH. Neither pure LiZnN nor Zn_3N_2 could be hydrogenated under the conditions tried, but a mixture resulting from the reaction was found to react with hydrogen to form LiNH$_2$ and Zn in a molar ratio of 1:1. The cyclability of the Li–Zn–N system (from both reactions) was examined by both IGA and HTP. Both mixtures were able to release gases under low pressure, 10 bar, and around 35 bar hydrogen. This system could release and take up hydrogen at temperatures above 275°C. Mg-doping in LiZnN was also examined in the hope of improving the reversibility of the Li–Zn–N system but was not successful.

Acknowledgements

Finally, I have now completed my thesis. There are many people who have helped and supported me during this work, and I want to give them all a great deal of thanks. First of all, I would like to thank my supervisor Paul Anderson for all his help and guidance over the last four years. I would like to thank the other members of Anderson's group, Matt, Rosie, Rachel, David, Tom, Ivan and Phil Chater. I would also like to thank other people on Floor 5, now and then, Marianna, Annabelle, Alaric, Laura, Phil, Claire,... for helping me have a good atmosphere place to work, especially Evin and Ben for caring of my problems. In Met & Mat I would like to thank David Book for the use of equipment, and especially Dan Reed for not only helping me with techniques but also encouraging me when I was losing my hope.

I would also like to thank many Vietnamese friends for treating me well and sharing my worries so that I can overcome many difficulties when studying far away from home and family. May I send my thanks to Chi, Chau, Khanh, Hoa, Dung, Ban, Huong, Huyen, Minh, Mai, Ngoc, Thinh,... and many others for that.

I would like to thank my family for their continued support; thanks to my parents, brothers, uncles, aunts, nieces and nephew.

Finally I would to thank my husband and my daughter for always loving me and believing in me to help me be strong enough to go to this stage.

Thank you all.

Contents

Chapter 1: Introduction

Because of the growth in world population and the use of technology, the world's energy demand has drastically risen, with this increase mostly met by fossil fuels. However, this source of energy is rapidly being exhausted. In addition, there is another harmful effect with the burning of fossil fuels which leads to an increase of the concentration of carbon dioxide in the atmosphere and this greenhouse gas has caused global climate change [1]. The requirement to find a low carbon, eco-friendly energy source becomes urgent. Recently hydrogen has been cited as the "fuel of the future" based on its availability from renewable resources and its clean, nontoxic combustion and high calorific content, producing 142 MJ/kg which is much greater than other chemical fuels [2]. Correspondingly, hydrogen is expected to satisfy both environmental and economic targets. ***Figure 1.1*** illustrates an ideal hydrogen cycle in which hydrogen is obtained from water through electrolysis using solar energy, and is stored reversibly in solid materials, and supplies energy demand [3].

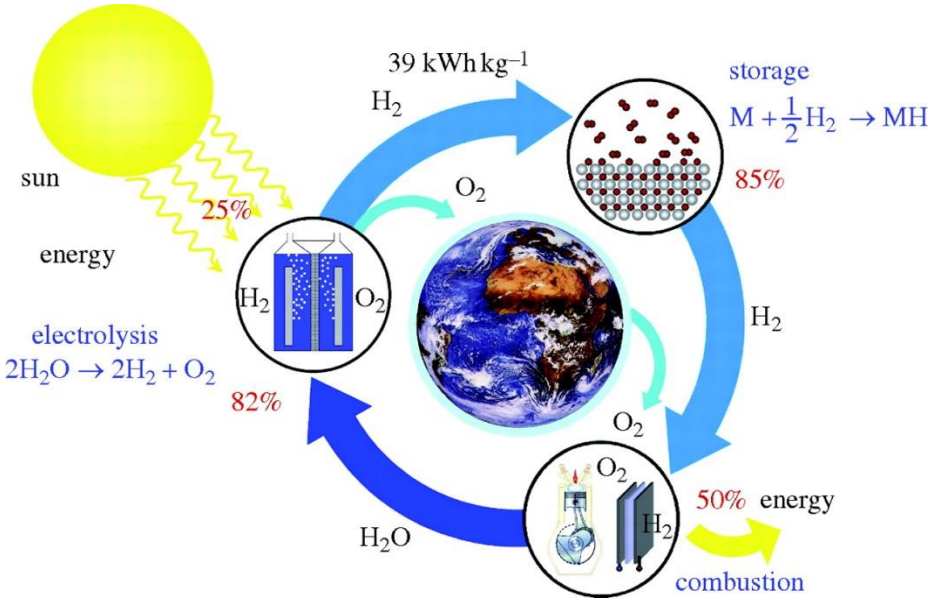

Figure 1.1 *Ideal hydrogen cycle* [3].

However, although hydrogen is the most abundant element throughout the cosmos, approximately 90% of the total atoms in the universe, and the tenth most abundant element by mass on Earth, its natural abundance is approximately one percent on Earth – therefore it must be produced [4]**.** Therefore, finding a suitable approach for hydrogen production is the main factor for application of this future energy.

1.1. Hydrogen production

Hydrogen can be obtained from fossil fuels and biomass as well as renewable sources including wind and solar electricity or from nuclear power.

Fossil fuels

Most hydrogen today is obtained from natural gas by steam reforming or from oil by a partial oxidation process [5]. Recently, interest has grown in producing hydrogen from coal gasification and reforming processes in which carbon dioxide is separated and

sequestered. These processes can, in principle, be used to manufacture large quantities of H_2 with a minor amount of greenhouse gas [6].

Biomass

Biomass is one of the most abundant renewable sources which is relatively safe for the atmosphere because carbon dioxide liberated from its combustion is offset by the absorption by plants during photosynthesis, producing a carbon neutral cycle. Biomass has been used for centuries, especially in pre-industrial times. Recently, biomass contributes about 12% of today's world energy supply, and that can be up to 40–50% in many developing countries [7]. However, similar to other sources of hydrogen, production from biomass will require appropriate hydrogen storage systems. Additionally, growing, harvesting and transporting biomass require high costs. Hence, it is not currently economically competitive with natural gas steam reforming [8].

Renewable sources

There are some other options for producing hydrogen from renewable sources such as wind, solar, and hydro electricity or from nuclear power. However, the production of hydrogen from these sources is not currently cost-competitive.

1.2. Hydrogen as a fuel

Since the 1970s the use of H_2 as a fuel has been investigated widely in the world as prices of oil rose significantly and recently has increased because of environmental problems in using fossil fuels. H_2 is considered as an excellent fuel for vehicles due to its high specific enthalpy and richest energy per unit mass.

Internal combustion engine (ICE)

The first ICE was produced by François Isaac de Rivaz in 1807, designed to run on a mixture of hydrogen and oxygen [9]. In an ICE, H_2 can be used as a fuel to convert the chemical energy of hydrogen to electricity, almost similar to a spark-ignited (SI) petrol engine [10]. Hydrogen ICEs allow a notable chance for a transition to a hydrogen economy. However, if the oxygen is supplied from the air, nitrogen oxides (NO_x) can also be created and react with water that can cause an acid rain effect. Utilizing pure oxygen would raise the cost of the system and also takes up additional storage space within the vehicles.

Fuel cells

Fuel cells are devices used for electrochemical energy conversion. There are many types of fuel cells with different electrolytes: alkaline, phosphoric acid, solid oxide, molten carbonate, and polymer electrolyte membrane. Fuel cells with hydrogen fuel from a sustainable source have been regarded by many as the ultimate in clean energy [11]. They are relatively simple, with hydrogen and oxygen used to create water and electricity. With a constant source of hydrogen fuel, fuel cells in vehicles can directly and continuously generate electricity.

Polymer electrolyte membrane fuel cells (PEMFC) have been developed with a number of advantages. They are able to operate at relatively low temperatures around 65°C with high efficiency and have rapid start up times, showing their potential for utilization in mobile applications [12]. Many cars containing PEM fuel cells have been produced by automobile manufacturers such as Honda, Hyundai etc. However, the operating

temperature of a PEM fuel cell has a considerable effect on the membrane. If the temperature is too high then the PEM can be dehydrated, leading to a drop in the efficiency of the stack. Due to the impurities in hydrogen supply such as CO, NH_3, NO_x, SO_x and organic compounds, PEM fuel cells can also suffer degradation in performance [13].

1.3. Hydrogen storage methods

Hydrogen storage is one of the issues which has been investigated profoundly develop a hydrogen economy. Efficient and compact hydrogen storage involves both thermodynamics and kinetics challenges: a large amount of hydrogen must be stored and the absorption/desorption of hydrogen must be quick and complete.

For transportation applications, volumetric and gravimetric energy density targets applied in 2020 and ultimate for acceptable materials for hydrogen storage were set by the U.S. Department of Energy (DOE) and shown in **Table 1** [14].

Since the early 1990s, research has been carried out to store hydrogen as a gas, liquid and in the solid state. A large amount of research has been carried out all over the world to discover economic and feasible solutions for hydrogen storage.

Table 1.1 Hydrogen storage system targets for Light-Duty Fuel Cell Vehicles

Storage Parameter	**Units**	**2020**	**Ultimate**
System Gravimetric Capacity	kWh/kg (kg H_2/kg system)	1.8 (0.055)	2.5 (0.075)
System Volumetric	kWh/L (kg H_2/L system)	1.3 (0.040)	2.3 (0.070)
Storage System Cost	$/kWhh net ($/kg H_2 stored)	10 333	8 266
Durability/Operrability - Operating ambient temperature - Min/max delivery temperature - Min/max delivery pressure from storage system	 °C °C bar (abs)	 -40/60(sun) -40/85 5/12	 -40/60(sun) -40/85 3/12
Charging/Discharging Rates System fill time (5 kg)	Min (kg H_2/min)	3.3 (1.5)	2.5 (2.0)
Fuel Quality (H_2 from storage)	% H_2	SAE J2719 and ISO/PDTS 14687-2 (99.97% dry basis)	

Besides those targets, materials need to meet environmental, health and safety issues.

Many kinds of materials have been investigated, some of which can match one or some of the above criteria but could not satisfy the others.

1.3.1 Hydrogen compressed gas

High pressure storage of hydrogen is currently the most understood and widely used commercial method. Hydrogen gas can be stored in gas cylinders made of carbon-fibre-reinforced composites at 700 bars at room temperature, enough for a car to run for 500 km without refuelling [15]. However, the volume which is much greater than petrol is too large to meet the volumetric capacity target. Additionally, a series of engineering challenges has to be overcome to handle hydrogen gas at high pressures up to 1000 bar or even higher. Also, there are a lot of safety issues concerned with storing gas at such high pressures.

1.3.2 Liquefied hydrogen

Hydrogen can also be stored as a cryogenic liquid or in other liquids such as $NaBH_4$ solutions. This is another approach to increase the volumetric energy density but it is not considered an economic alternative in a sustainable society due to requirement of a large amount of energy to cool the gas to 20 K (10 kWh/kg) and to keep the cryogenic tanks cold. They also lose hydrogen through evaporation.

A cryo-compressed tank system, which was designed by Salvador Aceves *et al.* can store hydrogen at cryogenic temperatures within a pressurized vessel [16]. Pressurized tank storage presently meets practical criteria of some car manufacturers (U.S. Department of Energy Hydrogen Program 2006) [14].

1.3.3 Solid state storage

Systems storing hydrogen in solid state using for on-board applications may be a good alternative for hydrogen storage due to the possibility of high volumetric and gravimetric density, and reversible hydrogen storage with long term stability, which does not suffer the disadvantages experienced by compressed and liquid hydrogen. However, the reversibility of these materials faces the obstacle of the bonding energy between hydrogen and the storage materials. If hydrogen is bound too strongly then it is not easy to be released while on the contrary hydrogen bound weakly is difficult to be replaced when refuelling [17]. Therefore, none of solid state storage materials is ideal for reversible storage applications.

Volumetric and gravimetric hydrogen storage densities of different techniques and various materials are shown in ***figure 1.2*** [18].

1.4. Hydrogen Storage Properties

Systems and materials require a number of different properties for hydrogen storage. Each property has its importance depending on the application or the aim of research. The following are the principal measured properties of hydrogen storage materials and systems.

1.4.1 Capacity

Capacity is the maximum steady state hydrogen content of a storage material. Capacity may mention different aspects including reversible capacity, usable capacity and excess material capacity. These kinds of capacity may be affected by the properties of the

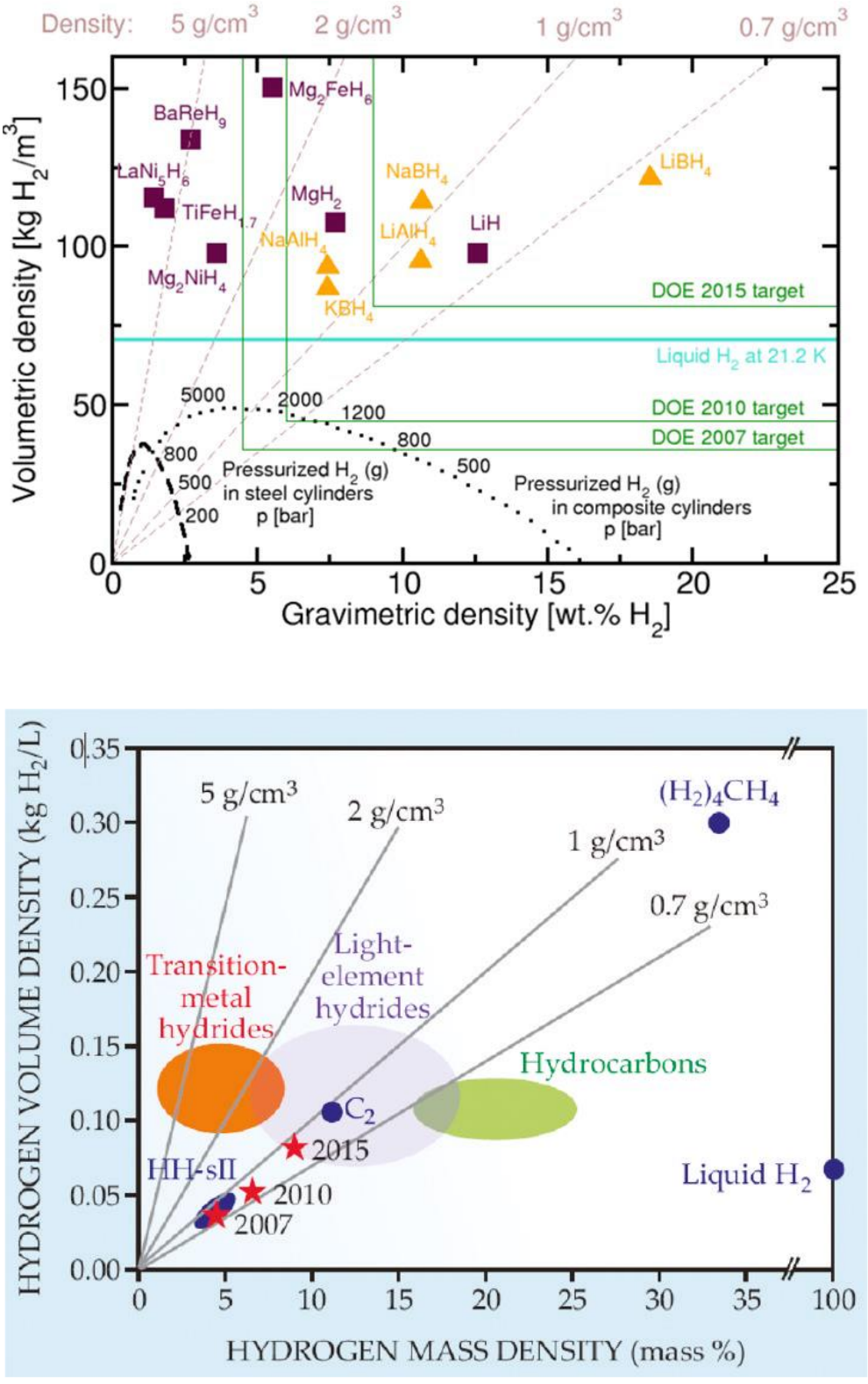

Figure 1.2 *Volumetric and gravimetric hydrogen storage densities of different techniques and various materials [3, 18].*

material such as stability, composition, temperature, pressure and number of cycles. [18–20]. Volumetric and gravimetric hydrogen storage densities of different techniques and various materials are presented in ***figure 1.2*** [3, 18].

1.4.2 Kinetics

Kinetics is the property relating to the rate of hydrogen sorption/desorption of a material. Kinetics depends on temperature and pressure and other parameters such as sample preparation, heat transfer capability, and the presence of catalysts and additives. There is an extreme difficulty in minimizing the strong influences of external effects on kinetics. [19–20, 22]

1.4.3 Thermodynamics

In a hydrogen material or system, thermodynamic properties affect many other parameters, especially the hydrogen capacity based on pressure and temperature. The relationship between temperatue and pressure and thermodynamic properties can be confused by slow kinetics [19, 21–22].

1.4.4 Cycle-life

Cycle-life measurement is applied for reversible hydrogen storage materials. Metal hydrides, complex hydrides, amides and physisorption materials are typical examples. Irreversible materials such as chemical slurries of hydrides can not be directly cycled. Cycle-life testing is used to investigate the influence of cycling on the capacity of materials. However, the change in effective capacity can occur through a change in

kinetics during cycling. Cycle-life depends on many factors, including impurities in hydrogen gas, phase changes, *etc.* [19, 23–24].

1.5 Potential hydrogen storage materials

Hydrogen can interact with porous materials *via* physisorption involving weak forces Van der Walls between hydrogen molecule and high surface areas materials. Hydrogen can also be stored in various types of materials through chemisorption which forms strong chemical bindings between H atoms and materials.

1.5.1 Porous materials

Hydrogen physisorption on porous materials has been expected to be a potential hydrogen storage approach. The adsorbents are generally kept at 77 K as the enthalpy of H_2 physisorption is typically in the range of 1–10 $kJmol^{-1}$ [25]. Various types of porous compounds have been highlighted as potential materials for hydrogen storage which include metal organic frameworks (MOFs) [17, 26–40], carbon-based materials [17, 30–31, 41–57], and inorganic compounds such as aluminosilicates, aluminophosphates, silicas *etc.* and microporous polymers [17, 31, 58–65]. However, these systems operate at low temperature around 77 K and a rapid decline in gravimetric density of adsorbed hydrogen can occur when temperature increase. In addition, it is difficult to measure accurately hydrogen storage capacity and understand the hydrogen absorption/adsorption mechanism of these systems. These are the major obstacles in developing physisorbed hydrogen storage materials [17, 31, 66–68].

Among porous materials, carbon-based materials ranging from porous activated carbons, carbon nanotubes, graphite *etc.* to carbide derived carbon have attracted scientists because of their high surface area and pore volume, stability and low cost [69]. Besides specific surface, other factors of porous carbon materials such as pore volume and pore size have been investigated to enhance physisorption of systems for hydrogen storage [70–71]. Zeolite templated porous carbon materials have been reported by Zang *et al* to have hydrogen storage capacity ~4.5 wt% at 77 K and 20 bar [72].

MOF materials, which has been considered another type of promising hydrogen storage materials, have attracted a great attention of many research groups due to their high volumetric capacity, potential reversibility, and an ability to store gas including hydrogen at low pressure. Modifying MOFs pore sizes [73–78], shaping powdered MOFS into compacted systems [79–82], and spillover (the ability of MOFs to operate at near room temperature) [83–100], which have been studied by many researchers has presented a promise to improve MOFs hydrogen storage capacity.

1.5.2 Metallic hydrides

Elemental hydrides can be divided into different types depending on the nature of bindings between metals and hydrogen. While ionic hydrides are formed by alkali metals and from calcium to barium of earth metals, covalent metal hydrides consist of hydrogen and non-metals, metallic hydrides are compounds of transition metals [101–104].

Metallic hydrides are other candidates for hydrogen storage applications due to their high hydrogen volumetric densities and fast kinetics for hydrogen up-take, release and transport [101, 105–106]. Thus, metallic hydrides were expected to be reversible solid-

state systems for hydrogen storage at low pressure in numerous studies [2, 22, 67, 107–111].

The metal–hydrogen compounds of Li, Be, B, Na, Mg, and Al are attractive due to their high volumetric capacity and light weight. Hydrides of heavier metals can be used in small proportions for alteration of properties or as catalysts [106].

Among metallic hydrides, MgH_2 is seriously studied because of the abundance of Mg in the Earth, high energy density (9 MJ/kg), high hydrogen capacity (7.7 wt %), and good reversibility [22, 112–118]. The main drawbacks of MgH_2 are high temperature of hydrogen release, poor hydriding/dehydriding kinetics, and low storage efficiency due to the high enthalpy of formation [114, 119–121]. Transition metals are used as dopants to enhance the absorption/desorption kinetics of MgH_2. Materials with formula $Mg_{\sim 7}MH_{\sim 16}$ – where M = Ti, Hf, Zr, Nb, Ta and V – have been synthesized. Although their reversibility are improved with reduction of dehydrogenation temperature, the required pressure from 4 GPa at 600^{o}C for their synthesis remains a major challenge for these materials [122]. Ball-milling was applied to improve surface activities and kinetics of MgH_2 and hydrogen release was observed at lower temperature than samples without ball-milling, from 200°C [22, 123–124]. MgH_2 mixed with $LiNH_2$ was reported to desorb hydrogen from 200°C [125–126]. Ball-milled mixture of them could release up to 6.1 wt% and 8.2 wt% hydrogen, experimental and density function theory (DFT) calculations, respectively [126–131].

Besides elemental hydrides, many intermetallic hydrides of heavy metals were reported to take up hydrogen such as ZrNi, Mg_2Ni, $TiFeH_2$ and $LaNi_5H_6$ [101, 132–135] *etc.*

However, pressures and temperatures are not in practical ranges of 0–100°C and 1–10 bar preventing them from practical usages [101].

1.5.3 Chemical hydrides

'Chemical hydrides' have recently been defined as compounds containing at least two chemically distinct non-hydrogen atoms where some of these atoms form bonds with one another such as NH_3BH_3, $LiNH_2BH_3$, *etc.*. [66]. Hydrolysis of these high-hydrogen-content compounds has attracted much attentiveness [136–140]. NH_3BH_3 possesses 19.6 wt% and 146 g L^{-1} gravimetric and volumetric, respectively, could release up to 6.5 wt% hydrogen *via* 3 steps at 100, 150 and above 500°C [141–153]. However, during desorption process, by-products including ammonia, diborane, and borazine were also observed.

Several studies have reported other kinds of chemicals which contain hydrogen and can be used for hydrogen storage including methanol and formic acid. These liquid organic hydrides (LOH) have hydrogen storage capacities in range of 6–8 wt% and are considered to be a potential means to supply hydrogen to PEMFCs [154–158].

In addition, decomposition of hydrous hydrazine (containing 8.0 wt% hydrogen) has been studied for obtaining hydrogen but this compound has a problem with toxicity need solving before being used [159–164].

Besides advantages, the development of chemical hydrides faces some challenges. In addition to the requirement for selective and efficient catalysts for dehydrogenation, this class of materials also needs to overcome limitations of heat transfer. Furthermore,

recycling of chemical hydrides has an additional economic obstacle with transportation cost [165–166].

1.5.4 Complex hydrides

Complex hydrides are salts of the aluminium hydride $[AlH_4]^-$ (also known as alanate) and borohydride $[BH_4]^-$ anions in which hydrogen is covalently bound to the central atoms. The general chemical formula of complex hydrides is $A_xMe_yH_z$, where A is metal in group I, II or many transition metals and Me is B or Al. Complex hydrides are other candidates for hydrogen storage materials due to their light weight and a large number of hydrogen atoms per metal atom [22, 101, 166].

1.5.4.1 Alanates

Alanates also have potentially usable storage capacities. A typical example is lithium alanate $LiAlH_4$ with high gravimetric capacity of 10.5 wt% hydrogen which has received much attention [167–180]. Theoretically, there are reversible reactions $LiAlH_4 \leftrightarrow Li_3AlH_6 \leftrightarrow LiH$ [169–171]. However, the reactions were found not to occur under practical conditions but require high pressure above 100 bar [172]. In addition of catalysts $TiCl_4$ or metallic Fe, $LiAlH_4$ was reported to transform into Li_3AlH_6, Al and H_2 [173–176]:

$$3LiAlH_4 \rightarrow Li_3AlH_6 + 2Al + 3H_2 \qquad (1.1)$$

$$Li_3AlH_6 \rightarrow 3LiH + Al + \frac{3}{2}H_2 \qquad (1.2)$$

$$3LiH + 3Al \rightarrow 3LiAl + \frac{3}{2}H_2 \qquad (1.3)$$

The presence of $NiCl_2$ could lower the decomposition temperature of this compound 50°C [177]. Mixtures of $LiAlH_4$-$Mg(BH_4)_2$, $Mg(NH_2)_2$-$LiAlH_4$, and $LiNH_2$-$LiAlH_4$ have also been studied and showed a considerable improvement of reversibility of hydrogen storage [178–181].

$NaAlH_4$ and Na_3AlH_6 are other promising alanates containing 7.4 and 5.9 wt%, respectively, having theoretical reversible reactions as descried in following equations [182–184]:

$$NaAlH_4 \Leftrightarrow \frac{1}{3}Na_3AlH_6 + \frac{2}{3}Al + H_2 \qquad (1.4)$$

$$\frac{1}{3}Na_3AlH_6 \Leftrightarrow NaH + Al + \frac{1}{2}H_2 \qquad (1.5)$$

Nevertheless, the reversibility of interconversion between them is a critical element for practical applications [105]. In a presence of Ti catalyst kinetics of reversible reaction of $NaAlH_4$ was remarkably improved to release hydrogen at 150°C and take up hydrogen at 170°C after 5 hour reaction under 152 bar hydrogen [185]. Reversible capacity could go up to 3-4 wt% [186].

Other alanates such as $KAlH_4$, $Ca(AlH_4)_2$ *etc.* have also been studied but the results have not met practical requirements for hydrogen storage materials [187–189].

In summary, up to now this class of material still has obstacles with hydrogen cycling capacities and kinetic performances that are suitable for on-board hydrogen storage vehicles [168].

1.5.4.2 Borohydrides

Among the borohydrides, $LiBH_4$ is a material has great potential of hydrogen storage because of a very high gravimetric density of hydrogen (18.5 wt %). However, it is very stable and releases most of its hydrogen at the relatively high temperature of 380°C [31]. Other borohydrides such as MBH_4 (M = Li, Na, and K), $Mg(BH_4)_2$, $Al(BH_4)_2$ and so on are also being investigated but the results have not yet met practical criteria [168].

Amide–borohydrides, with their high capacity, are others light complex hydrides for hydrogen storage. However, so far only a low amount of hydrogen has been reversibly released at temperature below 250°C [190]. More information about properties and destabilization to improve hydrogen desorption of borohydrides and amide–borohydrides will be presented in section **1.6**.

1.5.5 Li–N–H system

The Li–N–H system has been expected to be one of the most potential hydrogen storage materials. This reversible system readily met the specification of US DOE and was expected to be one of the most desirable lightweight systems for hydrogen storage. It involves the cycling between $LiNH_2$, Li_2NH and Li_3N [191–194].

Formation and crystal structure of $LiNH_2$

$LiNH_2$ was first synthesized by Titherley in 1894 using Li metal and NH_3 gas/liquid [195]. Later, there were other reports of the preparation of $LiNH_2$ by heating Li_3N at 220–250°C under hydrogen gas [196–197].

The crystal structure of $LiNH_2$ was first determined in 1951 by Juza and Opp [198] using XRD tetragonal symmetry with space group $I\bar{4}$ and lattice constant a = b =5.037 Å, c = 10.278 Å. Miwa *et al.* [199] reported that in $LiNH_2$, the amide ion $[NH_2]^-$ ionically bonds with Li. This is confirmed by a structural study *via* neutron diffraction [200]. The IR spectrum of $LiNH_2$ show two bands corresponding to stretches at 3260 cm^{-1} (symmetric) and 3315 cm^{-1} (asymmetric) [201]. With in situ Raman spectroscopy studies of $LiNH_2$ at high pressure up to 25 GPa, Chelleppa *et al.* [202] observed a phase transition of $LiNH_2$ from ambient pressure α-$LiNH_2$ to a β-NH_2 phase at 298 K.

Formation and crystal structure of Li_2NH

Li_2NH can be obtained from the decomposition of $LiNH_2$ at high temperature under vacuum or by the reaction between NH_3 gas and LiH [1, 203–204] or by reacting Li with NH_3 [205].

Noritake *et al.* showed that Li_2NH is face-centered cubic with $Fm\bar{3}m$ symmetry and lattice parameter a = 5.074 Å [206]. Investigations of Forman *et al.* based on NMR [207] and diffraction Balogh *et al.* using diffraction measurement [208] found that Li_2NH has a structural phase transition at the temperature above 360 K. They proposed that while the low temperature Li_2NH has $Fd\bar{3}m$ symmetry, it has $Fm\bar{3}m$ symmetry at high temperature.

Formation and crystal structure of Li_3N

Li_3N has three known polymorphs. The structure of α-Li_3N was first determined by Zintl and Brauer [209] and then confirmed by single crystal X-ray diffraction by Rabenau and

Schultz [210]. It is hexagonal with a = 3.648(1) Å, c = 3.875(1) Å and space group of *P*6*/mmm*.

α-Li_3N is stable at room temperature and pressure. α-Li_3N transforms into β-Li_3N at 300 K and ~0.5 GPa [211–212] whereas γ-Li_3N (isostructural with Li_3Bi) [211] completely transforms from β-Li_3N at 35–45 GPa and has high stability up to 200 GPa [213].

Thermodynamics and reaction mechanism of Li–N–H system

Li–N–H is a good example for a promising material for hydrogen storage due to its potential to store a large amount of hydrogen.

Chen *et al.* [191] reported that Li_3N could have high capacity hydrogen storage with a total theoretical gravimetric density of 10.4 wt % H_2. The reaction proceeds *via* a two-step reversible reaction (1.6) with an overall reaction heat of –161 $kJmol^{-1}$.

$$Li_3N + 2H_2 \leftrightarrow Li_2NH + LiH + H_2 \leftrightarrow LiNH_2 + 2LiH \quad (1.6)$$

Hu and Ruckenstein [214] proposed that the reaction proceeded with the release of NH_3 and an ultrafast reaction (less than 25ms) between LiH and NH_3 to form $LiNH_2$ and H_2.

$$LiNH_2 \rightarrow Li_2NH + NH_3 \quad (1.7)$$

$$NH_3 + LiH \rightarrow LiNH_2 + H_2 \quad (1.8)$$

Reaction (1.8) completes when all $LiNH_2$ and LiH convert into Li_2NH and H_2. The observation of NH_3 during two-step reaction was confirmed in many studies [193, 215–219].

With in situ ^1H NMR spectroscopy, Ichikawa *et al.* quantified the released NH_3 from reaction of $LiNH_2$ and LiH in 1:1 and 1:2 ratios [220] while Hua *et al.* reported a

suggestion of reaction between NH_3 and LiH at 150°C to add more details to the studies about reaction mechanism between $LiNH_2$ and LiH.

David *et al.*, using powder synchrotron X-ray diffraction on samples of hydrogenated and dehydrogenated $LiNH_2$–LiH mixture showed the continuous evolution from amide to imide (eqn 1.9) [221]. They suggested that Li^+ mobility is an important parameter in the mechanism of hydrogenation.

$$Li_{1+x}NH_{2-x} \rightarrow (1 - \varepsilon)Li_{1+y}NH_{2-y} + \varepsilon NH_3 \qquad (1.9)$$

where $(1 + y)(1 - \varepsilon) = (1+ x)$.

A study of the hydrogenation and dehydrogenation of $LiNH_2$ showed that $LiNH_2$ can be converted into LiH and NH_3 *via* reaction with H_2, whereas $LiNH_2$ is decomposed to Li_2NH and NH_3 under an Ar flow. The reaction between $LiNH_2$ and H_2 can be promoted by LiH or $TiCl_3$-doping [222].

With temperature programmed decomposition (TPD), Zhang *et al.* investigated the decompositions of $LiNH_2$ and Li_2NH with and without anion promoter [223]. They reported that $LiNH_2$ is decomposed into Li_2NH and NH_3 *via* two steps at the temperature of 300–450°C: forming first a stable intermediate compound ($Li_{1.5}NH_{1.5}$) and then Li_2NH. The decomposition of Li_2NH produced Li, N_2, and H_2 in the temperature range of 550–750°C without formation of Li_3N. The decompositions of $LiNH_2$ and Li_2NH can be accelerated by the presence of Cl^- ion. In the $LiNH_2$ sample, they observed the generation of a new NH_3 peak at temperature of 250°C. Moreover, increasing the molar ratio of Cl^- can decrease the decomposition temperature of Li_2NH from 645 to 530°C.

1.5.6 $LiNH_2$-based systems

The low absorption kinetics and relatively high operating temperature currently limit its practical applications. Taking the advantages of the Li–N–H system, mostly based on $LiNH_2$, various methods have been seriously applied to improve this system in a hope to have $LiNH_2$-based systems meeting targets of DOE for hydrogen storage.

Since Ichikawa *et al.* [193] first found that the presence of a small amount of $TiCl_3$ can lower the temperature of hydrogen discharge of Li–N–H system to 150–250^oC and improve the kinetics of hydrogen desorption, catalyst doping is one more option chosen to enhance the properties of these materials.

To investigate the effect of transition metal on Li–N–H system, Ti, Fe, Ni or Cr was used to substitute one of the Li sites in $LiNH_2$, and Li–Ti–N–H showed a marked reduction in reaction enthalpy with –46.6 $kJmol^{-1}$ compared with that of the Li–N–H system (–75.67 $kJmol^{-1}$). Another example is Li–Co–N–H system reported by Ma *et al.* shows a considerable improvement in desorption kinetics [224–225].

It was also reported by several research groups that on an addition of other catalysts including nano-Ti, nano TiO_2, halides or oxides of transition metals and oxides there was also a reduction on temperature of hydrogen release [193, 217, 223, 226–227]. A variety of ternary Li–M–N–H systems have also been investigated by mixing $LiNH_2$ with hydrides or halides of earth metals and to form Li–B–N–H, Li–Ca–N–H, Li–Mg–N–H… showed a remarkable reduction in temperature of hydrogen desorption to a low onset temperature around 100°C [190, 228–231].

The presence of LiH and lithium/magnesium halides were also found to have significant effects on the hydrogen desorption properties of the Li–N–H system. In the study of Anderson *et al.*, $LiNH_2$ and LiH were mixed with LiX and MgX_2 (X: Cl, Br, I). The results showed that in all cases, the halide-containing amides and imides released and absorbed hydrogen more rapidly than pure amides/imides [227, 232].

Zinc chloride was found to have different effects on $LiNH_2$ than lithium and magnesium chloride. Trang et al. reported that in the mixture of $LiNH_2$ and $ZnCl_2$, $LiNH_2$ could be decomposed into Li_2NH better than $LiNH_2$ alone at 200°C. From 250°C the mixture of them formed a binary nitride Zn_3N_2 and a ternary nitride LiZnN and release ammonia which can be converted into hydrogen in addition of LiH [233].

MgH_2 is one of the compound showing most significant effects to $LiNH_2$ and has attracted great interest of many researcher groups. Reaction between $LiNH_2$ and MgH_2 was predicted to have an enthalpy about 32 kJ mol^{-1} and release 8.2 wt% hydrogen but practical value of hydrogen observed below 8 wt% through following reactions 1.10 and 1.11 depends on the ratio between $LiNH_2$ and MgH_2 [234–250].

$2LiNH_2 + MgH_2 \rightarrow Li_2MgN_2H_2$ or $Li2Mg(NH)_2 + 2H_2$ (1.10)

$LiNH_2 + MgH_2 \rightarrow LiMgN + 2H_2$ (1.11)

Mixture of $LiNH_2$ and $LiBH_4$ is another candidate for hydrogen storage materials which will be detailed in section **1.6.**

Other amides such as $NaNH_2$ (5.1 wt%), $Mg(NH_2)_2$ (7.2 wt%), $Ca(NH_2)_2$ 5.5 wt%) *etc.* have also been studied but no system met DOE targets yet [168, 251–253].

1.6 $LiBH_4$-based systems

1.6.1 Synthesis of $LiBH_4$

$LiBH_4$ was first prepared in 1940 by Schlensinger *et al. via* the reaction of B_2H_6 and CH_3Li [254]. Schlesinger and Feddneva *et al.* later reported to produce $LiBH_4$ by a reaction between lithium hydride and boron trifluoride-ether [255] and a reaction of lithium hydride in diethyl ether with diborane [256]:

$$LiH + ½\ B_2H_6 \rightarrow LiBH_4 \qquad (1.12)$$

Lithium borohydride can also be formed from a reaction of lithium hydride and methyl [257] or directly from the elements *via* reaction of

$$Li + B + 2H_2 \rightarrow LiBH_4 \qquad (1.13)$$

at 650°C under 150 bar H_2 [258]. In 2005 Orimo *et al.* reported that lithium borohydride could be reformed from LiH and boron at 600°C under 350 bar hydrogen atmosphere and reversible and [259].

1.6.2 Structure of $LiBH_4$

$LiBH_4$ was firstly reported to have an orthorhombic with space group P*cmn* (a = 6.81 Å, b = 4.43 Å and c = 7.17 Å) in 1947 by Harris *et al.* [260]. Results from X-ray diffraction studied by Soulié *et al.* later showed that at low temperature $LiBH_4$ has an orthorhombic phase with a P*nma* space group (a = 7.17858 Å, b = 4.43686 Å, c = 6.80321 Å) [261] which was then confirmed by study of Züttel *et al.* [262]. It was changed to a hexagonal phase with a $P6_3mc$ space group (a = b = 4.27631 Å, c = 6.94844 Å) at high temperature of 381

K [263], 384 K [264] or 408 K [261], which is slightly different between different groups. Under high pressure, $LiBH_4$ was reported to form new phases of A*ma2* (1.2–10 GPa) [265] and F*m-3m* (> 10 GPa) [266]. The transformation between phases of $LiBH_4$ under different conditions of temperature and pressure has been studied [265, 267–271].

1.6.3 Thermal decomposition of $LiBH_4$

Thermal decomposition of $LiBH_4$ was reported to release hydrogen at 275°C by Schlensinger *et al.* in 1953 [254]. In 2003, $LiBH_4$ was studied its potential for hydrogen storage by Züttel *et al.* [262, 273]. $LiBH_4$ is considered to be a promising material for hydrogen storage because of its high weight percent of hydrogen (~18 wt%). However, this material liberates about 80% of its hydrogen at high temperature of 380°C [262] which is too high for application.

Züttel *et al.* reported that in addition of SiO_2 the decomposition of $LiBH_4$ could occur to release 9 wt% hydrogen below 400°C [272]. The addition of metals, metal hydrides and their chlorides such as Mg, MgH_2, $TiCl_3$, and $MgCl_2$ *etc.* showed a reduction on the decomposition temperature of $LiBH_4$ [273–274]. Many other catalysts including metals e.g. Ni, non-metal e.g. fullerenes and chlorides of transition metals including $FeCl_2$, $CoCl_2$ and $NiCl_2$ have been investigated. However, kinetics of dehydrogenation reaction was slightly improved while there was no enhancement of thermodynamics. [275–277]

Dehydrogenation properties of $LiBH_4$ can be significantly improved with the presence of $LiNH_2$ [278–287]. $LiBH_4$–$LiNH_2$ system was reported by Pinkerton *et al.* to release ≥ 10 wt%, and theoretically 11.9 wt% hydrogen from 250°C [279–282, 287] based on following reactions, depending on ratio of $LiBH_4$ and $LiNH_2$:

$3LiNH_2 + LiBH_4 \rightarrow Li_4BH_4(NH_2)_3$ or $Li_4BN_3H_{10}$ (1.13)

$2LiNH_2 + LiBH_4 \rightarrow Li_3BH_4(NH_2)_2$ or $Li_3BN_2H_8 \rightarrow Li_3BN_2 + 4H_2$ (1.14)

$LiNH_2 + LiBH_4 \rightarrow 2LiH + BN + 2H_2$ (1.15)

However, in practice, thermal decomposition of this system showed an evolution of ammonia [282]. This drawback has been tried to solve by addition of various transition metal catalysts of including Ni, Fe, Zn, Co, Pt, and Pd, or their chlorides or oxides and a reduction in ammonia discharge were achieved. Also, the temperature of hydrogen release was lowered to around 100°C in the presence of catalyst. However, the main product of this system Li_3BN_2 still showed poor rehydrogenation properties [280, 287–289].

Lately Zhang *et al.* published a paper showing significant effects of CoO in the reduction temperature of hydrogen desorption. This catalyst was also reported to improve the reversibility of products obtained after heating $LiBH_4$ and $LiNH_2$ in a molar ratio of 1:2 [290].

1.7 Zinc chloride, $ZnCl_2$

Magnesium chloride showed good results in forming new materials for hydrogen storage. Zinc has similar ionic radius to magnesium and therefore, zinc chloride attracts our interest. Zinc chloride has melting point and boiling point of 292°C and 756°C, respectively. This compound is hygroscopic and even deliquescent. Therefore, it needs to be kept out of moisture in the atmosphere. There are four known crystalline forms of $ZnCl_2$ named α, β, γ, and δ in which Zn^{2+} ions are tetrahedrally coordinated to four Cl^-

ions at ambient pressure. The structures of these crystalline forms are listed in **table 1.2** and ***figure 1.3*** [291–293].

Table 1.2 Structure parameters of four crystalline forms of $ZnCl_2$.

Phase	Crystal system	Space group	Lattice parameter (Å)
α	Tetragonal	$I\bar{4}2d$	a = b = 5.40, c = 10.35
β	Monoclinic	$P2_1/n$	a = 6.54, b = 11.31, c = 12.33
γ	Tetragonal	$P4_2/nmc$	a = b = 3.70, c = 10.67
δ	Orthorhombic	$Pna2_1$	a = 6.44, b = 7.69, c = 6.13

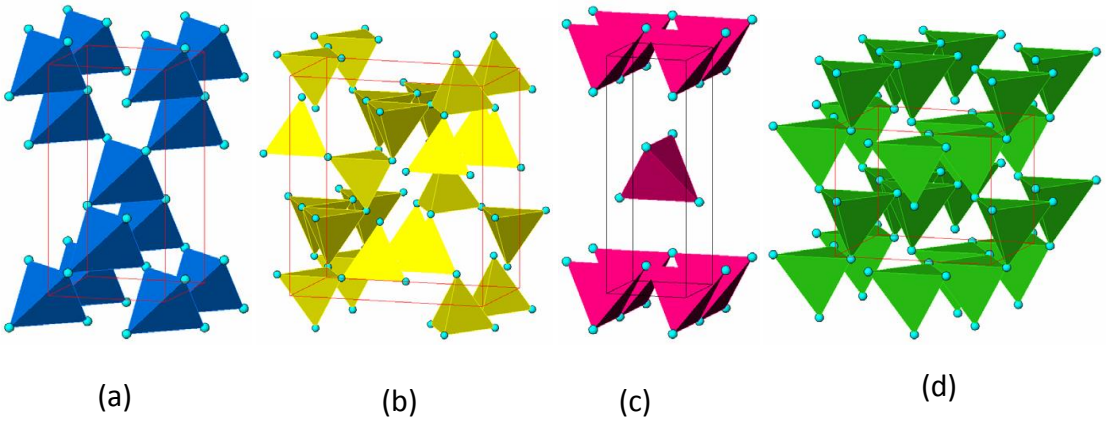

Figure 1.3 *Crystal structures of $ZnCl_2$: (a) α-$ZnCl_2$, (b) β-$ZnCl_2$, (c) γ-$ZnCl_2$ and (d) δ-$ZnCl_2$.*

The small blue circles represent Cl atoms, while Zn atoms are located inside the $ZnCl_4$ tetrahedra (not visible here).

Purely anhydrous $ZnCl_2$ has an orthorhombic structure (space group $Pna2_1$, a = 6.44 Å, b = 7.69 Å, c = 6.13 Å) but it can rapidly change to one of the three other forms due to water contamination.

Molten $ZnCl_2$ has a high viscosity at the melting point and a moderately low electrical conductivity that considerably increases with increasing temperature [294]. When $ZnCl_2$ was melt and rapidly cooled down it gives a glassy structure [295]. The melt $ZnCl_2$ studied by Raman and neutron scattering confirming the presence of polymeric structures [296–297].

$ZnCl_2$ was used in several studies of complex hydrides. It could react with NaBH4 or LiBH4 to form $Zn(BH_4)_2$ which has a capacity of 8 wt% hydrogen [298–301].

$ZnCl_2$ could also reduce temperature to release hydrogen of the mixture $LiBH_4$ + MgH_2 [302]. $ZnCl_2$ also performed as a catalyst in decomposition of $LiAlH_4$ [303].

1.8 Research Aims

Complex hydrides are regarded as particularly attractive candidates for hydrogen storage materials due to their high gravimetric storage capacities.

The aims of this work were to synthesise new mixed anion complex hydrides *via* reactions of either borohydride, chloride or nitride with amide and investigate their hydrogen desorption and reabsorption properties. A CoO catalyst was also used to add to mixture of xLiBH$_4$-yLiNH$_2$ in the hope of improving the hydrogen desorption/absorption of the system. In addition, Mg-doping of LiZnN was attempted to try and improve the reversibility of the Li–Zn–N system.

References

[1] T. M. Letcher, *Climate Change - Observed Impacts on Planet Earth*, Elsevier, 2009.

[2] L. Schlapbach and A. Züttel, *Nature*, 2001, 414, 353–358.

[3] P. Jena, *J. Phys. Chem. Lett.,* 2011, 2, 206–211.

[4] A. Züttel, *Mitig Adapt Strat Glob Change,* 2007, 12, 343–365.

[5] D. A. J. Rand, R. M. Dell, *Hydrogen Energy: Challenges and Prospects*, RSC Publishing, 2008.

[6] K. Hashimoto, M. Yahmasaki, S. Meguro, T. Sasaki, H. Katagini, K. Izumina, N. Kamagai, E. Akiyama, K. Asami, *Corrossion Science*, 2002, 44, 371–386.

[7] M. Ni, D. Y. C. Leung, M. K. H. Leung, K. Sumathy, *Fuel Pro. Tech.*, 2006, 87, 461–472.

[8] A. Demirbaş, *Energy conversion and Management*, 2001, 42, 1357–1378.

[9] L. M. Das, *Int. J. Hydrogen Energ.*, 1990, 15(6), 425–443.

[10] C. M. White, R. R. Steeper, and A. E. Lutz, *Int. J. Hydrogen Energ.*, 2006, 31, 1292–1305.

[11] P. P. Edwards, V. L. Kuznetsov, and W. I. F. David, *Phil. Trans. R. Soc. A*, 2007, 365, 1043–1056.

[12] F. Barbir and T. Gómez, *Int. J. Hydrogen Energ.*, 1997, 22(10–11), 1027–1037.

[13] X. Cheng, Z. Shi, N. Glass, L. Zhang, J. Zhang, D. Song, Z. Liu, H. Wang, and J. Shen, *J. Power Sources*, 2007, 165(2), 739–756.

[14] US Department of Energy Targets for Onboard Hydrogen Storage Systems for Light-Duty Vehicles Technical report, 2012.

[15] V. A. Yartys and M. V. Lototsky, *Hydrogen Materials Science and Chemistry of Carbon Nanomaterials, NATO Science Series,* 2005, 172, 75–104.

[16] S. M. Aceves, *DOE Hydrogen Program Annual Review*, 2003.

[17] G. Walker, *Solid-state hydrogen storage: Materials and chemistry*, Woodhead Publishing, 2008.

[18] R. Krishna, E. Titus, M. Salimian, O. Okhay, S. Rajendran, A. Rajkumar, J. M. G. Sousa, A. L. C. Ferreira, J. C. Gil and J. Gracio, *Hydrogen storage*, InTech, 2012.

[19] K. J. Gross, K. R. Carrington, S. Barcelo, A. Karkamkar, J. Purewal, *Recommended Best Practices for the Characterization of Storage Properties of Hydrogen Storage Materials*, Hydrogen Technology Consulting, 2010.

[20] G. Sandrock, *J. Alloy. Compd.,* 1999, 293–295, 877–888.

[21] W. Osborn, T. Markmaitree, L. L. Shaw, R.Ren, J. Hu, J. H. Kwak, and Z.Yang**,** *Materials in clean Power Systems*, 2009, 61, No. 4, 45–51.

[22] W. Grochala and P. P. Edwards, *Chem. Rev.,* 2004, 104, 1283–1315.

[23] Z. Dehouche, J. Goyette, T. K. Bose, *Int. J. Hydrogen Energ.*, 2003, 28, 983–988.

[24] K. J. Gross, P. Spatz, A. Züttel, *J. Alloy. Compd.,* 1996, 240, 206–213.

[25] A. Züttel, *Naturwissenschaften*, 2004, 91, 157–172.

[26] X. Lin, J. Jia, X. Zhao, K. M. Thomas, A. J. Blake, G. S. Walker, N. R. Champness, P. Hubberstey, and M. Schröder, *Angew. Chem., Int. Ed.*, 2006, 45, 7358–7364.

[27] B. Panella, M. Hirscher, *Adv. Mater.*, 2005, 17, 538–541.

[28] J. Sculley, D. Yuan, H-C. Zhou, *Energy Environ. Sci.*, 2011, 4, 2721–2735.

[29] L. R. Macgillivray, *Metal-organic Frameworks: Design and Application,* John Wiley & Sons, Inc., Publication, 2010.

[30] K. M. Thomas, *Catal. Today,* 2007, 120, 389–398.

[31] R. E. Morris and P. S. Wheatley, *Angew. Chem., Int. Ed.*, 2008, 47, 4966–4981.

[32] J. Ren, H. W. Langmi, B. C. North and M. Mathe, *Int. J. Energy Res.,* 2015, 39(5), 607–620.

[33] N. L. Rosi, J. Eckert, M. Eddaoudi, D. T. Vodak, J. Kim, M. O'Keefe and O. M. Yaghi, *Science*, 2003, 300, 1127–1129.

[34] M. Dinca and J. R. Long, *Angew. Chem., Int. Ed.,* 2008, 47, 6766.

[35] M. Hirscher, B. Panella and B. Schmitz, *Microporous Mesoporous Mater.,* 2010, 129, 335.

[36] Y. H. Hu and L. Zhang, *Adv. Mater.*, 2010, 22, E117.

[37] S. V. Kolotilov and V. V. Pavlishchuk, *Theor. Exp. Chem.*, 2009, 45, 277.

[38] L. J. Murray, M. Dinca and J. R. Long, *Chem. Soc. Rev.*, 2009, 38, 1294.

[39] K. M. Thomas, *Dalton Trans.*, 2009, 1487.

[40] B. Xiao and Q. C. Yuan, *Particuology*, 2009, 7, 129.

[41] S. S. Han, J. L. Mendoza-Cortes and W. A. Goddard, *Chem. Soc. Rev.*, 2009, 38, 1460.

[42] Y. Xia, Z. Yang and Y. Zhu, *J. Mater. Chem. A*, 2013, 1, 9365-9381.

[43] S. J. Yang, H. Jung, T. Kim, C. R. Park, *Prog. Nat. Sci. Mater. Int.*, 2012, 22, 631–638.

[44] H. Wang, Q. Gao, J. Hu, *J. Am. Chem. Soc.*, 2009, 131 (20), 7016–7022.

[45] A. C. Dillon, K. M. Jones, T. A. Bekkedahl, C. H. Kiang, D. S. Bethune, M. J. Heben, *Nature*, 1997, 386, 377–379.

[46] G. G. Tibbetts, G. P. Meisner, C. H. Olk, *Carbon*, 2001, 39, 2291–2301.

[47] O. V. Pupysheva, A. A. Farajian, B. I. Yakobson, *Nano Let.,* 2007, 8, 767–774.

[48] A. Chambers, C. Park, R. T. K. Baker, N. M. Rodriguez, *J. Phys. Chem. B*, 1998, 102, 4253–4256.

[49] C. Liu, Y. Chen, C-Z. Wu, S-T. Xu, H-M. Cheng, *Carbon*, 2010, 48, 452–455.

[50] Z. Yang, Y. Xia, and R. Mokaya, *J. Am. Chem. Soc.*, 2007, 129, 1673–1679.

[51] Y. Gogotsi, A. Nikitin, H. H. Ye, W. Zhou, J. E. Fischer, B. Yi, H. C. Foley and M. W. Barsoum, *Nature Mater.*, 2003, 2, 591–594.

[52] R. Dash, J. Chmiola, G. Yushin, Y. Gogotsi, G. Laudisio, J. Singer, J. Fischer and S. Kucheyev, *Carbon*, 2006, 44, 2489–2497.

[53] Y. Gogotsi, R. K. Dash, G. Yushin, T. Yildirim, G. Laudisio and J. E. Fischer, *J. Am. Chem. Soc.*, 2005, 127, 16006–16007.

[54] G. Yushin, R. Dash, J. Jagiello, J. E. Fischer and Y. Gogotsi, *Adv. Funct. Mater.*, 2006, 16, 2288–2293.

[55] J. M. Blackman, J. W. Patrick, A. Arenillas, W. Shi and C. E. Snape, *Carbon*, 2006, 44, 1376–1385.

[56] H. L. Wang, Q. M. Gao and J. Hu, *J. Am. Chem. Soc.*, 2009, 131, 7016–7022.

[57] A. Almasoudi and R. Mokaya, *J. Mater. Chem.*, 2012, 22, 146–152.

[58] M. Sevilla and R. Mokaya, *J. Mater. Chem.*, 2011, 21, 4727–4732.

[59] P. Bénard and R. Chahine, *Scr. Mater.*, 2007, 56, 803–808.

[60] J. Dong, X. Wang, H. Xu, Q. Zhao, J. Li, *Int. J. Hydrogen Energ.,* 2007, 32, 4998–5004.

[61] H. W. Langmi, D. Book, A. Walton, S. R. Johnson, M. M. Al-Mamouri, J. D. Speight, P. P. Edwards, I. R. Harris, and P. A. Anderson, *J. Alloys Compd.*, 2005, 404, 637–642.

[62] L. Chen, R. K. Singh, and P. Webley, *Micropor. Mesopor. Mater.*, 2007, 102, 159–170.

[63] J. Germain, J. M. Fréchet, F. Svec, *Small*, 2009, 5, 1098–1111.

[64] P. Budd, J. Selbie, K. Mahmood, N. B. McKeown, B. Ghanem, K. Msayib, D. Book, and A. Walton, *Phys. Chem. Chem. Phys.*, 2007, 9, 1802–1808.

[65] S. H. Jhung , H-K. Kim , J. W. Yoon , and J-S. Chang, *J. Phys. Chem. B*, 2006, 110 (19), 9371–9374.

[66] W. I. F. David, *Faraday Discuss.*, 2011, 151, 399–414.

[67] A. Züttel, *Mater. Today,* 2003, 6(9), 24–33.

[68] R. T. Yang, *Carbon*, 2000, 38, 623–626.

[69] B. Sakintuna and Y. Yurum, *Ind. Eng. Chem. Res.*, 2005, 44, 2893–2902.

[70] M. Felderhoff, C. Weidenthaler, R. von Helmolt and U. Eberle, *Phys. Chem. Chem. Phys.*, 2007, 9,2643-2653.

[71] K. Kadono, H. Kajiura and M. Shiraishi, *Appl. Phys. Lett.*, 2003, 83, 3392–3394.

[72] Z. Yang, Y. Xia, X. Sun and R. Mokaya, *J. Phys. Chem. B*, 2006, 110, 18424–18431.

[73] J. M. Ren, N. M. Musyoka, H. M. Langmi, B. C. North, M. Mathe, X. D. Kang, *Int. J. Hydrogen Energ,* 2014, 39, 14912–14917.

[74] I. Ahmed, S. H. Jhung, *Mater. Today,* 2014, 17, 136–146.

[75] Y. S. Bae, K. L. Mulfort, H. Frost, P. Ryan, S. Punnathanam, L. J. Broadbelt, J. T. Hupp, R. Q. Snurr, *Langmuir,* 2008, 24, 8592–8598.

[76] A. D. Burrows, *Cryst. Eng. Comm.,* 2011, 13, 3623–3642.

[77] H. Jiang, Y. Feng, M. Chen, Y. Wang, *Int. J. Hydrogen Energ.,* 2013, 38, 10950–10955.

[78] H. Lee, Y. N. Choi, S. B. Choi, J. H. Seo, J. Kim, I. H. Cho, S. Gang, C. H. Jeon, *J. Phys. Chem. C*, 2014, 118, 5691–5699.

[79] C. Xu, J. Yang, M. Veenstra, A. Sudik, J. J. Purewal, Y. Ming, B. J. Hardy, J. Warner, S. Maurer, U. Müeller, D. J. Siegel, *Int. J. Hydrogen Energ.,* 2013, 38, 3268–3274.

[80] J. Purewal, D. G. Liu, A. Sudik, M. Veenstra, J. Yang, S. Maurer, U. Müller, D. J. Siegel *J. Phys. Chem. C*, 2012, 116, 20199–20212.

[81] J. J. Purewal, D. Liu, J. Yang, A. Sudik, D. J. Siegel, S. Maurer, U. Müller, *Int. J. Hydrogen Energ.,* 2012, 37, 2723–2727.

[82] A. Dailly, E. Poirier, *Energy Environ. Sci.,* 2011, 4, 3527–3534.

[83] M. Boudart, M. A. Vannice, J. E. Benson, *Physikalische Chemie Neue Folge*, 1969, 64, 171–177.

[84] H. Chen, L. F. Wang, J. Yang, R. T. Yang, *J. Phys. Chem. C*, 2013, 117, 7565–7576.

[85] C. Y. Wang, C. S. Tsao, M. S. Yu, P. Y. Liao, T. Y. Chung, H. C. Wu, M. A. Miller, Y. R. Tzeng, *J. Alloys Comp.,* 2010, 492, 88–94.

[86] S. J. Yang, J. H. Cho, K. S. Nahm, C. R. Park, *Int. J. Hydrogen Energ.,* 2010, 35, 13062–13067.

[87] Y. W. Li, R. T. Yang, *J. Am. Chem. Soc.*, 2006; 128, 726–727.

[88] Q. X. Li, A. D. Lueking, *J. Phys. Chem. C,* 2011, 115, 4273–4282.

[89] K. S. Lin, A. K. Adhikari, K. C. Chang, M. T. Tu, W. Lu, *Catal. Today*, 2011, 164, 23–27.

[90] M. Anbia, S. Mandegarzad, *J. Alloys Compd.*, 2012, 532, 61–67.

[91] B. Y. Li, X. Huang, R. N. Gong, M. R. Ma, X. J. Yang, L. Y. Liang, B. Tan, *Int. J. Hydrogen Energ.,* 2012, 37, 12813–12820.

[92] L. F. Wang, N. R. Stuckert, H. Chen, R. T. Yang, *J. Phys. Chem. C*, 2011, 115, 4793–4799.

[93] A. D. Lueking AD, R. T. Yang, *Applied Catal. A: General*, 2004, 265, 259–268.

[94] Y. Li Y, R. T. Yang, *J. Am. Chem. Soc.*, 2006, 128, 8136–8137.

[95] N. R. Stuckert, L. F. Wang, R. T. Yang, *Langmuir,* 2010, 26, 11963–11971.

[96] A. J. Lachawiec Jr, Q. Qi, R. T. Yang, *Langmuir*, 2005, 21, 11418–11424.

[97] P. B. S. Rallapalli, M. C. Raj, D. V. Patil, K. P. Prasanth, R. S. Somani, H. C. Bajaj, *Inter. J. Energ. Res.,* 2013, 37, 746–753.

[98] O. Ardelean, G. Blanita, G. Borodi, M. Mihet, M. Coros, D. Lupu, *Int. J. Hydrogen Energ.,* 2012, 37, 7378–7384.

[99] Y. W. Li, R. T. Yang, C. J. Liu, Z. Wang, *Ind. Eng. Chem. Res.,* 2007, 46, 8277–8281.

[100] M. Hirscher, *Handbook of Hydrogen Storage: New Materials for Future Energy Storage*, WILEY-VCH Verlag GmbH & Co. KGaA, Weinheim, 2010.

[101] G. G. Libowitz, *The Solid-State Chemistry of Binary Metal Hydrides*, 1965, W.A. Benjamin, New-York.

[102] D. G. Ivey and D. O. Northwood, *J. Mater Sci.*, 1983, 18 (2), 321–347.

[103] A. J. Maeland, presented at the Hydrides for Energy Storage, Geilo, Norway, 1977.

[104] J. J. Reilly, *Z. Phys. Chem. N. F.*, 1979, 117, 155–184.

[105] B. Sakintuna, F. L. Darkrim, M. Hirscher, *Int. J. Hydrogen Energ.*, 2007, 32, 1121–1140.

[106] L. Zhou, *Renew Sustain Energy Rev.*, 2005, 9, 395–408.

[107] L. Zhou, Y. Zhou, Y. Sun, *Int. J. Hydrogen Energ.*, 2006, 31(2), 259–64.

[108] U. Eberle, G. Arnold, R. V. Helmholt, *J. Power Sour.*, 2006, 154(2), 456–60.

[109] M. Latroche, *J. Phys. Chem. Solids*, 2004, 65, 517–522.

[110] HyTRAIN: Hydrogen Storage Research Training Network, EC-MRTNCT-2004-512443. Website: http://www.imr.salford.ac.uk.

[111] M. Zhu, H. Wang, L. Z. Ouyang, M. Q. Zeng, *Int J Hydrogen Energy*, 2006, 31(2), 251–257.

[112] N. Hanada, T. Ichikawa, H. Fuji, *J. Phys. Chem. B,* 2005, 109, 7188–94.

[113] A. Zaluska, L. Zaluski, J. O. Ström-Olsen, *J Alloys Compds,* 1999, 288, 217–225.

[114] H. Imamura, K. Masanari, M. Kusuhara, H. Katsumoto, T. Sumi, Y. Sakata, *J. Alloys Compd.*, 2005, 386, 211–216.

[115] L. Zaluski, A. Zaluska, J. O. Ström-Olsen, *J. Alloys Compd.*, 1997, 253–254, 70–79.

[116] R. Wiswall, *Hydrogen Met. II*, 1978, 29, 209.

[117] Y. Fukai, *The metal–hydrogen system, basic bulk properties*, Springer series in materials science, 1993.

[118] B. Bogdanovi_c, K. Bohmhammel, B. Christ, A. Reiser, K. Schlichte, R. Vehlen, and U. Wolf, *J. Alloys Compd.*, 1999, 282(1-2), 84–92.

[119] O. Guteisch, N. S. de Boer, N. Ismail, M. Herrich, A. Walton, J. Speight, I. R. Harris, A. S. Pratt, and A. Züttel, *J. Alloys Compd.,* 2003, 356–357(1-2), 598–602.

[120] G. Barkhordarian, T. Klassen T, R. Bormann, *J. Alloys Compd.,* 2004, 364, 242–246.

[121] D. Moser, D. J. Bull, T. Sato, D. Noréus, D. Kyoi, T. Sakai, N. Kitamura, T. H. YusaTaniguchi, W. P. Kalisvaarte and P. H. L. Notten, *J. Mater. Chem.*, 2009, 19, 8150–8161.

[122] H. Aoyagi, K. Aoki, T. Masumoto, *J. Alloys Compd.,* 1995, 231, 804–809.

[123] R. W. P. Wagemans, J. H. V. Lenth, P. E. Jongh, A. J. V Dillen, K. P. Jong, *J. Am. Chem. Soc.*, 2005, 127, 16675–16680.

[124] J. Huot, E. Akiba, T. Takada, *J Alloys Compd.*, 1995, 231, 815–819.

[125] Y. Chen Y, C.-Z. Wu, P. Wang, H.-M. Cheng, *Int. J. Hydrogen Energ.*, 2006, 31, 1236–1240.

[126] W. Luo, *J Alloys Compd.,* 2004, 381, 284–287.

[127] Y. Liu, K. Zhong, M. Gao, J. Wang, H. Pan, Q. Wang, *Chem. Mater.*, 2008, 20, 3521–3527.

[128] S. V. Alapati, K. J. Johnson, D. S. Sholl, *J. Phys. Chem. B*, 2006, 110, 8769–8776.

[129] S. V. Alapati, K. J. Johnson, D. S. Sholl, *Phys. Chem. Chem. Phys.*, 2007, 9, 1438–1452.

[130] J. Lu, Z. Z. Fang, Y. J. Choi, H. Y. Sohn*, J. Phys. Chem. C*, 2007, 111, 12129–12134.

[131] W. Osborn, T. Markmaitree, L. L. Shaw, *J. Power Sources*, 2007, 172, 376–378.

[132] G. G Libowitz, H. F. Hayes, and T. H. P. Gibb*, J. Phys. Chem.*, 1958, 62, 76.

[133] J. J. Reilly and R. H. Wiswall, *Inorg. Chem.,* 1968, 7(11), 2254–2256.

[134] J. J. Reilly and R. H. Wiswall, *Inorg. Chem.,* 1974, 13(1), 218–222.

[135] J. H. N. van Vucht, F. A. Kuijpers, and H. C. A. M. Bruning, *Philips Res. Rep.*, 1970, 25, 133.

[136] Z. Huang and T. Autrey, *Energy Environ. Sci.*, 2012, 5, 9257–9268.

[137] H.-L. Jiang and Q. Xu, *Catal. Today*, 2011, 170, 56–63.

[138] C. W. Hamilton, R. T. Baker, A. Staubitz and I. Manners, *Chem. Soc. Rev.*, 2009, 38, 279–293.

[139] J. Hannauer, O. Akdim, U. B. Demirci, C. Geantet, J.-M. Herrmann, P. Miele and Q. Xu, *Energy Environ. Sci.*, 2011, 4, 3355–3358.

[140] U. B. Demirci and P. Miele, *Energy Environ. Sci.*, 2011, 4, 3334–3341.

[141] Z. Tang, X. Chen, H. Chen, L. Wu and X. Yu, *Angew. Chem. Int. Ed.*, 2013, 52, 5832–-5835.

[142] A. Gutowska, L. Li, Y. Shin, C. M. Wang, X. S. Li, J. C. Linehan, R. S. Smith, B. D. Kay, B. Schmid, W. Shaw, M. Gutowski and T. Autrey, *Angew. Chem. Int. Ed.*, 2005, 44, 3578–-3582.

[143] Z. Li, G. Zhu, G. Lu, S. Qiu and X. Yao, *J. Am. Chem. Soc.*, 2010, 132, 1490–1491.

[144] P. E. de Jongh and P. Adelhelm, *ChemSusChem*, 2010, 3, 1332–1348.

[145] X. Chen, L. Wan, J. Huang, L. Ouyang, M. Zhu, Z. Guo and X. Yu, *Carbon*, 2014, 68, 462–472.

[146] L. Li, X. Yao, C. Sun, A. Du, L. Cheng, Z. Zhu, C. Yu, J. Zou, S. C. Smith, P. Wang, H.-M. Cheng, R. L. Frost and G. Q. Lu, *Adv. Funct. Mater.*, 2009, 19, 265–271.

[147] C. A. Jaska, K. Temple, A. J. Lough and I. Manners, *J. Am. Chem. Soc.*, 2003, 125, 9424–9434.

[148] S.-K. Kim, W.-S. Han, T.-J. Kim, T.-Y. Kim, S. W. Nam, M. Mitoraj, Ł. Piekos, A. Michalak, S.-J. Hwang and S. O. Kang, *J. Am. Chem. Soc.*, 2010, 132, 9954–9955.

[149] S.-K. Kim, T.-J. Kim, T.-Y. Kim, G. Lee, J. T. Park, S. W. Nam and S. O. Kang, *Chem. Commun.*, 2012, 48, 2021–2023.

[150] M. E. Bluhm, M. G. Bradley, R. Butterick, U. Kusari and L. G. Sneddon, *J. Am. Chem. Soc.*, 2006, 128, 7748–7749.

[151] R. P. Shrestha, H. V. K. Diyabalanage, T. A. Semelsberger, K. C. Ott and A. K. Burrell, *Int. J. Hydrogen Energ.*, 2009, 34, 2616–2621.

[152] Z. Xiong, C. K. Yong, G. Wu, P. Chen, W. Shaw, A. Karkamkar, T. Autrey, M. O. Jones, S. R. Johnson, P. P. Edwards and W. I. F. David, *Nat. Mater.*, 2008, 7, 138–141.

[153] H. V. K. Diyabalanage, R. P. Shrestha, T. A. Semelsberger, B. L. Scott, M. E. Bowden, B. L. Davis and A. K. Burrell, *Angew. Chem. Int. Ed.*, 2007, 46, 8995–8997.

[154] M. Nielsen, E. Alberico, W. Baumann, H.-J. Drexler, H. Junge, S. Gladiali and M. Beller, *Nature*, 2013, 495, 85–89.

[155] R. E. Rodriguez-Lugo, M. Trincado, M. Vogt, F. Tewes, G. Santiso-Quinones and H. Grutzmacher, *Nat. Chem.*, 2013, 5, 342–347.

[156] S. Enthaler, J. von Langermann and T. Schmidt, *Energy Environ. Sci.*, 2010, 3, 1207–1217.

[157] M. Grasemann and G. Laurenczy, *Energy Environ. Sci.*, 2012, 5, 8171–8181.

[158] B. Loges, A. Boddien, F. Gartner, H. Junge and M. Beller, *Top. Catal.*, 2010, 53, 902–914.

[159] S. K. Singh, X.-B. Zhang and Q. Xu, *J. Am. Chem. Soc.*, 2009, 131, 9894–9895.

[160] S. K. Singh and Q. Xu, *J. Am. Chem. Soc.*, 2009, 131, 18032–18033.

[161] S. K. Singh, A. K. Singh, K. Aranishi and Q. Xu, *J. Am. Chem. Soc.*, 2011, 133, 19638–19641.

[162] S. K. Singh and Q. Xu, *Inorg. Chem.*, 2010, 49, 6148–6152.

[163] S. K. Singh and Q. Xu, *Chem. Commun.*, 2010, 46, 6545–6547.

[164] S. K. Singh, Y. Lizuka and Q. Xu, *Int. J. Hydrogen Energ.*, 2011, 36, 11794–11801.

[165] R. B. Biniwale, S. Rayalu, S. Devotta, M. Ichikawa, *Int. J. Hydrogen Energ.*, 2008, 33, 360–365.

[166] E. Y. Marrero-Alfonso, A. M. Beaird, T. A. Davis, and M. A. Matthews, *Ind. Eng. Chem. Res.,* 2009, 48, 3703–3712.

[167] S. Orimo, Y. Nakamori, J. R. Eliseo, A. Züttel, and C. M. Jensen, *Chem. Rev.,* 2007**,** 107, 4111–4132.

[168] I. P. Jain, P. Jain, A. Jain, *J. Alloys Compd.,* 2010*,* 503, 303–339.

[169] R. A. Varin, Z. S. Wronski, *Renewable Hydrogen Technologies, Chapter 13: Progress in Hydrogen Storage in Complex Hydrides,* Publisher: Elsevier, 2013.

[170] T. N. Dymova, D.P. Aleksandrov, V.N. Konoplev, T.A. Silina, A.S. Sizareva, *Russ. J. Coord. Chem.*, 1994, 20, 263.

[171] J. Chen, N. Kuriyama, Q. Xu, H. T. Takeshita, T. Sakai, *J. Phys. Chem. B*, 2001, 105, 11214.

[172] O. M. Løvvik, M. O. Susanne, W. B. Hendrik, C. H. Bjørn, *Phys. Rev. B,* 2004, 69 134117.

[173] J.-W. Jang, J.-H. Shim, Y. W. Cho, B.-J. Lee, *J. Alloys Comp.*, 2006, 420, 286–290.

[174] P. Balema Viktor, W. D.Kevin, K. Pecharsky Vitalij, *Chem. Commun.,* 2000 1665–1666.

[175] V. P. Balema, V. K. Pecharsky, K. W. Dennis, *J. Alloys Comp.,* 2000, 313, 69–74.

[176] V. P. Balema, J.W. Wiench, K.W. Dennis, M. Pruski, V.K. Pecharsky, J. *Alloys Comp.,* 2001, 329, 108–114.

[177] T. Sun, C. K. Huang, H. Wang, L. X. Sun, M. Zhu, *Int. J. Hydrogen Energ.,* 2008, 33, 6216–6221.

[178] Y. F. Liu, Y. J. Yang, Y. F. Zhou, Y. Zhang, M. X. Gao, H. G. Pan, *Int. J. Hydrogen Energ.,* 2012, 37, 17137–17145;

[179] Y. J. Yang, M. X. Gao, Y. F. Liu, J. H. Wang, J. Gu, H. G. Pan, Z.X. Guo, *Int. J. Hydrogen Energ.* 2012, 37, 10733–10742.

[180] Y. F. Liu, J. J. Hu, Z. T. Xiong, G. T. Wu, P. Chen, *J. Phys. Chem. C*, 2007, 111, 19161–19164.

[181] Z. T. Xiong, J. J. Hu, G. T. Wu, Y. F. Liu, P. Chen, *Catal. Today,* 2007, 120, 287–291.

[182] P. Claudy, B. Bonnetot and J. M. Lettoffe´ , *J. Therm. Anal.*, 1979, 15, 119–128.

[183] M. Mamatha, B. Bogdanovic´ , M. Felderhoff, A. Pommerin, W. Schmidt, F. Schüth and C. Weidenthaler, *J. Alloys Compd.,* 2006, 407, 78–86.

[184] Y. Kim, E.-K. Lee, J.-H. Shim, Y. W. Cho and K. B. Yoon, *J. Alloys Compd.*, 2006, 422, 283–287.

[185] B. Bogdanovi_c and M. Schwickardi, *J. Alloys Compd.,* 1997, 253-254, 1–9.

[186] S. S. Srinivasan, H. W. Brinks, B. C. Hauback, D. Sun, and C. M. Jensen, *J. Alloys Compd.*, 2004, 377(1-2), 283–289.

[187] H. Morioka, K. Kakizaki, S.-C. Chung, A. Yamada, *J. Alloys Comp.,* 2003, 353, 310–314.

[188] J. R. Ares, K.-F. Aguey-Zinsou, F. Leardini, I. J. Ferrer, J.-F. Fernandez, Z.-X. Guo, C. Sanchez, *J. Phys. Chem. C*, 2009, 113, 6845.

[189] A. Klaveness, P. Vajeeston, P. Ravindran, H. Fjellvag, A. Kjekshus, *J. Alloys Comp.* 2007, 433, 225–232.

[190] P. A. Chater, P. A Anderson, J. W. Prendergast, A. Walton, V. S. J. Mann, D. Book, W. I. F. David, S. R. Johnson, P.P. Edwards, *J Alloy Compd.*, 2007, 446–447, 350–354.

[191] P. Chen, Z. Xiong, J. Luo, J. Lin and K. L.Tan, *Nature,* 2002, 420, 302–304.

[192] P. Chen, Z. Xiong, J. Luo, J. Lin and K. L.Tan, *J. Phys. Chem. B,* 2003, 107, 10967–10970.

[193] T. Ichikawa, S. Isobe, N. Hanada, H. Fujii, *J. Alloys Compd.,* 2004, 365, 271–276.

[194] S. Isobe, T. Ichikawa, N. Hanada, H. Y. Leng, M. Fichtner, O. Fuhr, H. Fujii, *J. Alloys Compd,* 2005, 404–406, 439–442.

[195] A. W. Titherley, *J. Am. Soc., Trans.*, 1894, 65, 504–522.

[196] F. W. Dafert, R. Miklanz, *Manotsh. Chem.,* 1910, 31, 981.

[197] O. Ruff, H. Geoges, *Ber. Dtsh. Chem. Ges.,* 1911, 44, 501–502.

[198] R. Juza and K. Opp, Z. *Anorg. Allg. Chem.,* 1951, 266, 313–325.

[199] K. Miwa, N. Ohba, S. Towata, *Phys. Rev. B,* 2005, 71, 195109.

[200] J. B. Yang, X. D. Zhou, Q. Cai, W. J. James, W. B. Yelon, *Appl. Phys. Lett.*, 2006, 88, 041914.

[201] Y. Kojima, Y. Kawai, *J. Alloys Compd.,* 2005, 395, 236–239.

[202] R. S. Chellappa and D. Chandra, *J. Phys. Chem. B,* 2007, 111, 10785–10789.

[203] W. J. Jolly, *Inorganic Chemistry of Nitrogen, W. A. Benjamin, Inc., New York*, 1964, 19–46.

[204] E. C. Franklin, *The Nitrogen System of Compounds, Reinhold, New York*, 1935, 53–63.

[205] Y. H. Hu and E. Ruckenstein, *Ind. Eng. Chem. Res,* 2006, 45, 182–186.

[206] T. Noritake, H. Nozaki, M. Aoki, S. Towata, G. Kitahara, Y. Nakamori, S. Orimo, *J. Alloys Compd.,* 2005, 393, 264–268.

[207] R. A. Forman, *J. Chem. Phys.,* 1971, 55, 1987.

[208] M. P. Balogh, C. Y. Jones, J. F. Herbst Jr., L. G. Hector, M. Kundrat, *J. Alloys Compd.,* 2006, 420, 326–336.

[209] E. Zintl and G. Brauer, *Z. Elektrochem.,* 1935, 41, 102.

[210] A. Rabenau and H. Schulz, *J. Less-Common Met.,* 1976, 50, 155.

[211] M. Mali, J. Roos and D. Binkmann, *Phys. Rev. B,* 1987, 36, 3888.

[212] H. J. Beister, S. Haag, R. Kniep, K. Strössner and K. Syassen, *Angew. Chem. lnt. Ed. Engl.*, 1988, 27, No. 8.

[213] A. Lazicki, B. Maddox, W. J. Evans, C. S. Yoo, A. K. McMahan, W. E. Pickett, R. T. Scalettar, M. Y. Hu and P. Chow, *Phys. Rev. Lett.,* 2005, 95, 165503.

[214] Y. H. Hu, E. Ruckenstein, *J. Phys. Chem. A,* 2003, 107, 9737–9739.

[215] S. Hino, T. Ichikawa, N. Ogita, M. Udagawa, H. Fujii, *Chem. Commun*., 2005, 181, 3038–3040.

[216] T. Ichikawa, N. Hanada, S. Isobe, H.Y. Leng, H. Fujii, *J. Alloys Compd.,* 2005, 404–406, 435–438.

[217] J. H. Yao, C. Shang, K. F. Aguey-Zinsou, Z.X. Guo, *J. Alloys Compd.*, 2007, 432, 277–282.

[218] T. Ichikawa, N. Hanada, S. Isobe, H. Leng, H. Fujii, *J. Phys. Chem. B*, 2004, 108, 887–7892.

[219] L. Shaw, R. Ren, T. Markmaitree, W. Osborn, *J. Alloys Compd.*, 2008, 448, 263.

[220] J. Z. Hua, J. H. Kwaka, Z. Yanga, W. Osbornb, T. Markmaitreeb, L. L. Shawb, *J. Power Sources*, 2008, 181, 116‑119.

[221] W. I. F. David, M. O. Jones, D. H. Gregory, C. M. Jewell, S. R. Johnson, A. Walton and P. P. Edwards, *J. Am. Chem. Soc.,* 2007, 129, 1594–1601.

[222] H. Y. Leng, T. Ichikawa, S. Hino, H. Fujii, *J. Alloys Compd.,* 2008, 463, 462–465.

[223] J. Zhang and Y. H. Hu, *Ind. Eng. Chem. Res.,* 2011, 50, 8058–8064.

[224] L. Ma, P. Wang, H. Dai, L. Kong, H. Cheng, *J. Alloys Compd.*, 2008, 466, L1–L4.

[225] Q. Wang, Z. Chen, W.Yu, Y. Chen, and Y. Li, *Ind. Eng. Chem. Res,* 2010, 49, 5993–5996.

[226] S. Isob, T. Ichikawa T and N. Hanada, 2005 *J. Alloys Compd.* **404** 439.

[227] H. Leng, Z. Wu, W. Duan, G. Xia, Z. Li, *Int. J. Hydrogen Energ.,* 2012, 37, 903–907.

[228] Z. T. Xiong, G. T. Wu, H. J. Hu, P. Chen, *Adv. Mater*., 2004, 16, 1522–1525.

[229] Y. Kojima, M. Matsumoto, Y. Kawai, T. Haga, N. Ohba, K. Miwa, S. Towata, Y. Nakamori, S. Orimo, *J. Phys. Chem. B,* 2006, 110, 9632–9636.

[230] K. Toyokoda, S. Hino, T. Ichikawa, K. Okamoto, H. Fujii, *J. Alloys Compd.*, 2007, 439, 337–341.

[231] H. Wu, *J. Am. Soc.,* 2008, 130, 6515–6522.

[232] P. A. Anderson, P. A. Chater, David R. Hewett and P. R. Slater, *Faraday Discuss.,* 2011, 151, 271–284.

[233] T. T. T. Nguyen, D. Reed, D. Book, P. A. Anderson, *J. Alloys Compd.,* 2015, 645, S295–298.

[234] W. Luo, *J. Alloys Compd.*, 2004, 381, 284–287.

[235] W. Luo, E. Rönnebro, *J. Alloys Compd.*, 2005, 404-406, 392–395.

[236] W. Luo, S. Sickafoose, *J. Alloys Compd.,* 2006, 407, 274–281.

[237] T. Ichikawa, H. Y. Leng, S. Isobe, N. Hanada, H. Fujii, *J. Power Sourc.,* 2006, 159, 126–131.

[238] Y. Chen, P. Wang, C. Liu, H.-M. Cheng, *Int. J. Hydrogen Energ.,* 2007, 32, 1262–1268.

[239] J. Lu, Z. Z. Fang, Y. J. Choi, H. Y. Sohn, *J. Phys. Chem. C,* 2007, 111, 12129–12134.

[240] R. R. Shahi, T. P. Yadav, M. A. Shaz, O. N. Srivastava, *Int. J. Hydrogen Energ.,* 2008, 33, 6188–6194.

[241] Y. Liu, K. Zhong, M. Gao, J. Wang, H. Pan, Q. Wang, *Chem. Mater.* 2008, 20, 3521–3527.

[242] C. Liang, Y. Liu, K. Luo, B. Li, M. Gao, H. Pan, Q. Wang, *Chem. Eur. J.* 2010, 16, 693–702.

[243] O. Dolotko, N. Paulson, V. K. Pecharsky, *Int. J. Hydrogen Energy* 2010, 35, 4562–4568.

[244] D. Pottmaier, F. Dolci, M. Orlova, G. Vaughan, M. Fichtner, W. Lohstroh, M. Baricco, *J. Alloys Compd*., 2011, 509S, S719–S723.

[245] C. Price, J. Gray, R. Lascola Jr., D. L. Anton, *Int. J. Hydrogen. Energ.*, 2012, 37, 2742–2749.

[246] T. Durojaiye, Goudy, *Int. J. Hydrogen Energ.*, 2012, 37, 3298–3304.

[247] W. Luo, V. Stavila, L. E. Klebanoff, *Int. J. Hydrogen Energ.,* 2012, 37, 6646–6652.

[248] S. V. Alapati, J. K. Johnson, D. S. Sholl, *Phys. Chem. Chem. Phys.* 2007, 9, 1438–1452.

[249] R. A. Varin, L. Zbroniec, M. Jang, *Eng. Rev.*, 2011, 31, 111–123.

[250] R. Parviz, R. A. Varin, *Int. J. Hydrogen Energ.,* 2013, 8(20), 8313–8327.

[251] H. Leng, T. Ichikawa, S. Hino, N. Hanada, S. Isobe, H. Fujii, *J. Power Sources*, 2006, 156, 166–170.

[252] S. Hino, T. Ichikawa, H. Leng, H. Fujii, *J. Alloys Comp.*, 2005, 398, 62–66.

[253] Y. Kojima, T. Ichikawa, and H. Fujii, *Encyclopedia of Electrochemical Power Sources, Part: Fuel – Hydrogen storage: Complex hydrides*, Elservier, 2013, 473–484.

[254] H. I. Schlesinger and H. C. Brown*, J. Am. Chem. Soc.*, 1940, 62, 3429–3435.

[255] E. M. Fedneva, V. I. Alpatova, and V. I. Mikheeva*, Russ. J. Inorg. Chem.*, 1964, 9 (6), 826-827.

[256] H. I. Schlesinger, H. C. Brown, B. Abraham, A. C. Bond, N. Davidson, A. E. Finholt, J. R. Gilbreath, H. Hoekstra, L. Horvitz, E. K. Hyde, J. J. Katz, J. Knight, R. A. Lad, D. L. Mayfield, L. Rapp, D. M. Ritter, A. M. Schwartz, I. Sheft, L. D. Tuck, and A. O. Walker, *J. Am. Chem. Soc.*,1953. 75, 186–190.

[257] H. Noth and G. Mikulaschek*, Angewandte Chemie,* 1961. 73 (11), 371–383.

[258] D. Goerrig, *Synthesis of $LiBH_4$ from the elements*, 1985, Germany, Patent Number 1077644.

[259] S. Orima, Y. Nakamori, G. Kitahara, K. Miwa, N. Ohba, S. Towata, and A. Züttel, *J. Alloys Comp.,* 2005, 404, 427–430.

[260] P. M. Harris, E. P. Meibohm, *J. Am. Chem. Soc.*, 1947, 69, 1231–1232.

[261] J. P. Soulié, G. Renaudin, R. Cerny, and K. Yvon, *J. Alloys Comp.,* 2002, 346, 200–205.

[262] A. Züttel, S. Rentsch, P. Fischer, P. Wenger, P. Sudan, P. Mauron, and C. Emmenegger*, J. Alloys Comp.,* 2003, 356, 515–520.

[263] M. R. Hartman, J. J. Rush, T. J. Udovic Jr, R. C. Bowman, S.-J. Hwang, *J. Solid State Chem.,* 2007, 180, 1298–1305.

[264] Y. Filinchuk, D. Chernyshov, R. Cerny, *J. Phys. Chem. C*, 2008, 112, 10579–10584.

[265] Y. Filinchuk, D. Chernyshov, A. Nevidomskyy, V. Dmitriev, *Angew Chem. Int. Ed.*, 2008, 47, 529–532.

[266] A. Tekin A, R. Caputo R, A. Züttel, *Phys. Rev. Lett.*, 2010, 104, 215501.

[267] H. Takamura, Y. Kuronuma, H. Maekawa, M. Matsuo, S. Orimo, *Solid State Ionics*, 2010, doi:10.1016/j.ssi.2010.02.011.M.

[268] B. Sundqvist, O. Andersson, *Int. J. Thermophys.*, 2009, 30, 1118–1129.

[269] A. V. Talyzin, O. Andersson, B. Sundqvist, A. Kurnosov, L. Dubrovinsky, *J. Solid State Chem.*, 2007, 180, 510–517.

[270] CWFT, Pistorius, *Z. Phys. Chem. Neue Folge*, 1974, 88, 253.

[271] V. Dmitriev, Y. Filinchuk, D. Chernyshov, *Phys. Rev. B*, 2008, 77, 174112.

[272] A. Züttel, P. Wenger, S. Rentsch, P. Sudan, P. Mauron, and C. Emmenegger*, J. Power Sources,* 2003, 118, 1–7.

[273] M. Au, A. Jurgensen, and K. Zeigler*., J. Phys. Chem. B*, 2006, 110, 26482–26487.

[274] M. Au, A. R. Jurgensen, W. A. Spencer, D. L. Anton, F. E. Pinkerton, S. J. Hwang, C. Kim, and R. C. Bowman, *J. Phys. Chem. C,* 2008, 112, 18661–18671.

[275] G. L. Xia, Y. H. Guo, Z. Wu, X. B. Yu, *J. Alloys Compd.,* 2009, 479, 545–548.

[276] M. S. Wellons, P. A. Berseth, R. Zidan, *Nanotechnology,* 2009, 20, 204022.

[277] B. J. Zhang, B. H. Liu, *Int. J. Hydrogen Energ.,* 2010, 35, 7288–7294.

[278] S. V. Alapati, J. K. Johnson, D. S. Sholl, *J. Phys. Chem. B*, 2006, 110, 8769–8776.

[279] F. E. Pinkerton, G. P. Meisner, M. S. Meyer, M. P. Balogh, and M. D. Kundrat, *J. Phys. Chem. B,* 2005, 109, 6–8.

[280] F. E. Pinkerton, G. P. Meisner, M. S. Meyer, M. P. Balogh, *J. Phys. Chem. B*, 2006, 110, 7967–7974.

[281] G. P. Meisner, M. L. Scullin, M. P. Balogh, F. E. Pinkerton, M. S. Meyer, *J. Phys. Chem. B*, 2006, 110, 4186–4192.

[282] H. Wu, W. Zhou, K. Wang, T. J. Udovic, J. J. Rush, T. Yildirim, *et al., Nanotechnology,* 2009, 20, 204002.

[283] W. S. Tang, G. Wu, Tao Liu, A. T. S. Wee, C. K. Yong, Z. Xiong, A. T. S. Hor and P. Chen, *Dalton Trans.,* 2008, 2395–2399.

[284] M. Aoki, K. Miwa, T. Noritake, G. Kitahara, Y. Nakamori, S. Orimo, *et al., Appl. Phys. A*, 2005, 80, 1409–1412.

[285] Y. Nakamori, A. Ninomiya, G. Kitahara, M. Aoki, T. Noritake, K. Miwa, *et al., J. Power Sourc.*, 2006, 155, 447–455.

[286] T. Noritake, M. Aoki, S. Towata, A. Ninomiya, Y. Nakamori, S. Orimo, *Appl. Phys. A,* 2006, 83, 277–279.

[287] F. E. Pinkerton, M. S. Meyer, *J. Phys. Chem. C*, 2009, 113, 11172–11176.

[288] F. E. Pinkerton, G. P. Meisner, M. S. Meyer, M. P. Balogh, *J. Alloys Compd.,* 2007, 433, 282–291.

[289] Y. F. Liu, K. Luo, Y. F. Zhou, M. X. Gao, H. Pan, *J. Alloys Compd.,* 2009, 481, 473–479.

[290] Y. Zhang, Y. Liu, T. Liu, M. Gao, H. Pan, *Int. J. Hydrogen Energ.,* 2013, 38, 13318–13327.

[291] B. Brehler, *Z. Kristallogr.*, 1961, 115, 373–402.

[292] J. Brynestad, and H. L. Yakel, *Inorg. Chem.*, 1978, 17 (5), 1376–1377.

[293] A Sen, M. N. Rao, R. Mittal and S. L. Chaplot, *J. Phys. Condens. Matter*, 2005, 17, 6179–6192.

[294] H. S. Ray, *Introduction to Melts: Molten Salts, Slags and Glasses,* Allied Publishers, 2006.

[295] J. D. Mackenzie, W. K. Murphy, *J. of Chem. Phys.,* 1960, 33, 366.

[296] V. Danek, *Physico-Chemical Analysis of Molten Electrolytes,* Elsevier, 2006.

[297] D. L. Price, M. L. Saboungi, S. Susman, K. J. Volin, A. C. Wright, *J. Phys. Condens. Matter,* 1991, 3, 9835–9842.

[298] S. Narashimhan, R. Balakumar, *Aldrichimica Acta* 1998, 31, 1, 19–26.

[299] P. Edwards, W. Grochala, D. Book, I. R. Harris, *PCT Int. Appl.* 2004, 21.

[300] E. Jeon, Y. W. Cho, *J. Alloys Compd*. 2006, Article in press.

[301] S. Srinivasan, E. Stefanakos, Y. Goswami, WHEC 16, 2006 – Lyon France.

[302] Luis A. Rivera, *Destabilization and characterization of $LiBH_4/MgH_2$ complex hydride for hydrogen storage*, PhD thesis, University of South Florida, 2007.

[303] S. L. Suib, *New and Future Developments in Catalysis: Batteries, Hydrogen Storage and Fuel Cells*, Elsevier, 2013.

Chapter 2: Experimental

2.1 Materials Synthesis under Inert Gas

All synthesis reactions in this work were carried out under inert conditions due to a high reactivity with moisture and oxygen of materials used.

Starting materials were ground together in a pestle and mortar by hand in the desired mole ratio in an argon-atmosphere glove box (MBraun, UniLab, < 10 ppm O_2, <0.1ppm H_2O). Prepared samples were then transferred into a quartz reaction tube (0.5"O/D), sealed with a Young's tap T-piece with an Ultra-torr® fitting before being taken out the glove box. The reaction tube was then placed inside a vertical tube (Lenton Furnaces, LTF 12/25/250 fitted with a Eurotherm 3216P1 controller). The T-piece was then connected to the gas line for argon gas to be flowed through. The Young's tap was then open during the reaction. In general, a sample is heated up to desired temperature with a heating rate of 2°C/min then held for 12 hours. After the reaction finishes and the furnace cooling down to room temperature, the Young's tap was closed and removed from the gas line then taken into the glove box.

2.2 Crystallography

Crystallography is concerned with the structure and properties of crystalline materials [1-3].

Crystals are solids where the atoms adopt regular arrangements of atoms with respect to each other in three dimensions which is known as a lattice. These arrangements are

repeating by a unit called the unit cell, the smallest repeating unit which shows the full symmetry of a crystal structure. The unit cell can produce crystal lattice via translational symmetry.

The size and shape of a unit cell are determined by the lengths of three unit cell edges denoted *a*, *b*, and c and three angles between them α, β, and γ (the angle between *b* and *c* is α, between *a* and *c* is β, and between *a* and *b* is γ). A set of these six values are used to define unit cell and termed lattice parameters. By having different combinations and relationships between these lattice parameters, seven crystal systems including triclinic, monoclinic, orthorhombic, tetragonal, trigonal, hexagonal and cubic are formed.

In crystals in three dimensions there are four lattice types. The primitive cell (P) is the simplest one containing only a single lattice point at the corners of the cell. The body centred (I) cell has an additional lattice point at the centre of the unit cell. The face centred cell (F) contains an extra lattice point in the centre of each face of the cell. The side-centred or base-centred (C) cell contains one additional lattice point at the centre of each face of one pair of parallel faces of the cell.

By combining one of the seven crystal systems with one of the lattice types, a total of 14 lattice types known as the Bravais lattices are produced (***figure 2.1***).

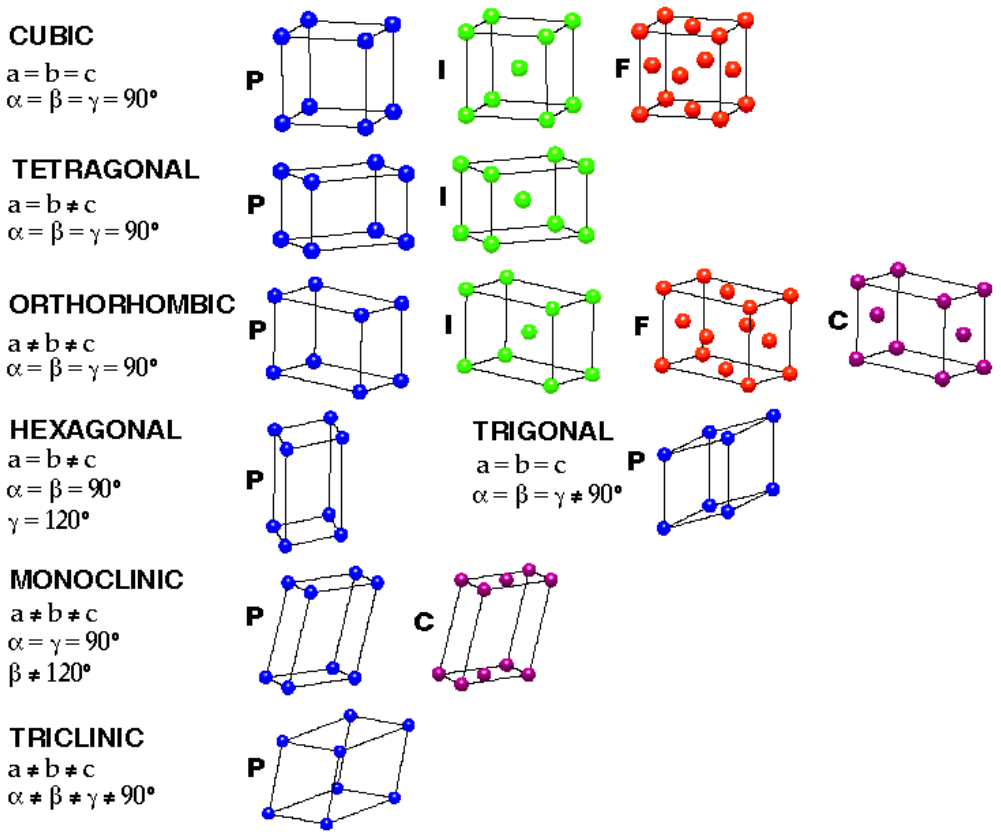

Figure 2.1 *The 14 Bravais lattices*

The Bravais lattices show the intrinsic translational symmetry of a unit cell by describing the geometrical arrangement of the lattice points. Crystal structures are described by lattice parameters, positions of atoms in the unit cell, and the supplementary symmetry elements of the cell.

Atomic positions are expressed as fractional coordinates along each unit cell direction from one corner of the cell.

In addition to atoms in the unit cell, the symmetry elements of the unit cell including non-translational symmetry elements (inversion centre, reflection, and rotation) and

translational symmetry elements (glide planes and screw axes) must be considered in three dimensions.

With the combination of all the symmetry elements 230 space groups can be derived which then completely describe the symmetry of the crystal structure.

2.3 Powder X-ray Diffraction

Powder X-ray diffraction is a powerful and widely used technique for characterizing a crystalline material. The distance between the atoms (ions) in crystalline solids is around a few angstroms (Å) similar to the wavelength of X-rays, and interference between the scattered X-rays can occur.

Not all scattering can cause X-ray diffraction patterns, only that whose conditions satisfy Bragg's law (equation (2.1)). Where Bragg's law is not met destructive interference occurs and no peak intensity is seen in the diffraction pattern [2].

$$n\lambda = 2d\sin\theta \qquad (2.1)$$

where

n is an integer,

λ is the wavelength of incident X-ray,

d is the lattice spacing,

θ *is* the Bragg angle (the angle between incident radiation and scattered plane).

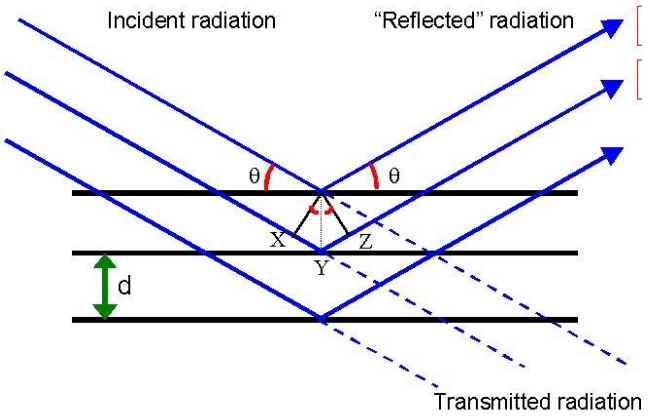

Figure 2.2 *Geometry used for Bragg's law*

X-ray generation

X-rays are produced when a metal target is bombarding by an electron beam which is accelerated towards the target by a high electric field. If the energy of the arriving electrons is high enough, an electron in an inner electron shell will be ejected and that creates a vacancy. An electron in an outer electron shell then fills the vacancy and emits an X–ray radiation. A typical X-ray spectrum of the most widely used target, copper, is shown in ***figure 2.3***.

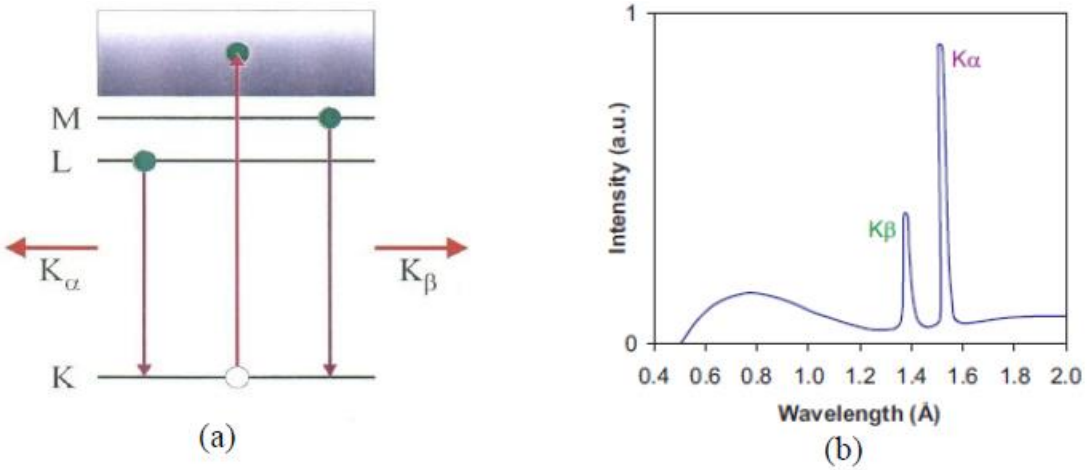

Figure 2.3 *Generation of a vacancy (a) and X-ray spectrum obtained (b) [4]*

In this work, the powder diffraction data were measured using a Bruker D8 diffractometer operating in transmission mode with automatic sample changer, monochromatic Cu radiation, LynxEye position-sensitive detector and a Bruker D5000 Diffractometer operating in capillary mode, monochromatic Cu radiation, Braun position-sensitive detector.

2.4 Rietveld Analysis

Rietveld analysis, invented by Hugo M. Rietveld, is an advanced diffraction analysis technique with whole pattern fitting refinement [4]**.** This is now widely accepted to be an exceptionally valuable method for structural analysis of many classes of crystalline materials not available as single crystals. Using this software accurate quantitative information about the sample can be obtained including unit cell parameters, the atomic positions, site occupancy factors, and thermal motions. The Rietveld refinement process has the advantage, over other quantitative methods that no standards are required and results accurate to within ±1% can be obtained in favourable cases.

In this refinement process, the parameters in the model are adjusted using a least-squares method until the observed diffraction pattern achieves a best fit. This process minimizes the residual (S_y) in the equation 2.2:

$$S_y = \sum_i w_i(y_i(obs) - y_i(calc))^2 \qquad (2.2)$$

where

$w_i = 1/y_i(obs)$,

$y_i(obs)$ = observed intensity at the i^{th} step,

$y_i(calc)$ = calculated intensity at the i^{th} step, and the sum is overall data points [5].

Peak intensity

Peak intensities are determined by positions of atoms in the unit cell. The calculated intensity is a combination of factors shown in equation 2.3.

$$y_{i(calc)} = S \sum_j L_{(hkl)} |F_{(hkl)}|^2 \emptyset_i (2\theta_i - 2\theta_k) P_{(hkl)} A + y_{bi} \qquad (2.3)$$

Where **S** is the scale factor,

$\boldsymbol{L_{(hkl)}}$ contains the Lorentz, polarization and multiplicity factors,

Φ_i is the reflection profile function,

$\mathbf{2\theta_i}$ is 2θ position of the i^{th} profile point in the diffraction pattern,

$\mathbf{2\theta_k}$ is the calculated 2θ position of the k^{th} reflection,

$\boldsymbol{P_{(hkl)}}$ is the preferred orientation,

A is the sample absorption factor,

$\boldsymbol{F_{(hkl)}}$ is the structure factor, and

$\boldsymbol{y_{bi}}$ is background intensity at the i^{th} step.

Background

Background can be caused by absorption, amorphous phases of samples or instrumental factors, experimental factors including sample holder. Background is described by geometric functions that best fit the background, typically a polynomial function such as Chebyschev or other equations.

Peak profile Functions

Peak shapes can be described by different profile functions such as Gaussian, Lorentzian, Cauchy, Pearson VII, etc. The convolution of a Gaussian and a Lorentzian give pseudo-Voigt function which is used in practice for refining parameters of width and intensity of a peak shape [6].

It is essential to choose the correct starting model to determine accurate crystal structures of the phases present in an observed diffraction pattern. When the calculated diffraction pattern has a good fit with the observed one, the difference line will be close to a straight line. Other factors measuring the quality of the Rietveld refinement are 'R-values' including pattern (R_p) and weighted pattern (R_{wp}). They show how good the fit is and the effects of changing parameters in the model on the fit. The methods for calculating them are shown in equations (2.4) and (2.5):

$$R_p = 100\sqrt{\frac{\sum|y_i(obs) - y_i(calc)|}{\sum y_i(obs)}} \qquad (2.4)$$

$$R_{wp} = 100\sqrt{\frac{\sum w_i[y_i(obs) - y_i(calc)]^2}{\sum w_i[y_i(obs)]^2}} \qquad (2.5)$$

The R_{wp} factor is the more valuable as its absolute value does not depend on the absolute value of the intensities. With a high background it is better to look at the R_{wp} background subtracted.

The best possible R-value for a data set is called expected pattern factor (R_{exp}) which is expressed in equation 2.6.

$$R_{exp} = 100\sqrt{\frac{N - P - C}{\sum w_i[y_i(obs)]^2}} \qquad (2.6)$$

where N = the number of observables,

P = the number of refined parameters,

C = the number of constraints used.

The R_{exp} is the minimum R_{wp} value reachable using a certain number of refineable parameters. R_{exp} indicates the quality of data being used.

A further statistical measure is defined from the above values (equation 2.7):

$$\chi^2 = [\frac{R_{wp}}{R_{exp}}]^2 \qquad (2.7)$$

This is the final value used to describe the quality of fit with desirable value approaching to 1. This is an important value because it contains the number of refinable parameters use to process the refinement. Using a large number of refined parameters can enhance the fit of the observed data. However, utilizing parameters with low data qualities can lead to model inaccuracies.

2.4.1 Quantitative Phase Analysis (QPA)

Rietveld refinement can also give a very accurate estimate of relative weight fraction of each phase for a mixture of some phases. In multiphase refinement, quantitative phase analysis (QPA) bases on equation 2.8.

$$W_p = \frac{S_p(ZMV)_p}{\sum_i^n S_i(ZNV)_i} \qquad (2.8)$$

where W_p is the relative weight fraction of phase p in a mixture of n phases,

S is the Rietveld scale factor

Z is the number of formula units per unit cell

M is the mass of the formula unit, and

V is the unit cell volume (Å) [2].

In this work in most cases, the lattice parameters and thermal parameters of known phases were refined and reported. When necessary, atomic positions and occupancies were also refined. The estimated weight percentages and standard errors for reaction products were reported by Topas and were converted into mole percent values when it is necessary. Phases with proportions below 5 wt% were generally excluded from refinements unless the diffraction patterns provided clear evidence for their presence.

2.5 Temperature Programmed Desorption with Mass Spectrometry (TPD–MS)

Temperature programmed desorption involves heating a sample while gaseous desorption products are monitored. A controlled rate of heat under a flowing

atmosphere is used for heating the sample whilst the gaseous desorption products are detected by a mass spectrometer (TPD–MS).

In this study, TPD experiments were conducted using a TPD apparatus under a flowing argon atmosphere coupled to a quadrupole mass spectrometer (HPR-20, Hiden Analytical). The schematic of this apparatus is illustrated in ***figure 2.4***.

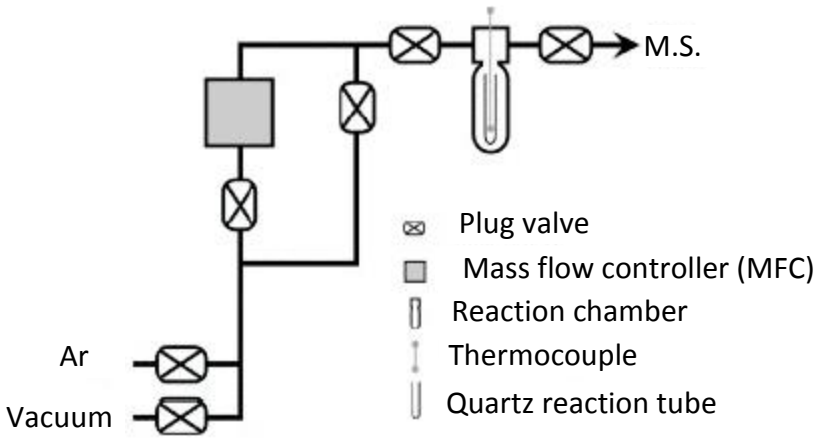

Figure 2.4 *Schematic diagram of the TPD–MS apparatus [7].*

Sample Preparation for Temperature Programmed Desorption

The sample was weighed (≈ 0.1 g) and held in a quartz reaction tube (7 mm O/D, 4 mm I/D) inside an argon-filled glove box and sealed within the reaction chamber.

The sealed reaction chamber was then transferred to the TPD apparatus, protecting the sample from the effect of the atmosphere. A barrel heater was placed around the reaction chamber and was controlled by a thermocouple contacting with the sample. Endothermic and exothermic events from the sample were visible in the temperature trace. The argon carrier gas was regulated by a mass flow controller (Hastings 200 series, Teledyne) at a constant flow of 100 ml min^{-1}. The amounts of gaseous desorption

products from the sample were measured using a quadrupole mass spectrometer with a secondary electron multiplier (SEM).

In this study, samples were heated at 2°C/minute to 350–400°C and held at that temperature for 2 hours before cooling.

2.6 Hydrogenation

Hydrogenation is used to test an ability of a sample to be hydrogenated by high-pressure (HP) rig reactor which can be heated up to 640°C under 100 bar hydrogen.

A sample for hydrogenation reaction was prepared in a similar way to that for TPD–MS. The prepared sample was loaded into a quartz reaction tube (7 mm O/D, 4 mm I/D) and then placed into the HP rig reactor. The reactor was then sealed using a torque wrench before being taken out of the glove box.

The reactor was then placed into a vessel furnace and connected to an argon-filled manifold system. The system was evacuated and purged with a low pressure of hydrogen. After leaks in the whole system have been checked carefully by a hydrogen detector, hydrogen was flowed and set at 90 bar. Desired temperature and time were then set using a furnace program. When the reaction completed, the system was vented hydrogen before being evacuated and purged with argon. The sample reactor was then removed from the system and placed back inside the glove box.

2.7 Gravimetric Analysis (IGA)

The Intelligent Gravimetric Analyser (IGA), Hiden Isochema, is a gravimetric system which provides the accurate measurement of sample mass under different temperatures (-196 to 500°C) and pressures (10 mbar to 20 bar). The IGA is capable high degree of stability for both temperature and pressure over extended time periods (days/weeks) along with low balance drift over time allows for the direct measurement of hydrogen uptake and release of materials with slow kinetics.

The schematic of the IGA is shown in ***figure 2.5***, and works by measuring the displacement of balance head **(a)** as the mass of loading a sample **(d)** changes as a function of time, pressure and/or temperature. The sample is connected to the balance head by a tungsten wire hang-down **(b)** and counter balanced by counterweight **(c)**, all the balance components are housed within a stainless steel reactor, that can be opened to allow samples to be changed. Thermal analysis can be performed by changing the temperature using furnace **(e)** in conjunction with a platinum resistance thermometer (PRT) located next to the sample. The pressure (and atmosphere) around the sample can be changed through stepper motors **(f)** that open and close by small amounts to regulate the flow of gas in and out of the reactor, which contains a pressure transducer to record (and feedback to the stepper motors to regulate pressure).

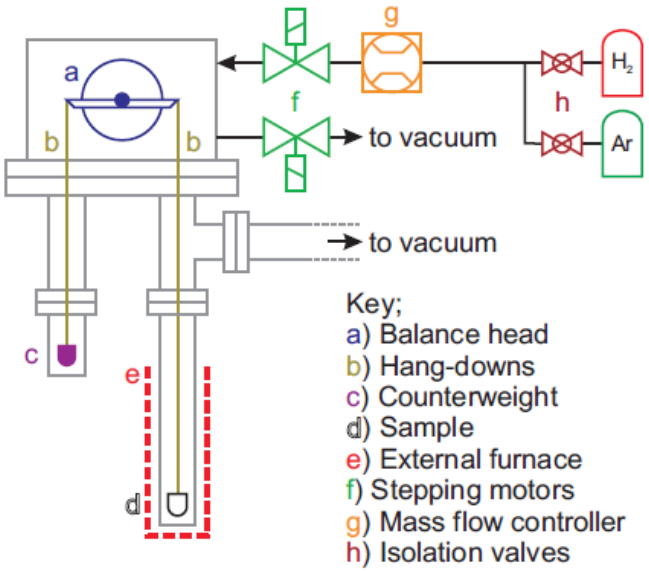

Figure 2.5 *Schematic diagram of an IGA [8]*

Inert sample transfer was achieved by loading the sample (~ 100mg) into a pre-weighed stainless steel sample holder in an argon-filled glove box, and sealing in inside an airtight stainless steel transfer tube. The transfer tube was then loaded onto a Perspex dry loaded (Hiden Isochema) where argon was cycled between 1050 and 1500 mbar 500 times through the IGA gas control system (***figure 2.5***) to displace air with argon. The cap of the transfer tube was then removed allowing the sample to be loaded onto the balance hang down, and the reactor sealed.

The IGA can be used in several modes, **Isothermal mode**: measuring the change in mass at a fixed temperature whilst varying pressure, **thermogravimetric mode**: measuring the dynamic change in mass as a function of temperature at a constant pressure (or flow) and **kinetics mode**: where a constant pressure and temperature are maintained and the change in mass is observed as a function of time (multiple measurements of this nature are combined in isothermal mode).

In this work measurements were performed in kinetic mode, where the desired pressure set and maintained before the sample was heated (at 2°C/min) to the desired temperature and the change in sample mass was recorded over time.

As the decomposition and absorption measurements are performed at a constant pressure and temperature, it is possible to ignore the influence buoyancy on the mass as the density of gas will remain constant during the bulk of the measurements.

2.8 Volumetric Analysis using Sieverts' method (HTP)

Volumetric measurements were performed based on the Sieverts' method using a Hiden Isochema HTP. The HTP is able to operate accurately from -196 to 500°C and from dynamic vacuum to 200 bar.

The Sieverts' method is an indirect method of determining uptake or release of gas from a sample, based on the relationship between pressure and moles of gas, where by the change in pressure is measured as a function of time at a constant temperature. Whereby a release of gas is observed as an increase in pressure and an uptake observed as a decrease in pressure.

A schematic of the internal pipe work of the HTP is shown in ***figure 2.6***. Where the sample, in the form of a powder, is loaded in a gold coated sample holder and sealed into the reactor **(a)**. The pressure within the system is changed and controlled via a series of pneumatically actuated diaphragm valves (PCV*X*) and mass flow controllers (FCV*X*). There are two known volumes within the system, a **dose volume (b)** consisting of the pipework between valves PCV1, PCV2, PCV3, PCV5 and PCV4 and the **reactor**

volume (a), containing the sample reactor and the interconnecting pipework between PCV4, PCV6 and PCV7. The whole of the dose volume is located within the body of the system and temperature controlled to a constant 35°C, there reactor volume, however, has thermal control around the sample reactor (-196 to 500°C) and temperature gradients within the interconnecting pipework. In the HTP pressure is always measured within the dose volume, and only in the reactor volume when PCV4 is open.

Isothermal measurements are performed by setting an initial pressure in the dose volume through a combination of PCV1 (for H_2), PCV3 (for He) or PCV5 (vacuum) whilst PCV4 remains closed. Once the initial pressure ($P_{initial}$) has stabilised and been recorded PCV4 is opened and the pressure between the dose and reactor volumes allowed to reach equilibrium. Once an equilibrium pressure is reached, PCV4 is closed and final pressure (P_{final}) is recorded after a stabilisation period. The process is then repeated with a new initial pressure to generate an isotherm. The amount of uptake (mmol) is determined using the change in pressure (P_{final}-$P_{initial}$) within a real gas equation with, as all measurements were performed at elevated temperatures and relatively modest pressures (<50 bar) meaning uncertainties arising from the compressibility of hydrogen will have little effect these measurements. As this method relates the change of pressure to the amount of gas uptake or release it cannot distinguish between different gasses, therefore it is not possible to distinguish if the gas released is H_2, N_2 or NH_3, however, and any uptake is assumed to be solely due to H_2.

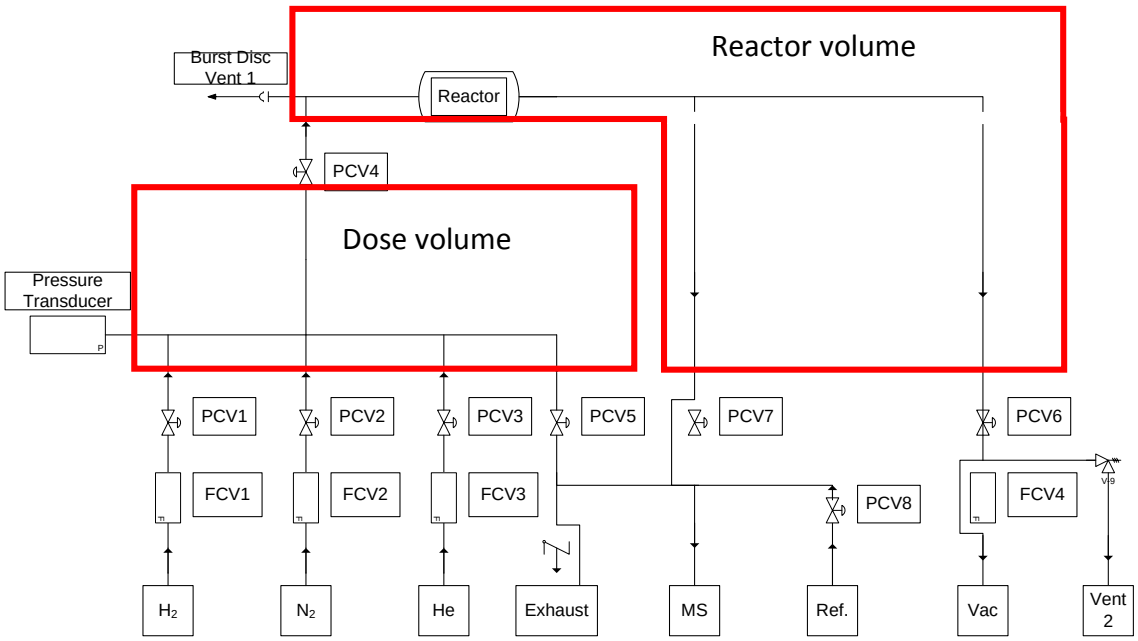

Figure 2.6 *Schematic of the Valves and pipe work on the Hiden Isochema HTPS-2 [9]*

Determination of the dose and reactor volumes of the system performed by dosing He (50 bar) into the system in using the method above, with and without the addition of standard displacement volumes added to the reactor. The volume displaced by the samples is determined using He pycnometry, where 5 bar He is dosed from a starting vacuum, and the pressure difference between reactor with and without sample compared to determine the volume displaced.

In this work, a hydrided sample was inertly loaded using an attached argon purged glove box, a hydrogen pressure of 100 bar was then applied before heating (5°C/min) to 400 °C. A desorption isotherm was then performed to ascertain the equilibrium pressure for desorption and the amount of gas desorbed. Subsequent cycling measurements were performed as a series of isotherms at different temperatures.

It is important to note that this method has several limitations, and experimental artefacts that appear in the obtained results.

- As this is an indirect measure of uptake and release it is not possible to distinguish between different gas species (H_2, N_2, NH_3, *etc.*).

- Errors are compounded during isothermal measurements, as the same indirect measurements are repeatedly performed, meaning that any errors or uncertainties in the uptake are the sum of all the errors and uncertainties of all the previous points within the isotherm.

- The pressure measurement is only taken from the dose volume errors are generated during desorption isotherms at high temperature, as the hot gas flows from the reactor into the dose volume and slowly cools, giving a lower than 'expected' pressure, which the system wrongly converts to an apparent slight uptake.

This final artefact is observed only on desorption, and appears to show the material uptakes a small amount of hydrogen (<50 mmol) when observed as an isotherm, whilst the individual points (pressure against time) do not exhibit any uptake, and therefore any uptake observed during desorption can be ignored, unless commented upon specifically.

2.9 Raman

Raman spectroscopy is a common technique used to study vibrations in a system [10]. In a Raman experiment, a sample is irradiated by monochromatic light (from infrared to ultraviolet). The radiation may be absorbed or scattered or pass through the molecule. If the radiation scattered from the molecule is shifted by one vibrational unit of energy, it will be detected.

In Raman scattering, the molecule interacts with the light and the cloud of electrons round the nuclei is polarized to form a short-live state called virtual state. This is an unstable state and the electron relaxes and releases a photon of different energy and go back to vibrational state and producing Stokes scattering.

When an electron is excited and promotes from a vibrational state ($\nu = 1$) to a virtual state then relaxes back to ground vibrational state ($\nu = 0$), anti-Stokes scattering is generated.

If only the electron cloud is involved in the scattering, the energy difference between the photons is small. The scattering is regarded as elastic scattering and called Rayleigh scattering. This is the most common scattering.

In this work, Raman data were collected from a Renishaw InVia Raman microscope Ar ion laser at wavelengths of 488 nm and 633 nm (of 2400 and 1800 lines/mm, respectively). Samples were loaded in an Instec sample cell in an argon-filled glove box. The sample cell was then transferred to the microscope and was flowed by 1 bar argon gas during data collection.

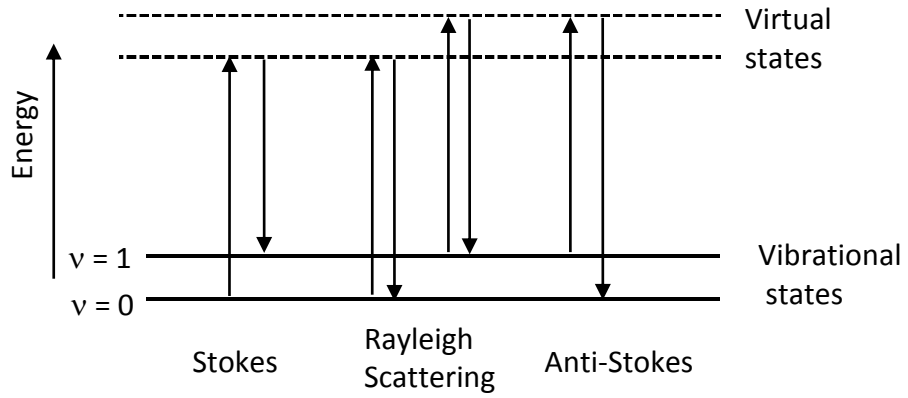

Figure 2.7 *Diagram of the Rayleigh and Raman scattering processes*

2.10 Scanning Electron Microscopy (SEM)

Scanning electron microscopy (SEM) is a popular technique used for studying the morphology (texture), crystalline structure, and the surface features of powder and solid samples. In SEM an electron beam from a suitable cathode filament (typically tungsten) is scanned across a sample's surface. When electrons in the sample are excited by the incident beam, secondary electrons, backscattered electrons could be produced and used to produce images of the sample. This technique can produce high resolution imagines of samples on a small scale which will be used to study desired properties of samples.

In this work the size and shape of particles in samples were investigated by a JOEL 6060 SEM fitted with an Oxford instrument Inca 300 EDS system.

References

[1] G. Burns and A. M. Glazer, Space Groups for Solid State Scientists, Academic Press, 1978.

[2] R. E. Dinnerbier and S. J. L. Billinge, *Powder Diffraction – Theory and Practice*, RSC Publishing, 2008.

[3] C. Hammond, *The Basics of Crystallography and Diffraction*, IUCr Monographs on Crystallography, Oxford University Press, 2nd ed., 2001.

[4] H. M. Rietveld, *J. Appl. Cryst.*, 1969, 2, 65–71.

[5] R. A. Young, *The Rietveld Method*, Oxford University Press, 1993.

[6] Topas technical reference manual. A. Coelho; Bruker AXS, 2005.

[7] P. A. Chater, P. A. Anderson, J. W. Prendergast, A. Walton, V. S. J. Mann, D. Book, W. I. F. David, S. R. Johnson, P. P. Edwards, *J. Alloys Comp.,* 2007, 446–447,350–354.

[8] P. A. Chater, Mixed Anion Complex Hydrides for Hydrogen Storage, PhD thesis, University of Birmingham, 2009.

[9] D. T. Reed, *An Investigation into the Synthesis and Characterisation of Metal Borohydrides for Hydrogen Storage*, PhD thesis, University of Birmingham, 2009.

[10] E. Smith, G. Dent, *Modern Raman Spectroscopy: A practical Approach*, John Wiley & Sons Ltd, 2005.

Chapter 3: xLiBH$_4$ + yLiNH$_2$ + zCoO

3.1. Introduction

$LiBH_4$–$LiNH_2$ system has been subject of much recent research as potential hydrogen storage and delivery materials. A mixture of $LiBH_4$ and $LiNH_2$ in a molar ratio of 1:2 was reported to release ≥ 10 wt% hydrogen from 250°C. The drawbacks of this system are an evolution of ammonia (2-3 mol%) and a lack of reversibility of the main product Li_3BN_2 [1-2].

A reduction in hydrogen release temperature and a depression in ammonia discharge were achieved by the presence of various transition metal catalysts of including Ni, Fe, Zn, Co, Pt, and Pd, or their chlorides or oxides [3–6].

Zhang *et al.* [6] reported that the addition of small amount of CoO could help to reduce the onset hydrogen desorption temperature of a $LiBH_4$–$2LiNH_2$ mixture to 100°C and more importantly, the majority of the hydrogen release occurred at the melting temperature of the product mixture obtained around 220°C.

The presence of the cobalt (II) oxide catalyst was also found to improve rehydrogenation of this system. The 0.05CoO sample after dehydrogenation absorbed approximately 1.1 wt% of hydrogen at 350°C and 110 bar while the catalyst-free sample absorbed about 0.2 wt% under the same conditions.

The reactions between $LiNH_2$ and $LiBH_4$ in various ratios have been studied by Anderson *et al*. [7] and Singer *et al.* [8] and the thermodynamic products were presented in ***figure 3.1***.

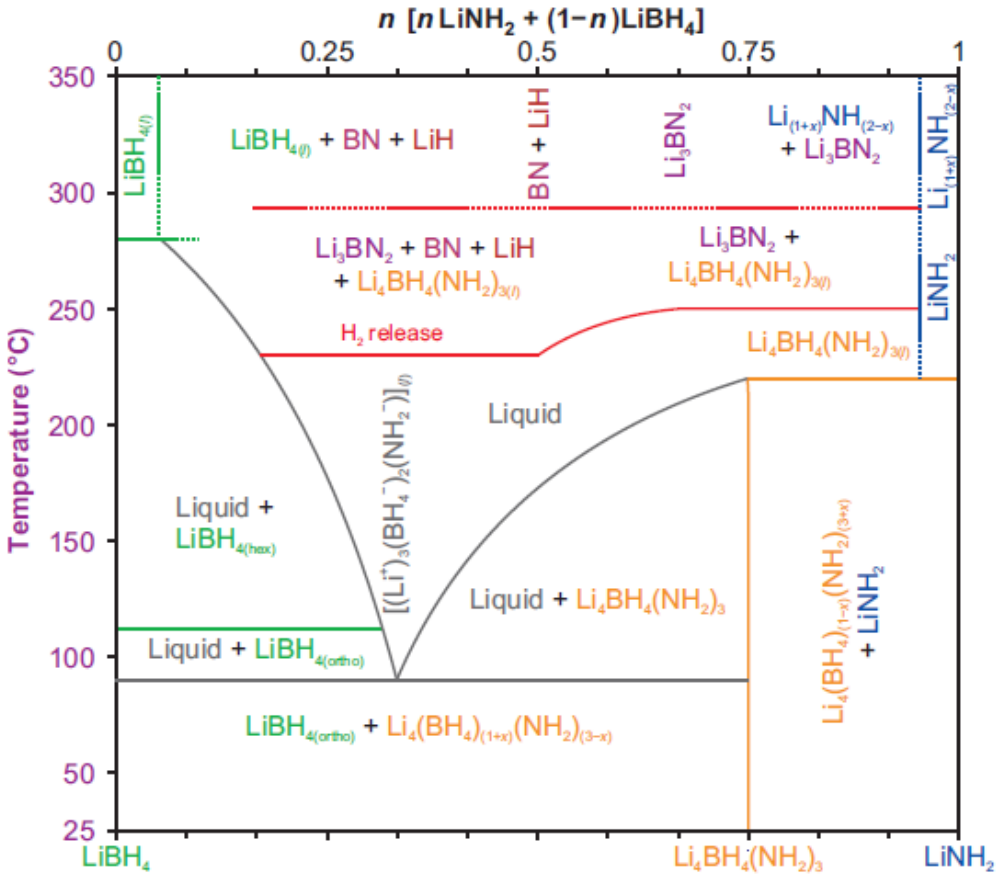

Figure 3.1 *Schematic phase diagram for the $nLiNH_2 + (1-n)LiBH_4$ system reported by Anderson et al. [7].*

It can be seen from ***figure 3.1*** that the melting point of borohydride-rich mixtures can be much lower than that of the $LiBH_4$–$2LiNH_2$ mixture. Therefore, the effects of a CoO catalyst on these mixtures were examined to see whether a lower temperature of hydrogen release and perhaps better absorption properties could be achieved.

In this work I have studied reactions of $LiBH_4$ with $LiNH_2$ at different stoichiometries with different amounts of CoO. The decomposition of mixtures and rehydrogenation properties of products were investigated. Effects of ball-milling were also examined in the hope of improving the reversibility of the system.

3.2. Experimental

Mixtures of lithium borohydride (Sigma-Aldrich, 95%), lithium amide (Sigma-Aldrich, 95%), and cobalt (II) oxide (Sigma-Aldrich, −325 mesh) were ground together in an argon-filled glove box. The samples were prepared in various ratios in quartz tubes and heated under flowing argon at temperatures up to 400°C for up to 12 hours.

Powder X-ray diffraction data were collected on a Bruker D8 Advance diffractometer in transmission geometry with a Cu-K_α (λ_1 = 1. 5406 Å) X-ray source and analysed using the Topas computer software (**section 2.4**).

Temperature-programmed desorption with mass spectrometry (TPD–MS) and Raman spectroscopy data were also collected and analysed. Particle size and morphology were studied using SEM. Rehydrogenation measurements were carried out as described in chapter 2.

3.3 $LiBH_4$–$2LiNH_2$–*a*CoO

A series of $LiBH_4$−$2LiNH_2$−*a*CoO mixtures (where *a* = 0, 0.01, 0.03, 0.05 and 0.1) were prepared and heated up to 400°C.

3.3.1 Powder X-ray diffraction

Reaction of $LiBH_4$ and $LiNH_2$ in a molar ratio of 1:2 at 350°C formed two polymorphs of Li_3BN_2 - tetragonal $I4_1/amd$ and monoclinic $P2_1/c$ along with a small amount of LiH. The $P2_1/c$ polymorph was the dominant phase with the $P2_1/c$:$I4_1/amd$ ratio ~ 2:1. A small amount of Li_2O, originating as an impurity in the $LiNH_2$ used, was also observed. The third known phase of Li_3BN_2 (tetragonal $P4_22_12$) was not obtained under the reaction conditions used. The products of the reaction of $LiBH_4$–$2LiNH_2$ at 350°C are shown in ***figure 3.2***.

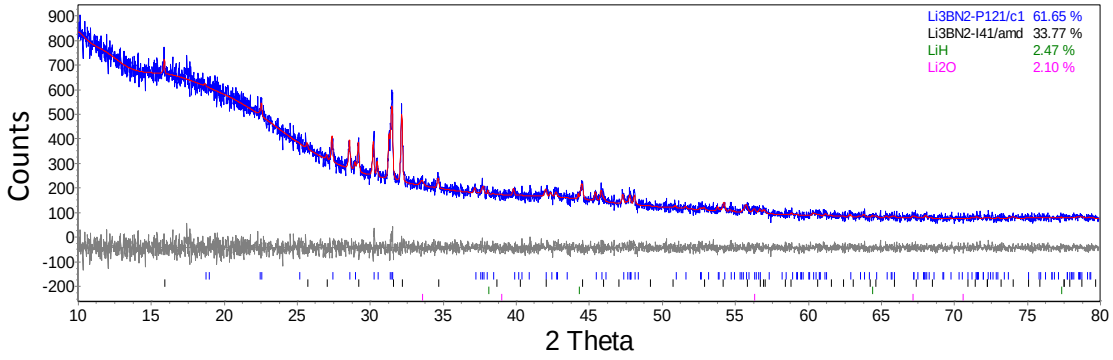

Figure 3.2 *Powder XRD pattern of the products of the reaction of $LiBH_4$–$2LiNH_2$ at 350℃ showing observed (blue), Rietveld fit (red) and difference (grey) plots. Peak positions for refined compounds are shown underneath.*

Lithium boron nitride is known to be formed *via* equation (3.1)

$$LiBH_4 + 2LiNH_2 \rightarrow Li_3BN_2 + 4H_2 \qquad (3.1)$$

LiH could be formed from reaction (3.2)

$$LiBH_4 + LiNH_2 \rightarrow 2LiH + BN + 2H_2 \qquad (3.2)$$

which is known to compete with reaction (3.1) [7]. The boron nitride product of reaction (3.2) is amorphous and therefore not visible in the XRD pattern. However, the high amorphous background in ***figure 3.2*** is consistent with the presence of amorphous BN.

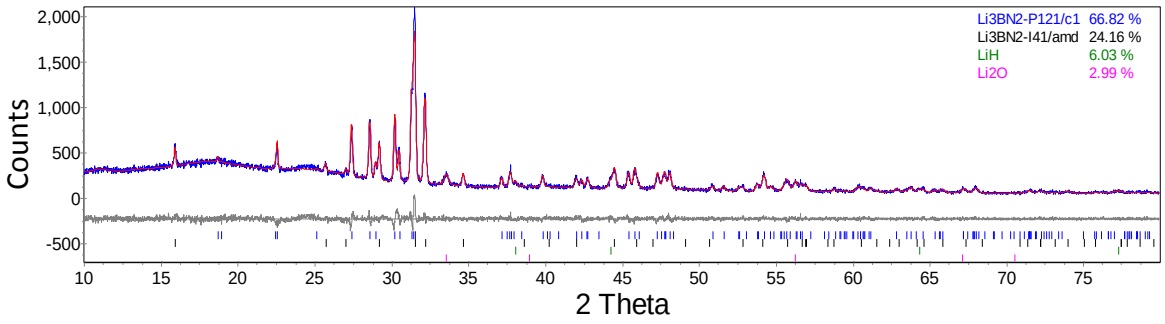

Figure 3.3 *Powder XRD pattern of the products of the reaction of $LiBH_4$–$2LiNH_2$ at 400 ℃ showing observed (blue), Rietveld fit (red) and difference (grey) plots. Peak positions for refined compounds are shown underneath.*

At the higher temperature of 400°C, the same products were obtained but the amount of Li_3BN_2 $P2_1/c$ increased while that of Li_3BN_2 $I4_1/amd$ decreased (***figure 3.3***).

These results are consistent with previous work of Anderson group [9-10] (***figure 3.4***), Pinkerton *et al.* [11] and Meisner *et al.* [12].

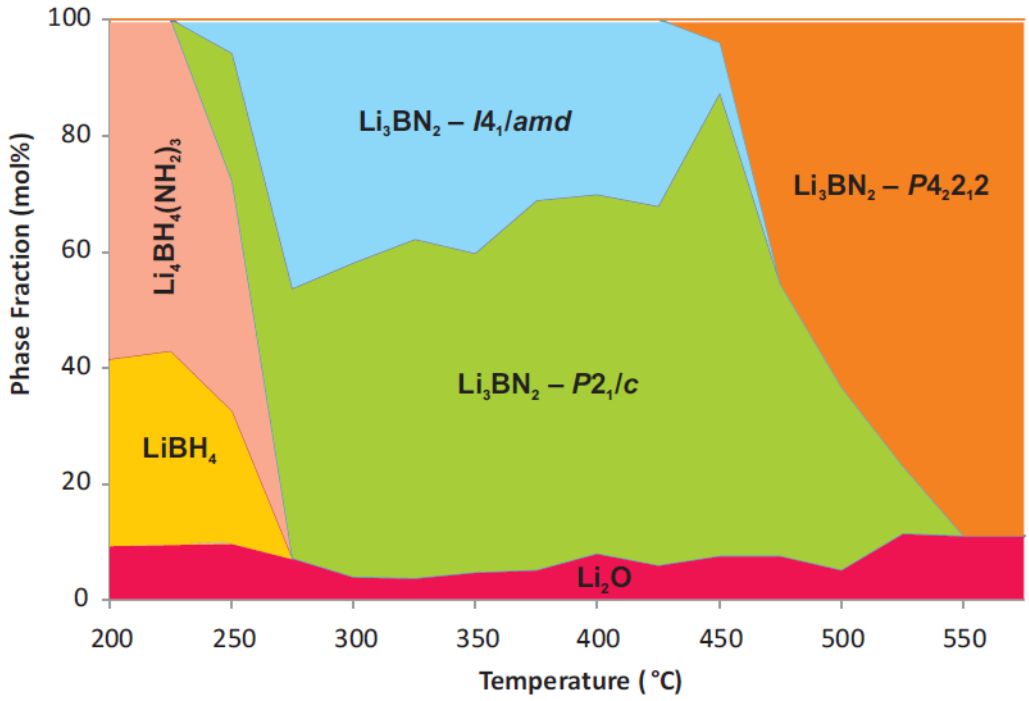

Figure 3.4 *Phase map of the products from reaction of $LiBH_4$–$2LiNH_2$ at different temperatures heated at 2 ℃/minute and held for 12 hours [9].*

With the addition of CoO, LiH was not observed in the reaction products. When a = 0.01, the main products after heating at 400°C were a mixture of two polymorphs of Li_3BN_2 $I4_1/amd$ and $P2_1/c$. In this case the favoured product was the $I4_1/amd$ polymorph. The products of reaction of $LiBH_4 + 2LiNH_2$ in a presence of CoO (a = 0.01) catalyst are shown in ***figure 3.5***.

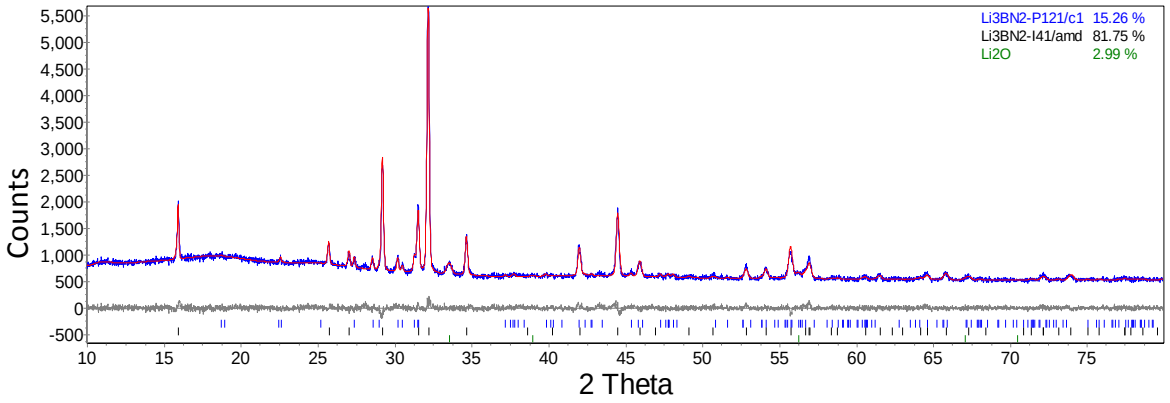

Figure 3.5 *Powder XRD pattern of the products of the reaction of $LiBH_4$–$2LiNH_2$–0.01CoO at 400℃ showing observed (blue), Rietveld fit (red) and difference (grey) plots. Peak positions for refined compounds are shown underneath.*

With the presence of more CoO ($a \geq 0.03$) only the tetragonal Li_3BN_2 $I4_1/amd$ was obtained (~98 wt%) alongside a small amount of Li_2O impurity (***figure 3.6***). Catalyst may favour the formation of the $I4_1/amd$ polymorph.

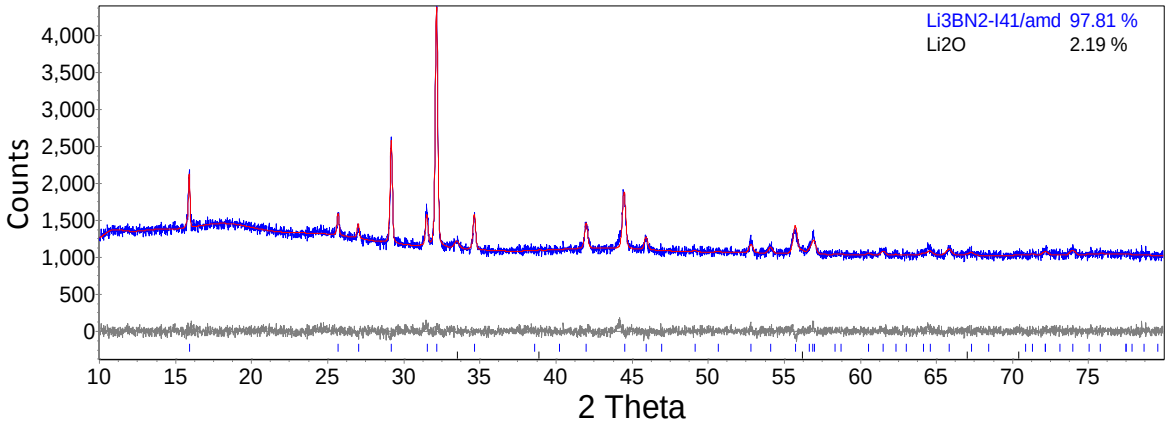

Figure 3.6 *Powder XRD pattern of the products of the reaction of $LiBH_4$–$2LiNH_2$–0.03CoO at 400℃ showing observed (blue), Rietveld fit (red) and difference (grey) plots. Peak positions for refined compounds are shown underneath.*

Powder XRD patterns of samples of $LiBH_4$–$2LiNH_2$–aCoO after heating at 400°C are shown in ***figure 3.7***. It can be seen that the proportion of catalyst has affected the products of reaction between $LiBH_4$ and $LiNH_2$. Samples with more CoO produced more of the $I4_1/amd$ polymorph.

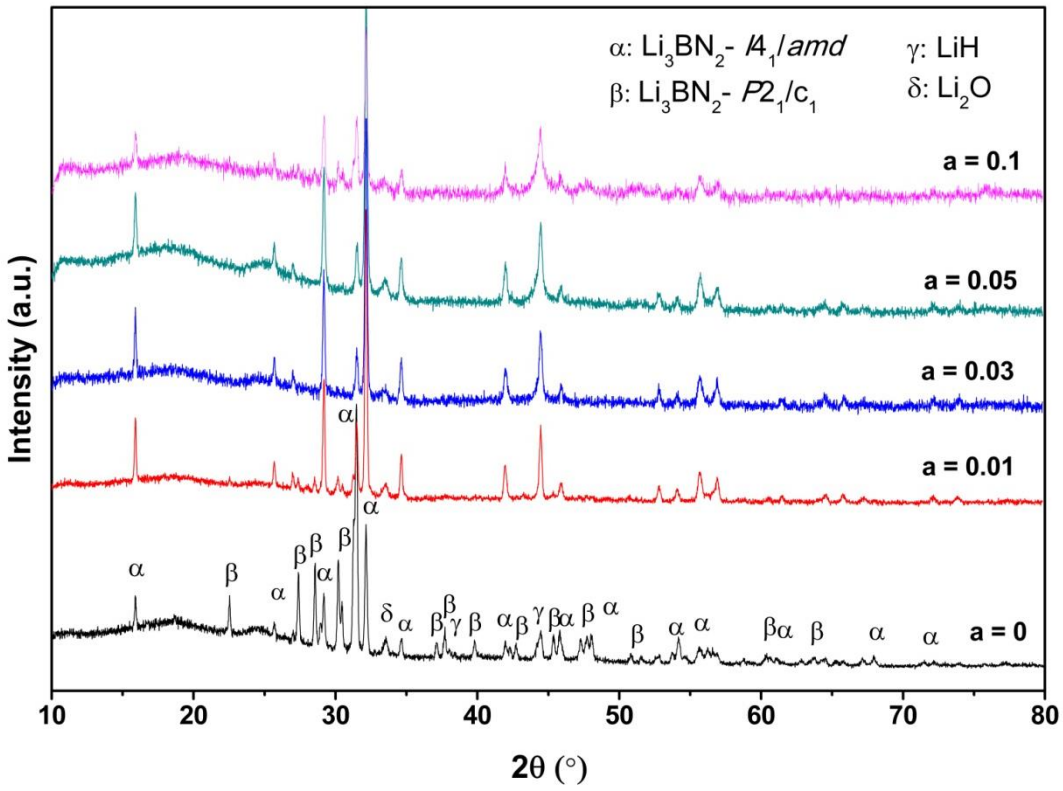

Figure 3.7 *Powder XRD pattern of the products of the reaction of $LiBH_4$–$2LiNH_2$–aCoO at 400℃ where a = 0, 0.01, 0.03, 0.05 and 0.1.*

The products of samples with different amounts of CoO at 400°C obtained from powder X-ray diffraction were analysed and are presented in ***Figure 3.8***.

In all the reactions studied, peaks showing the presence of CoO have not been observed in XRD patterns. Using data from XAFS, Zhang *et al.* concluded CoO was converted into Co acted as a catalyst for the formation of B–N bonds [8].

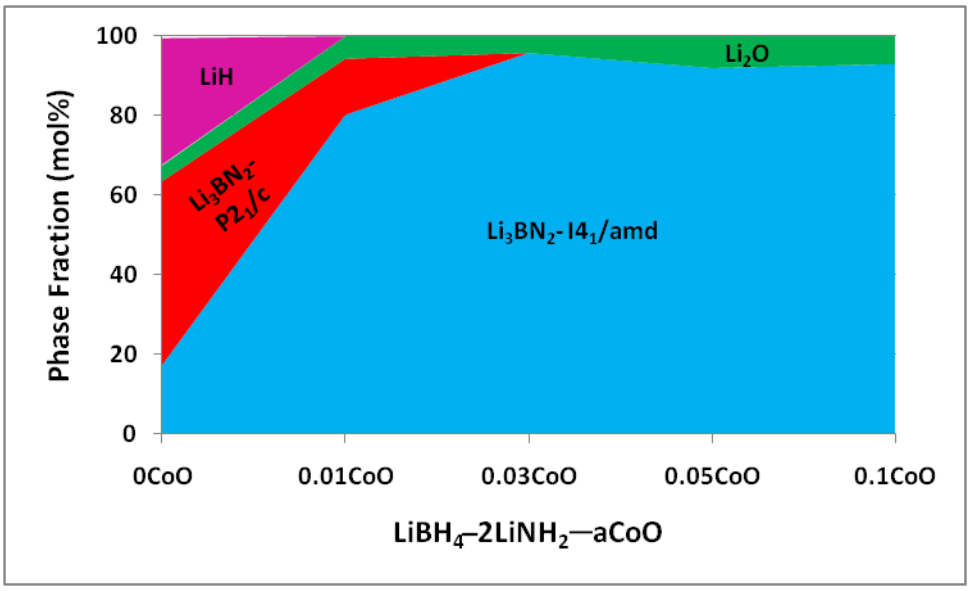

Figure 3.8 *Phase map of the products of the reaction of $LiBH_4$–$2LiNH_2$–aCoO heated at 400℃ in the TPD–MS apparatus, where a = 0, 0.01, 0.03, 0.05 and 0.1.*

3.3.2 Raman

The Raman spectra of the three polymorphs of Li_3BN_2 ($I4_1$/amd, $P4_22_12$, and $P2_1$/c,) were reported to have peaks at wave numbers of 1050.5 cm^{-1}, 1054.5 cm^{-1}, and 1067.0 cm^{-1}, respectively, caused by B–N bond lengths of $I4_1$/amd > $P4_22_12$ > $P2_1$/c [9].

In this work, the Raman spectra of catalyst-free and 0.05CoO samples after heating at 400°C in the TPD–MS were obtained using the Renishaw InVia Raman microscope Ar ion laser at wavelengths of 488 nm and 633 nm. Peaks from the $I4_1$/amd and $P2_1$/c polymorphs were observed in the Raman spectra of catalyst-free and 0.01CoO samples, while only the peak from the $I4_1$/amd polymorph was seen in samples containing higher amounts of CoO (***figure 3.9***)

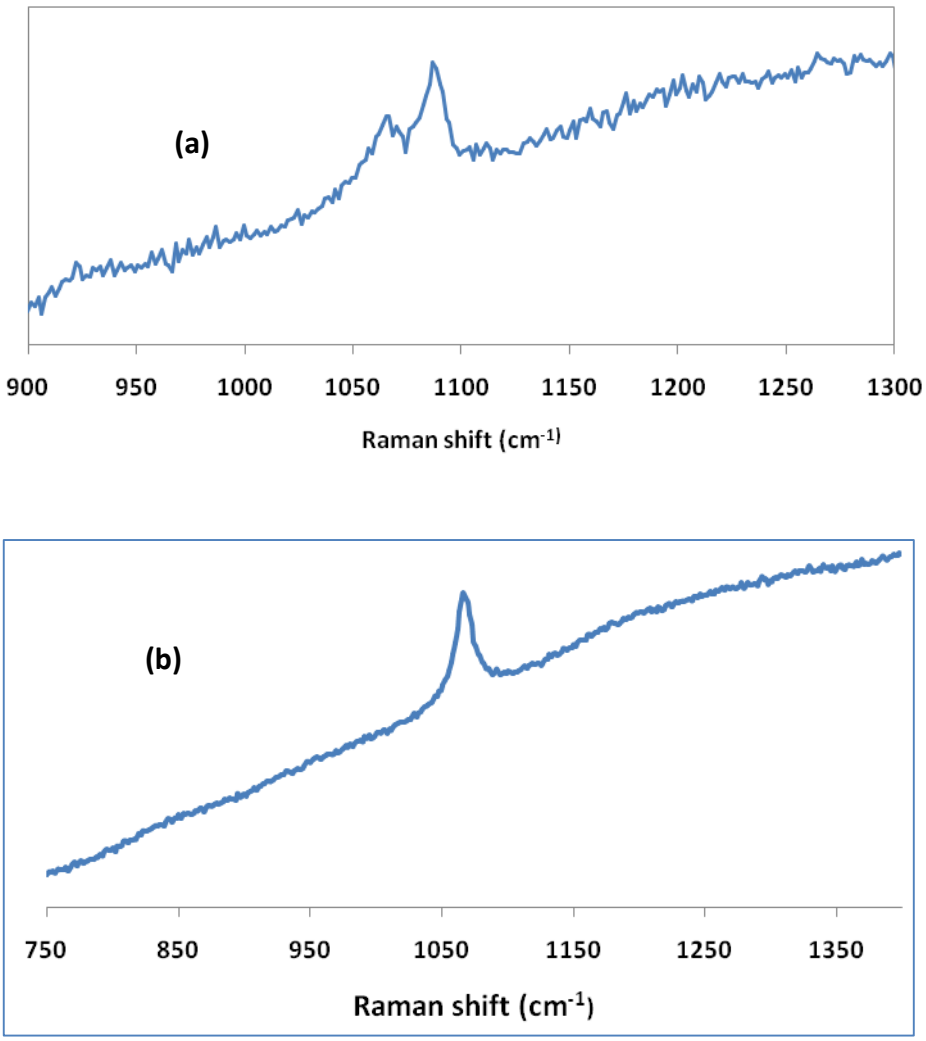

Figure 3.9 *The Raman spectra of catalyst-free* ***(a)*** *and 0.05CoO* ***(b)*** *samples after heating at 400℃ in the TPD–MS.*

3.3.3 Temperature-Programmed Desorption – Mass Spectrometry (TPD-MS)

In this section the hydrogen desorption properties of mixtures of $LiBH_4$–$2LiNH_2$–aCoO were tested. The samples were all heated with the same heating rate of 2°C/min to 350°C–400°C and held for 2 hours.

In catalyst-free samples hydrogen release started from 240°C and peaked around 290°C, which is in agreement with values in the literature [9–10]. A small amount of ammonia was also observed. The gases released from the reaction of $LiBH_4$–$2LiNH_2$ are shown in ***figure 3.10.***

In theory, the amount of hydrogen released could be up to 11.9 wt% (equation 3.1). In practice, the amount of hydrogen calculated based on TPD–MS data showed a much lower value of ~2.3wt%. TPD–MS data for $LiBH_4$–$2LiNH_2$ on heating to 400°C are shown in ***figure 3.10***.

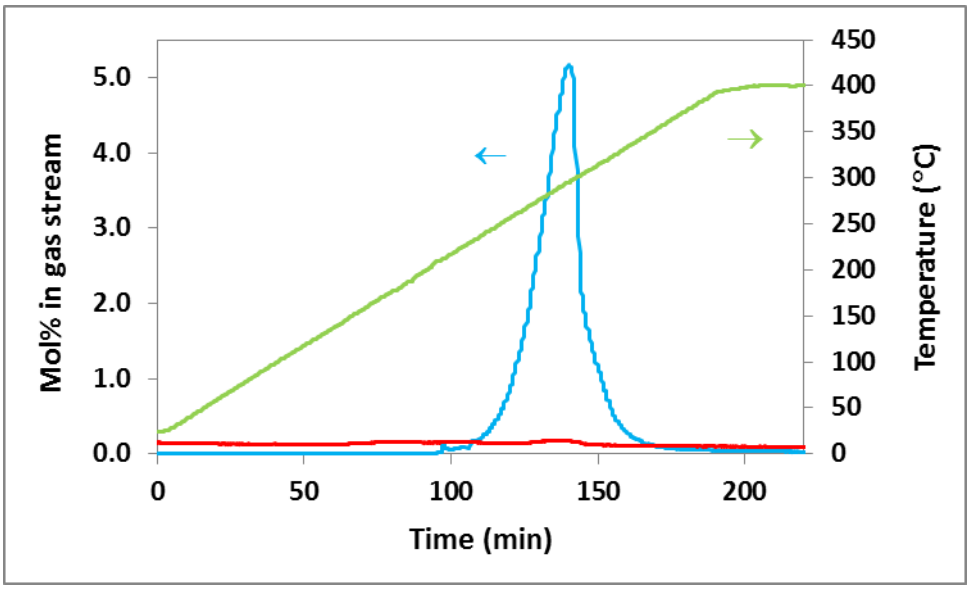

Figure 3.10 *TPD–MS traces of the reaction of $LiBH_4$–$2LiNH_2$ heated at 2℃/minute to 400℃, showing hydrogen (blue), ammonia (red) and temperature (green).*

On addition of cobalt (II) oxide catalyst, a remarkable reduction in the temperature of hydrogen emission was achieved. With a small amount of CoO (a = 0.01), a small hydrogen evolution was observed around 160°C. The main peak of hydrogen release

was at around 240°C followed by a smaller peak around 290°C. With thermal desorption data shown in ***figure 3.11***, it can be seen that decomposition occurred *via* multiple steps. The second peak is in the same place as the peak in the catalyst-free sample. This suggests that in most of the sample there is a different reaction pathway, but some of the sample remains unaffected.

The total amount of hydrogen desorbed was ~ 3.2 wt%, which is higher than that without the addition of CoO. Moreover, there was a suppression of ammonia evolution. Interestingly, the ammonia release is absent from the main peak, but still present in the higher temperature one, so again consistent with the suggestion that this comes from parts of the sample unaffected by CoO. Clearly, the presence of CoO has a significant effect mechanism of reaction of $LiBH_4 + 2LiNH_2$.

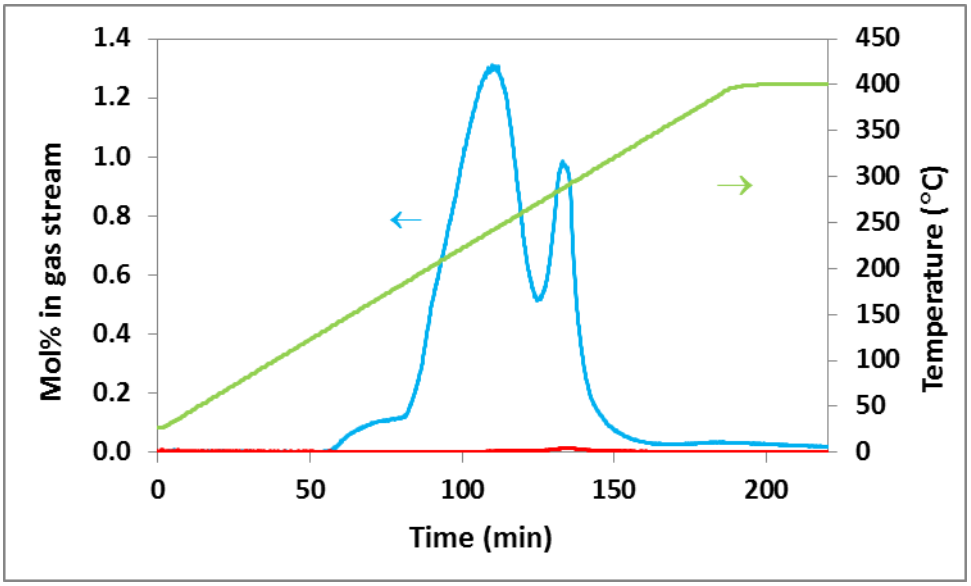

Figure 3.11 *TPD–MS trace of the reaction of $LiBH_4$–$2LiNH_2$–0.01CoO heated at 2 ℃/minute to 400 ℃, showing hydrogen (blue), ammonia (red) and temperature (green).*

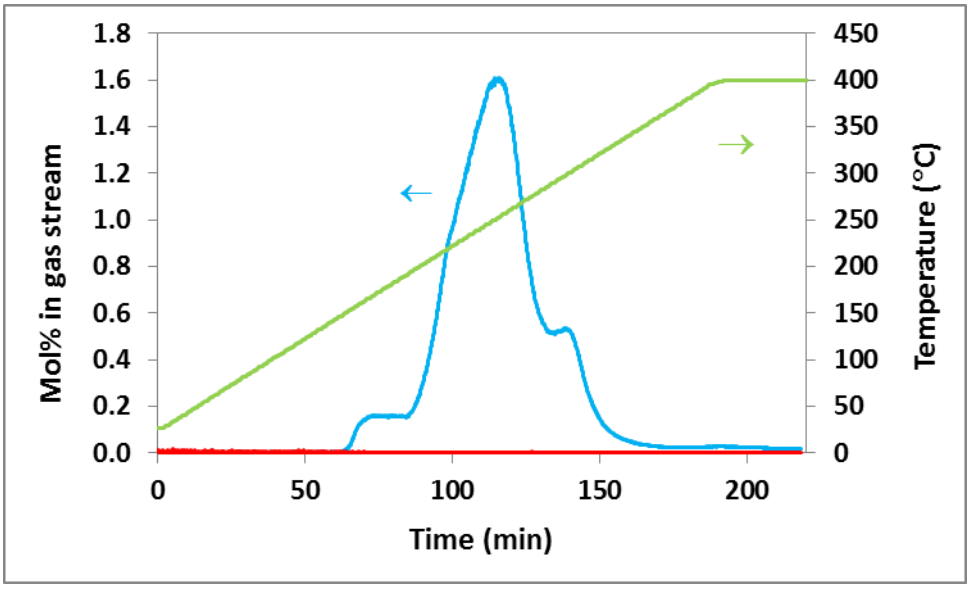

Figure 3.12 *TPD–MS traces of the reaction of $LiBH_4$–$2LiNH_2$–0.03CoO heated at 2 ℃/minute to 400 ℃, showing hydrogen (blue), ammonia (red) and temperature (green).*

With a greater portion of CoO (*a* = 0.03), slightly more hydrogen was released at the first step around 160°C and most hydrogen was desorbed by 270°C. There was also a small peak of hydrogen release at 290°C (***figure 3.12***). The amount of ammonia released was further reduced and was below the detection limit of our apparatus for this and greater proportions of catalyst. The amount of hydrogen release was ~ 3.7wt%.

A direct comparison of the hydrogen desorption of $LiBH_4$–$2LiNH_2$–*a*CoO samples studied using TPD–MS is shown in ***figure 3.13***. It can be seen clearly that CoO catalyst has a remarkable effect on dehydrogenation of the system. These traces show that the shoulders often correspond to the peaks observed with a different amount of catalyst. This may indicate inhomogeneities in the distribution of catalyst, which is possible as the samples were mixed by hand.

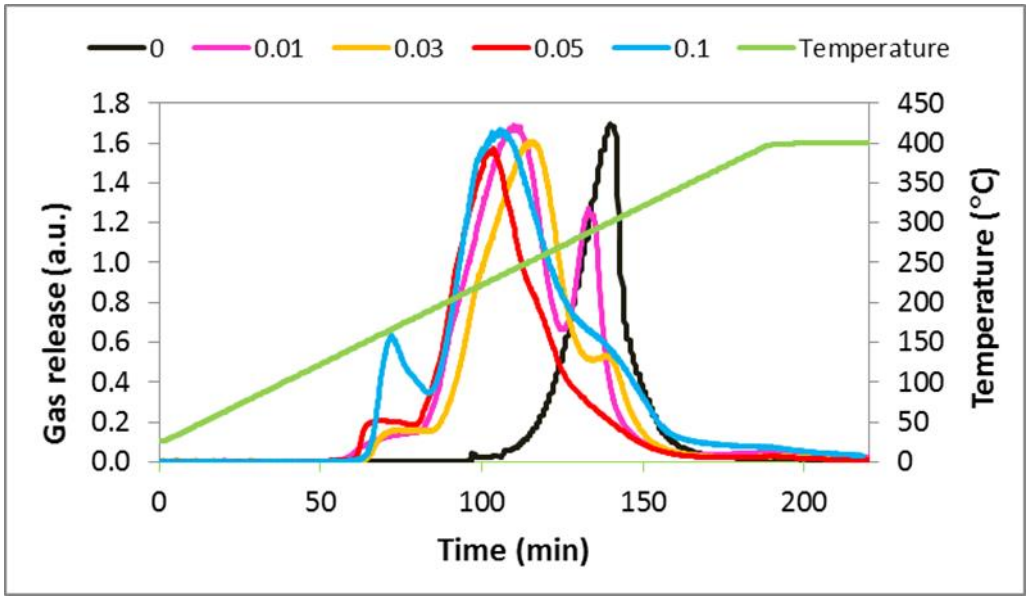

Figure 3.13 *TPD–MS hydrogen traces of the reactions of $LiBH_4$–$2LiNH_2$–$aCoO$ heated at 2 ℃/minute to 400 ℃.*

The samples with CoO have a much lower temperature of hydrogen release. Decomposition of products obtained during dehydrogenation was also changed showing a slight difference in traces of hydrogen liberation. Possibly there are at least 4 hydrogen release pathways. The large increase in the lowest temperature one with CoO content suggests that it may involve CoO as a reagent rather than a catalyst in the strictest sense.

More hydrogen was release at the main peak around 240°C while the amount of catalyst increased. With a = 0.05, the hydrogen release peaked around 240°C, and the third step was reduced to a shoulder on the main peak. About 4.0 wt% H_2 released. When the amount of CoO was increased to a = 0.1 the temperature of hydrogen release was not lowered further. However, the main dehydrogenation peak was broader and a tail was observed in the hydrogen release above 340°C.

A slightly greater amount of H_2 was obtained (~4.2 wt%). Taking all things into consideration *a* = 0.05 was identified as the optimum amount of cobalt (II) oxide of the ratios studied. Consequently, this proportion of catalyst was chosen to test the rehydrogenation properties of samples in the next section.

3.3.4 Rehydrogenation

The effects of CoO on the rehydrogenation properties of the mixture of $LiBH_4$ and $2LiNH_2$ were examined under 90 bar pressure of hydrogen. The samples used were the products of desorption reactions at 350–400°C in the absence and presence of 0.05CoO. The masses of samples before and after the rehydrogenation reaction were recorded to determine any weight gain.

The phases present in the sample without catalyst after heating under hydrogen gas flow for 24 hours remained unchanged. In the presence of CoO, after rehydrogenation similar results were obtained for samples heated both to 350°C and 400°C, with no observation of hydrided compounds. No change in mass of sample after rehydrogenation was achieved, suggesting no hydrogen absorption occurred under the conditions studied. However, the $P2_1/c$ phase of Li_3BN_2, which was absent before reaction, was observed. This result is different from those in a previous study of samples without CoO catalyst, which showed no observation of the $P2_1/c$ phase [9]. Trace hydrogen absorption in the CoO-containing sample might effect a transformation from Li_3BN_2-$I4_1/amd$ to Li_3BN_2-$P2_1/c$, though the effect of pressure may be more likely. Powder X-ray diffraction patterns of products obtained after hydrogenation of sample heated to 400°C are shown in ***figure 3.14***.

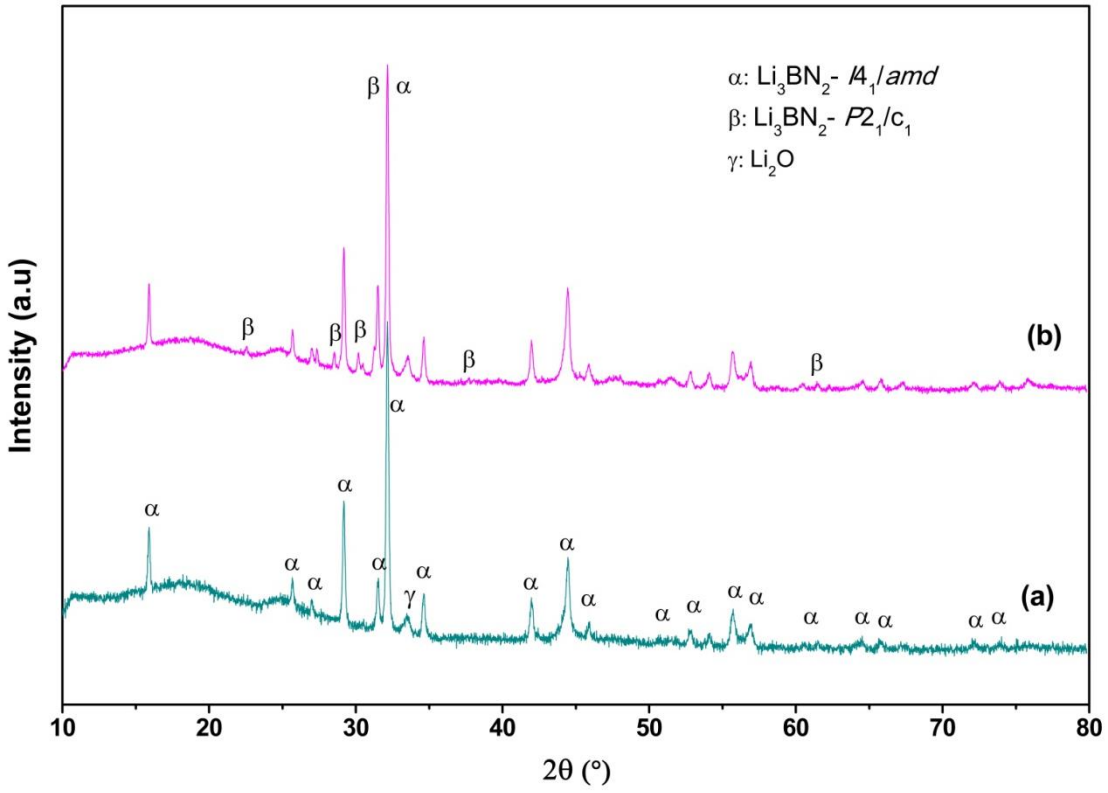

Figure 3.14 *Powder XRD patterns of the products of $LiBH_4$–$2LiNH_2$–0.05CoO heated at 400℃ before (a) and after (b) hydrogenation at 300℃ for 24 hours.*

The transformation from Li_3BN_2-*I*4_1/*amd* to the *P*2_1/c polymorph under pressure may be caused by a difference in densities of the two polymorphs which are shown in **table 3.1**.

Table 3.1 Densities of Li_3BN_2 $I4_1/amd$ and $P2_1/c$

	Density ρ (g/cm^3)	
	$I4_1/amd$	**$P2_1/c$**
Pinkerton *et al.* [11]	1.7488(1)	1.7371
0.05CoO	1.7632(1)	-
0.05CoO after hydrogenation	1.7632(1)	1.7429(7)

In order to examine whether particle size can improve the rehydrogenation properties of the dehydrogenated products obtained, the sample with catalyst was ball-milled for 10 hours before hydrogenation reaction. After ball-milling the width of the peaks had increased indicating that the particle size had decreased.

In the products of the ball-milled sample after rehydrogenation Li_3BN_2 – $I4_1/amd$ phase but no $P2_1/c$ phase was observed. A small amount of Li_2O and hexagonal BN were also observed. No hydrided product can be seen in the XRD pattern. Therefore, it can be concluded that reducing the size of the particles did not help to improve the reversibility of lithium boron nitride under conditions studied. The high background of the powder XRD patterns is caused by the amount of cobalt present (***figure 3.15***).

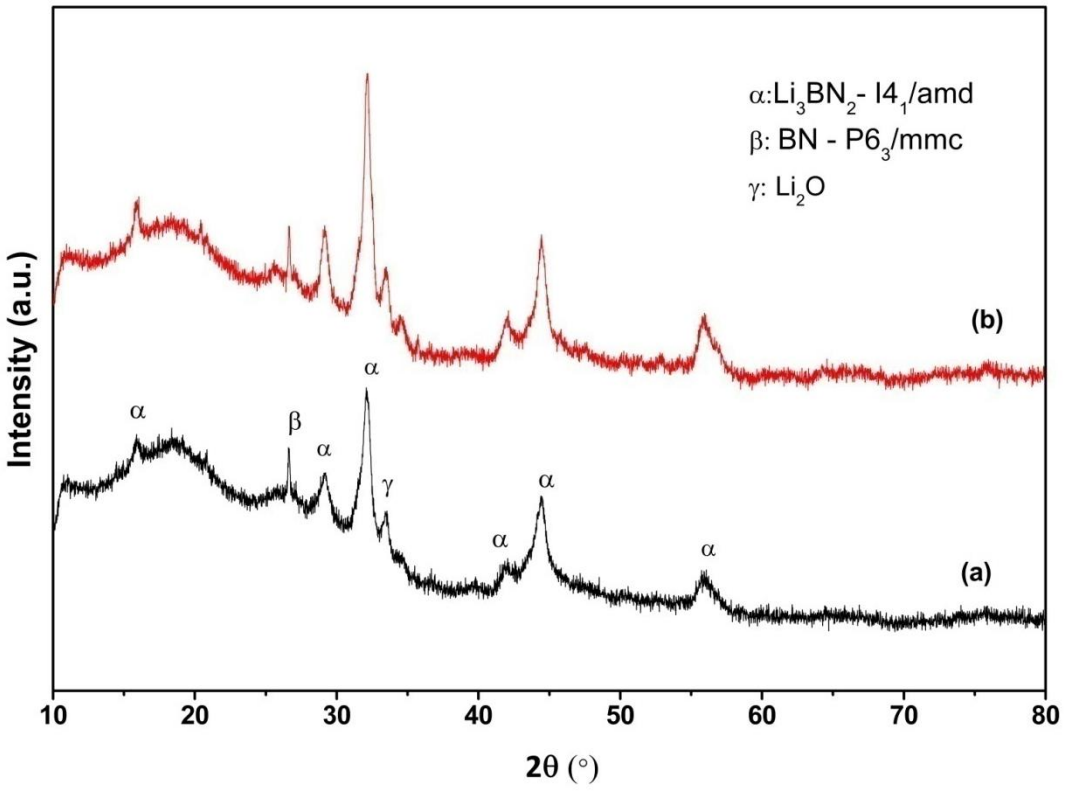

Figure 3.15 *Powder XRD patterns of the products of ball-milled $LiBH_4$–$2LiNH_2$–0.05CoO heated at 400℃ before* ***(a)*** *and after* ***(b)*** *hydrogenation at 300℃ for 24 hours.*

3.4 $LiBH_4$–$LiNH_2$–*b*CoO

Reactions of $LiBH_4$–$LiNH_2$–*b*CoO (where *b* = 0.01, 0.02, 0.03, 0.04, 0.05, and 0.1) were studied under the same conditions as the ratio of $LiBH_4$: $2LiNH_2$ in **section 3.3**.

3.4.1 Powder X-ray Diffraction

Anderson *et al*. [7] reported that in a molar ratio of $LiBH_4$:$LiNH_2$ = 1:1 a rhombohedral phase $Li_2BH_4NH_2$ can be obtained pure by quenching a mixture of $LiBH_4$ + $LiNH_2$ heated to 190°C (equation 3.3). This compound was then converted into the more stable phases

$Li_4(BH_4)(NH_2)_3$, $LiBH_4$ and $LiNH_2$ when heated further and decomposed to Li_3BN_2, LiH, BN and H_2 at high temperature as shown in equation (3.1) and (3.2).

$$LiNH_2 + LiBH_4 \rightarrow Li_2BH_4NH_2 \qquad (3.3)$$

In this study, powder XRD showed (in ***figure 3.16***) that the products of reaction $LiBH_4$ + $LiNH_2$ at 350°C were a mixture of Li_3BN_2 and LiH along with a large amount of $LiBH_4$ remaining from starting materials. The high background with broad peaks at 2θ = 18° and 25° may indicate the presence of amorphous phase of BN because of stoichiometry in equation (3.2).

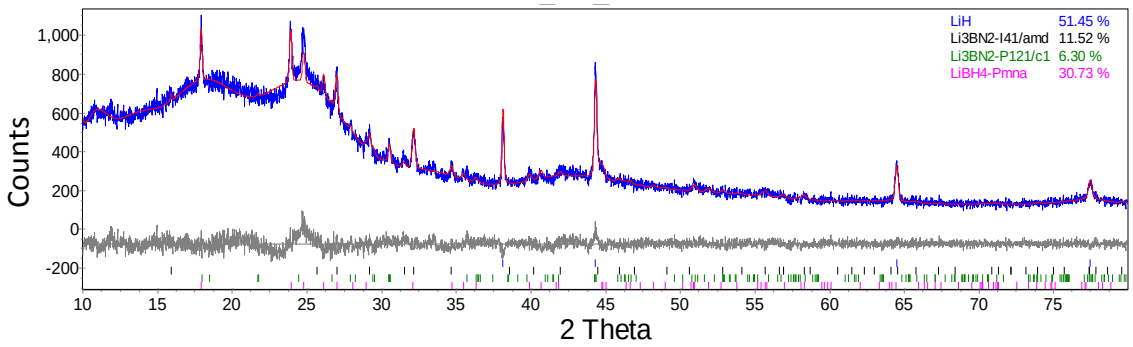

Figure 3.16 *Powder XRD pattern of the products of the reaction of $LiBH_4$–$LiNH_2$ at 350℃ showing observed (blue), Rietveld fit (red) and difference (grey) plots. Peak positions for refined compounds are shown underneath.*

At the higher temperature of 400°C, most $LiBH_4$ was decomposed leading to a marked decrease in proportion of this material after heating. A slightly larger amount of lithium boron nitride was obtained.

The powder XRD patterns of the products of the reactions $LiBH_4$ + $LiNH_2$ + *b*CoO are shown in ***figure 3.17***.

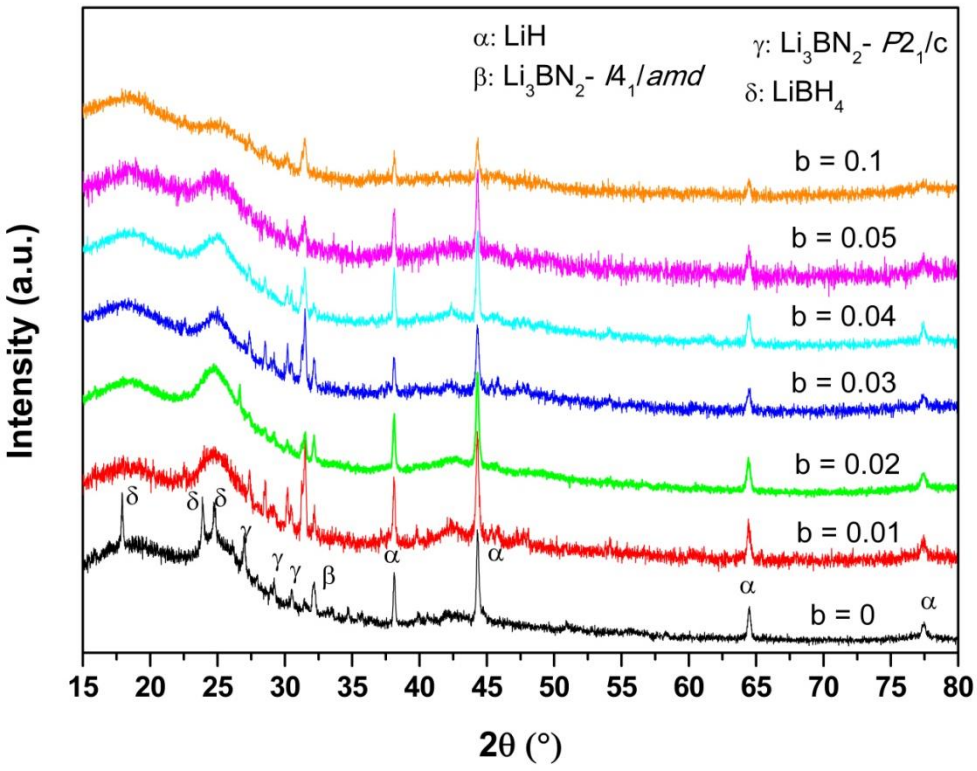

Figure 3.17 *Powder XRD patterns of the products of the reactions of $LiBH_4$–$LiNH_2$–$bCoO$ at 400℃.*

In the products of samples with CoO catalyst present, there was no observation of remaining $LiBH_4$, indicating a complete decomposition of this compound. On addition of $b \leq 0.05$ CoO, increasing the amount of catalyst did not cause much change in the products on heating. In the products of reactions at a 1:1 ratio, both $P2_1/c$ and $I4_1/amd$ polymorphs of lithium boron nitride were seen. In the products of the 0.05CoO sample, a considerable amount of $P2_1/c$ phase was observed, which is different from the 1:2 ratio, which contained only the $I4_1/amd$ polymorph (***figure 3.18)***. With a larger amount of CoO (b = 0.1), only the $P2_1/c$ phase was observed alongside LiH.

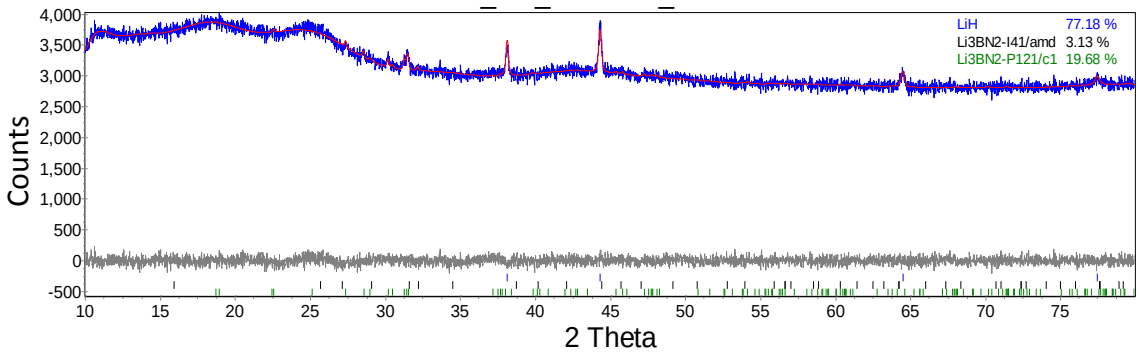

Figure 3.18 *Powder XRD pattern of the products of the reaction of $LiBH_4$–$LiNH_2$–0.05CoO at 400℃ showing observed (blue), Rietveld fit (red) and difference (grey) plots. Peak positions for refined compounds are shown underneath.*

The proportions of the products obtained from catalysed 1:1 $LiBH_4$–$LiNH_2$ mixtures heated at 400°C are shown in ***figure 3.19***.

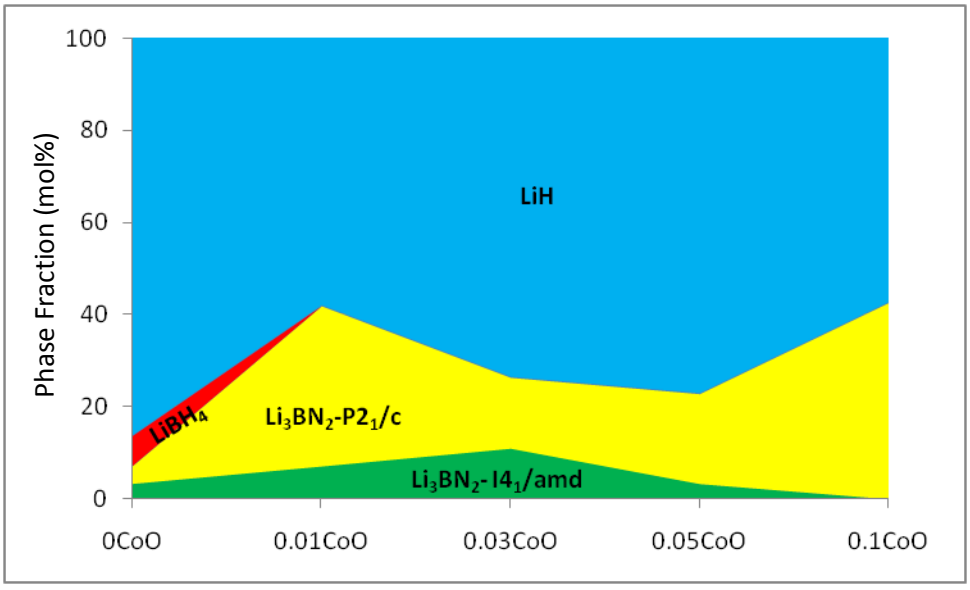

Figure 3.19 *Proportions of products from the reactions of $LiBH_4$–$LiNH_2$–bCoO at 400℃.*

3.4.2 Temperature Programmed Desorption

Hydrogen desorption properties of mixtures of $LiBH_4$–$LiNH_2$–*b*CoO were tested. The samples were treated under the same conditions as in **section 3.3.2.**

During thermal desorption of a mixture of $LiBH_4$–$LiNH_2$ up to 400°C the TPD apparatus, an endotherm was observed around 100°C which could be caused by the formation of $Li_4BH_4(NH_2)_3$. Hydrogen release was observed from 225°C and peaked at 315°C, lower than that of the 1:2 ratio, in agreement with the earlier results of Anderson *et al.* [7]. Desorption of ammonia was insignificant. Another desorption around 380°C could be seen, which can be from a decomposition of remaining $LiBH_4$ (***figure 3.20***). ~ 2.2 wt% H_2 was obtained.

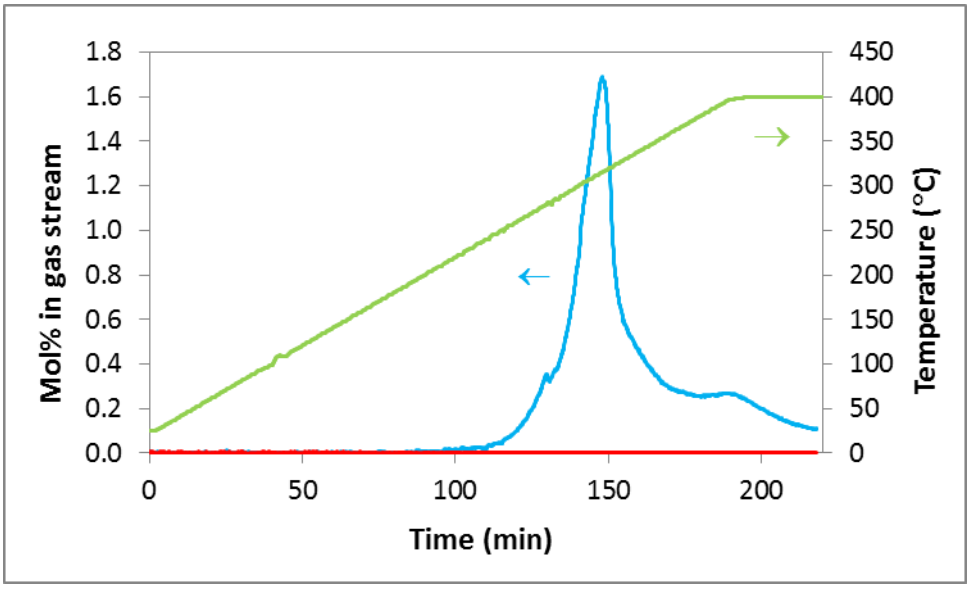

Figure 3.20 *TPD–MS traces of the reactions of $LiBH_4$–$LiNH_2$ heated at 2 ℃/minute to 400 ℃, showing traces for hydrogen (blue), ammonia (red) and temperature (green).*

In the presence of a small amount of CoO (b = 0.01), the onset temperature for hydrogen release was dramatically reduced by around 90°C from 225°C to 135°C. The peak of the hydrogen desorption was around 250°C. The absorption around 380°C was much weaker, which may be because most of remaining $LiBH_4$ was decomposed at lower temperature. The total amount of hydrogen release was not much greater than that in the absence of catalyst, which was about 2.3 wt% hydrogen. The evolution of ammonia was below the detection limits (***figure 3.21***).

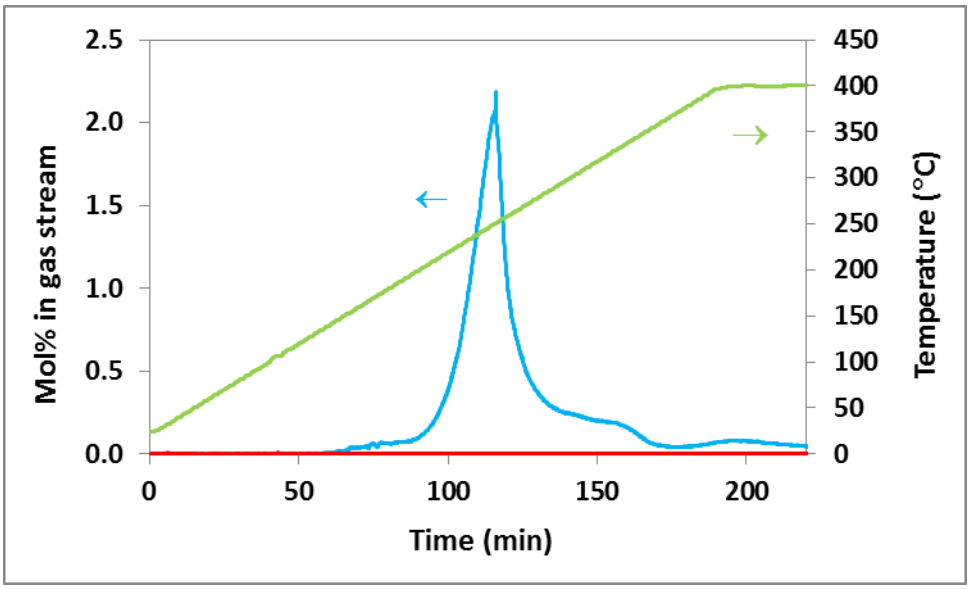

Figure 3.21 *TPD–MS traces of the reactions of $LiBH_4$–$LiNH_2$–0.01CoO heated at 2℃/minute to 400℃, showing traces for hydrogen (blue), ammonia (red) and temperature (green).*

Desorption traces for hydrogen from samples containing different amounts of CoO catalyst are presented in ***figure 3.22***. As the amount of catalyst rose from 0.02 to 0.05CoO, the main peak of hydrogen emission shifted gradually to lower temperature, from 230°C to 190°C. When 0.1CoO was used, the small peak around 90°C became much

stronger indicating a greater amount of hydrogen released at this temperature. However, the total hydrogen release measured by TPD–MS was less than 4 wt%.

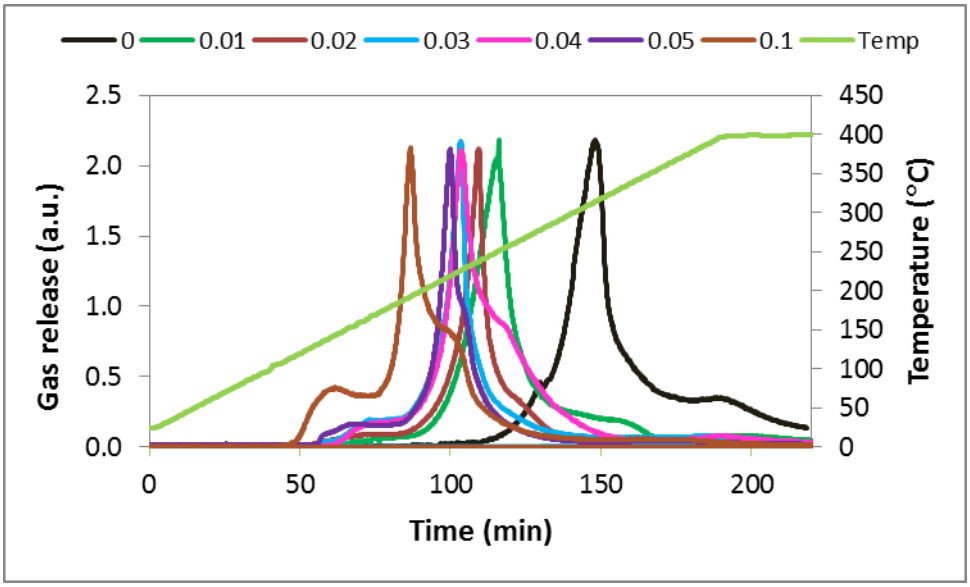

Figure 3.22 *TPD–MS traces of hydrogen release from the reactions of $LiBH_4$–$LiNH_2$–bCoO (b = 0.01-0.1) heated at 2 ℃/minute to 400 ℃.*

3.4.3 Rehydrogenation

The rehydrogenation properties of mixtures of $LiBH_4$ and $LiNH_2$ after heating at 350–400°C in the absence and presence of 0.05CoO were examined under the same conditions used in **section 3.3.3.**

The powder XRD patterns of samples before and after rehydrogenation under 90 bar hydrogen at 300°C are shown in ***figure 3.23.*** The patterns showed no change in products which is similar to the ratio of 1:2.

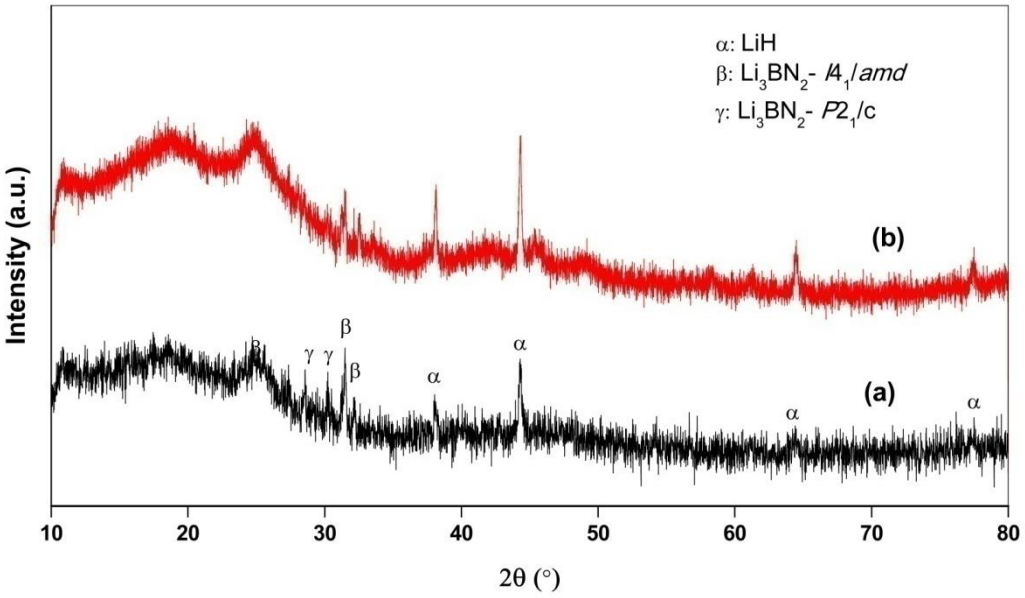

Figure 3.23 *Powder XRD patterns of the products of $LiBH_4$–$LiNH_2$–0.05CoO heated at 400℃ before (a) and after (b) hydrogenation at 300℃ for 24 hours*

The 0.05CoO samples heated at 350°C and 400°C were ball-milled for 10 hours before hydrogenation in the hope of improving the reversibility of the dehydrogenation products obtained. These ball-milled samples were then heated to 300°C under 90 bar hydrogen for 24 hours. Again there was no evidence of hydrogen absorption in the samples examined (***figure 3.24***).

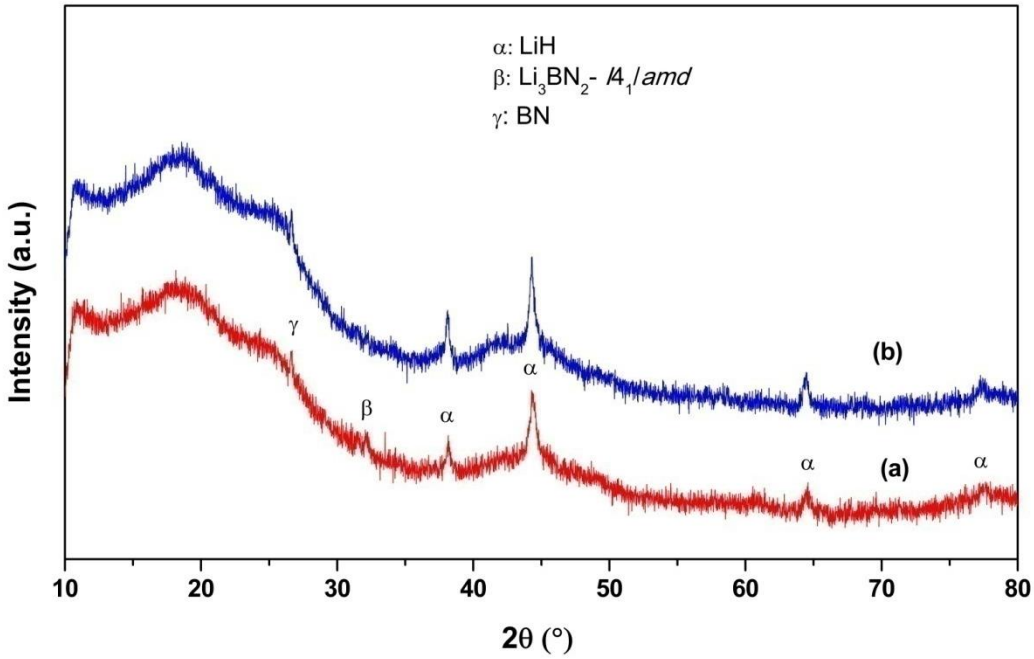

Figure 3.24 *Powder XRD patterns of the products of ball-milled $LiBH_4$–$LiNH_2$–0.05CoO heated at 350℃ before (a), after (b) hydrogenation at 300℃ for 24 hours.*

In order to examine any possible effect of longer reaction time and changes in pressure on rehydrogenation, the sample was heated to 300°C and held for 24 hours, then cooled down to ambient temperature at atmospheric pressureand heated to 300°C under 90 bar hydrogen again and held for another 24 hours. However, there was no observation of hydrided products after rehydrogenation. Similar results were obtained with a sample heated at 400°C.

3.5 $2LiBH_4$–$LiNH_2$–*c*CoO

3.5.1 Powder X-ray Diffraction

Reactions of $2LiBH_4 + LiNH_2$ were studied under the same conditions used in sections **3.3** and **3.4**. The main reaction product at 350°C was LiH along with a large amount of unreacted $LiBH_4$ remaining (***figure 3.25***).

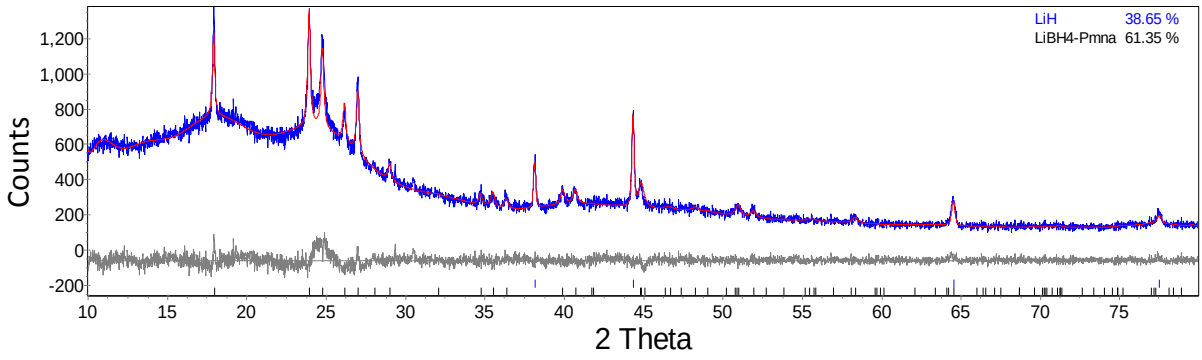

Figure 3.25 *Powder XRD pattern of the products of the reaction of $2LiBH_4$–$LiNH_2$ at 350℃ showing observed (blue), Rietveld fit (red) and difference (grey) plots. Peak positions for refined compounds are shown underneath.*

The borohydride-rich mixture was heated at 400°C. $LiBH_4$ was still seen in products obtained indicating reaction was not complete. This result is consistent with the fact that the reaction mixture contained $LiBH_4$ far in excess of the amount needed for reaction 3.1 – 3.3, even though 400°C is above the decomposition temperature of $LiBH_4$ [13].

The large background and broad features observed in the diffraction pattern in ***figure 3.26*** indicate the presence of amorphous BN, makes forming Li_3BN_2 less likely.

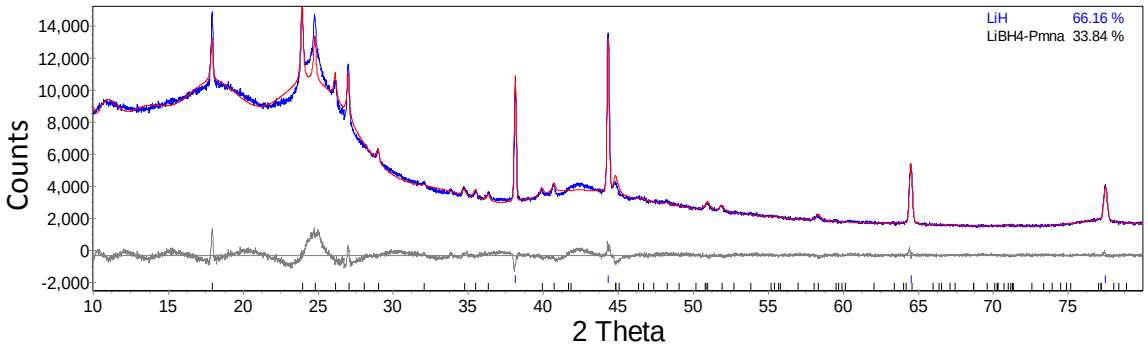

Figure 3.26 *Powder XRD pattern of the products of the reaction of $2LiBH_4–LiNH_2$ at 400 ℃ showing observed (blue), Rietveld fit (red) and difference (grey) plots. Peak positions for refined compounds are shown underneath.*

Cobalt (II) oxide was also doped into mixtures of $2LiBH_4–LiNH_2$ to investigate its effect on temperature and amount of hydrogen release. Samples of $2LiBH_4–LiNH_2–cCoO$ where (c = 0.01 – 0.1) were heated up to 400°C and held for up to 12 hours.

The presence of CoO catalyst may advance decomposition of $LiBH_4$ as a larger amount of CoO led to no $LiBH_4$ in product. ***Figure 3.27*** shows that when c = 0.05 LiH was the only product obtained. Therefore, CoO may help excess $LiBH_4$ to decompose under conditions studied. Similar result was achieved with more CoO (c = 0.1) used.

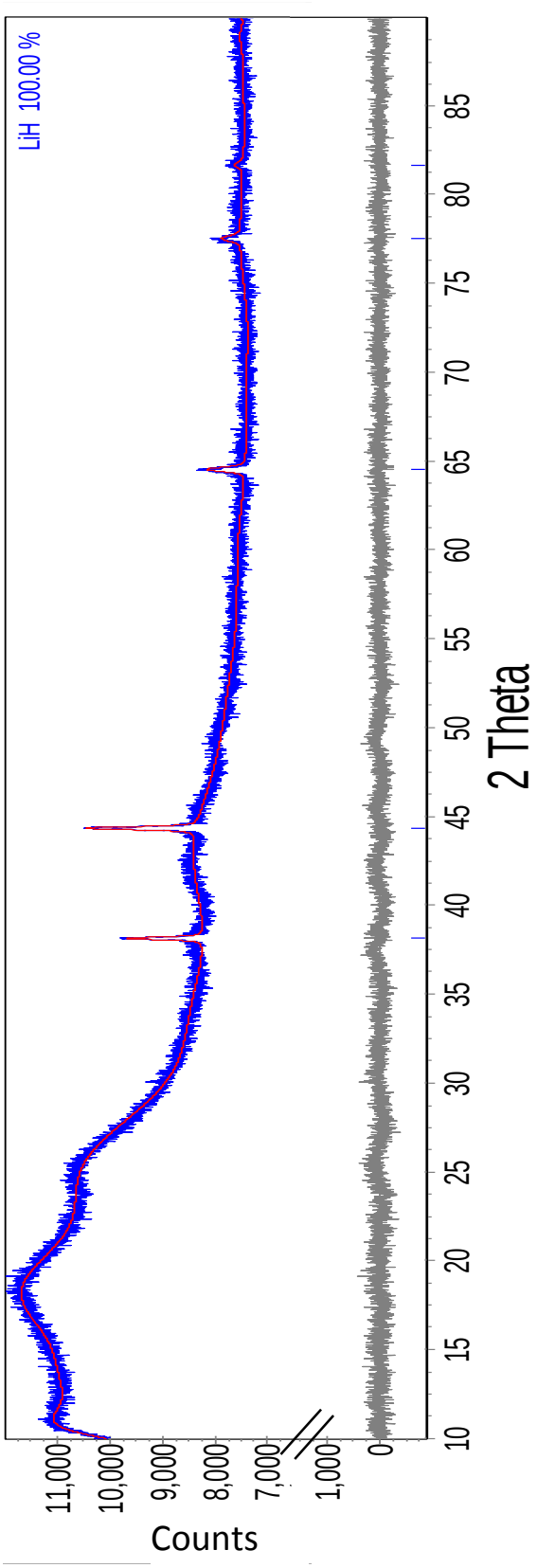

Figure 3.27 *Powder XRD pattern of the products of the reaction of $2LiBH_4$–$LiNH_2$–0.05CoO at 400 °C showing observed (blue), Rietveld fit (red) and difference (grey) plots. Peak positions for refined compounds are shown underneath.*

3.5.2 Temperature Programmed Desorption

Mixtures of $2LiBH_4$–$LiNH_2$–cCoO were all heated with the same heating rate of 2°C/min to 350–400°C and held for 1.5–2h to study their hydrogen desorption properties.

Hydrogen was emitted from 220°C and peaked around 300°C when a mixture of $2LiBH_4$–$LiNH_2$ was heated up to 350°C using TPD. There was another strong peak of hydrogen around 400°C when sample was heated further to 400°C which may correspond to the decomposition of unreacted $LiBH_4$. This result is consistent with the large amount of $LiBH_4$ shown in the powder XRD pattern in ***figure 3.28***. The total amount of hydrogen release was about 2.4 wt%.

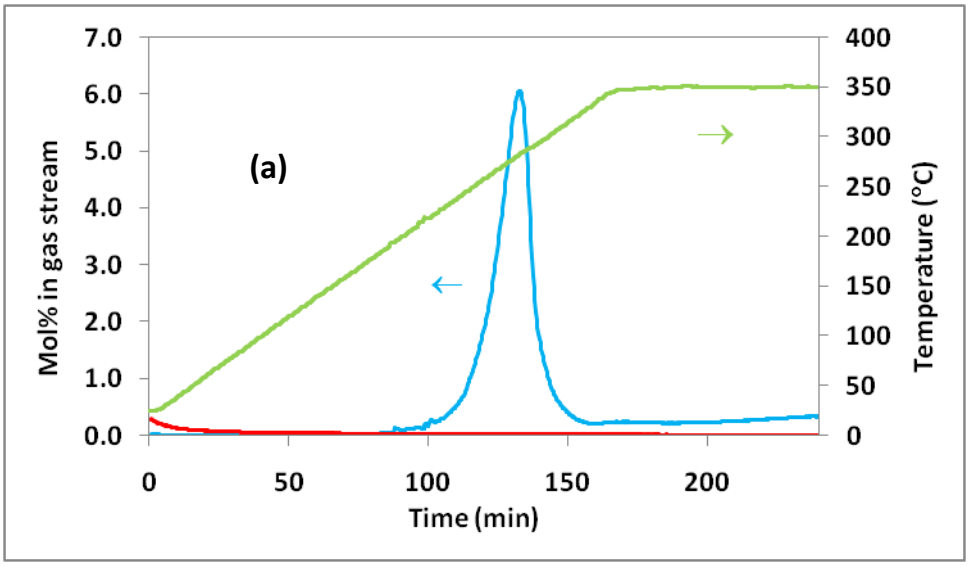

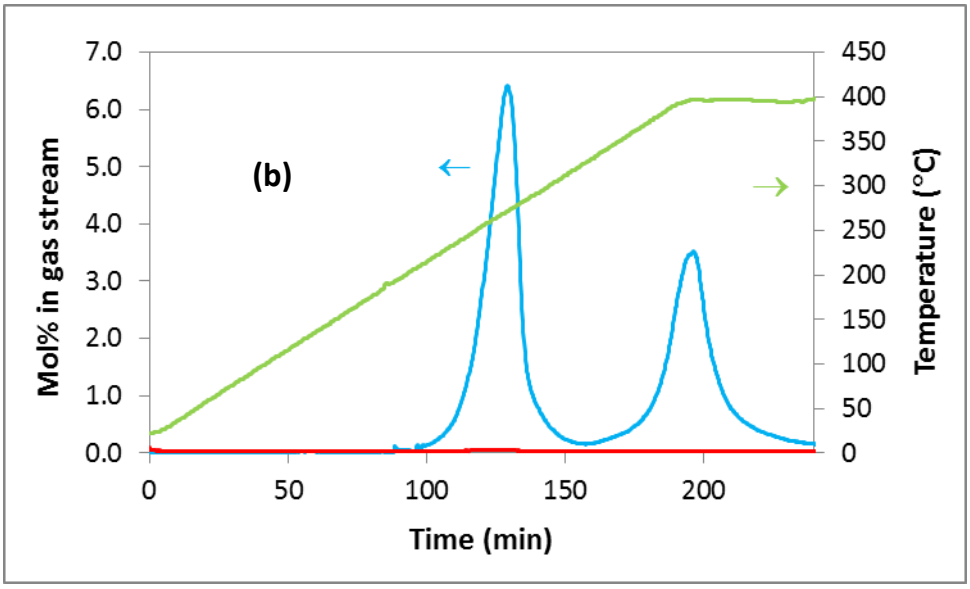

Figure 3.28 *TPD-MS trace of the reaction of $2LiBH_4$–$LiNH_2$ heated at 2 ℃/minute to* ***(a)*** *350 ℃ and* ***(b)*** *400 ℃, showing traces for hydrogen (blue), ammonia (red) and temperature (green).*

The addition of CoO reduced the onset temperature of hydrogen release by about 100°C. In the 0.05CoO sample hydrogen was released from 120°C, slightly higher than the eutectic point at around 90°C of the borohydride-rich system reported by Anderson *et al*. [7] (***figure 3.1***). The main hydrogen release was achieved at low temperature around 200°C. There was also a trend of hydrogen release at higher temperature probably due to the decomposition of remaining $LiBH_4$.

Figure 3.29 shows that when 0.1CoO was used the excess $LiBH_4$ remaining after reaction was decomposed. The amount of hydrogen release was about 2.4 wt%.

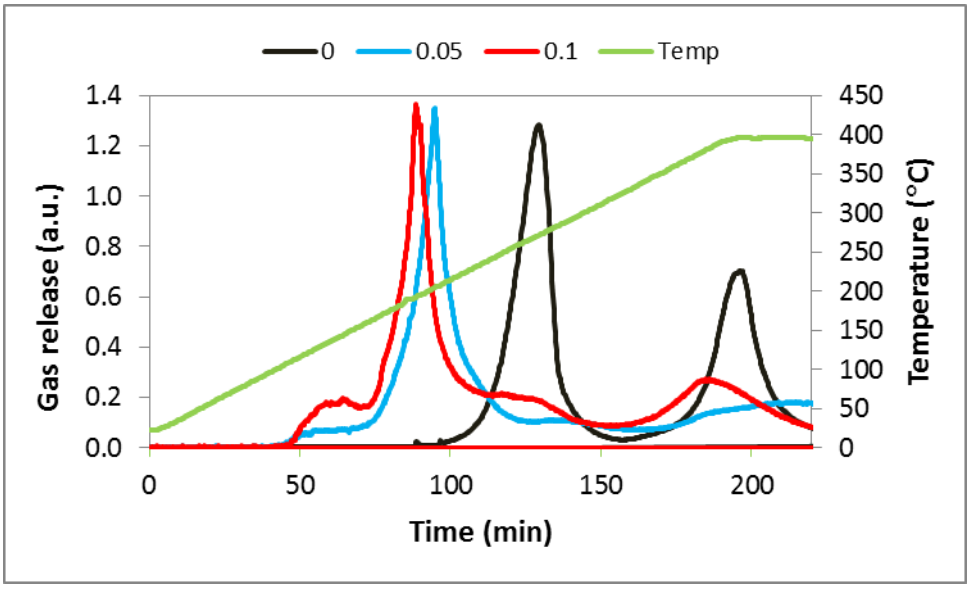

Figure 3.29 *TPD–MS traces of the reaction of $LiBH_4$–$2LiNH_2$–$cCoO$ heated at 2 ℃/minute to 400 ℃, showing hydrogen (blue), ammonia (red) and temperature (green).*

3.6 Effects of ball-milling

The presence of catalyst CoO could help to reduce the onset temperature of hydrogen desorption of $LiBH_4$–$LiNH_2$ systems. However, the amounts of hydrogen release were still much lower than in theory. These results may be caused by samples hand-grinding. Therefore, starting materials of those systems on addition of 0.05CoO were ball-milled for 10 hours before testing desorption by TPD–MS.

3.6.1 Ball-milled $LiBH_4$–$2LiNH_2$–0.05CoO

Products obtained after ball-milling of $LiBH_4$–$2LiNH_2$–0.05CoO were examined by powder XRD and shown in ***figure 3.30***.

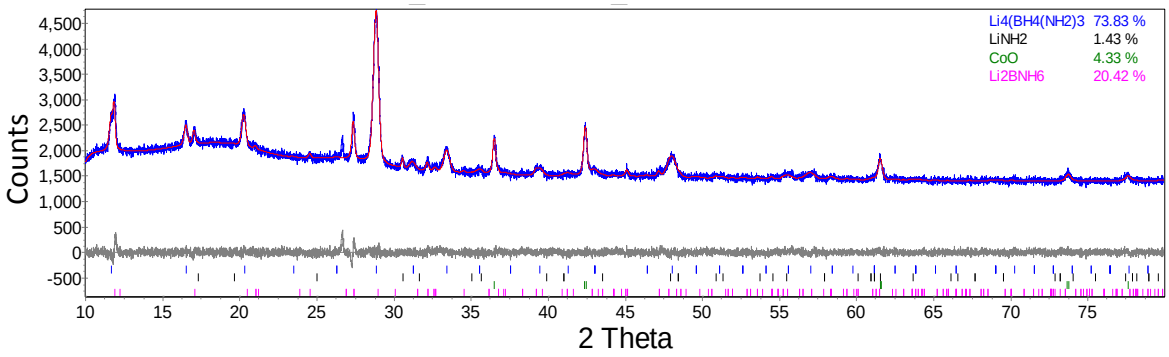

Figure 3.30 *Powder XRD pattern of the products of $LiBH_4$–$2LiNH_2$–0.05CoO after ball-milling for 10 hours showing observed (blue), Rietveld fit (red) and difference (grey) plots. Peak positions for refined compounds are shown underneath.*

Reaction between $LiBH_4$ and $LiNH_2$ at a molar ratio of 1:2 occurred under ball-milling conditions studied with the observation of a main product α-phase $Li_4BH_4(NH_2)_3$ and a rather large amount of β-phase Li_2BNH_6 ($LiBH_4NH_2$) along with a small amount of

remaining $LiNH_2$. There was also an observation of CoO with the similar amount to that before ball-milling. That means CoO did not take part in the reaction under conditions used. There was also a small unidentified peak at $2\theta = 26.6°$.

This mixture were then heated up to 400°C and held for 1.5 hour to test desorption properties. Products post TPD was only Li_3BN_2-$I4_1/amd$ ***(figure 3.31)***.

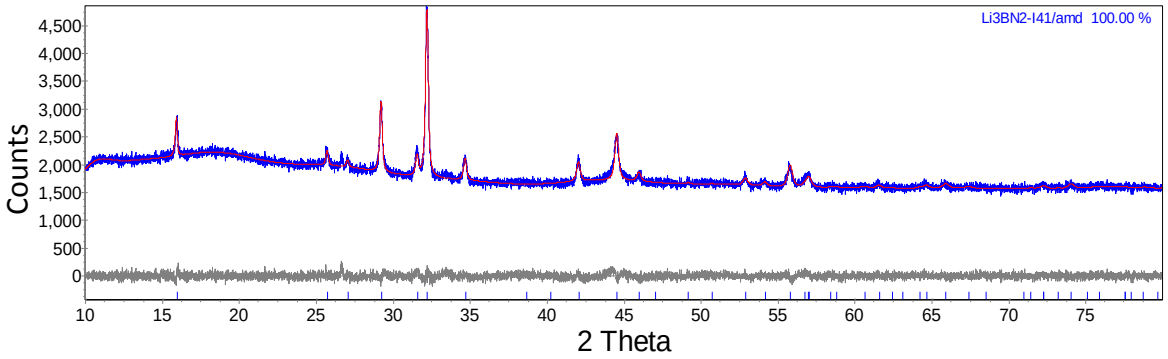

Figure 3.31 *Powder XRD pattern of the products of ball-milled $LiBH_4$–$2LiNH_2$–$0.05CoO$ after heating by TPD at 400℃ showing observed (blue), Rietveld fit (red) and difference (grey) plots. Peak positions for refined compounds are shown underneath.*

With the assistance of ball-milling, there was a further reduction in temperature of hydrogen release showing only one main peak which was around 220°C. More interestingly, the amount of hydrogen release meaured by MS raised up to 10.7 wt%, significantly greater than that of not ball-milled sample. Ammonia evolution was negligible (***figure 3.32***).

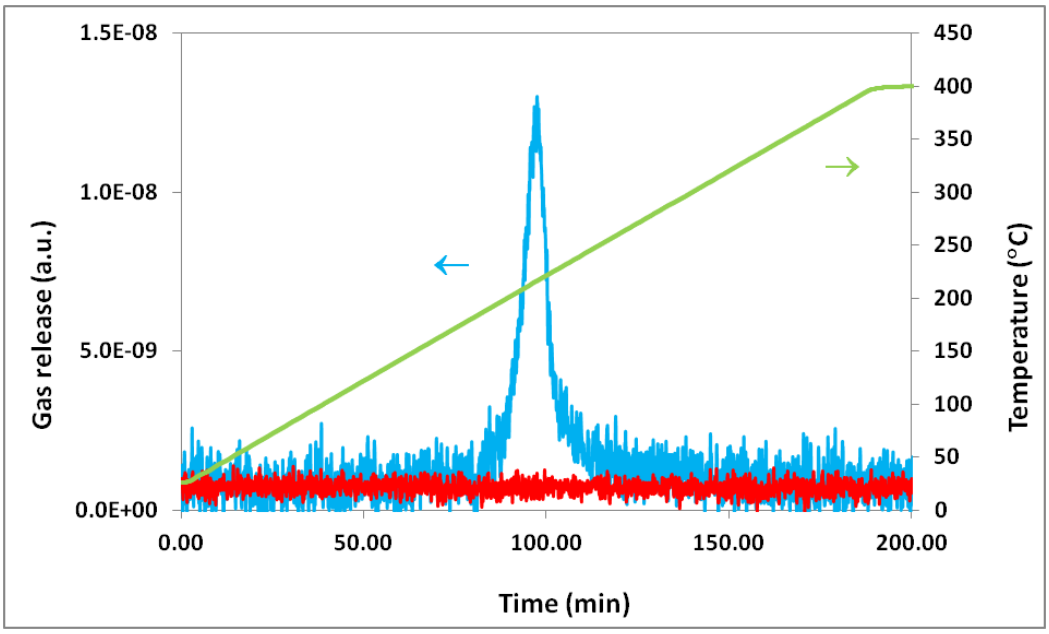

Figure 3.32 *TPD–MS traces of the reactions of ball-milled $LiBH_4$–$2LiNH_2$–0.05CoO heated at 2 ℃/minute to 400 ℃, showing traces for hydrogen (blue), ammonia (red) and temperature (green).*

3.6.2 Ball-milled $LiBH_4$–$LiNH_2$–0.05CoO

In the products obtained after ball-milling of $LiBH_4$–$LiNH_2$–0.05CoO the proportion of α-phase $Li_4BH_4(NH_2)_3$ is much lower while that of β-phase Li_2BNH_6 ($LiBH_4NH_2$) is much greater than those of $LiBH_4$–$2LiNH_2$–0.05CoO. There was also a small quantity of unreacted $LiBH_4$ beside a small amount of remaining $LiNH_2$. CoO remained nearly unchanged (***figure 3.33***).

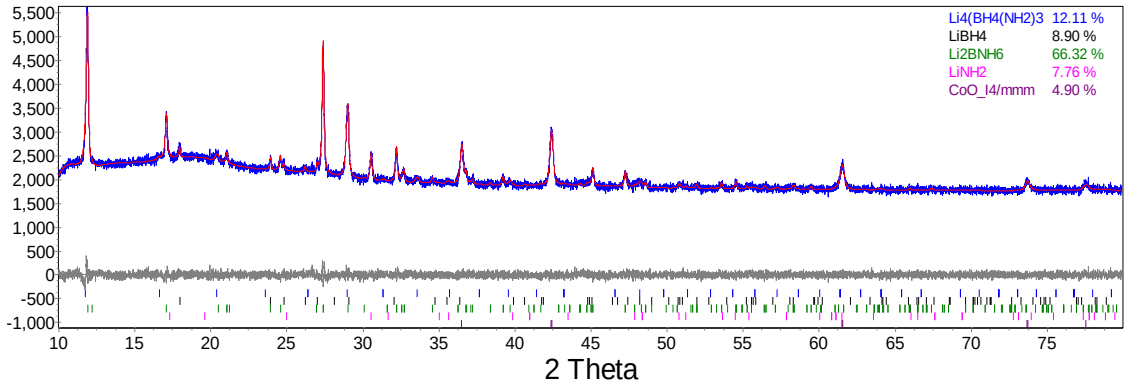

Figure 3.33 *Powder XRD pattern of the products of $LiBH_4$–$LiNH_2$–0.05CoO after ball-milling for 10 hours showing observed (blue), Rietveld fit (red) and difference (grey) plots. Peak positions for refined compounds are shown underneath.*

After heating in the TPD apparatus, the crystalline products were a mixture of LiH with a lesser amount of Li_3BN_2-$P2_1/c$ (***figure 3.34***).

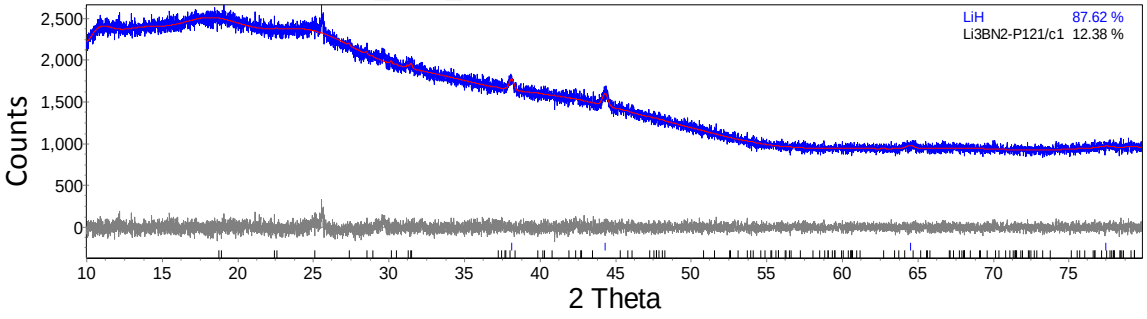

Figure 3.34 *Powder XRD pattern of the products of ball-milled $LiBH_4$–$LiNH_2$–0.05CoO after heating in the TPD apparatus at 400 ℃ showing observed (blue), Rietveld fit (red) and difference (grey) plots. Peak positions for refined compounds are shown underneath.*

The powder XRD pattern does not look good partly because there is quite a lot of cobalt there, but mainly because the products are amorphous such as BN and probably some boron from decomposition of $LiBH_4$ as in equation (3.4) [13]

$LiBH_4 \rightarrow LiH + B + 3/2H_2$ (3.4)

The background clearly shows this, and suggests that at this ratio, reaction 3.2 is more important than 3.1, which is probably to be expected.

A desorption of hydrogen started around 160°C and peaked around 220°C. Similar amount of hydrogen release (10.7 wt%) was seen at low temperature below 250°C (***figure 3.35***).

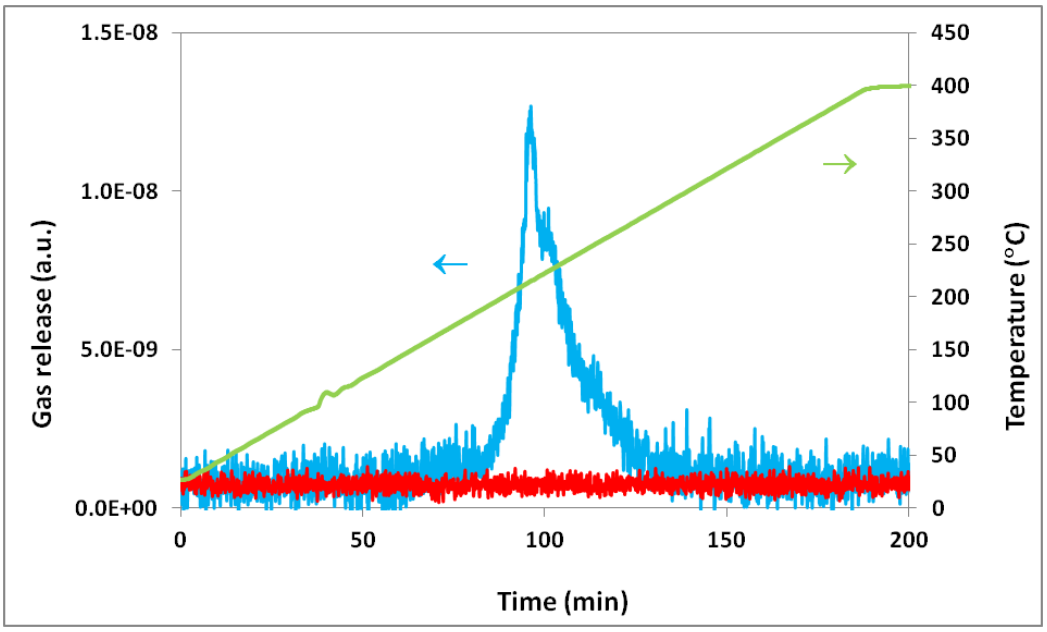

Figure 3.35 *TPD–MS traces for the reactions of ball-milled $LiBH_4$–$LiNH_2$–0.05CoO heated at 2℃/minute to 400℃, showing hydrogen (blue), ammonia (red) and temperature (green).*

3.6.3 Ball-milled $2LiBH_4–LiNH_2–0.05CoO$

In products after ball-milling of the mixture of $2LiBH_4–LiNH_2–0.05CoO$ α-phase $Li_4BH_4(NH_2)_3$ and $LiNH_2$ were not observed but a large amount of unreacted $LiBH_4$. CoO was seen approximately its proportion before ball-milling (***figure 3.36).***

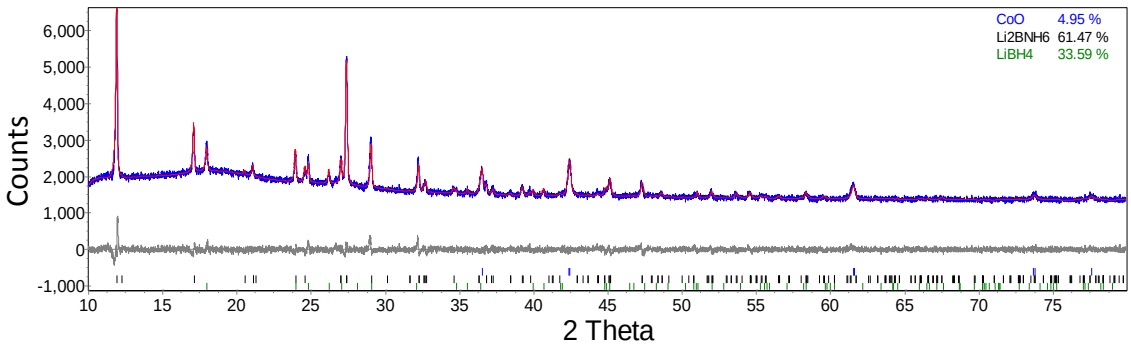

Figure 3.36 *Powder XRD pattern of the products of $2LiBH_4–LiNH_2–0.05CoO$ after ball-milling for 10 hours showing observed (blue), Rietveld fit (red) and difference (grey) plots. Peak positions for refined compounds are shown underneath.*

The main product obtained after TPD was LiH along with a small amount of impurity Li_2O (***figure 3.37***).

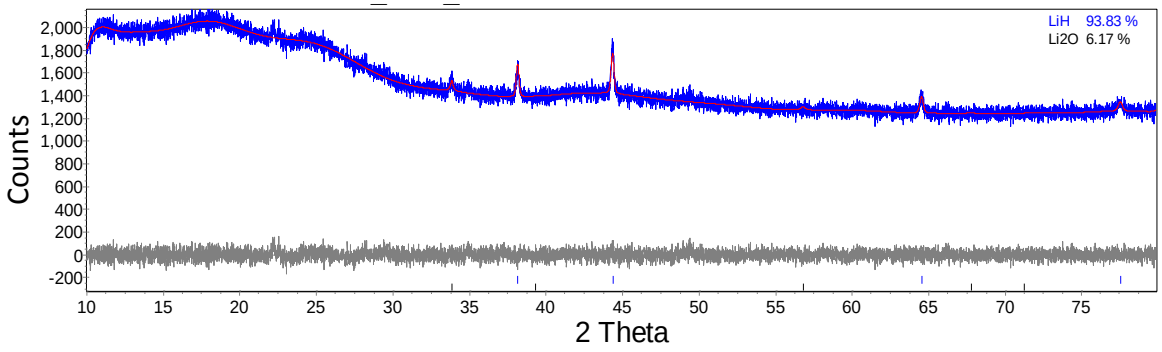

Figure 3.37 *Powder XRD pattern of the products of ball-milled $2LiBH_4–LiNH_2–0.05CoO$ after heating by TPD at 400 ℃ showing observed (blue), Rietveld fit (red) and difference (grey) plots. Peak positions for refined compounds are shown underneath.*

Most hydrogen was observed to emit around 220°C. However, there was still an observation of hydrogen releasing above 380°C – decomposition temperature of $LiBH_4$ (***figure 3.38***). Total amount of hydrogen desorbed was 10.7 wt%.

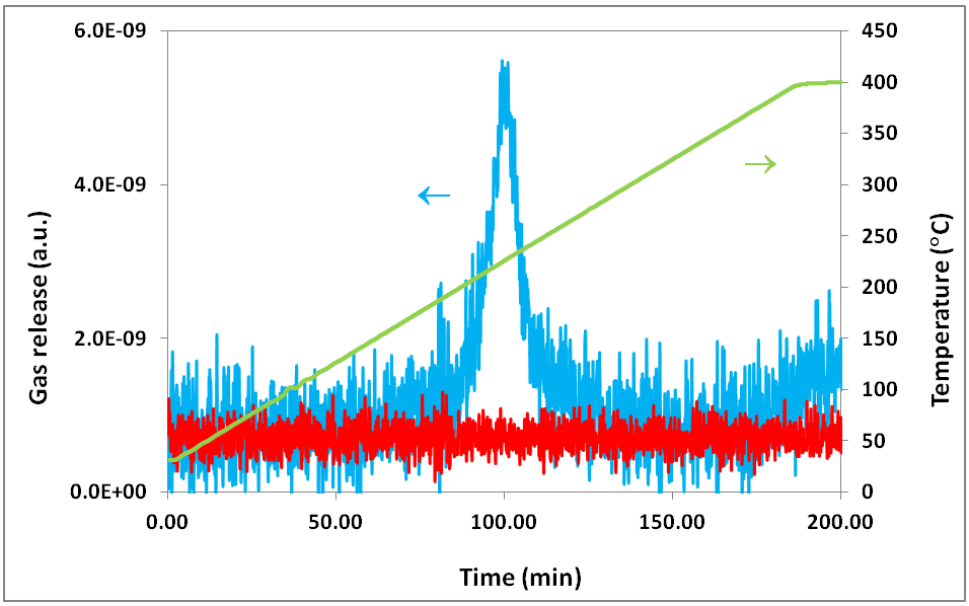

Figure 3.38 *TPD–MS traces for the reactions of ball-milled $2LiBH_4–LiNH_2–0.05CoO$ heated at 2 ℃/minute to 400 ℃, showing hydrogen (blue), ammonia (red) and temperature (green).*

3.7 SEM

There was a remarkable difference in hydrogen release between samples with and without ball-milling. That may be caused by a change in particle size and morphology of samples after ball-milling, which could affect kinetics of hydrogen uptake. Therefore, SEM was applied to studied particle size and surface of samples before and after ball-milling and shown in ***figure 3.39***.

It can be seen that the particle sizes of ball-milled samples are generally smaller and more homogeneous than their hand-mixed counterparts.

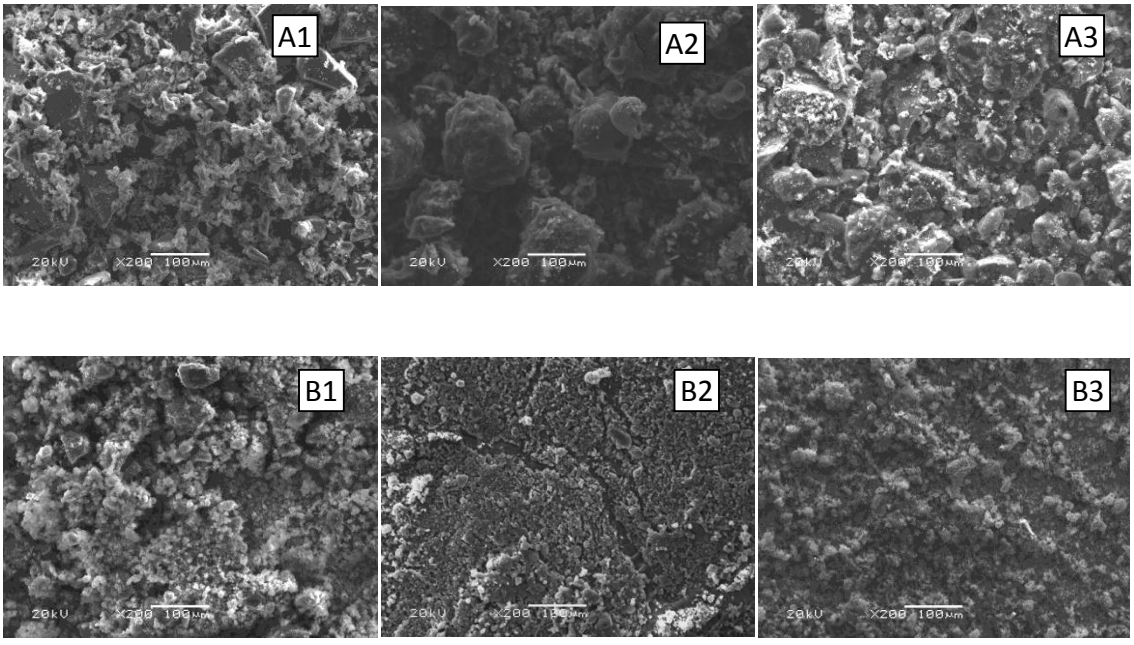

Figure 3.39 *Scanning electron microscopy images of at the scale of 100 μm of samples before ball-milling of $LiBH_4$–$2LiNH_2$–0.05CoO (A1), $LiBH_4$–$LiNH_2$–0.05CoO (A2), $2LiBH_4$–$LiNH_2$–0.05CoO (A3) and after ball-milling of $LiBH_4$–$2LiNH_2$–0.05CoO (B1), $LiBH_4$–$LiNH_2$–0.05CoO (B2), and $2LiBH_4$–$LiNH_2$–0.05CoO (B3).*

For the samples without ball-milling, the particles are inhomogeneous including big particles of about 100-150 μm along with small particles of 10-50 μm. The ball-milled samples have more homogeneous particles and smaller size around 5-10 μm.

3.8 Discussion and conclusions

The system $LiBH_4$ + $LiNH_2$ + CoO has been studied using powder XRD, TPD–MS, Raman and SEM. Data collected from different ratios under various conditions in the absence and presence of catalyst CoO have been analysed.

At a 1:2 ratio of $LiBH_4$:$LiNH_2$ the main products were a mixture of two polymorphs of lithium boron nitride, the tetragonal $I4_1/amd$ and the monoclinic $P2_1/c$, along with a small amount of LiH, and Li_2O from the starting materials. After rehydrogenation under 90 bar hydrogen at 300°C, no hydrided compounds were observed. That can be caused by kinetically limited desorption of Li_3BN_2 which make rehydrogenation unlikely.

On addition of CoO catalyst, LiH was not observed. Proportions of the two polymorphs of Li_3BN_2 were affected by the amount of catalyst with increasing $I4_1/amd$ phase observed with a greater amount of CoO. The presence of CoO was found to reduce temperatures of hydrogen release by up to 100°C. Moreover, the amounts of ammonia obtained were negligible in most CoO-doped samples, and often below detection limits. The addition of CoO may change the mechanism of hydrogen release from the $x$$LiBH_4$-$y$$LiNH_2$ systems. No improvement in the hydrogenation properties of Li_3BN_2 was observed under conditions studied. However, there was a transformation from the tetragonal $I4_1/amd$ phase to the monoclinic $P2_1/c$ phase under hydrogen pressure.

Ball-milling was applied to enhance the homogeneity and decrease the particle size of reaction mixtures. The temperature of hydrogen release was not significantly improved but the amount of hydrogen was drastically increased from 3–4 wt% to 10.7 wt%.

At the 1:1 and 2:1 ratios of $LiBH_4$:$LiNH_2$, LiH was the main crystalline product although there was also some lithium boron nitride and evidence for amorphous products such as boron nitride and boron. Similar reduction in temperature of hydrogen evolution was seen in these two ratios, showing hydrogen release from 135°C, peaking around 250°C. Ball-milling also helped to raise the amounts of hydrogen desorbed from these ratios up to greater than 10 wt%. The results obtained in this study suggest that the $LiBH_4$ + $LiNH_2$ + CoO system could be used as a hydrogen delivery system in some applications, though reversibility remains problematic.

It has been reported that incorporation of Li_3BN_2 into carbon nanoscaffolds resulted in some rerehydrogenation ability [14]. This may be a way forward to improve the rehydrogenation properties of Li_3BN_2.

References

[1] F. E. Pinkerton, G. P. Meisner, M. S. Meyer, M. P. Balogh, and M. D. Kundrat, **,** *J. Phys. Chem. B,* 2005, 109, 6–8.

[2] F. E. Pinkerton, G. P. Meisner, M. S. Meyer, M. P. Balogh, *J. Phys. Chem. B*, 2006, 110, 7967–7974.

[3] F. E. Pinkerton, G. P. Meisner, M. S. Meyer, M. P. Balogh, *J. Alloys Compd.,* 2007, 433, 282–291.

[4] W. S. Tang, G. Wu, Tao Liu, A. T. S. Wee, C. K. Yong, Z. Xiong, A. T. S. Hor and P. Chen, *Dalton Trans.,* 2008, 2395–2399.

[5] Y. F. Liu, K. Lu, Y. F. Zhou, M. X. Gao, H. G. Pan, *J. Alloys Compd.,* 2009, 481, 473–479.

[6] Y. Zhang, Y. Liu a, T. Liu, M. Gao, H. Pan, *Int. J. Hydrogen Energy,* 2013, 38, 13318–13327.

[7] P. A. Anderson, P. A. Chater, W. I. F. David, I. C. Evans and A. L. Kersting, *Mat. Res. Soc. Symp. Proc.,* 2009, 1219:W09–05.

[8] J. P. Singer, M. S. Meyer, R.M. Speer, and F. E. Pinkerton, *J. Phys. Chem. C* 2009, *113,* 18927–18934.

[9] D. R. Hewett, Mixed Anion Amides for Hydrogen Storage, PhD thesis, 2009, University of Birmingham.

[10] P. A. Chater, W. I. F. David, S. R. Johnson, P. P. Edwards, and P. A. Anderson, *Chem. Commun.*, 2006, 23, 2439–2441.

[11] F. E. Pinkerton and J. F. Herbst, *J. Appl. Phys.* 99, 113523–113525.

[12] G. P. Meisner, M. L. Scullin, M. P. Balogh, F. E. Pinkerton, and M. S. Meyer**,** *J. Phys. Chem. B,* 2006, 110, 4186–4192.

[13] A. Züttel, P. Wenger, S. Rentsch, P. Sudan Ph. Mauron, Ch. Emmenegger, *J. Power Sources,* 2003, 118, 1–7.

[14] H. Wu, W. Zhou, K. Wang, T. J. Udovic, J. J. Rush*,* T. Yildirim, L. A Bendersky, A. F. Gross, S. L. Van Atta, J. J. Vajo, F. E Pinkerton and M. S. Meyer, *Nanotechnology*, 2009, 20, 204002.

Chapter 4: $ZnCl_2$-based systems

4.1 Introduction

The Li–N–H system, which involves cycling between $LiNH_2$, Li_2NH and Li_3N, has attracted considerable attention as one of the most promising lightweight systems for reversible hydrogen storage. However, the slow absorption kinetics and relatively high operating temperature currently limit its practical applications [1–3].

Lithium and magnesium halides were found to have significant effects on the hydrogen desorption properties of the Li–N–H system [4–6]. Anderson *et al.* heated $LiNH_2$ and Li_2NH with LiX and MgX_2 (X = Cl, Br, I) to form a range of new amide halides. On reaction with LiH, in all cases the halide-containing amides and imides released and absorbed hydrogen more rapidly than pure amides/imides [4–6].

$$3LiNH_2 + LiCl \rightarrow Li_4(NH_2)_3Cl \quad (4.1)$$

$$6LiNH_2 + MgCl_2 \rightarrow 2Li_3Mg_{0.5}(NH_2)_3Cl \quad (4.2)$$

Zinc is a metal which has many similar chemical properties to magnesium: they have a common oxidation state of +2 and their ionic radii are similar in size (Zn, 86 pm; Mg, 88 pm).

Therefore, it was decided to investigate whether zinc chloride would react with lithium amide to form a zinc-chloride-amide system similar to the magnesium-based one.

$$6LiNH_2 + ZnCl_2 \rightarrow 2Li_3Zn_{0.5}(NH_2)_3Cl \quad (4.3)$$

In this chapter, the reactions between $ZnCl_2$ and $LiNH_2$, with and without the presence of LiH, under different conditions of stoichiometry and temperature have been studied.

The hydrogen absorption/desorption properties of these products have been investigated.

4.2 Experimental

$ZnCl_2$ (Sigma-Aldrich, 99.99%) and $LiNH_2$ (Sigma-Aldrich, 95%) were ground together in different molar ratios in an argon-filled glove box (O_2 content < 5 ppm, H_2O < 1 ppm) and heated under argon gas at different temperatures.

The reactions between $ZnCl_2$ and $LiNH_2$ were studied at molar ratios of 1:2, 1:3, 1:4, 1:5, and 1:6 in the temperature range 150–600°C. The heating rate was 2°C/minute and the reactions were kept at the set temperature for up to 12 hours.

TPD–MS and rehydrogenation measurements were carried out as in chapter 3.

4.3 $ZnCl_2$ + *n*$LiNH_2$ (*n* = 1-6)

4.3.1 Reaction in a ratio of 1:2

Reactions between $LiNH_2$ and $ZnCl_2$ in a ratio of 1:2 at different temperatures for 12 hours were studied and powder XRD patterns of the products of the reactions are shown in ***figure 4.1***.

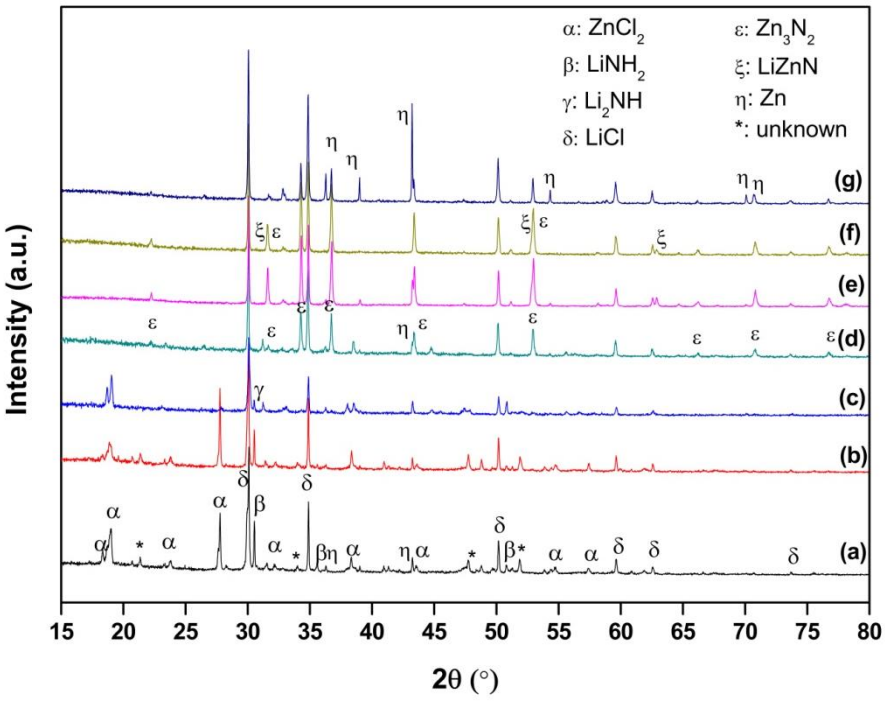

Figure 4.1 *Powder XRD patterns of the products of reactions between $LiNH_2$ and $ZnCl_2$ in a ratio of 1:2 at 150 ℃* ***(a)****, 200 ℃* ***(b)****, 250 ℃* ***(c)****, 300 ℃* ***(d)****, 400 ℃* ***(e)****, 500 ℃* ***(f)****, and 600 ℃* ***(g)*** *for 12 hours.*

Reaction occurred at 150°C, as the presence of LiCl and a small amount of Zn was observed in the products. The reaction was not complete, however, as there were significant amounts of $LiNH_2$ and δ-$ZnCl_2$ in the products. The presence of LiCl is believed to result from a salt metathesis reaction such as that in equation (4.4).

$$ZnCl_2 + 2LiNH_2 \rightarrow 2LiCl + Zn(NH_2)_2 \qquad (4.4)$$

The presence of Zn may be from the decomposition of $Zn(NH_2)_2$ or a further reaction of $Zn(NH_2)_2$ and LiCl. There were also some unmatched peaks present in the XRD pattern which have not yet been identified (***figure 4.2***). These peaks do not belong to any known zinc-based or lithium-based compounds such as ZnO, LiH, Li_2O, LiOH, Li_2ZnCl_4, *etc.* These

may belong to zinc amide, for which no XRD pattern has yet been reported. Alternatively some of the unidentified peaks may belong to a zinc amide chloride phase. Indexing of the peaks has been attempted but with no success.

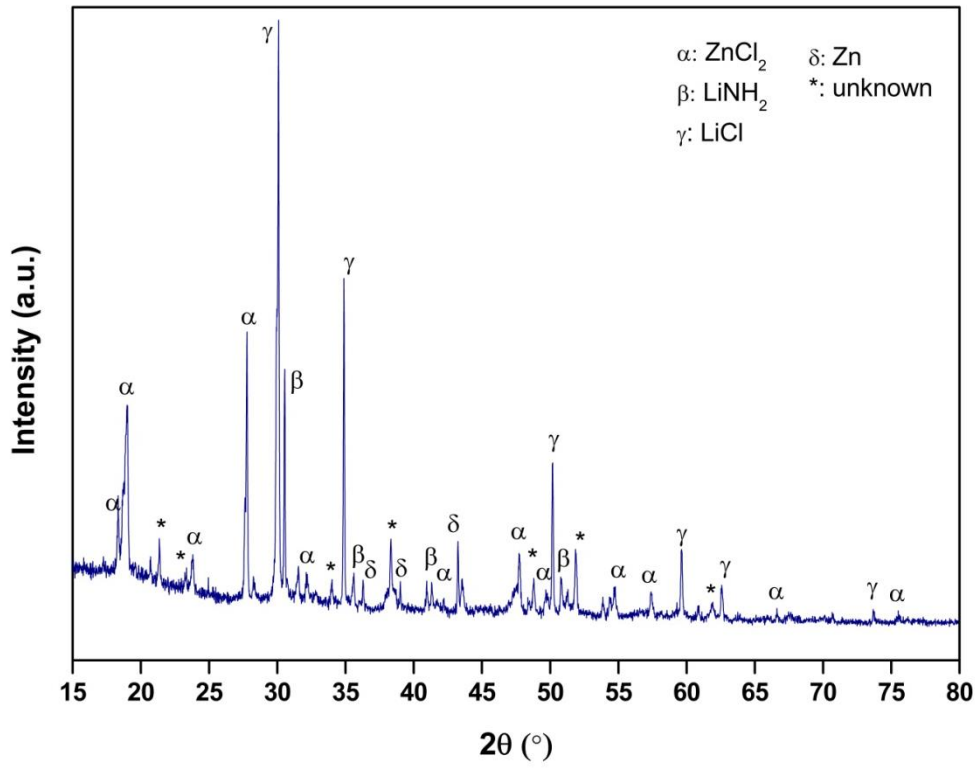

Figure 4.2 *Powder XRD patterns of the products of the reaction of $ZnCl_2$–$2LiNH_2$ at 150℃ for 12 hours.*

Similar products were obtained at 200°C, including similar unmatched peaks. The products after reaction at 250°C were significantly different from those at lower temperatures. A considerable proportion of $LiNH_2$ was decomposed into Li_2NH at 250°C although it was reported that at this temperature, $LiNH_2$ was decomposed only to a small extent [7]. This result may be caused by the effect of Cl^- ion, which is in agreement with study of Zhang *et al.* [8]. A small amount of zinc nitride Zn_3N_2 was also obtained. Some of the unmatched peaks observed at lower temperatures were not seen.

It can be seen from the XRD patterns that the products of the reaction at 300°C were different from those of the reaction at 250°C (***figure 4.3***).

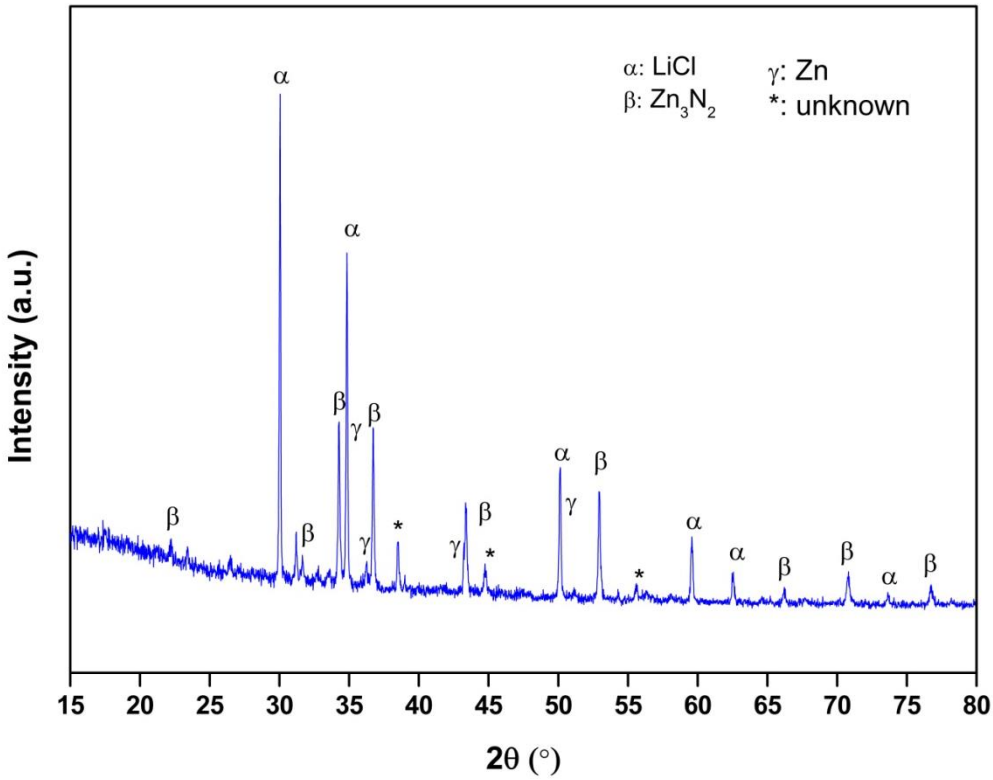

Figure 4.3 *Powder XRD pattern of the products of the reaction of $ZnCl_2$–$2LiNH_2$ at 300℃ for 12 hours.*

At this temperature $LiNH_2$ was completely decomposed; no lithium amide or imide was observed. There was also no remaining $ZnCl_2$. The proportion of Zn_3N_2 present after reaction at 300°C was much greater than that after reaction at 250°C. Some unidentified was peaks still observed in the pattern. The peak at 2θ = 31.2° may belong to LiZnN, which has been observed in products from reactions between $ZnCl_2$ and $LiNH_2$ in other ratios. However, this value of 2θ is lower than other values for position of LiZnN obtained from this work (~31.6°). Therefore the peak was not confirmed to belong to LiZnN.

For the sample heated to 400°C, besides LiCl and Zn_3N_2, the ternary nitride LiZnN was observed. A small amount of Zn was also obtained (***figure 4.4***). The peak at 2θ = 31.2° was also observed in the pattern.

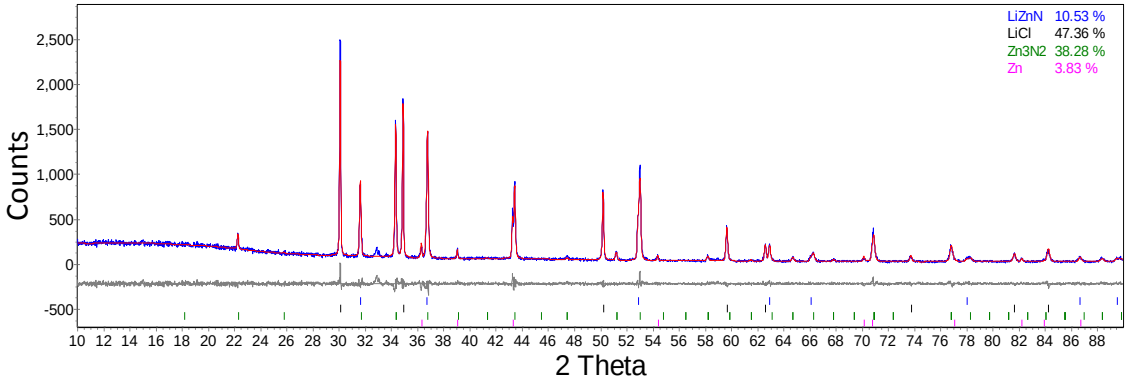

Figure 4.4 *Powder XRD patterns of the products of the reaction of $ZnCl_2$–$2LiNH_2$ at 400 ℃ for 12 hours showing observed (blue), Rietveld fit (red) and difference (grey) plots. Peak positions for refined compounds are shown underneath.*

The products of the reactions at 500°C (***figure 4.5)*** were similar to those at 400°C. However, there was no observation of Zn.

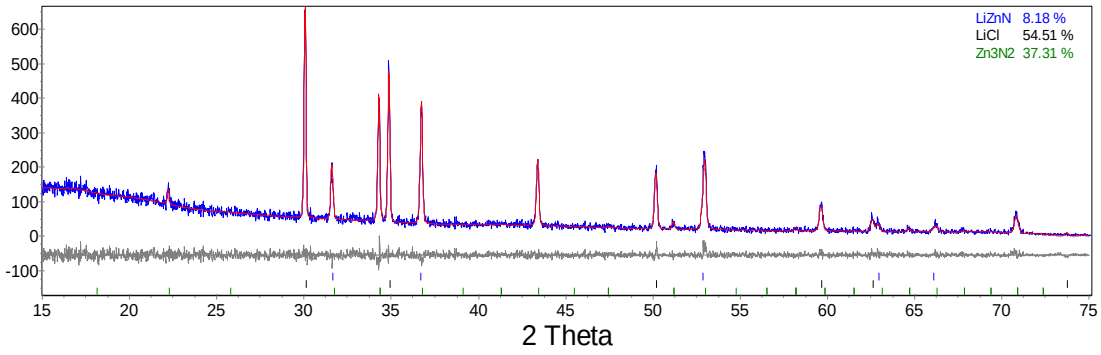

Figure 4.5 *Powder XRD pattern of the products of the reaction of $ZnCl_2$–$2LiNH_2$ at 500℃ for 12 hours showing observed (blue), Rietveld fit (red) and difference (grey) plots. Peak positions for refined compounds are shown underneath.*

At 600°C, the presence of a much smaller amount of Zn_3N_2 was observed. Zn was obtained in a greater amount than that at lower temperatures. The large amount of Zn here may be contributed to by the decomposition of LiZnN which occurs above 500°C. There was also a significant presence of Li_2O impurity (***figure 4.6***).

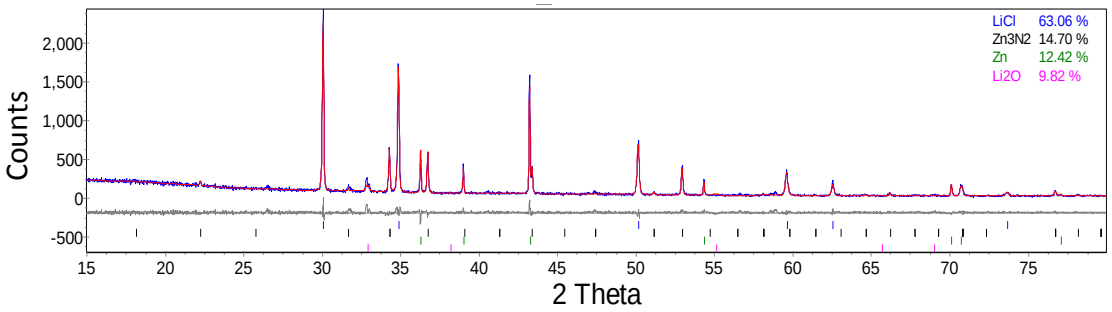

Figure 4.6 *Powder XRD pattern of the products of the reaction of $ZnCl_2$–$2LiNH_2$ at 600℃ for 12 hours showing observed (blue), Rietveld fit (red) and difference (grey) plots. Peak positions for refined compounds are shown underneath.*

In summary, reaction of $ZnCl_2$ and $LiNH_2$ in the ratio of 1:2 occurred from 150°C and the main products were LiCl and Zn_3N_2. There was also observation of a smaller amount of the ternary nitride LiZnN.

4.3.2 Reaction in a ratio of 1:3

Reactions between $LiNH_2$ and $ZnCl_2$ in a ratio of 1:3 at different temperatures for 12 hours were studied and powder XRD patterns of the products of the reactions are shown in ***figure 4.7***.

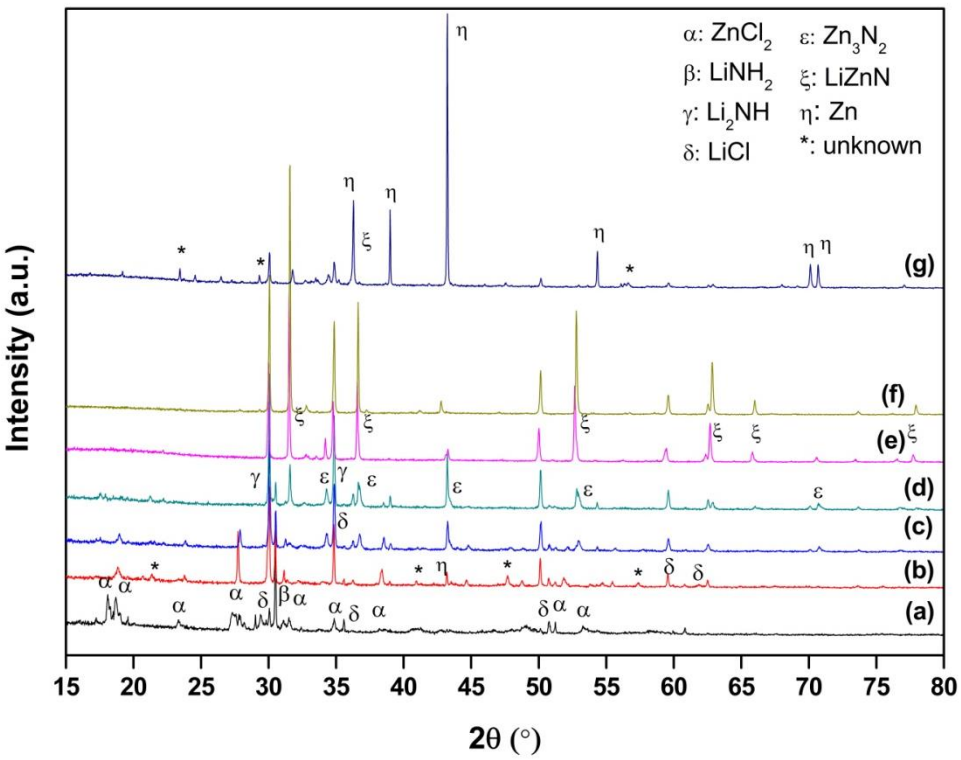

Figure 4.7 *Powder XRD patterns of the products of the reactions of $ZnCl_2$–3$LiNH_2$ at 150 ℃* ***(a)****, 200 ℃* ***(b)****, 250 ℃* ***(c)****, 300 ℃* ***(d)****, 400 ℃* ***(e)****, 500 ℃* ***(f)****, and 600 ℃* ***(g)*** *for 12 hours.*

In the temperature range 150–250°C the products of reactions were similar to those of reactions in the ratio of 1:2, also including some unmatched peaks. However, at 150°C Zn was not seen in the products.

Products of the reaction in the ratio of 1:3 at 300°C were a mixture of Li_2NH, Zn, Zn_3N_2 and LiZnN along with unreacted $LiNH_2$ (***figure 4.8***).

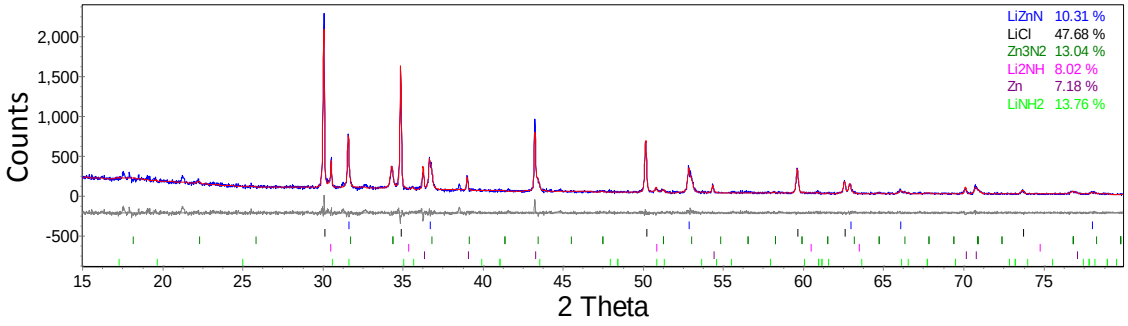

Figure 4.8 *Powder XRD patterns of the products of the reaction of $ZnCl_2$–$3LiNH_2$ at 300 ℃ for 12 hours showing observed (blue), Rietveld fit (red) and difference (grey) plots. Peak positions for refined compounds are shown underneath.*

All the remaining Li_2NH was decomposed at 400°C. The proportion of LiZnN was much higher than that of the ratio 1:2 with 42.5 wt% while that of Zn_3N_2 was smaller with 10.9 wt% (***figure 4.9***).

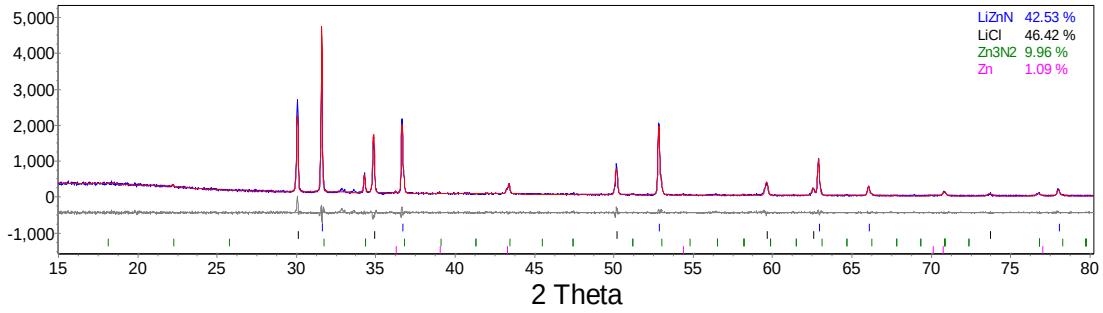

Figure 4.9 *Powder XRD pattern of the products of the reaction of $ZnCl_2$–$3LiNH_2$ at 400℃ for 12 hours showing observed (blue), Rietveld fit (red) and difference (grey) plots. Peak positions for refined compounds are shown underneath.*

At 500°C Zn_3N_2 was no longer observed and the final products were a mixture of LiCl and LiZnN in a mole ratio of approximately 2:1 and a very small amount of Zn (***figure 4.10***). All residual LiZnN was decomposed at 600°C. The pattern of products of the reaction at this temperature contained some unmatched peaks.

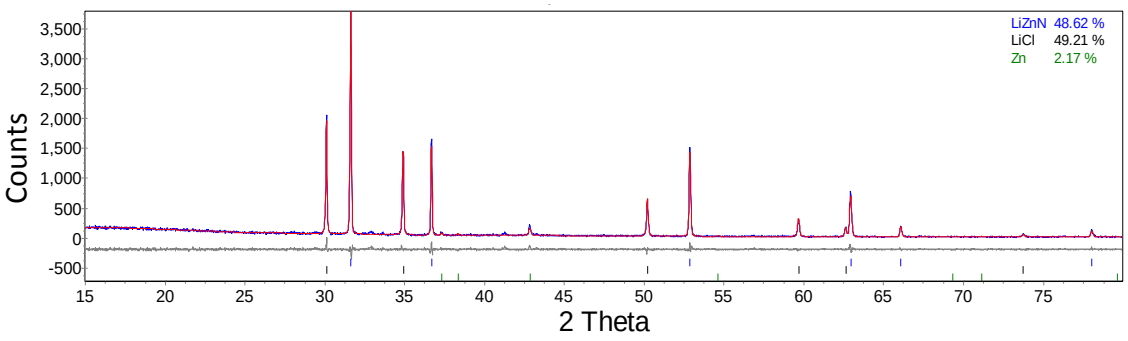

Figure 4.10 *Powder XRD pattern of the products of the reaction of $ZnCl_2$–$3LiNH_2$ at 500℃ for 12 hours showing observed (blue), Rietveld fit (red) and difference (grey) plots. Peak positions for refined compounds are shown underneath.*

In the ratio of 1:3, LiZnN appeared from 300°C then its proportion increased with increasing temperature up to 500°C. From 500°C Zn_3N_2 was not observed.

4.3.3 Reaction in a ratio of 1:4

Reactions between $LiNH_2$ and $ZnCl_2$ in a ratio of 1:4 at different temperatures for 12 hours were studied and the powder XRD patterns of the products of the reactions are shown in ***figure 4.11***.

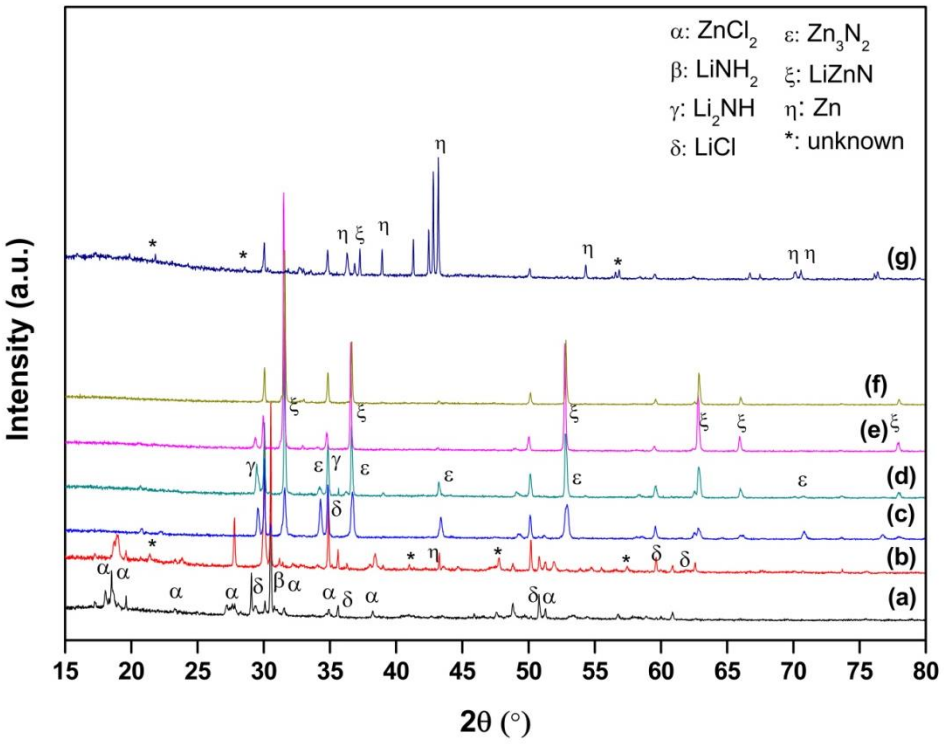

Figure 4.11 *Powder XRD patterns of the products of reactions the reaction of $ZnCl_2$–$4LiNH_2$ at 150 ℃* ***(a)****, 200 ℃* ***(b)****, 250 ℃* ***(c)****, 300 ℃* ***(d)****, 400 ℃* ***(e)****, 500 ℃* ***(f)****, and 600 ℃* ***(g)*** *for 12 hours.*

The products of reactions between $LiNH_2$ and $ZnCl_2$ in a ratio of 1:4 below 300°C were not much different from those of the reactions in the ratio of 1:3.

At 300°C the percentage of LiZnN in the products of reaction in a ratio of 1:4 was considerably greater than those of the two ratios above (~31 wt%). Also, more Li_2NH

was observed in the products than in the ratio of 1:3. This increased with increasing amount of $LiNH_2$ from a ratio of 1:2 to 1:4 (***figure 4.12***).

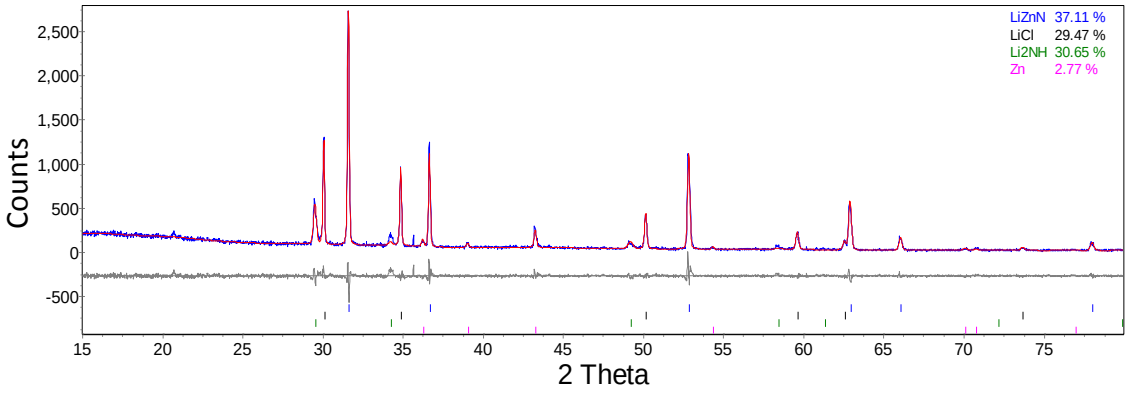

Figure 4.12 *Powder XRD pattern of the products of the reaction of $ZnCl_2$–$4LiNH_2$ at 300℃ for 12 hours showing observed (blue), Rietveld fit (red) and difference (grey) plots. Peak positions for refined compounds are shown underneath.*

It can be seen in ***figure 4.13*** that considerable amount of lithium imide was observed in the reaction products from this ratio at 400°C. Lithium imide is a product of the thermal decomposition of lithium amide.

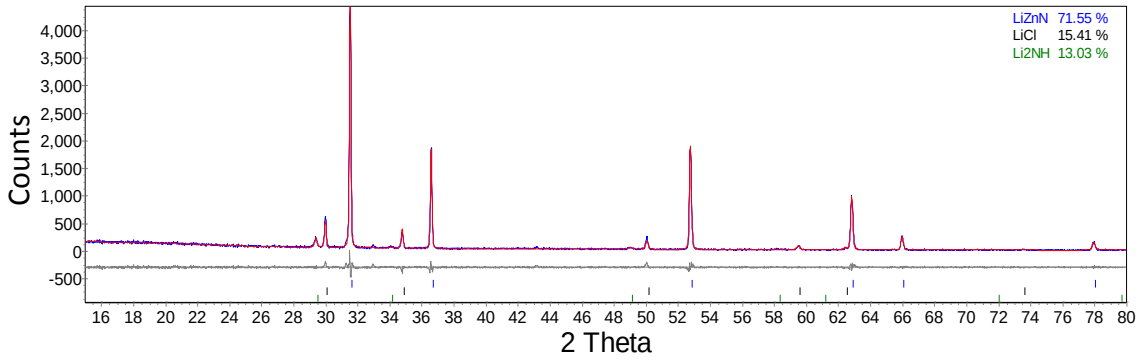

Figure 4.13 *Powder XRD pattern of the products of the reaction of $ZnCl_2$–$4LiNH_2$ at 400℃ for 12 hours showing observed (blue), Rietveld fit (red) and difference (grey) plots. Peak positions for refined compounds are shown underneath.*

That may be because of the amount of lithium amide which was not required for reactions to form LiZnN and Zn_3N_2. The main product was LiZnN (72 wt%) while Zn_3N_2 was not observed, contrast to previous ratios.

When the temperature of reaction was raised to 500°C, all Li_2NH was decomposed. Products were a mixture of LiZnN and LiCl in a molar ratio of LiZnN : LiCl ~ 1 : 1. There was also a very small amount of Zn (***figure 4.14***).

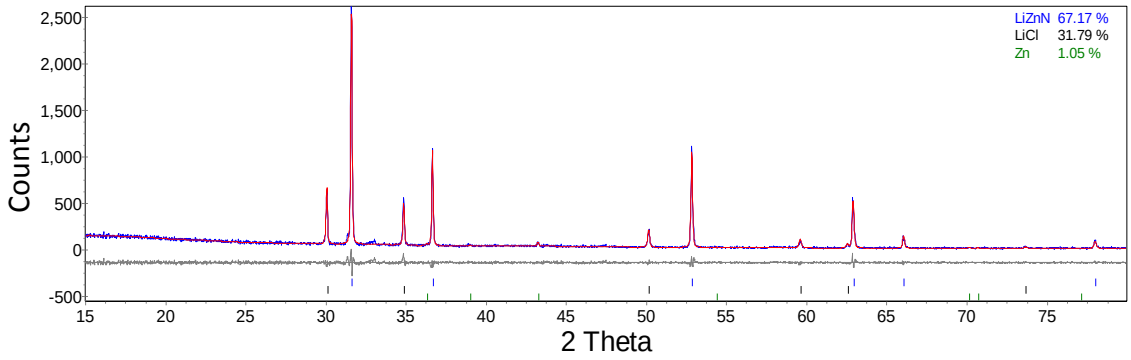

Figure 4.14 *Powder XRD pattern of the products of the reaction of $ZnCl_2$–$4LiNH_2$ at 500℃ for 12 hours showing observed (blue), Rietveld fit (red) and difference (grey) plots. Peak positions for refined compounds are shown underneath.*

There was no observation of LiZnN at 600°C. Instead, LiZn and Zn were obtained along with LiCl.

Overall, in the ratio of 1:4 the products were similar to those of the ratio of 1:3. However, Li_2NH was present in much greater amount at 300°C and was observed at 400°C, while there was no observation of this compound at 400°C at lower ratios.

4.3.4 Reaction in a ratio of 1:5

Reactions between $LiNH_2$ and $ZnCl_2$ in a ratio of 1:5 at different temperatures for 12 hours were studied and powder XRD patterns of the products of the reactions are shown in ***figure 4.15***.

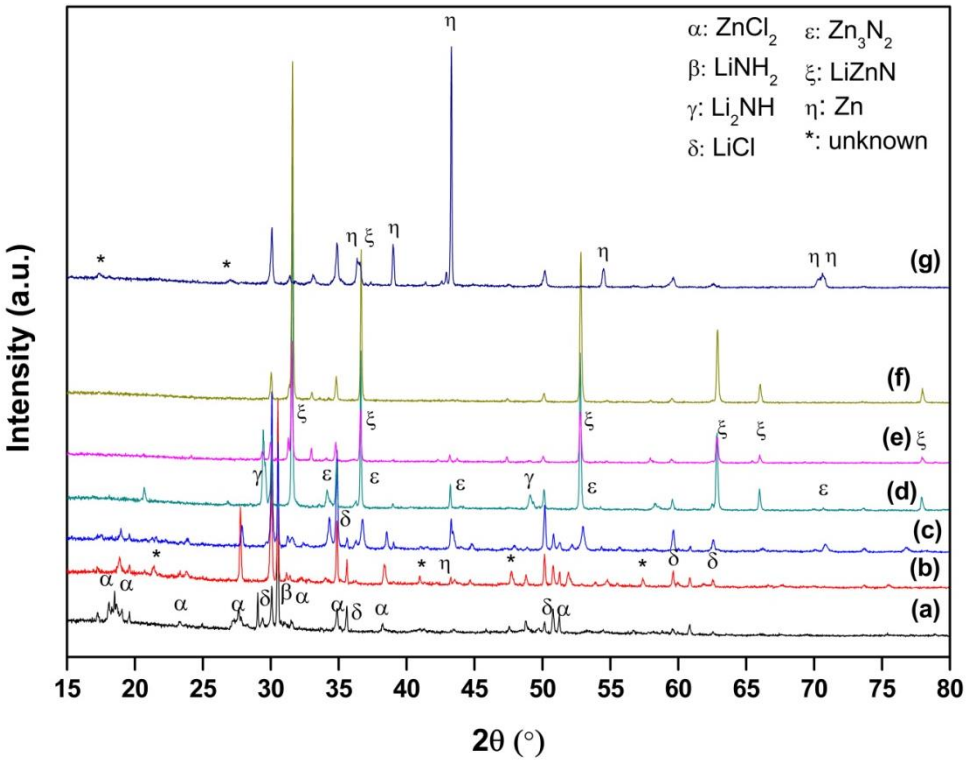

Figure 4.15 *Powder XRD patterns of the products of the reaction of $ZnCl_2$–$5LiNH_2$ at 150 ℃* ***(a)****, 200 ℃* ***(b)****, 250 ℃* ***(c)****, 300 ℃* ***(d)****, 400 ℃* ***(e)****, 500 ℃* ***(f)****, and 600 ℃* ***(g)*** *for 12 hours.*

In the temperature range 150–200°C the products of the reactions were similar to those of reactions in the ratios of 1:2 to 1:4. At 250°C $LiNH_2$ was observed while there was no Li_2NH in the products, different from the above ratios. The amount of LiZnN increased with increasing temperatures up to 400°C while that of Zn_3N_2 decreased. The highest proportion of LiZnN (~85.8 wt %) was obtained at 500°C (***figure 4.16***) and then this was completely decomposed at 600°C. The molar ratio of LiZnN:LiCl was ~ 3:1.

4.3.5 Reaction in a ratio of 1:6

Powder XRD patterns of the products of reactions between $LiNH_2$ and $ZnCl_2$ in a ratio of 1:6 at different temperatures for 12 hours are shown in ***figure 4.17***.

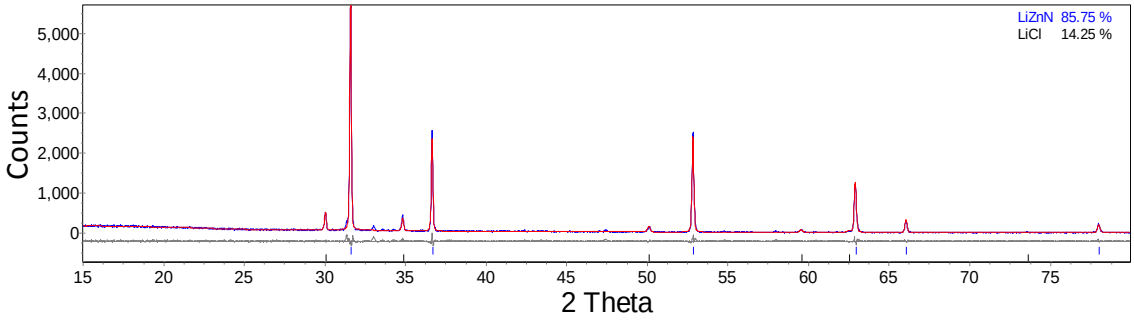

Figure 4.16 *Powder XRD pattern of the products of the reaction of $ZnCl_2$–5$LiNH_2$ at 500 ℃ for 12 hours showing observed (blue), Rietveld fit (red) and difference (grey) plots. Peak positions for refined compounds are shown underneath.*

Overall, the products in the ratio of 1:5 were similar to those in the ratio of 1:4.

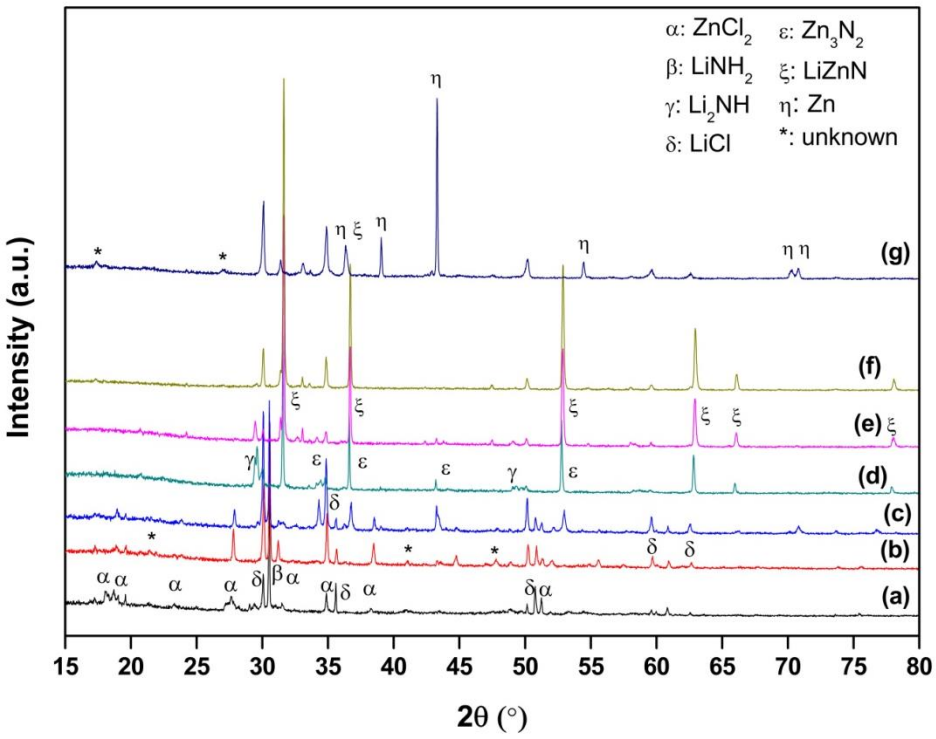

Figure 4.17 *Powder XRD patterns of the products of the reactions of $ZnCl_2$–6$LiNH_2$ at 150 ℃ (**a**), 200 ℃ (**b**), 250 ℃ (**c**), 300 ℃ (**d**), 400 ℃ (**e**), 500 ℃ (**f**), and 600 ℃ (**g**) for 12 hours.*

The same compounds were obtained in the products of reactions at 150°C and 200°C in a ratio of 1:6 as those from the ratio of 1:5. In products of reactions in the temperature range from 250°C to 500°C, LiZnN was achieved in larger amounts at higher temperatures. However, at 500°C the amount of LiZnN was slightly smaller than that in the ratio of 1:5 at the same temperature (80.4 wt%) (***figure 4.18***). This may be caused by the lack of Zn in starting materials to form more LiZnN. The molar ratio of LiZnN:LiCl was ~ 2:1.

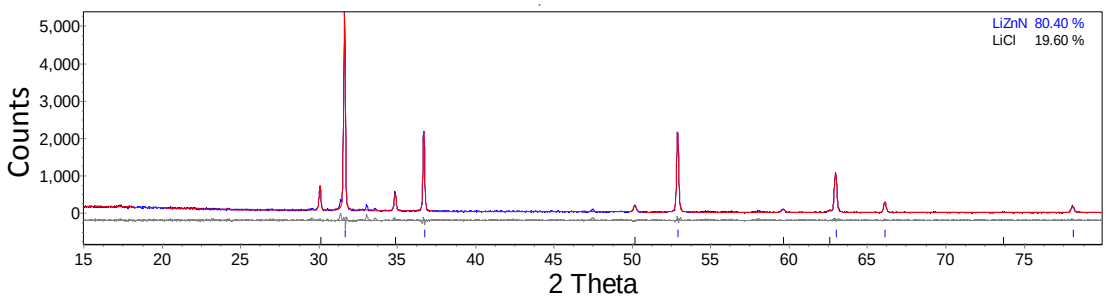

Figure 4.18 *Powder XRD pattern of the products of the reaction of $ZnCl_2$–$6LiNH_2$ at 500 ℃ for 12 hours showing observed (blue), Rietveld fit (red) and difference (grey) plots. Peak positions for refined compounds are shown underneath.*

The proportions of products corresponding to each temperature in the ratios of 1:2 and 1:3 in weight percentages including errors corresponding to each temperature in the ratios of 1:2 and 1:3 have been calculated by Topas software. The values were then converted into molar percent and listed in **Table 4.1**.

Table 4.1 Products of reactions between $ZnCl_2$ and $LiNH_2$ in the ratio of 1:2 and 1:3 at different temperatures.

Products (mole %)	Temperature (°C)							
	250		300		400		500	
	1:2	1:3	1:2	1:3	1:2	1:3	1:2	1:3
$ZnCl_2$	5.21	2.99	-	-	-	-	**-**	**-**
$LiNH_2$	31.12	39.12	-	26.14	-	-	-	-
Li_2NH	27.31	16.11	-	12.24	-	-	-	-
LiCl	33.15	37.38	89.74	49.08	76.08	66.42	81.68	66.06
Zn_3N_2	0.57	2.50	8.58	2.54	11.63	2.69	10.57	-
LiZnN	-	-	-	5.21	8.31	29.88	7.75	32.05
Zn	2.63	1.89	1.68	4.79	3.99	1.01	-	1.89

It can be seen from **table 4.1** that at 250°C $LiNH_2$ was partly decomposed into $LiNH_2$ and Zn_3N_2 was observed in both ratios of 1:2 and 1:3 of $ZnCl_2$:$LiNH_2$. At 300°C the main products of reaction of $ZnCl_2$–$2LiNH_2$ were a mixture of Zn_3N_2 and LiCl along with a small amount of Zn. At this temperature, in the products of reaction of $ZnCl_2$–$3LiNH_2$ there

was an observation of the ternary nitride LiZnN. Li_2NH and remaining $LiNH_2$ were also observed. At 400°C while in the products of the ratio of 1:2 the proportion of Zn_3N_2 is higher than that at 300°C, similar amount of Zn_3N_2 but much greater amount of LiZnN was obtained in the ratio of 1:3. At 500°C there was a remaining of a substantial amount of Zn_3N_2 in the product of the 1:2 ratio but all Zn_3N_2 was converted into LiZnN in the 1:3 ratio.

The data obtained for the different ratios are consistent with the suggestion that the stoichiometric reactions given by equations (4.5), (4.6) and (4.7):

$$3ZnCl_2 + 6LiNH_2 \rightarrow Zn_3N_2 + 6LiCl + 4NH_3 \quad (4.5)$$

(Molar ratio of $ZnCl_2$:$LiNH_2$ = 1:2)

$$Zn_3N_2 + 3LiNH_2 \rightarrow 3LiZnN + 2NH_3 \quad (4.6)$$

Reaction (4.5) occurred from 250 °C to below 500°C. However, from 300°C Zn_3N_2 formed from reaction (4.5) reacted with $LiNH_2$ to form LiZnN as described in reaction (4.6) and this reaction may be complete at 500°C to form LiZnN and LiCl.

Overall reaction:

$$3ZnCl_2 + 9LiNH_2 \rightarrow 3LiZnN + 6LiCl + 6NH_3$$

$$\text{Or } ZnCl_2 + 3LiNH_2 \rightarrow LiZnN + 2LiCl + 2NH_3 \quad (4.7)$$

(Molar ratio of $ZnCl_2$:$LiNH_2$ = 1:3; molar ratio of LiZnN:LiCl = 1:2)

4.3.6 Temperature-Programmed Desorption with Mass Spectrometry (TPD–MS)

The hydrogen desorption properties of the reaction between $ZnCl_2$ and $LiNH_2$ at ratios of 1:2 to 1:6 were tested using the home-built temperature-programmed desorption with mass spectrometry (TPD–MS) apparatus described earlier. $LiNH_2$ and $ZnCl_2$ were ground in the ratios of 1:2 to 1:6 and heated at 2°C/minute to 400°C and held for 2 hours in the TPD apparatus.

4.3.6.1 Reaction in a ratio of 1:2

The powder XRD pattern and proportions of the products of the reactions between $ZnCl_2$ and $LiNH_2$ in the ratio of 1:2 after TPD are shown in ***figure 4.19***. The main reaction occurring was the formation of Zn_3N_2. A very small amount of LiZnN was formed. That may be because while reaction (4.5) occurred slowly, reaction (4.6) also happened. Impurity Li_2O which was present in starting material $LiNH_2$ was also observed. A small amount of Zn was observed.

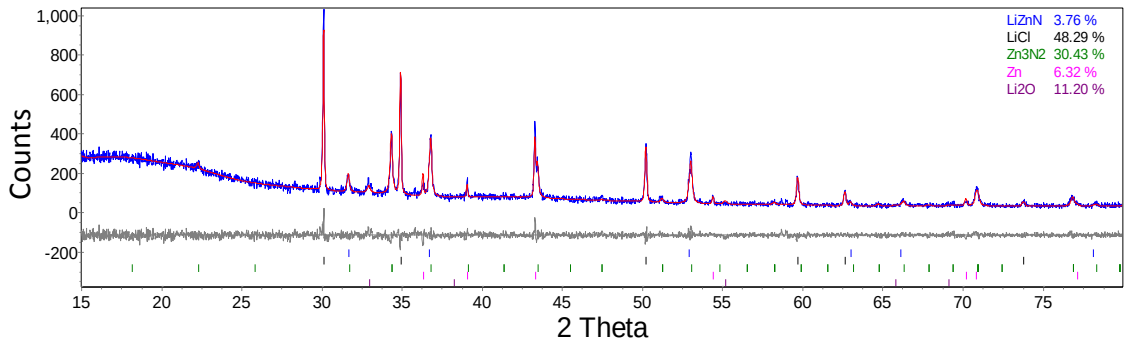

Figure 4.19 *Powder XRD pattern of the products of the reaction of $ZnCl_2$–$2LiNH_2$ heated in the TPD apparatus to 400℃ showing observed (blue), Rietveld fit (red) and difference (grey) plots. Peak positions for refined compounds are shown underneath.*

At about 280°C, there was a broad desorption peak observed for ammonia gas. The amounts of hydrogen and ammonia gas released during TPD are indicated in ***figure 4.20***. This is consistent with reactions (4.5) and (4.6) occurring with release of ammonia gas. A lesser amount of hydrogen gas was also observed beginning above 300°C and peaking at the higher temperature of about 400°C. The appearance of a small amount of hydrogen here may be from the decomposition of NH_3.

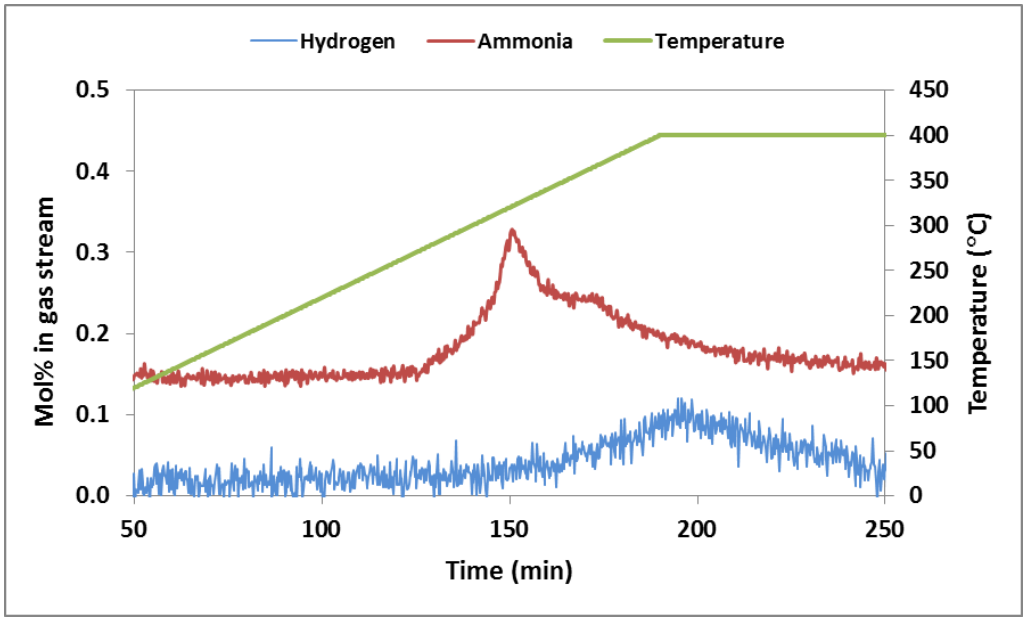

Figure 4.20 *TPD–MS trace of the reaction of $ZnCl_2$–$2LiNH_2$, heated at 2 ℃/minute to 400 ℃, showing traces for hydrogen (blue), ammonia (purple) and temperature (green).*

4.3.6.2 Reaction in a ratio of 1:3

The powder XRD pattern and proportions of products of reactions between $ZnCl_2$ and $LiNH_2$ in the ratio of 1:3 are shown in ***figures 4.21***. There was an observation of LiZnN, LiCl, and Zn also present after reaction in the ratio of 1:2, but Zn_3N_2 was not obtained. A much greater amount of LiZnN was found and the molar ratio of LiZnN: LiCl was ~ 1:2.

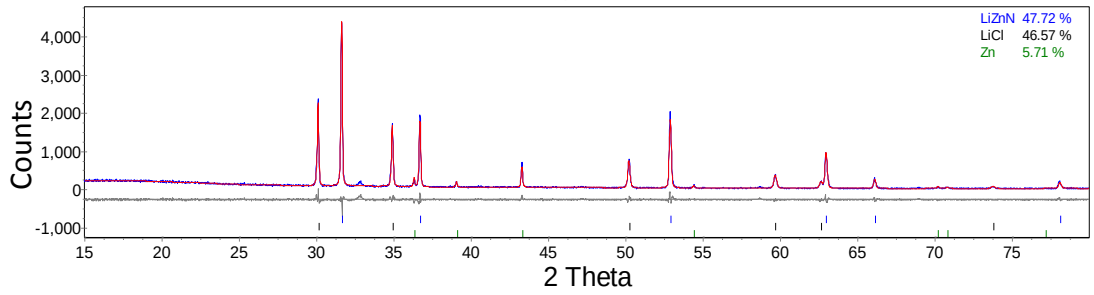

Figure 4.21 *Powder XRD pattern of the products of reaction between $LiNH_2$ and $ZnCl_2$ in the ratio of 1:3 heated in the TPD apparatus to 400 ℃ showing observed (blue), Rietveld fit (red) and difference (grey) plots. Peak positions for refined compounds are shown underneath.*

For the ratio of 1:3, it has been observed that the rate of ammonia release peaked at 300°C with a large amount of ammonia gas obtained. The sharpness of this release suggests that reaction 4.7 may be quicker than 4.6, and therefore Zn_3N_2 formed could be converted into LiZnN in the presence of excess $LiNH_2$.

This result is consistent with reaction (4.7) with a stoichiometric ratio between $ZnCl_2$ and $LiNH_2$ of 1:3. Hydrogen release started at this temperature and gradually increased to 400°C (***figure 4.22***).

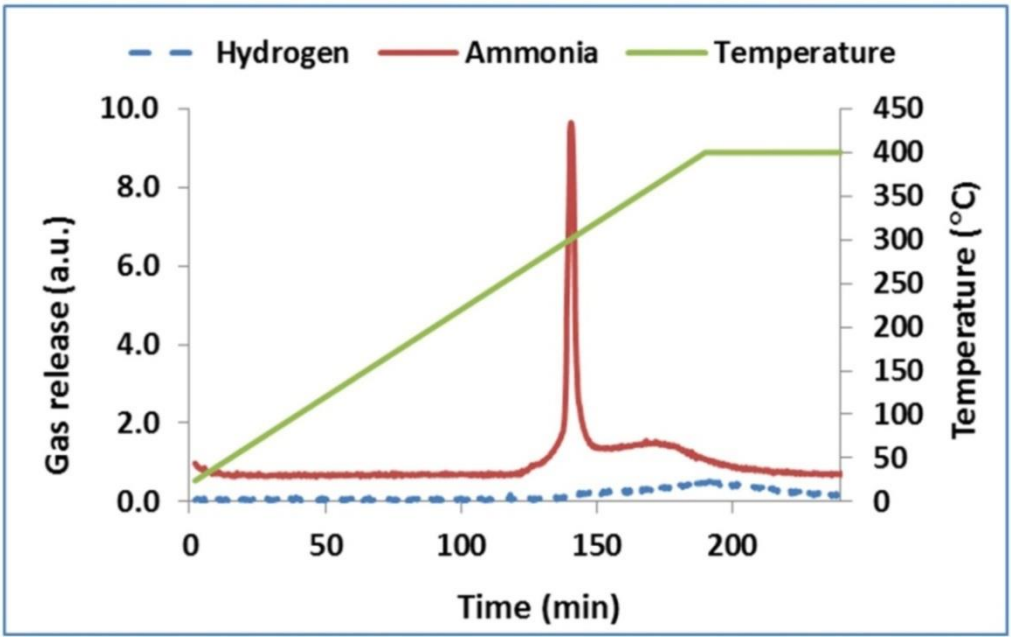

Figure 4.22 *TPD–MS trace of the reaction of $ZnCl_2$ + 3$LiNH_2$, heated at 2 ℃/minute to 400 ℃, showing traces for hydrogen (blue), ammonia (purple) and temperature (green).*

4.3.6.3 Reaction in ratios 1:4, 1:5, and 1:6

Gas release traces at ratios of 1:4 to 1:6 were collected using TPD–MS and shown in ***figure 4.23***. The trace of ammonia release from a ratio of 1:3 is also included for comparison. It can be seen that temperatures of gases release and peaks shapes are similar indicating similar reactions occurred. After the main peak, desorption of NH_3 should be from the decomposition of excess $LiNH_2$ used.

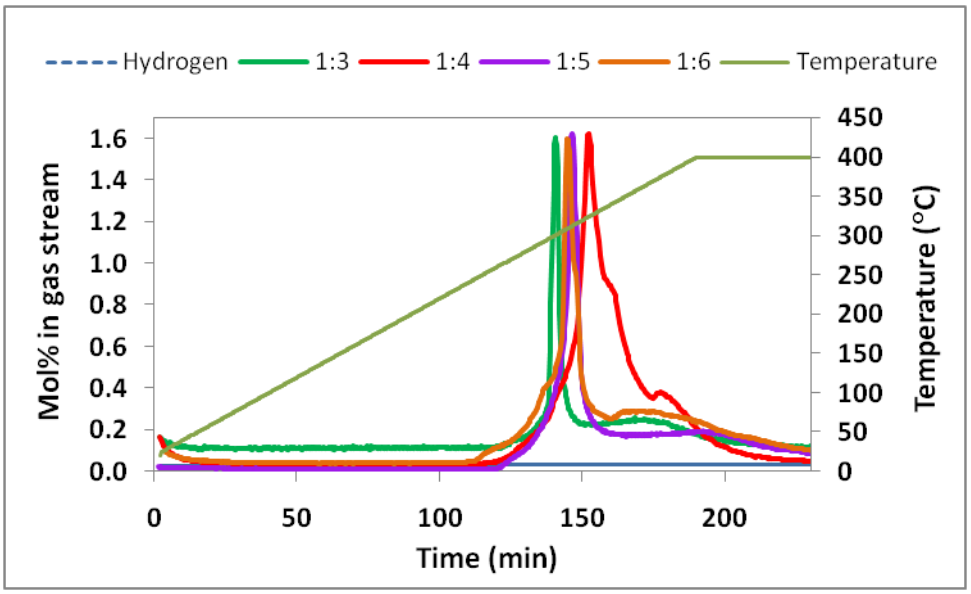

Figure 4.23 *TPD–MS trace of the reaction of $ZnCl_2$ + $nLiNH_2$ (n = 4, 5, 6), heated at 2 ℃/minute to 400 ℃, showing traces for hydrogen (where n = 4) (blue), ammonia and temperature (green). Hydrogen traces where n = 5 and n = 6 are similar to the trace of hydrogen shown above (where n = 4).*

The data obtained, are consistent with the conclusion that $ZnCl_2$ reacts stoichiometrically with $LiNH_2$ at the molar ratios of 1:2 and 1:3 as with different reaction products Zn_3N_2 and LiZnN, respectively and the release of ammonia gas.

4.4 Reaction of $ZnCl_2$ and $LiNH_2$ in the presence of LiH

4.4.1 Powder X-ray Diffraction

The results in the previous section confirmed the reaction scheme proposed above. However, the main gas released was ammonia while our aim was to produce hydrogen. Therefore, a different approach was adopted.

Yu and Ruckenstein [9] proposed that the decomposition reaction of $LiNH_2$ proceeded *via* the release of NH_3 and with the presence of LiH, an ultrafast reaction (less than 25 ms) between LiH and NH_3 would occur to form $LiNH_2$ and H_2.

Therefore, LiH (Sigma Aldrich 95%) was chosen to add into the mixture of $LiNH_2$ and $ZnCl_2$ with the aim of converting NH_3 gas into H_2 based on the reactions (4.7) and (4.8):

$$2LiH + 2NH_3 \rightarrow 2LiNH_2 + 2H_2 \qquad (4.8)$$

The overall reaction between $ZnCl_2$, $LiNH_2$ and LiH would then be the sum of reaction (4.7) and (4.8) as follows:

$$ZnCl_2 + LiNH_2 + 2LiH \rightarrow LiZnN + 2LiCl + 2H_2 \qquad (4.9)$$

4.4.1.1 Reaction at 150℃

Reaction occurred from 150°C, and the products (shown in ***figure 4.24***) were a mixture of Zn and LiCl along with remaining unreacted starting materials $LiNH_2$ and $ZnCl_2$ (α-$ZnCl_2$ and δ-$ZnCl_2$). The presence of Zn at this temperature could not be from direct decomposition of LiZnN, which was confirmed in **section 4.3.1** to decompose at a much higher temperature around 500°C. However, ZnH_2 has been reported to decompose into the elements at 90–120°C [10]. Therefore, it is possible that Zn could be formed from reaction of LiH and $ZnCl_2$ as in equation (4.10):

$$2LiH + ZnCl_2 \rightarrow 2LiCl + Zn + H_2 \qquad (4.10)$$

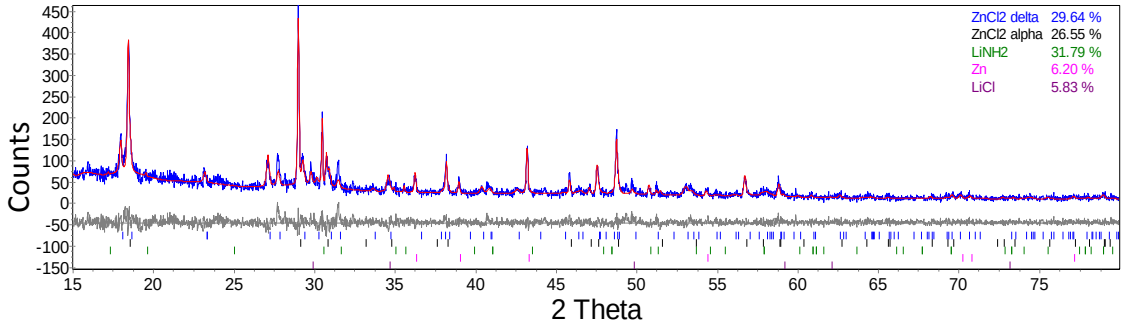

Figure 4.24 *Powder XRD pattern of the products of reaction between $ZnCl_2$, $LiNH_2$ and LiH at 150℃ for 12 hours showing observed (blue), Rietveld fit (red) and difference (grey) plots. Peak positions for refined compounds are shown below.*

4.4.1.2 Reaction at 200℃

At 200°C, a greater amount of Zn was obtained. About 25 wt% of $ZnCl_2$ (δ-$ZnCl_2$) remained unreacted. Most of the $LiNH_2$ present at 150°C was converted into Li_2NH (***figure 4.25***).

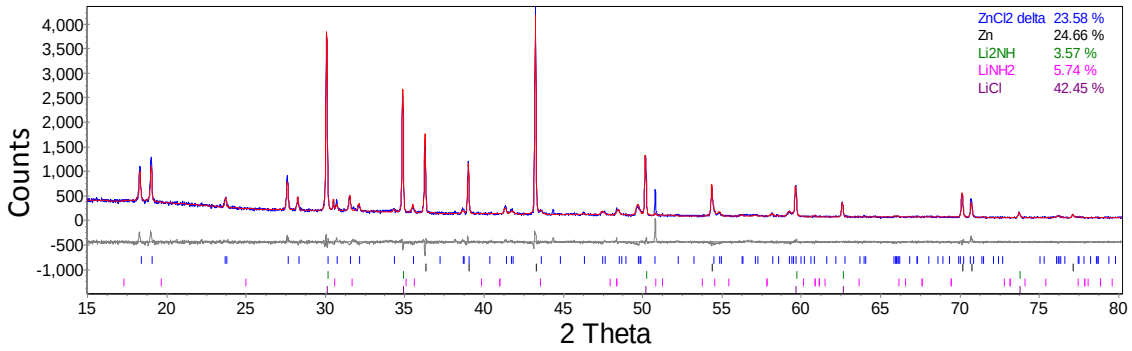

Figure 4.25 *Powder XRD pattern of the products of reaction between $ZnCl_2$, $LiNH_2$ and LiH at 200℃ for 12 hours showing observed (blue), Rietveld fit (red) and difference (grey) plots. Peak positions for refined compounds are shown below.*

4.4.1.3 Reaction at 300℃

The powder XRD pattern of the products of reactions between $ZnCl_2$, $LiNH_2$ and LiH at 300°C for 12 hours is shown in ***figure 4.26***.

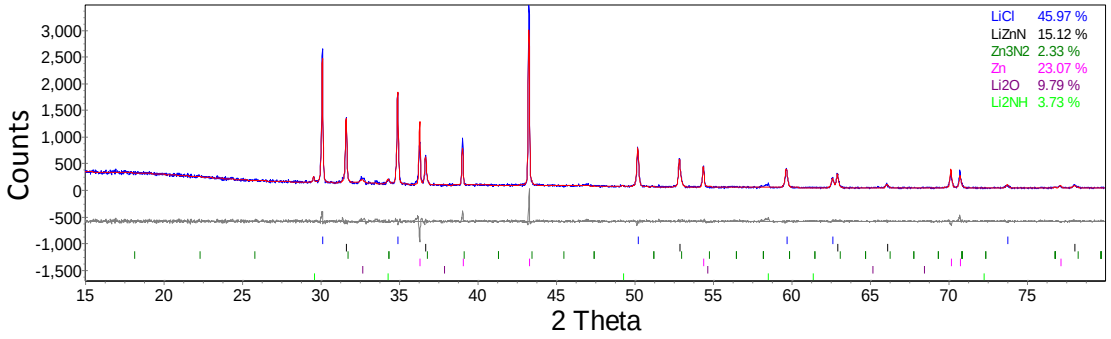

Figure 4.26 *Powder XRD pattern of the products of reaction between $ZnCl_2$, $LiNH_2$ and LiH at 300℃ for 12 hours showing observed (blue), Rietveld fit (red) and difference (grey) plots. Peak positions for refined compounds are shown below.*

The products were significantly different from those of reaction between $LiNH_2$ and $ZnCl_2$ under the same conditions. The addition of LiH into the mixture of $LiNH_2$ and $ZnCl_2$ led to the formation of a much larger amount of Zn than in the absence of LiH besides formation of LiZnN and Zn_3N_2. A small amount of Li_2NH was observed.

4.4.1.4 Reaction at 400℃

At 400°C, the amount of LiZnN was higher while that of Zn was lower (***figure 4.27***).

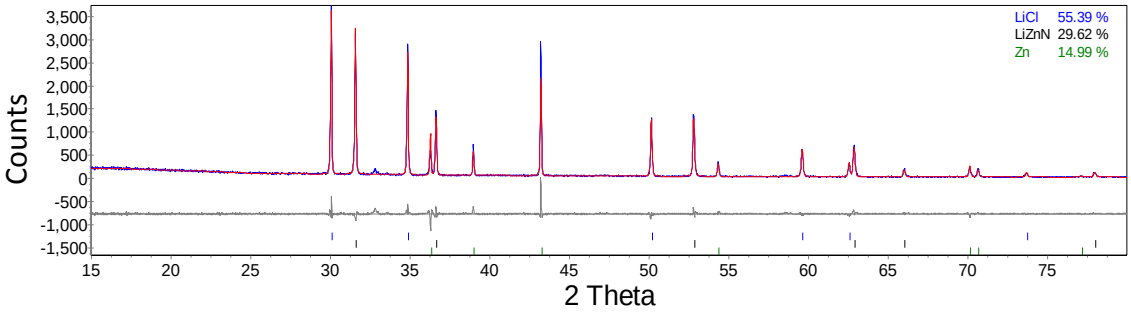

Figure 4.27 *Powder XRD pattern of the products of reaction between $ZnCl_2$, $LiNH_2$ and LiH at 400℃ for 12 hours showing observed (blue), Rietveld fit (red) and difference (grey) plots. Peak positions for refined compounds are shown below.*

4.4.1.5 Reaction at 500℃

At 500°C, besides products obtained at 400°C, a small amount of LiZn appeared. This compound may come from the decomposition of LiZnN, which has been reported by Juza *et al.* [11] and Toyoura *et al.* [12]. This is slightly lower than the temperature it was obtained through reaction of $LiNH_2$ and $ZnCl_2$ alone. The reaction may not be complete with some unidentified peaks present (***figure 4.28***).

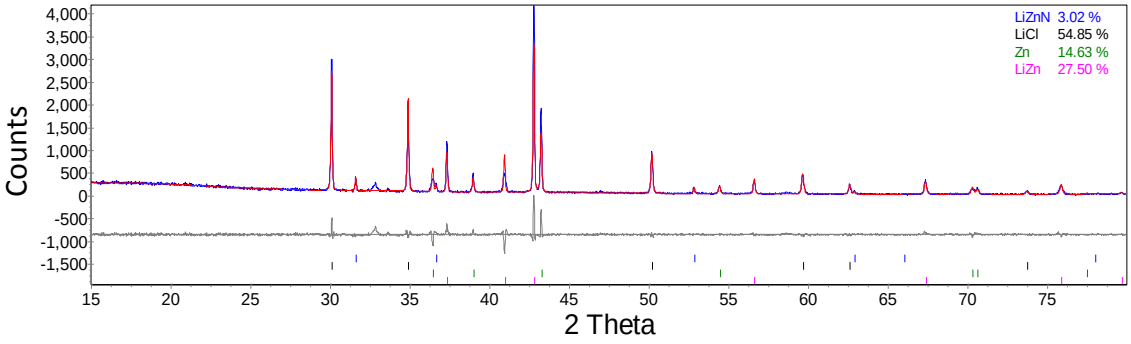

Figure 4.28 *Powder XRD pattern of the products of reaction between $ZnCl_2$, $LiNH_2$ and LiH at 500℃ for 12 hours showing observed (blue), Rietveld fit (red) and difference (grey) plots. Peak positions for refined compounds are shown below.*

4.4.2 Temperature-Programmed Desorption with Mass Spectrometry (TPD–MS)

The hydrogen desorption properties of the reaction between $ZnCl_2$, $LiNH_2$ and LiH in a ratio of 1:1:2 were tested using TPD–MS. All of the samples were heated at 2°C/minute to 400°C and held for 2 hours. Products obtained after TPD were shown in ***figure 4.29.***

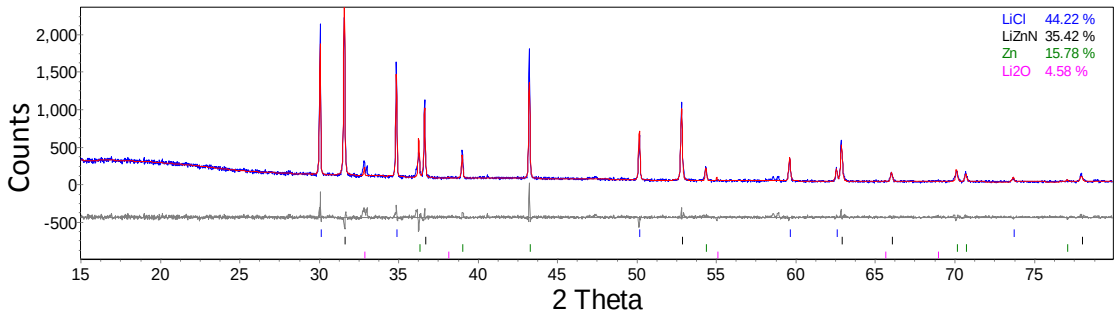

Figure 4.29 *Powder XRD pattern of the products of reaction between $ZnCl_2$, $LiNH_2$ and LiH in the ratio of 1:1:2 heated in the TPD apparatus to 400 ℃ showing observed (blue), Rietveld fit (red) and difference (grey) plots. Peak positions for refined compounds are shown underneath.*

The traces of hydrogen and ammonia gas released during TPD are shown in ***figure 4.30***. The peak present for ammonia gas was at a similar temperature to those of the reactions without LiH but much reduced in intensity. There was a significant change in temperature and amount of hydrogen released. Two peaks at quite low temperatures of about 220°C and 300°C were observed. The peaks of hydrogen and ammonia at around 300°C are consistent with the release of NH_3 gas converted to H_2 by reaction (4.8), and reaction (4.9) occurring overall. The observation of hydrogen from 90°C and peaking at about 220°C was different from the reaction without LiH. Clearly, here a

different reaction pathway is in operation. One possibility is that ZnH_2 was formed transiently from LiH and $ZnCl_2$ and then decomposed into Zn and H_2 as mentioned above.

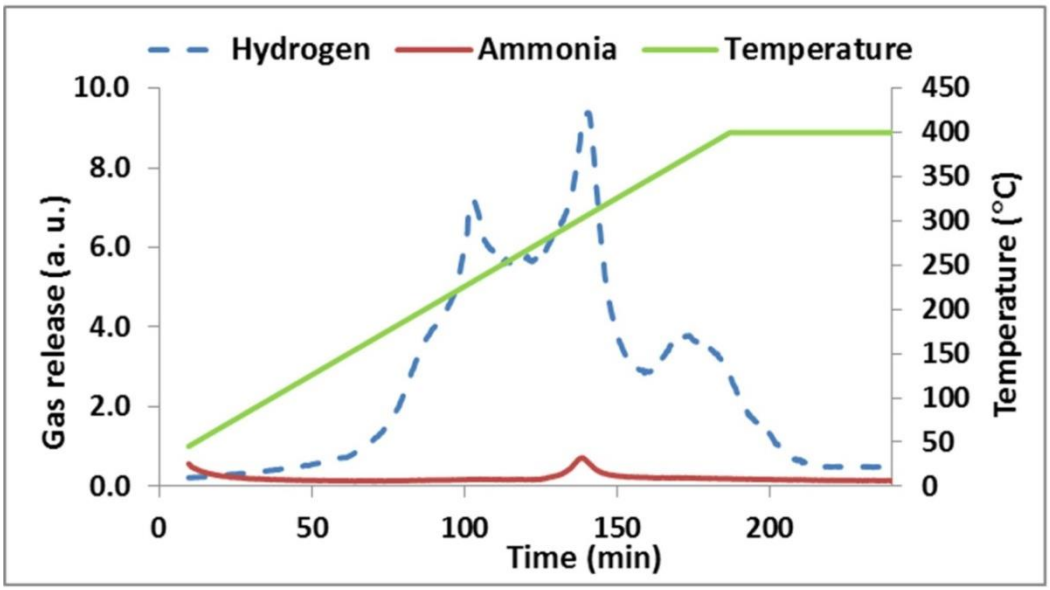

Figure 4.30 *TPD–MS trace of the reaction of $ZnCl_2$ + $LiNH_2$ + 2LiH, heated at 2 ℃/minute to 400 ℃, showing traces for hydrogen (blue), ammonia (purple) and temperature (green).*

4.5 Reaction of $ZnCl_2$ and LiH

In order to check whether Zn and H_2 can be obtained directly from LiH and $ZnCl_2$ at low temperature, reaction between $ZnCl_2$ and LiH in a ratio of 1:2 was investigated at a range of temperature of 100–300°C.

After reaction at 100°C for 1 hour, the products were LiCl and Zn along with a small amount of remaining α-$ZnCl_2$. Results confirmed the occurence of reaction between $ZnCl_2$ and LiH at low temperature of 100°C. There was also a small amount of LiZn which may come from reaction between LiH and Zn (***figure 4.31***).

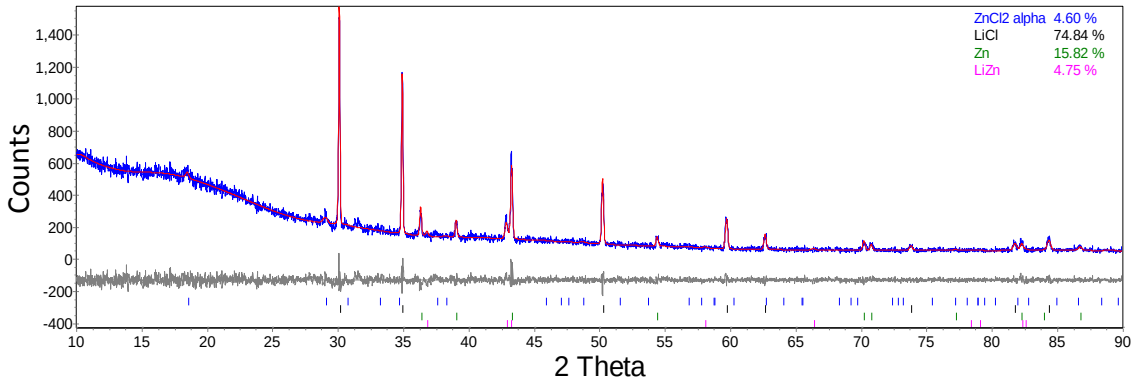

Figure 4.31 *Powder XRD pattern of the products of reaction between $ZnCl_2$ and LiH at 100℃ for 12 hours showing observed (blue), Rietveld fit (red) and difference (grey) plots. Peak positions for refined compounds are shown below.*

The reaction was studied at higher temperatures up to 300°C with the same products obtained. However, there were also some unidentified peaks.

A sample of $ZnCl_2$ and LiH was then measured by TPD–MS. Gas traces of ammonia and hydrogen are shown in ***figure 4.32***.

Hydrogen can be seen to to released at low temperature from around 100°C, peaking around 280°C. The very sharp exothermic desorption peak is consistent with a very fast reaction.

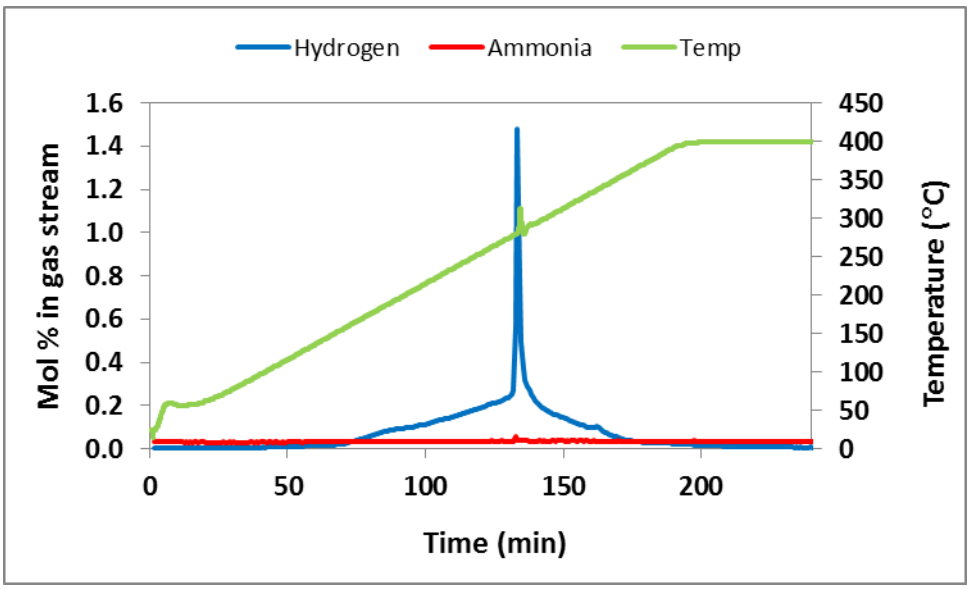

Figure 4.32 *TPD–MS trace of the reaction of $ZnCl_2$ + $LiNH_2$ + 2LiH, heated at 2 ℃/minute to 400 ℃, showing traces for hydrogen (blue), ammonia (purple) and temperature (green).*

4.6 Rehydrogenation

Hydrogenation of mixtures of LiZnN + 2LiCl (from the reaction of $ZnCl_2$ + $3LiNH_2$ at 500°C), was attempted at 200–300°C for 12–24 hours under 90 bar H_2.

Samples were prepared as discussed in chapter 3 and began with a heating temperature of 200°C. No hydrogenated product was observed. A small amount of LiZnN was converted into Zn and LiZn (***figure 4.33***).

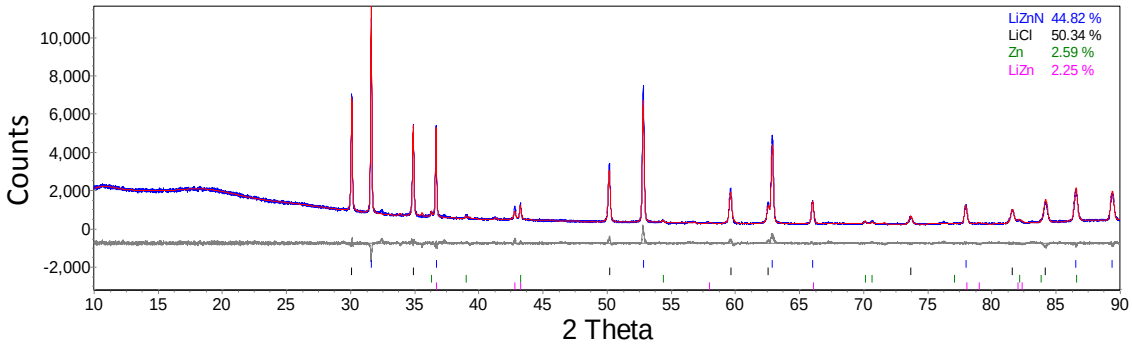

Figure 4.33 *Powder XRD pattern of products from hydrogenation of a mixture of LiZnN and LiCl under 90 bar H_2, at 200 ℃ for 24 hours showing observed (blue), Rietveld fit (red) and difference (grey) plots. Peak positions for refined compounds are shown underneath.*

Hydrogenation was therefore studied at the higher temperature of 300°C. After 20 hours the mixture of LiZnN and LiCl showed the formation of Li_2NH (20 wt%), along with Zn (32 wt%) and Li_2O (3 wt%) in company with residual LiZnN and LiCl (***figure 4.34***). This indicates that rehydrogenation is possible, however, the presence and stability of LiCl may prevent the formation of $ZnCl_2$, and therefore full reversibility is unlikely to be possible.

The reaction may occur as equation 4.11:

$$2LiZnN + 2H_2 \rightarrow Li_2NH + Zn + NH_3 \qquad (4.11)$$

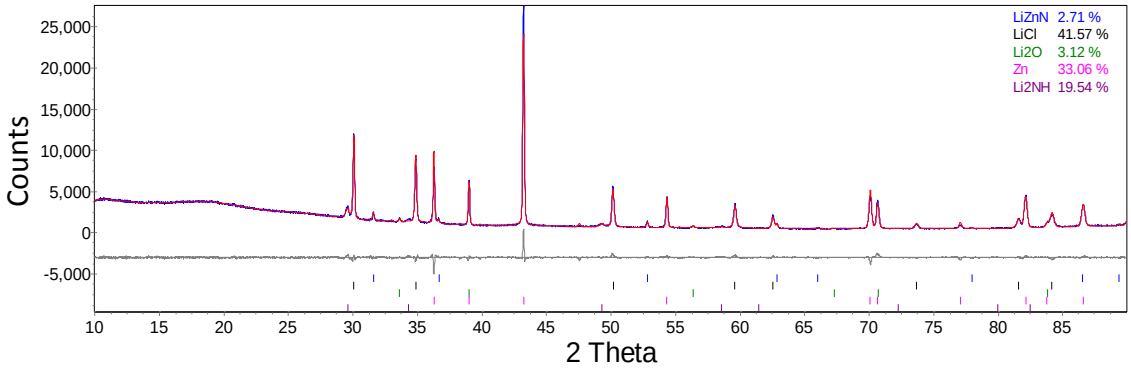

Figure 4.34 *Powder XRD pattern of products from hydrogenation of a mixture of LiZnN and LiCl under 90 bar H_2, at 300 ℃ for 20 hours showing observed (blue), Rietveld fit (red) and difference (grey) plots. Peak positions for refined compounds are shown underneath.*

4.7 Mg-doping

A mixture of LiZnN and LiCl obtained from reaction between $ZnCl_2$ and $LiNH_2$, did not perform well with regard to hydrogen absorption, while LiMgN is known to have good rehydrogenation properties [13-15]. For that reason, Mg-doping of LiZnN was attempted to try and perhaps improve the reversibility of the Li–Zn–N system. $MgCl_2$ was used to replace some of the $ZnCl_2$ in the reaction with $LiNH_2$.

4.7.1 Powder Diffraction Study

Samples of $(1-n)ZnCl_2 + nMgCl_2 + 3LiNH_2$ (where n = 0; 0.1; 0.2; 0.3; 0.4; 0.5) were heated up to 500°C and held for 12 hours.

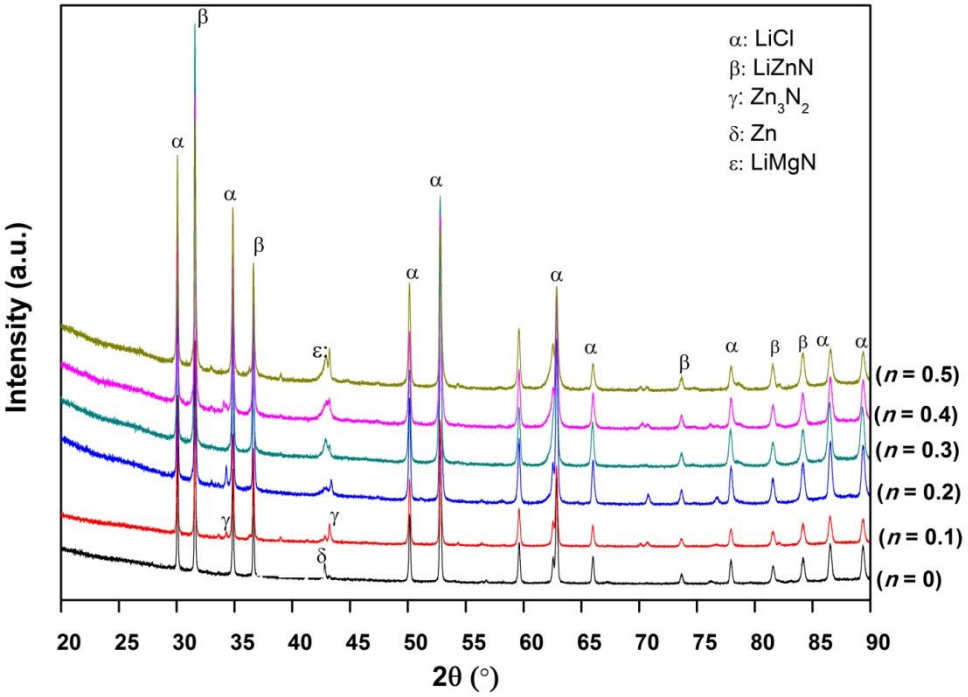

Figure 4.35 *Powder XRD patterns of the products of reactions $(1-n)ZnCl_2 + nMgCl_2 + 3LiNH_2$ at 500 ℃ for 12 hours.*

Powder XRD patterns of the products of the reactions are shown in ***figure 4.35***.

On addition of 0.1$MgCl_2$, the main products of reaction were LiZnN and LiCl, similar to those of reaction between $ZnCl_2$ + 3$LiNH_2$ along with small amount of Zn and LiZn which may come from the decomposition of LiZnN. However, a small amount of Zn_3N_2 was also obtained. There was also a small amount of Li_2O impurity (***figure 4.36***). When *n* = 0.2, the reaction products were similar to *n* = 0.1 but LiZn was not observed.

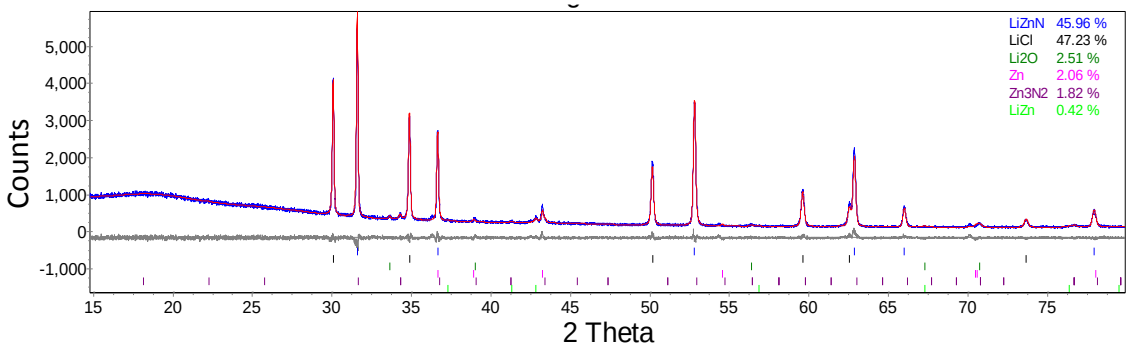

Figure 4.36 *Powder XRD patterns of the products of reactions 0.9$ZnCl_2$ + 0.1$MgCl_2$ + 3$LiNH_2$ at 500℃ for 12 hours showing observed (blue), Rietveld fit (red) and difference (grey) plots. Peak positions for refined compounds are shown underneath.*

When 0.3$MgCl_2$ was used Zn_3N_2 was not observed. Products were LiZnN and LiCl and a small amount of Zn (***figure 4.37***).

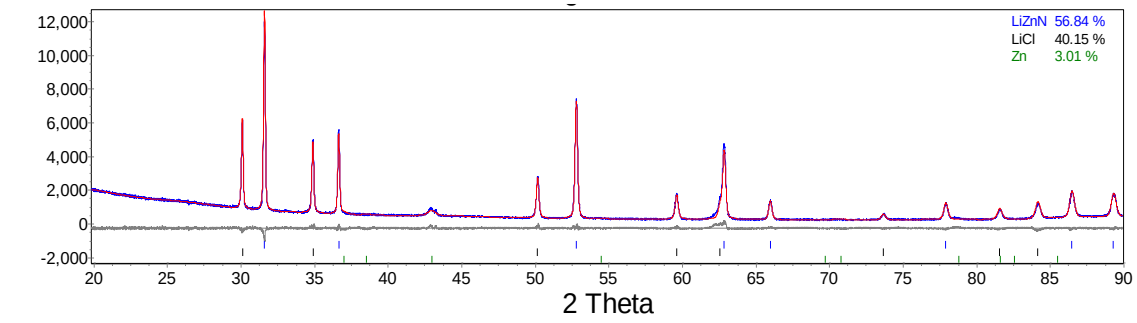

Figure 4.37 *Powder XRD patterns of the products of reactions $0.7ZnCl_2 + 0.3MgCl_2 + 3LiNH_2$ at 500℃ for 12 hours showing observed (blue), Rietveld fit (red) and difference (grey) plots. Peak positions for refined compounds are shown underneath.*

When *n* = 0.4, besides LiZnN, LiCl, and Zn there was an observation of a cubic phase of LiMgN I2$_1$3 in the products (***figure 4.38***). More $MgCl_2$ used with *n* = 0.5 products were similar to *n* = 0.4 but the amount of LiMgN was slightly higher (~ 9 wt%).

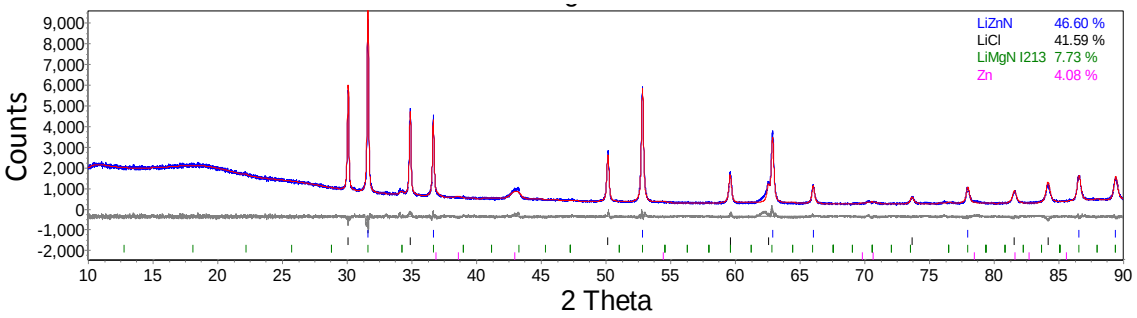

Figure 4.38 *Powder XRD patterns of the products of reactions $0.6ZnCl_2 + 0.4MgCl_2 + 3LiNH_2$ at 500℃ for 12 hours showing observed (blue), Rietveld fit (red) and difference (grey) plots. Peak positions for refined compounds are shown underneath.*

4.7.2 Rietveld Refinement

The lattice parameter of LiZnN obtained from products of reactions $(1-n)ZnCl_2 + nMgCl_2 + 3LiNH_2$ at 500°C for 12 hours and the occupancies of atoms in LiZnN were refined and shown in **table 4.2**.

Table 4.2 The lattice parameter of LiZnN and the occupancies of atoms in LiZnN obtained from products of reactions $(1-n)ZnCl_2 + nMgCl_2 + 3LiNH_2$

$MgCl_2$ used	**Lattice parameter of LiZnN (Å)**	**Occupancy**	
		Zn site	**Mg in Zn site**
n = 0	4.89438(7)		
n = 0.1	4.89958(4)	0.702(12)	0.298(12)
n = 0.2	4.89902(3)	0.701(9)	0.299(9)
n = 0.3	4.90198(5)	0.733(9)	0.267(9)
n = 0.4	4.89838(7)	0.742(13)	0.258(13)
n = 0.5	4.89847(7)	0.733(15)	0.267(15)

The lattice parameter of LiZnN was slightly increased when $0.1MgCl_2$ was used, from 4.89438(7) Å to 4.89958(4) Å. Values of Li site and N did not change when being refined then they were set to be 1. A presence of Mg in Zn site was examined. Value of Zn in Zn

site is 0.702(12) and value of Mg in Zn site is 0.298(12). The results suggest a compositional difference.

The lattice parameter of LiZnN when *n* = 0.2, 4.89902(3) Å, is nearly the same as value of that when *n* = 0.1. Similar occupancy values of Zn and Mg to those of *n* = 0.1 were observed, which are 0.701(9) and 0.299(9) respectively.

When *n* = 0.3, the lattice parameter of LiZnN (4.90198(5) Å) and the occupancy of Zn in Zn site (0.733(9)) are slightly higher than the values of $n \leq 0.2$.

However, the lattice parameter of LiZnN becomes smaller when more $MgCl_2$ (*n* = 0.4 and *n* = 0.5) was used. In a comparison to the value of occupancy of Zn in Zn site when *n* = 0.3, value of that when *n* = 0.4 is higher while that is the same when *n* = 0.5. Values collected were then presented in ***figure 4.39.***

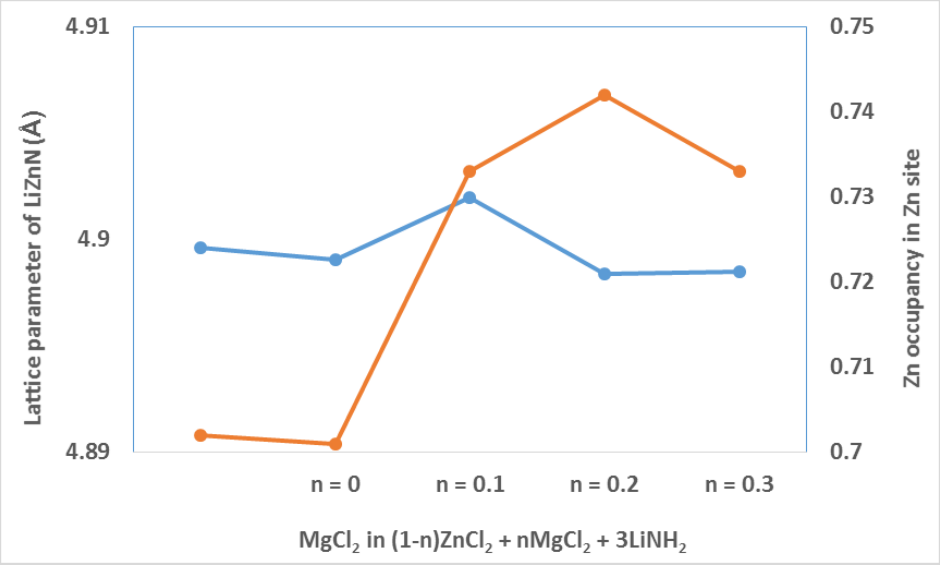

Figure 4.39 *Rietveld refinement values of lattice parameter of LiZnN and Zn occupancy in Zn site in LiZnN after reaction of* $(1-n)ZnCl_2 + nMgCl_2 + 3LiNH_2$ *(1-n).*

4.7.3 Hydrogenation

Products from reaction of $0.5ZnCl_2 + 0.5MgCl_2 + 3LiNH_2$ at 500°C for 12 hours were rehydrogenated under 90 bar hydrogen at 300°C for 24 hours. Similar products to those from the reaction of $ZnCl_2 + MgCl_2 + 3LiNH_2$ were obtained. The hydrogenation products were Li_2NH and Zn. LiCl and a small amount of LiZnN remained unreacted (***figure 4.40***).

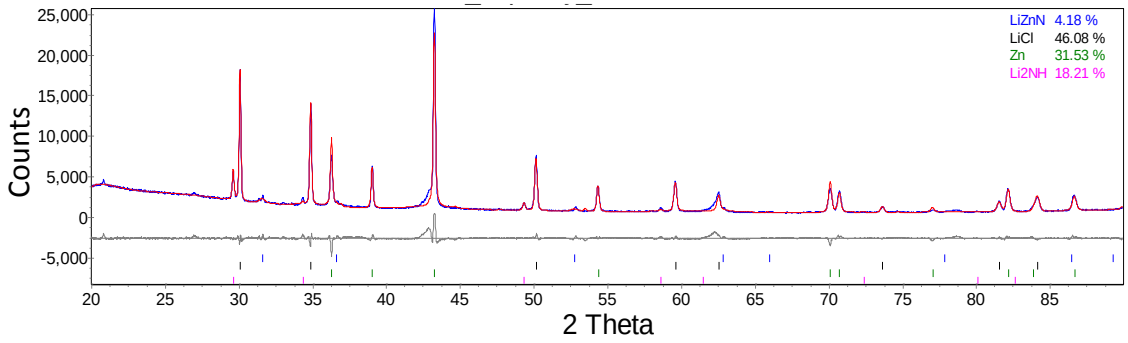

Figure 4.40 *Powder XRD pattern of products from hydrogenation of a mixture of LiZnN and LiCl (obtained from the reaction of reactions $0.5ZnCl_2 + 0.5MgCl_2 + 3LiNH_2$ at 500 ℃ for 12 hours) under 90 bar H_2, at 300 ℃ for 20 hours showing observed (blue), Rietveld fit (red) and difference (grey) plots. Peak positions for refined compounds are shown underneath.*

In summary, with a replacement of $ZnCl_2$ in the reaction of $ZnCl_2 + 3LiNH_2$ by different amounts of $MgCl_2$, the lattice parameter of LiZnN was changed. Also, there was an observation of Mg in the Zn site in LiZnN. However, Li–Zn–N after doping did not show an improvement in its the hydrogenation properties.

4.8 Conclusions

Reactions of $ZnCl_2$ + *n*$LiNH_2$ at a range of molar ratios and temperatures gave a mixture of Zn_3N_2 and LiZnN as products; no stable amide chloride, imide chloride or nitride chloride phases were identified. Temperature-programmed desorption with mass spectrometry (TPD–MS) showed that the main gas emitted was ammonia (NH_3). The addition of lithium hydride (LiH) changed the main gaseous product from NH_3 to H_2, which was released at a low temperature beginning around 90°C. Mixtures of LiZnN and LiCl reacted with H_2 at 300°C to form Li_2NH and zinc metal. Mg-doping to Li–Zn–N showed a change in lattice parameter of this compound but no enhancement of hydrogenation properties.

References

[1] P. Chen, Z. Xiong, J. Lou, J. Lin and K.L. Tan, *J. Phys. Chem. B*, 2003, 107, 10967–10970.

[2] T. Ichikawa, S. Isobe, N. Hanada, H. Fujii, *J. Alloys Comp.,* 2004*,* 365, 271–276.

[3] S. Isobe, T. Ichikawa, N. Hanada, H. Y. Leng, M. Fichtner, O. Fuhr, H. Fujii, *J. Alloys Comp.*, 2005, 404–406, 439–442.

[4] P. A. Chater, P. A. Anderson, J. W. Prendergast, A. Walton, V. S. J. Mann, D. Book, W. I. F. David, S. R. Johnson, P. P. Edwards, *J. Alloys Comp.,* 2007, 446–447, 350–354.

[5] P. A. Anderson, P. A. Chater, D. R. Hewett and P.R. Slater, *Faraday Discuss.,* 2011, 151, 271–284.

[6] R. A. Davies, P. A. Anderson, *Int. J. Hydrogen Energy,* 2015, 40, 3001–3005.

[7] F.E. Pinkerton, *J. Alloys and Comp.*, 2005, 400, 76–82.

[8] J. Zhang, Y.H. Hu, *Ind. Eng. Chem. Res.,* 2001, 50, 8058–8064.

[9] Y. H. Hu and E. Ruckenstein, *J. Phys. Chem. A,* 2003, 107, 9737–9739.

[10] E. Wiberg, W. Henle, *Z. Naturforsch*., 1951, 6b, 393.

[11] V. R. Juza and F. Hund, *Z. Anorg. Allg. Chem.*, 1948, 257, 1–13.

[12] K .Toyoura, T. Goto, K. Hachiya, R. Hagiwara, *J. Electrochem. Soc.*, 2006, 153, G83–G86.

[13] Z. T. Xiong, G. T. Wu, H. J. Hu, P. Chen, *Adv. Mater.,* 2004, 16, 1522–1525.

[14] J. Lu, Y. J. Choi, Z. Z. Fang, H. Y. Sohn, *J. Power Sources,* 2010, 195, 1992–1997.

[15] W. Lou, S. Sickafoose, *J. Alloys Comp.*, 2006, 407, 274–281.

Chapter 5: Chloride-free LiZnN system

5.1 Introduction

In chapter 4, it was shown that LiZnN was obtained in the products of the reaction between $ZnCl_2$ and $LiNH_2$ and that it could be rehydrogenated. However, it was thought that the presence of LiCl in the product, which has very high lattice energy, may prevent the reaction from being reversible. Moreover, LiZnN is known to have some similar structure properties to a polymorph of LiMgN (zinc blende-like structure, a = 4.955(5) Å for LiMgN and a = 4.902(5) Å for LiZnN) [1–2], which has good hydrogen storage properties as mentioned in chapter 4. It was suggested in reaction (5.1) that LiZnN formed through reaction between Zn_3N_2 and $LiNH_2$.

$$Zn_3N_2 + 3LiNH_2 \rightarrow 3LiZnN + 2NH_3 \qquad (5.1)$$

For these reasons, in this chapter, reaction (5.1) was investigated to see whether zinc nitride would indeed react with lithium amide to form the ternary nitride LiZnN. The reaction between Zn_3N_2 and $LiNH_2$ in the presence of LiH under different conditions was studied as an alternative synthesis route. The hydrogenation and cyclability of the products obtained, chloride free in this case, were also investigated.

5.2 Experimental

Zn_3N_2 (Sigma-Aldrich, 99.99%) and $LiNH_2$ (Sigma-Aldrich, 95%) were ground together in an argon-filled glove box (O_2 content < 5 ppm, H_2O < 1 ppm) and heated under argon

gas at heating rate of 2°C/minute to different temperatures and kept at the set temperature for up to 24 hours.

The cyclability of the Li-Zn-N system was investigated by rehydrogenation in a hydrogenator, and intelligent gravimetric analyser (IGA) and Sieverts' method measurements. The crystal structure of LiZnN prepared was analysed through Rietveld refinement as described in chapter 2.

For QPA analysis, where possible, atomic coordinates and thermal parameters were taken from reported structures and in some cases attempts were made to refine the atomic positions and site occupancies of the majority phases.

5.3 Reaction between Zn_3N_2 and $LiNH_2$

5.3.1 Reaction between Zn_3N_2 and $LiNH_2$ in a ratio of 1:3 at 300–500°C

In order to check whether the reaction (4.6) was plausible, Zn_3N_2 and $LiNH_2$ were mixed in a 1:3 molar ratio of Zn_3N_2:$LiNH_2$ as starting materials. The samples were then studied after heating at 300–500°C for up to 24 hours.

At 300°C the reaction may not occur as LiZnN was not observed but starting materials. Reaction occurred slowly at 400°C with the observation of about 27 wt% LiZnN along with unreacted starting materials Zn_3N_2 and $LiNH_2$. There was also a very small amount of Zn (***figure 5.1).***

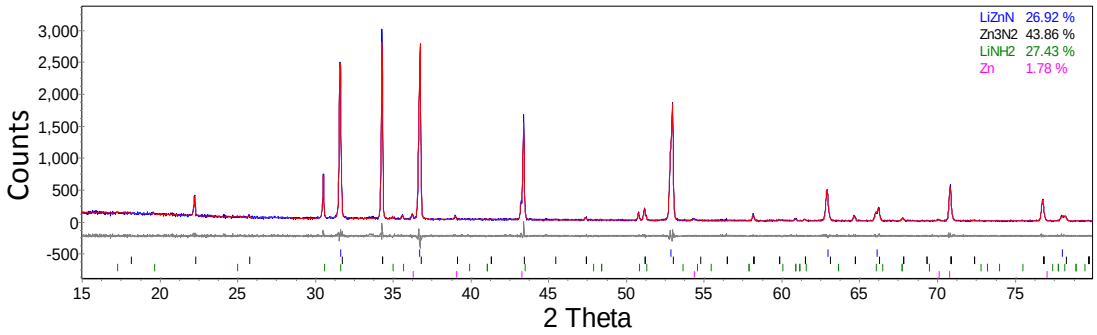

Figure 5.1 *Powder XRD pattern of the products of reaction of Zn_3N_2 + 3$LiNH_2$ at 400℃ for 12 hours showing observed (blue), Rietveld fit (red) and difference (grey) plots. Peak positions for refined compounds are shown underneath.*

After a 12 hour reaction at 500°C almost all the product was LiZnN (~ 92 wt%) with a small proportion of remaining Zn_3N_2 (~ 8 wt%) (***figure 5.2***).

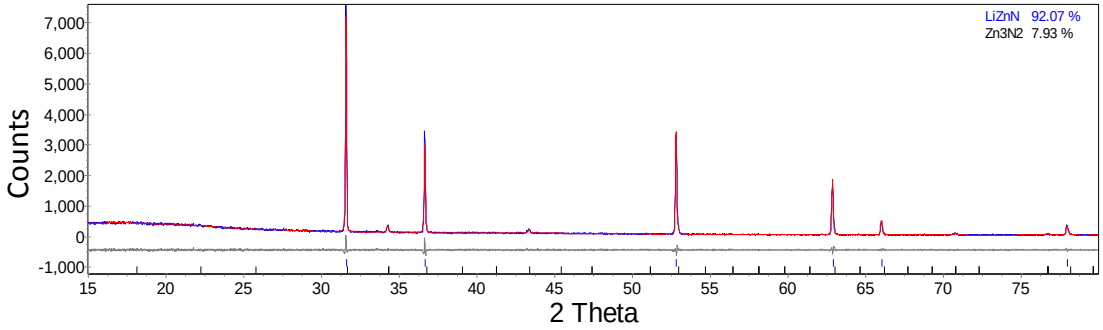

Figure 5.2 *Powder XRD pattern of the products of reaction of Zn_3N_2 + 3$LiNH_2$ at 500℃ for 12 hours showing observed (blue), Rietveld fit (red) and difference (grey) plots. Peak positions for refined compounds are shown underneath.*

A longer reaction time of 24 hours was applied to study whether the remaining Zn_3N_2 could be converted into LiZnN. However, there was still a small amount of Zn_3N_2 unreacted (~ 6 wt%) (***figure 5.3***).

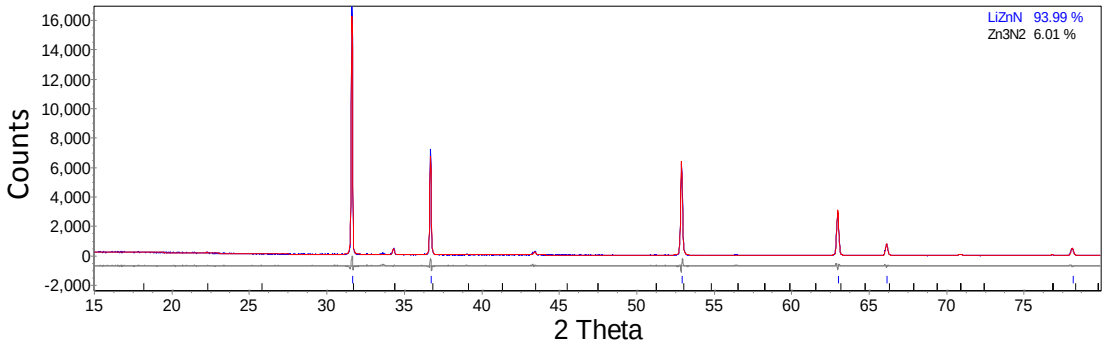

Figure 5.3 *Powder XRD pattern of the products of reaction of Zn_3N_2 + 3$LiNH_2$ at 400℃ for 12 hours showing observed (blue), Rietveld fit (red) and difference (grey) plots. Peak positions for refined compounds are shown underneath.*

5.3.2 Second firing of the products of reaction in a ratio of 1:3 with additional 10 wt% $LiNH_2$

To convert the rest of the Zn_3N_2 in the products of the reaction between Zn_3N_2 and $LiNH_2$ at 500°C for 12 hours into LiZnN, a small amount of the products were mixed with $LiNH_2$ in a weight ratio of 90%:10% and held at 500°C for up to 12 hours. After a 6 hour reaction the remaining Zn_3N_2 was changed into LiZnN and pure LiZnN was obtained (***figure 5.4***).

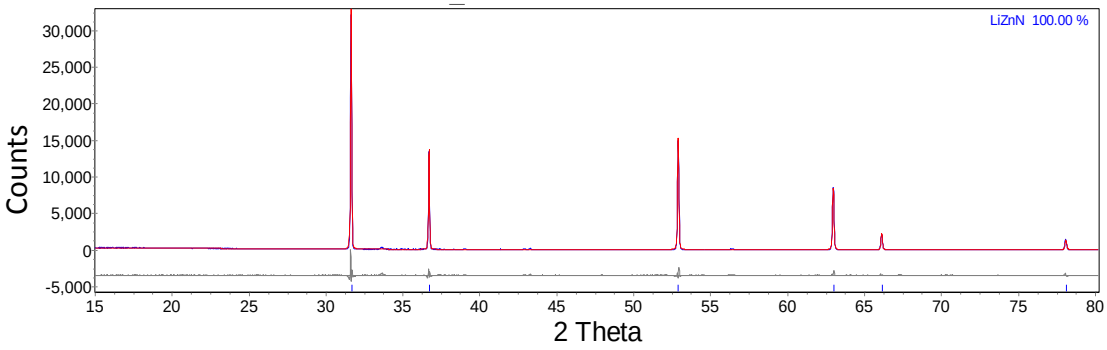

Figure 5.4 *Powder XRD pattern of the products of reaction between LiZnN and $LiNH_2$ in a ratio 1:3 with 10% additional $LiNH_2$ at 500℃ for 6 hours showing observed (blue), Rietveld fit (red) and difference (grey) plots. Peak positions for refined compounds are shown underneath.*

5.3.3 Reaction between Zn_3N_2 and $LiNH_2$ with excess $LiNH_2$

The reaction between Zn_3N_2 and $LiNH_2$ at 500°C for 12 hours was examined with 10–40% excess $LiNH_2$. The remaining Zn_3N_2 decreased with increasing amount of $LiNH_2$. With an approximate ratio of $1Zn_3N_2$:$4LiNH_2$, after a 12 hour reaction, phase-pure LiZnN was obtained (***figure 5.5***). It was reported in literature that LiZnN was obtained after 1 hour and LiZnN was decomposed about 500°C [3]. Therefore, a reaction of Zn_3N_2 + $4LiNH_2$ at 490°C for 1 hour was also studied and pure LiZnN was also achieved.

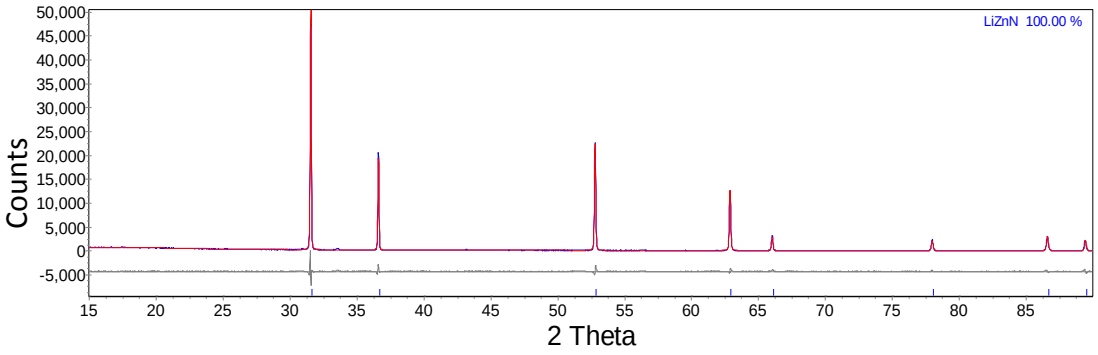

Figure 5.5 *Powder XRD pattern of the products of reaction of Zn_3N_2 + 4$LiNH_2$ at 490℃ for 1 hour showing observed (blue), Rietveld fit (red) and difference (grey) plots. Peak positions for refined compounds are shown underneath.*

In summary, LiZnN could be synthesized via the reaction of Zn_3N_2 and $LiNH_2$ in an approximate molar ratio of 1:4 at 490°C after an hour reaction.

5.3.4 Zn_3N_2 + Li_3N

It was decided to investigate whether LiZnN could be synthesized more easily through direct reaction of Zn_3N_2 and Li_3N *via* following equation:

$$Zn_3N_2 + Li_3N \rightarrow 3LiZnN \qquad (5.2)$$

The reaction between Zn_3N_2 and Li_3N under ammonia gas flow was reported to produce LiZnN by Juza *et al.* [3]. However, ratio of Zn_3N_2:Li_3N used in starting materials and purity of LiZnN were not reported.

In this study, Zn_3N_2 and Li_3N are mixed in a molar ratio of 1:1 and heated up to 500°C for 24 hours under argon gas flow. After 12 hour reaction at 500°C LiZnN was obtained but about 19 wt% Zn_3N_2 remained. The reaction was studied at a longer time of 24 hours. Besides LiZnN, there was an observation of about 8 wt% Zn_3N_2 in the products.

When 20% excess $LiNH_2$ was used, products of the reaction of Zn_3N_2 + Li_3N heated to 500°C for 12 hours still contained a small amount (6 wt%) of unreacted Zn_3N_2 (***figure 5.6***).

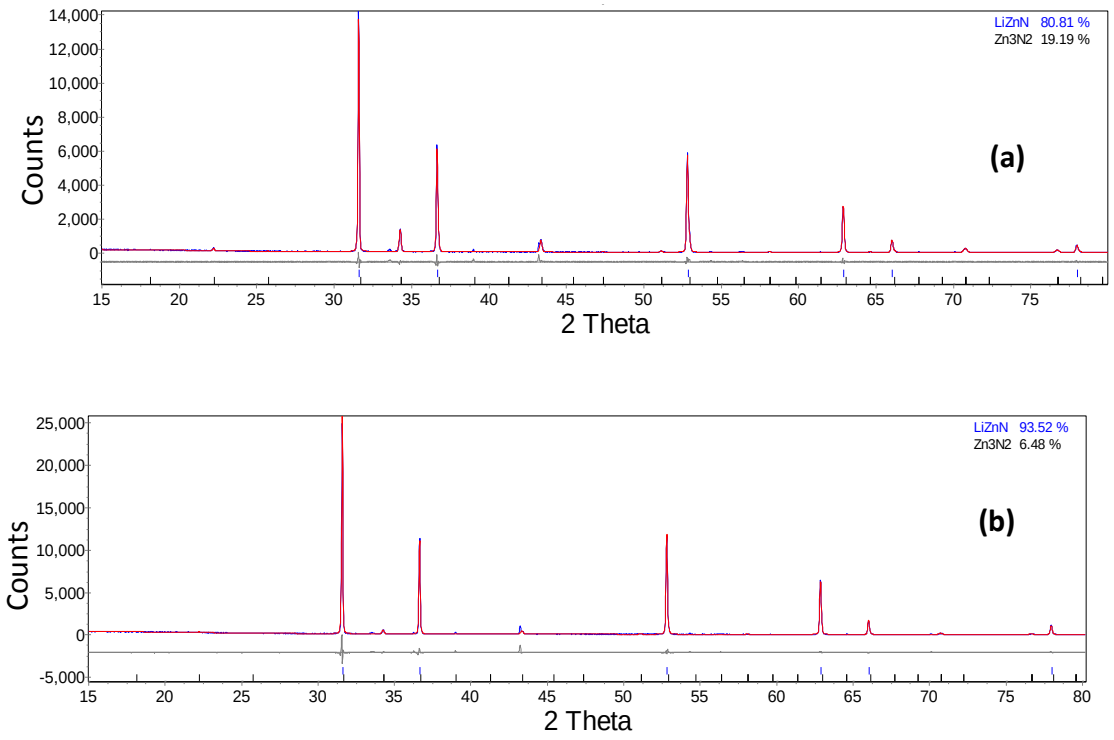

Figure 5.6 *Powder XRD pattern of the products of reaction of Zn_3N_2 + Li_3N in a molar ratio of 1:1* ***(a)*** *and 20% excess Li_3N* ***(b)*** *at 500 ℃ for 12 hours showing observed (blue), Rietveld fit (red) and difference (grey) plots. Peak positions for refined compounds are shown underneath.*

5.3.5 Temperature-Programmed Desorption with Mass Spectrometry (TPD–MS)

The hydrogen desorption properties of the reaction between Zn_3N_2 and $LiNH_2$ at molar ratios of 1:3 and 1:4 were tested using TPD–MS. The sample was heated at 2°C min^{-1} to 400°C and held for 2 hours.

Similar results were obtained for both ratios with the main product of LiZnN along with remaining Zn_3N_2 and Li_2O impurity but a larger amount of LiZnN and smaller amount of Zn_3N_2 were seen in the ratio of 1:4. The presence of unreacted Zn_3N_2 indicated that the reactions did not go to completion under TPD conditions. The powder XRD patterns and proportions of the products of the reaction between Zn_3N_2 and $LiNH_2$ in the ratio of 1:4 after TPD are shown in ***figure 5.7***.

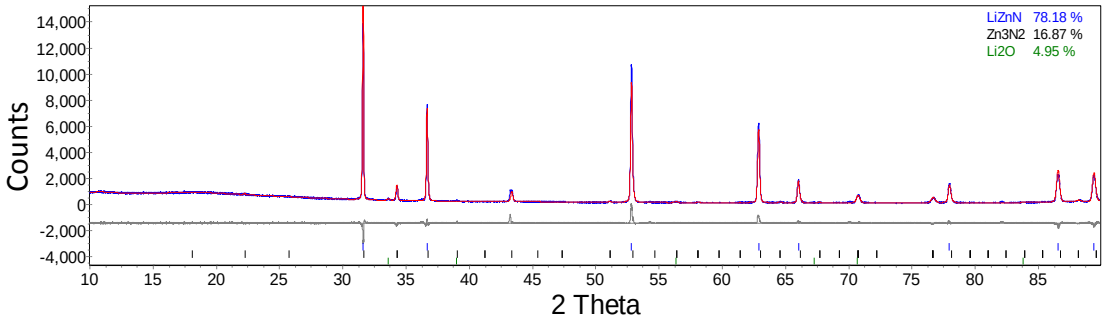

Figure 5.7 *Powder XRD pattern of the products of reaction of Zn_3N_2 + 4$LiNH_2$ heated in the TPD apparatus at 400℃ for 2 hours showing observed (blue), Rietveld fit (red) and difference (grey) plots. Peak positions for refined compounds are shown underneath.*

For both ratios, ammonia was the main gas released while no hydrogen release was observed from this reaction. At about 370°C a desorption peak of ammonia gas was observed. Amounts of hydrogen and ammonia gas released during TPD of the reaction of Zn_3N_2 + 4$LiNH_2$ are indicated in ***figure 5.8***. This is consistent with reaction (5.1) occurring with release of ammonia gas, though it is possible that some of the ammonia may come from a decomposition of excess $LiNH_2$.

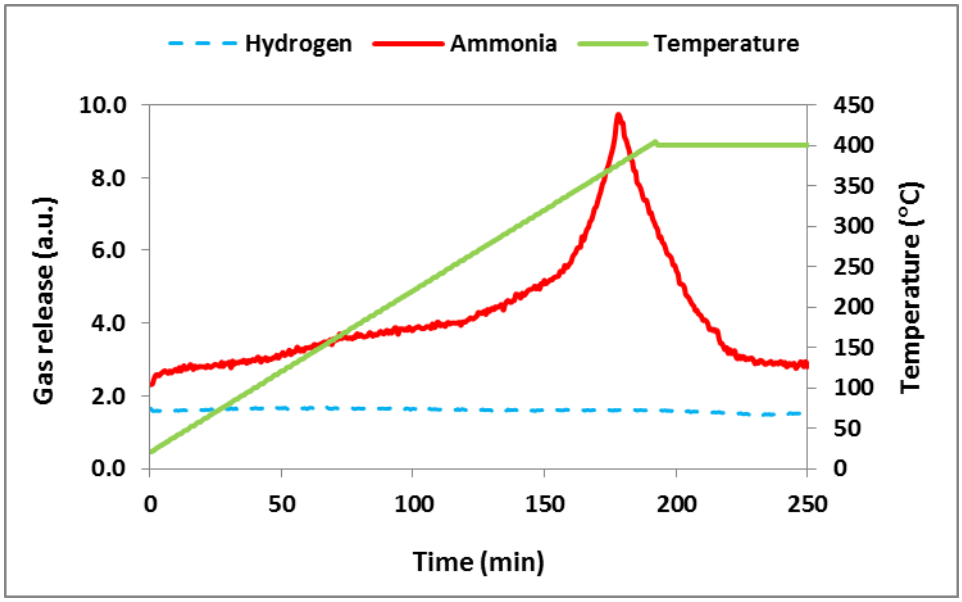

Figure 5.8 *TPD–MS trace of the reaction of Zn_3N_2 + 4$LiNH_2$ heated at 2 °C min^{-1} to 400 °C, showing traces for hydrogen (blue), ammonia (purple) and temperature.*

Taken together the data obtained from powder XRD diffraction and TPD–MS measurements appear to confirm reaction of Zn_3N_2 and $LiNH_2$ to form LiZnN and NH_3 gas.

5.4 Reaction of Zn_3N_2 and $LiNH_2$ in the presence of LiH

The reaction between Zn_3N_2 and $LiNH_2$ was confirmed to occur to form LiZnN with the release of ammonia gas. As discussed in chapter 4, in order to convert ammonia gas into hydrogen, LiH was added to the mixture of Zn_3N_2 and $LiNH_2$ in a molar ratio of 1:1:2.

The reactions between Zn_3N_2, $LiNH_2$, and LiH was expected to occur through the following reactions:

$Zn_3N_2 + 3LiNH_2 \rightarrow 3LiZnN + 2NH_3$ (5.3)

$2NH_3 + 2LiH \rightarrow 2LiNH_2 + 2H_2$ (5.4)

Overall reaction:

$Zn_3N_2 + LiNH_2 + 2LiH \rightarrow 3LiZnN + 2H_2$ (5.5)

Phase pure LiZnN was achieved after a 2 hour reaction at 400°C and shown in ***figure 5.9***.

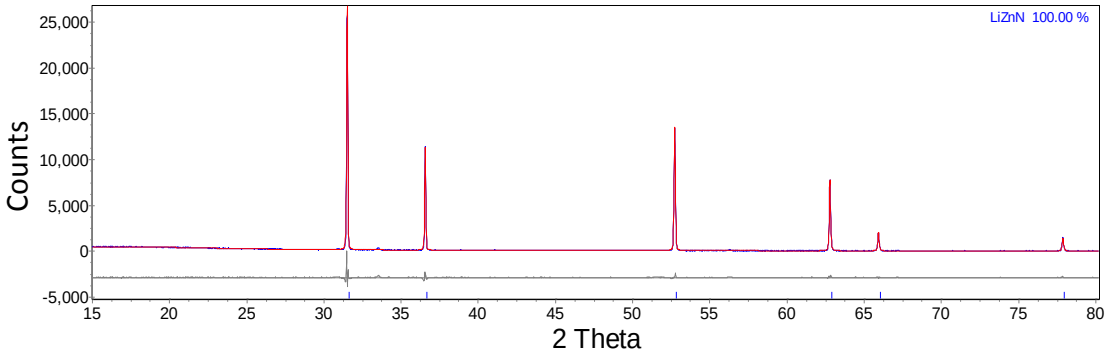

Figure 5.9 *Powder XRD pattern of the products of reaction between Zn_3N_2, $LiNH_2$, and LiH in a ratio of 2:1:1 at 400℃ for 2 hours showing observed (blue), Rietveld fit (red) and difference (grey) plots. Peak positions for refined compounds are shown underneath.*

In the products of reaction at 500°C for 2 hours there was about 17 wt% of Zn beside LiZnN (***figure 5.10***). With the addition of LiH, more Zn was obtained than that in the reaction without LiH.

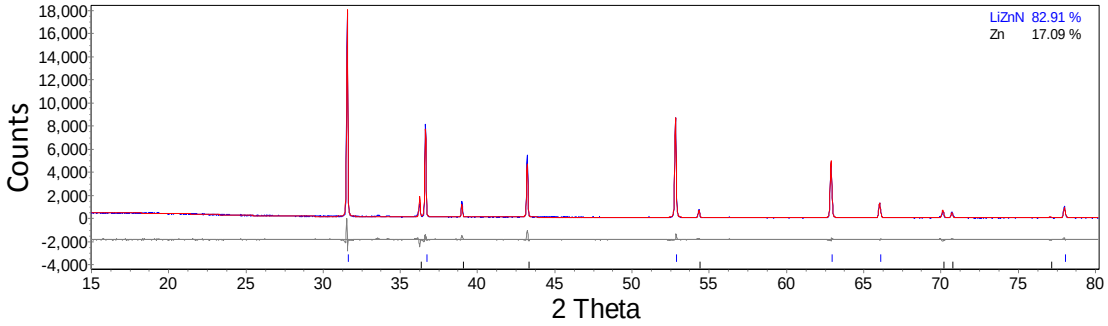

Figure 5.10 *Powder XRD pattern of the products of reaction between Zn_3N_2, $LiNH_2$, and LiH in a ratio of 1:1:2 at 500 ℃ for 2 hours showing observed (blue), Rietveld fit (red) and difference (grey) plots. Peak positions for refined compounds are shown underneath.*

5.4.1 Temperature-Programmed Desorption with Mass Spectrometry

The hydrogen desorption properties of the reaction between Zn_3N_2, $LiNH_2$ and LiH in a molar ratio of 1:1:2 were tested using TPD–MS. The sample was heated at 2°C min^{-1} to 400°C and held for 2 hours.

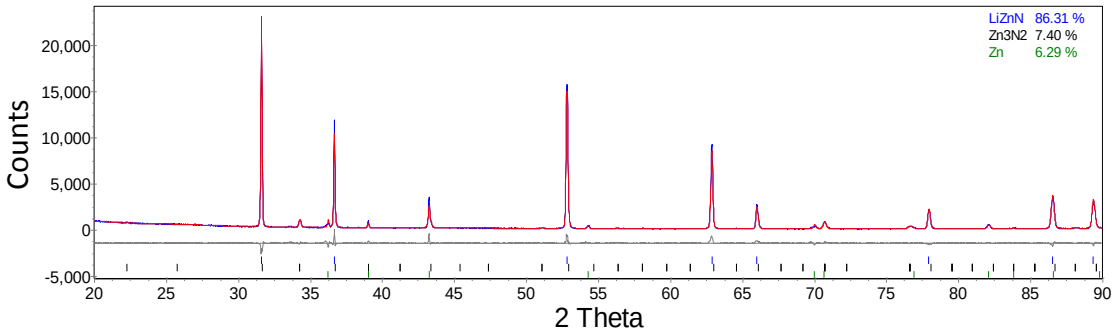

Figure 5.11 *Powder XRD pattern of the products of reaction between Zn_3N_2, $LiNH_2$ and LiH in a molar ratio of 1:1:2 heated in the TPD apparatus at 400 ℃ for 2 hours showing observed (blue), Rietveld fit (red) and difference (grey) plots. Peak positions for refined compounds are shown underneath.*

The powder XRD patterns and proportions of the products after TPD are shown in ***figure 5.11***. Besides LiZnN (~ 86 wt%) and Zn_3N_2 (~ 7 wt%) as in the products of the reactions between $LiNH_2$ and Zn_3N_2, ~6 wt% of Zn was also obtained.

The amounts of hydrogen and ammonia gas released during TPD are indicated in ***figure 5.12***. There was a significant change in temperature and amount of hydrogen released: hydrogen release was observed from about 180°C and peaked at about 330°C. The amount of ammonia release was insignificant.

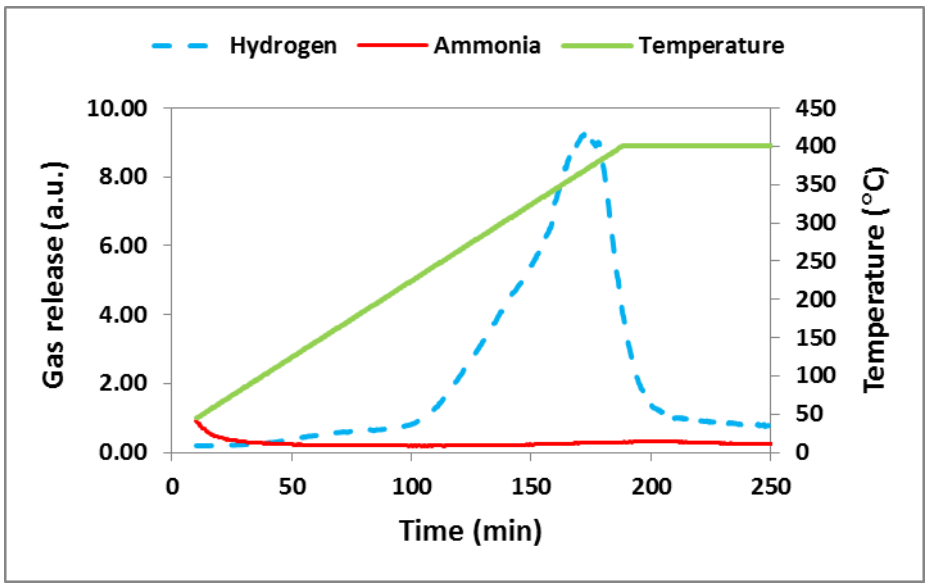

Figure 5.12 *TPD–MS trace of the reaction between Zn_3N_2, $LiNH_2$, and LiH in a ratio of 1:1:2 at 400℃ heated at 2℃ min^{-1} to 400℃, showing traces for hydrogen (blue), ammonia (purple) and temperature (green).*

Reaction of Zn_3N_2 and $LiNH_2$ with the addition of LiH was found to form LiZnN and hydrogen, consistent with reaction 5.3.

5.5 Crystal structure of synthesized LiZnN

LiZnN was first synthesized by heating a mixture of Li_3N and Zn_3N_2 at 400°C for 1 hour in a flow of NH_3 gas by Juza and Hund [3]. Polycrystalline LiZnN has a deep red colour, is hygroscopic and oxidizes rapidly in air. LiZnN has an antifluorite structure, space group $F\bar{4}3m$ with lattice constant a = 4.877(2) Å [3]. It was then reported by Kuriyama *et al.* to be formed by a direct reaction between NH_3 and LiZn alloy at 490°C for 5 hours with a slightly larger lattice parameter of a = 4.902(5) Å [4–5]. LiZnN can be also produced by an electrochemical method via a reaction between zinc nitride and lithium [6] or electrolysis using Zn electrode at 0.7 V (Li^+/Li) in LiCl–KCl–Li_3N at 400°C [7].

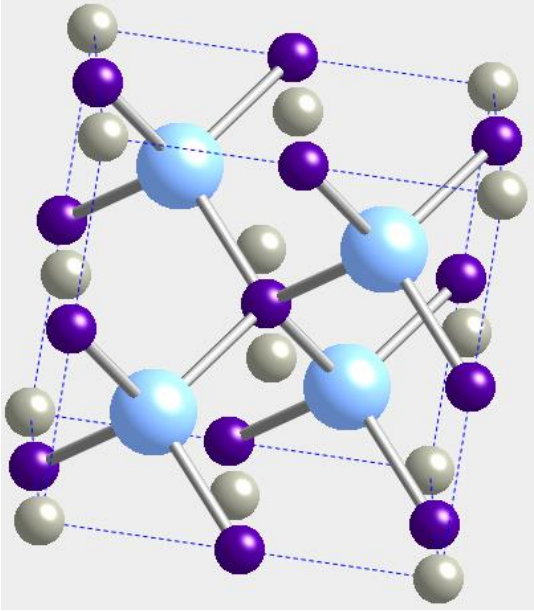

Figure 5.13 *Crystal structure of LiZnN. Zn is shown in grey, Li in purple and N in blue.*

In LiZnN both Zn and Li are coordinated to four N atoms, but N is coordinated to four Zn and four Li nearest atoms (***figure 5.13***). There are two phases of LiZnN: α phase with Li^+ near the anion and the β phase with Li^+ near the cation [7–8]. LiZnN was reported to

decompose above 500°C in a stream of nitrogen and hydrogen [3]. Results from calculations of Toyoura *et al.* suggested that decomposition of LiZnN could start above 500 K (223°C) [9]. LiZnN has been investigated as semiconductor with direct band gap of 1.9 eV [5]. It can absorb green light in a range of wavelength 400–600 nm therefore this material has a potential to be used in red-green-blue LEDs [10].

In this study, LiZnN was achieved at 490°C after heating Zn_3N_2 and $LiNH_2$ in a molar ratio of 1:4 for 1 hour or at 400°C after 2 hours on addition of LiH. The lattice parameters for LiZnN were 4.89333(4) Å and 4.89761(5) Å, respectively. LiZnN with a lattice parameter of 4.89655(5) Å could also been produced nearly pure (~ 6.4 wt% or 2.4 mol% Zn_3N_2 remained) after the 24 hour reaction of Zn_3N_2 and Li_3N under argon flow. The new methods developed in this study have some advantages over those previously reported [3–7] as they do not require either the use of ammonia gas or an electrochemical reaction. In addition, pure LiZnN can be obtained at lower temperature and after a much shorter reaction time.

A summary of conditions for the synthesis of LiZnN reported in literature and in this study are shown in table 5.1, along with lattice parameters for the LiZnN formed.

Table 5.1 Summary of conditions for the synthesis of LiZnN and lattice parameters of the product.

	Reactants and Conditions	**Lattice parameter (Å)**
Juza and Hund [1]	Li_3N and Zn_3N_2, flow of NH_3 gas, 400°C for 1 hour	4.877(2)
Kuriyama *et al.*[2]	NH_3 and LiZn alloy, 490°C for 5 hours	4.902(5)
Pereira *et al.* [4]	Electrochemical method, Zn_3N_2 and Li	-
Toyoura *et al.* [5]	Electrolysis, Zn electrode at 0.7 V (Li^+/Li) in LiCl–KCl–Li_3N, 400°C	4.90
This study	Zn_3N_2 + 4$LiNH_2$, 490°C, 1 hour	4.89047(4)
	Zn_3N_2 + $LiNH_2$ + 2LiH, 400°C, 2 hours	4.89762(4)
	Zn_3N_2 + Li_3N, 500°C, 12 hours	4.89655(5)

Diffraction data from synthesized LiZnN were obtained using a powder X-ray diffractometer operating in capillary mode and are shown in ***figure 5.14***.

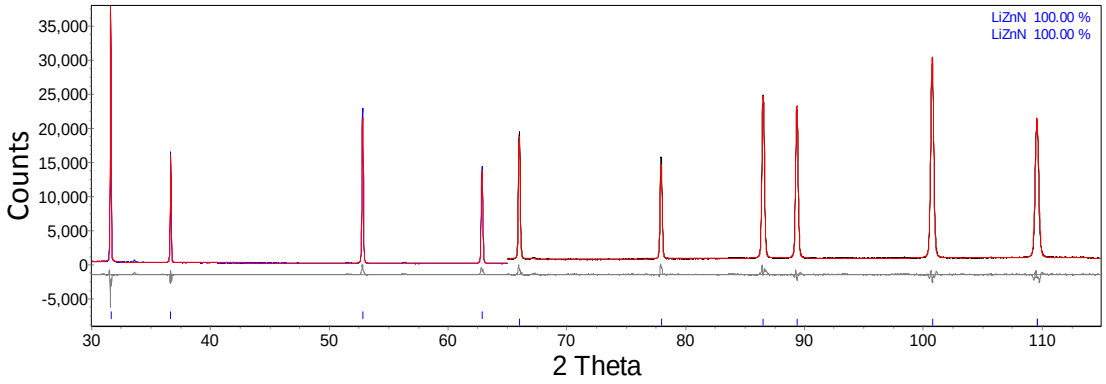

Figure 5.14 *Powder XRD patterns of the products of reaction of Zn_3N_2 + $4LiNH_2$ at 500 ℃ for 1 hour showing observed (blue), Rietveld fit (red) and difference (grey) plots. Peak positions for refined compounds are shown underneath.*

A full Rietveld refinement of crystal structure of LiZnN was carried out using Topas software. The refined parameters including lattice constant and thermal parameter are shown in **table 5.2**. Within error, refined atomic occupancies all showed values of 1 and so were fixed at this value. This indicates that the product was highly ordered and free from defects.

Table 5.2 Refined crystal structure data for LiZnN.

Atom	Site	x	y	z	Occupancy	B_{iso}
Li1	4b	1/2	1/2	1/2	1	0.41(4)
Zn1	4a	0	0	0	1	0.41(4)
N1	4c	1/4	1/4	1/4	1	0.41(4)

Space group: $F\bar{4}3m$; a = 4.89047(4) Å;

R_{exp} = 6.01%; R_{wp} = 11.05%; χ^2 = 3.380

5.6 Hydrogenation

Pure synthesized LiZnN, commercial Zn_3N_2 and mixtures of LiZnN and Zn_3N_2 in different weight ratios were ground and sealed in reaction vessels in an argon-filled glove box and then put in the hydrogenation apparatus. Hydrogenation properties of these samples were tested at 200°C and 300°C under 90 bar H_2 for up to 24 hours.

5.6.1 Hydrogenation of pure LiZnN

The samples were studied at 200°C and 300°C for up to 24 hours. After hydrogenation at 200°C only starting material was observed indicating no hydrogen absorption occurred under conditions studied.

At a higher temperature of 300°C for 24 hours a reaction occurred as about 12 wt% Zn was obtained. A small amount of Zn_3N_2 was also observed (***figure 5.15***).

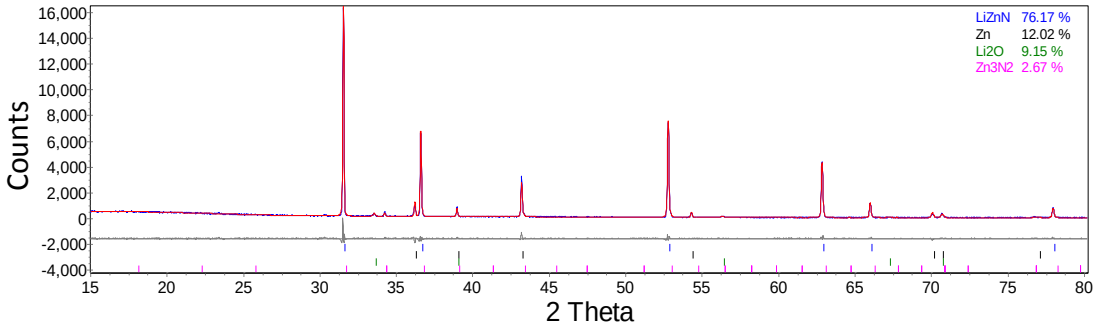

Figure 5.15 *Powder X-ray diffraction pattern of products from hydrogenation of pure LiZnN under 90 bar H_2, at 300 ℃ for 24 hours showing observed (blue), Rietveld fit (red) and difference (grey) plots. Peak positions for refined compounds are shown underneath.*

5.6.2 Hydrogenation of Zn_3N_2 (99%)

The hydrogenation properties of this compound were studied at 300°C for 24 hours. A reaction may occur and produced ~7 wt% (~21 mol%) of Zn along with mostly remaining Zn_3N_2 (***figure 5.16***).

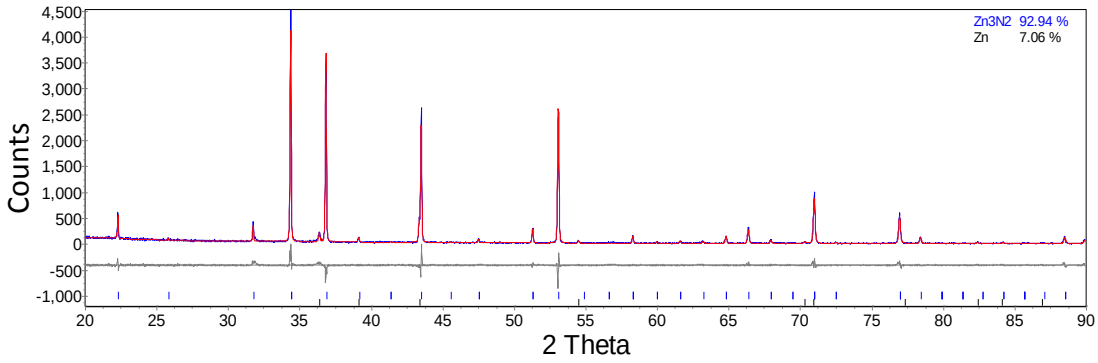

Figure 5.16 *Powder X-ray diffraction pattern of products from hydrogenation of Zn_3N_2 (99%) under 90 bar H_2, at 300 °C for 24 hours showing observed (blue), Rietveld fit (red) and difference (grey) plots. Peak positions for refined compounds are shown underneath.*

5.6.3 Hydrogenation of mixture of LiZnN and Zn_3N_2

A mixture of ~86 wt% (94 mol%) LiZnN and ~14 wt% (6 mol%) Zn_3N_2 obtained from reaction of Zn_3N_2 and $LiNH_2$ was hydrogenated at 200°C and 300°C for 24 hours. The reaction at 200°C for 12 hours did not show a clear difference in proportions of the compounds in the products from those in starting materials. The products of the hydrogenation at higher temperature of 300°C were a mixture of Zn and $LiNH_2$ in a molar ratio of approximately 1:1 (***figure 5.17***). Unlabelled peaks in the patterns belong to Li_2O and impurity.

The hydrogenation of LiZnN may occur through the following reaction:

$$LiZnN + 2H_2 \rightarrow LiNH_2 + Zn + H_2 \text{ or } LiZnN + H_2 \rightarrow LiNH_2 + Zn \quad (5.4)$$

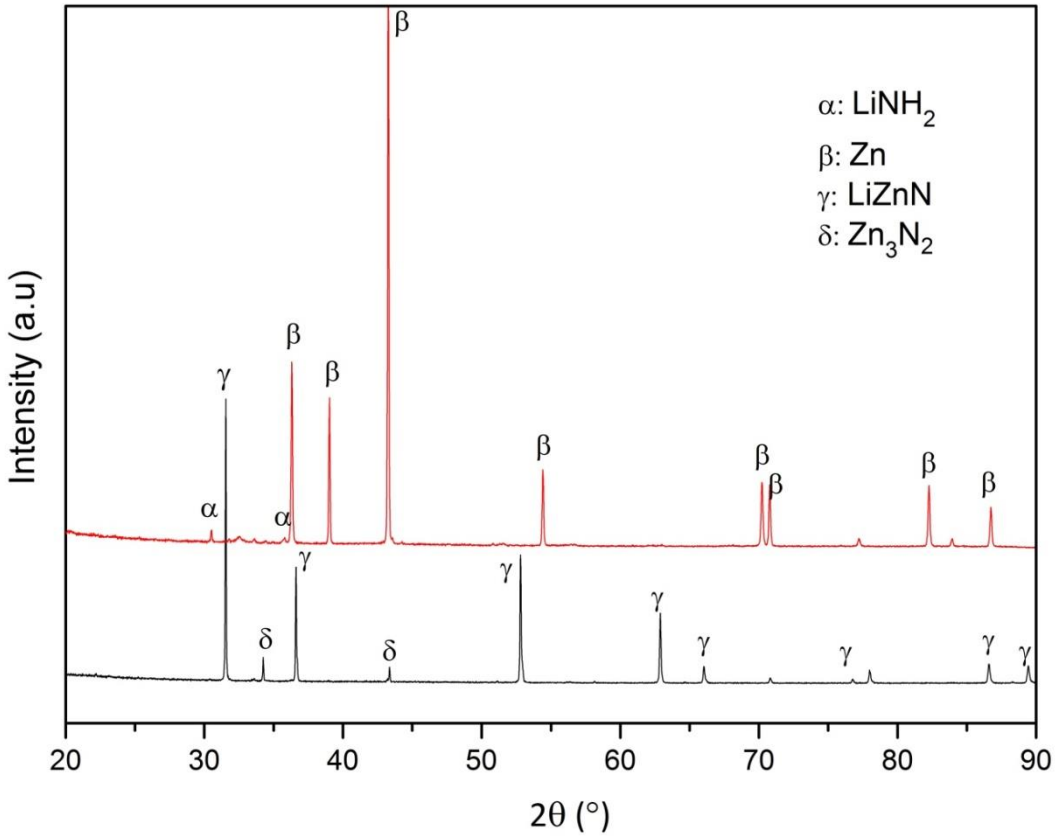

Figure 5.17 *Powder X-ray diffraction pattern of products from hydrogenation of a mixture of LiZnN (~86 wt %) and Zn_3N_2 (~14 wt %) obtained from reaction of Zn_3N_2 and $LiNH_2$, under 90 bar H_2, at 300 ℃ for 24 hours.*

5.7 SEM

With the purpose of investigating the effects of particle size and morphology on rehydrogenation properties of LiZnN, Zn_3N_2 and a mixture of both, samples were examined with SEM.

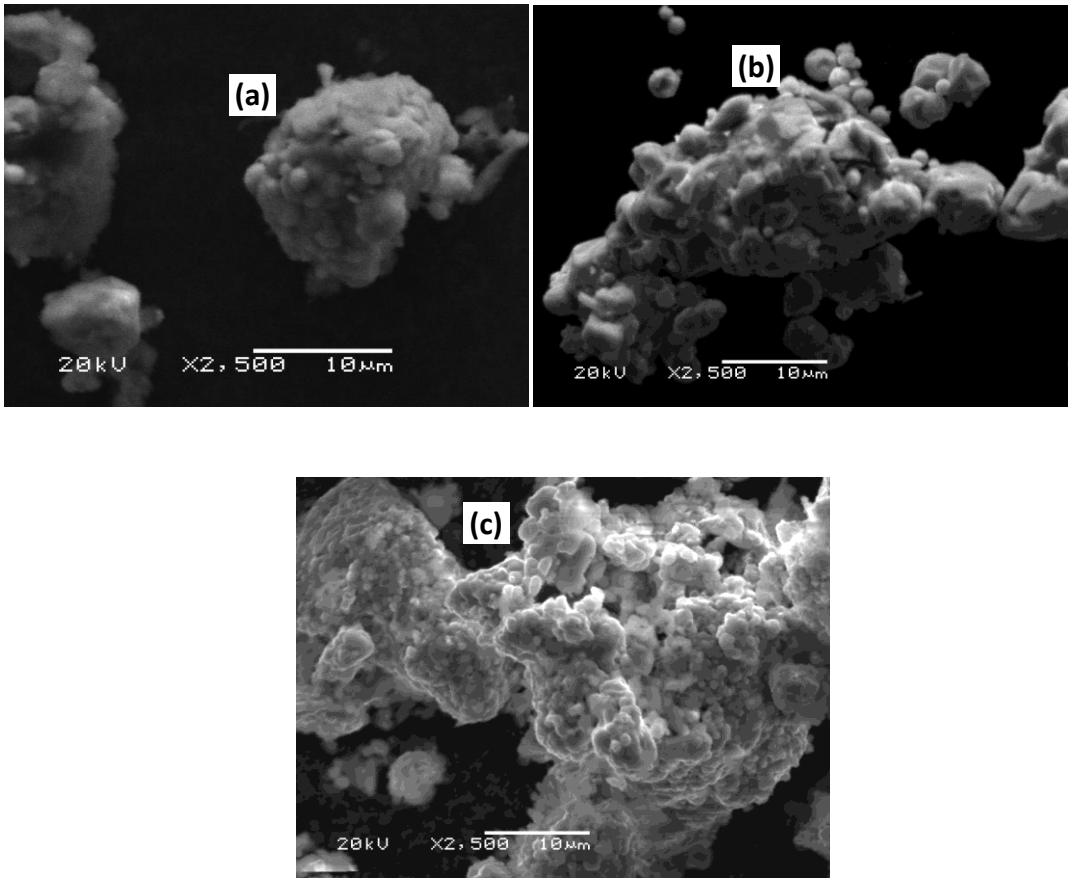

Figure 5.18 *Scanning electron micrographs at the scale of 10 µm of samples of LiZnN (**a**), commercial Zn_3N_2 (**b**), and a mixture of both obtained from reaction of Zn_3N_2 and $LiNH_2$ (**c**).*

It can be seen in ***figure 5.18*** that commercial Zn_3N_2 has bigger particle size than LiZnN and its particles are not of uniform size. The mixture of Zn_3N_2 and LiZnN had the finest particles and the greatest homogeneity. This may enhance its ability to react with hydrogen during the rehydrogenation process.

5.8 Ball-milling

In order to test whether a smaller particle size of LiZnN could improve diffusion and the kinetics of the rehydrogenation, synthesized LiZnN was ball-milled for 10 hours before rehydrogenation. After heating up to 300°C for 24 hours under 90 bar hydrogen, ball-milled LiZnN was hydrogenated to form $LiNH_2$ and Zn as can be seen in the powder XRD pattern in ***figure 5.19***.

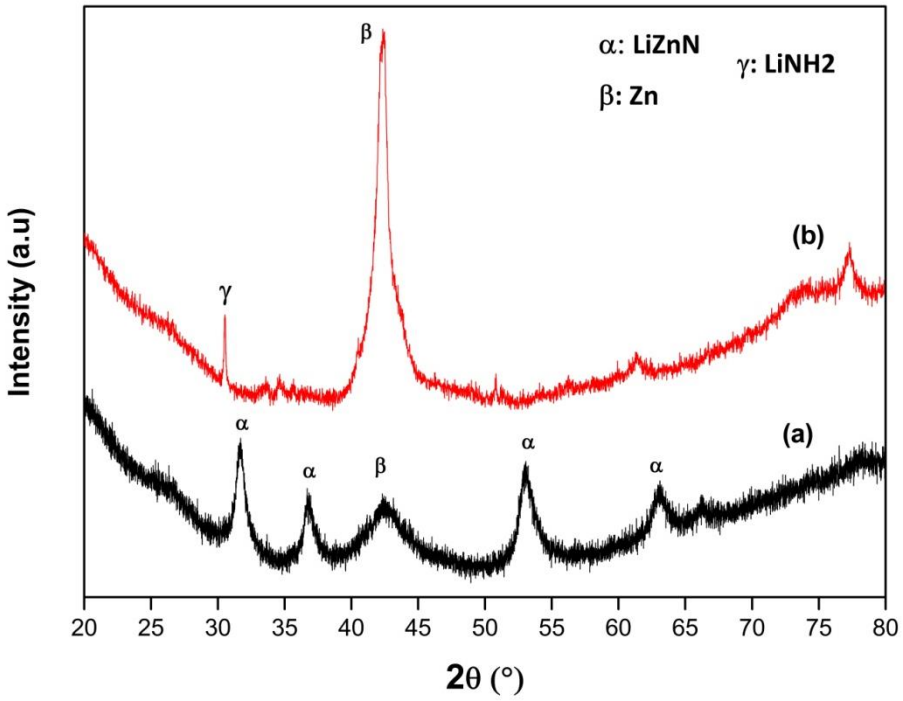

Figure 5.19 *Powder X-ray diffraction patterns of ball-milled LiZnN* ***(a)*** *and products after hydrogenation under 90 bar H_2 at 300 ℃ for 24 hours* ***(b)***.

5.9 Reaction of Zn + $LiNH_2$

In order to examine whether the Li–Zn–N system could potentially be reversible, the reaction of Zn and $LiNH_2$ in a molar ratio of 1:1 was studied in the temperature range of 300–500°C.

At 300°C reaction did not occur as the starting materials remained unchanged. Reaction happened slowly at 400°C with the observation of about 8 wt% LiZnN. The reaction between Zn and $LiNH_2$ may occur according to the following equation:

$$Zn + LiNH_2 \rightarrow LiZnN + H_2 \qquad (5.5)$$

In the products of reaction at 490°C a much larger amount ~58 wt% of LiZnN was observed along with unreacted Zn (~42 wt%) was observed. $LiNH_2$ was not seen, which is not surprising as any remaining $LiNH_2$ which did not react with Zn would have decomposed at this temperature (***figure 5.20***).

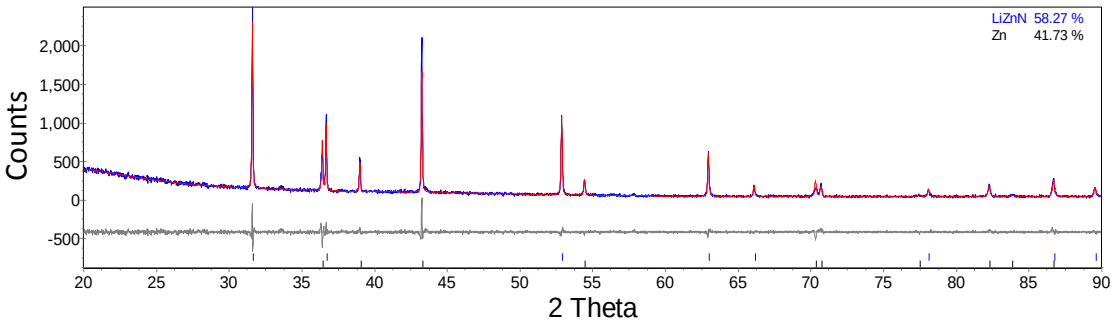

Figure 5.20 *Powder XRD pattern of the products of reaction of Zn + $LiNH_2$ at 490°C for 12 hours showing observed (blue), Rietveld fit (red) and difference (grey) plots. Peak positions for refined compounds are shown underneath.*

With the aim of examining whether excess $LiNH_2$ can could increase the conversion of Zn to LiZnN, 40% excess $LiNH_2$ was used. However, there was still a large amount of unreacted Zn. In addition, a small amount of LiZn was observed (***figure 5.21***).

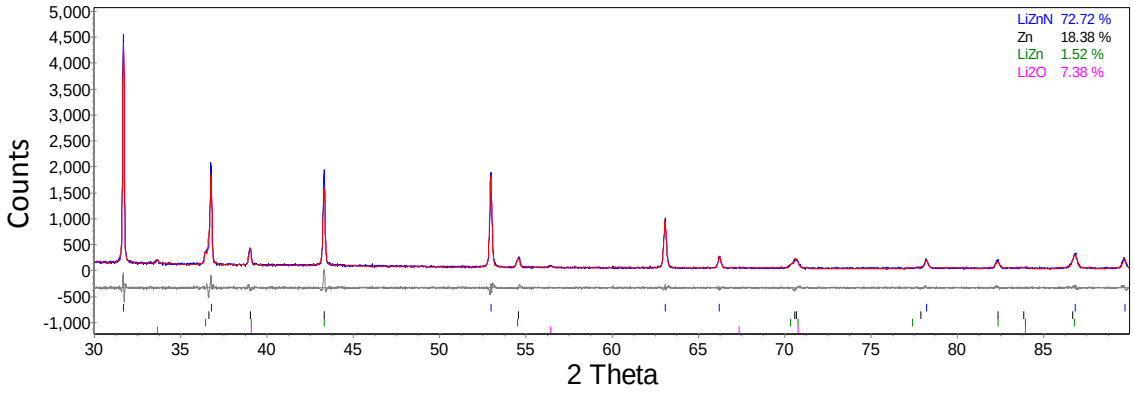

Figure 5.21 *Powder XRD pattern of the products of reaction of Zn + 1.4$LiNH_2$ at 490℃ for 12 hours showing observed (blue), Rietveld fit (red) and difference (grey) plots. Peak positions for refined compounds are shown underneath.*

5.10 Reversibility of Li–Zn–N system

5.10.1. Intelligent Gravimetric Analysis (IGA)

5.10.1.1 Desorption of Zn3N2 + $LiNH_2$ + 2LiH at 400℃

It was shown in previous sections that LiZnN can be hydrogenated. To obtain more information in a hope to understand the kinetics of this process, samples were studied using an intelligent gravimetric analyzer (IGA).

A sample of Zn_3N_2, $LiNH_2$, and LiH in a ratio of 1:1:2 was placed into an IGA under 18.5 bar hydrogen and heated at 2°C/min to 400°C for 48 hours.

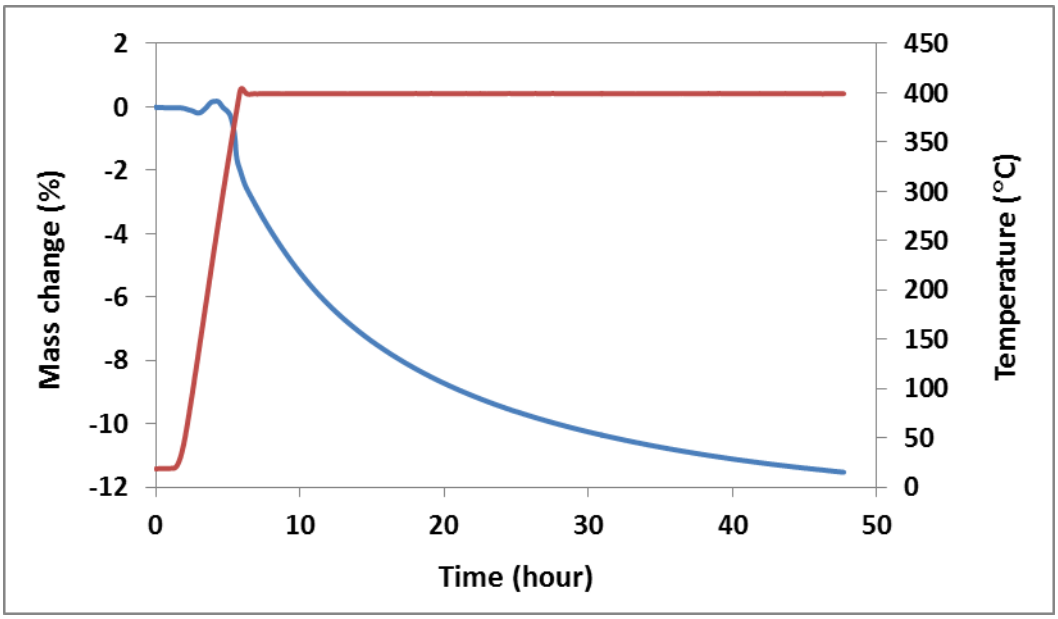

Figure 5.22 *IGA trace of Zn_3N_2 + $LiNH_2$ + 2LiH heated at 400℃ under 18.5 bar H_2 for 48 hours.*

A mass decrease of about 11 wt% was observed after 48 hours and would continue to lose mass as shown in ***figure 5.22***. This reduction is much larger than the mass drop of

hydrogen release which is about 1.5 wt% based on reaction (5.2). This may be caused by a release of nitrogen (*e.g.* decomposition of LiZnN) or ammonia from a decomposition of $LiNH_2$. As the measurement was performed at 18.5 bar it was not possible to determine whether the mass loss was from nitrogen or ammonia.

5.10.1.2 Desorption/Absorption of Zn_3N_2 + $LiNH_2$ + 2LiH at 150–300 ℃

The desorption and absorption of the products of the mixture of Zn_3N_2 + $LiNH_2$ + 2LiH obtained from **section 5.10.1.1** were then studied at lower temperatures between 150–300°C. At 150°C there was a small increase in mass of sample (~0.5 wt%). The result obtained may indicate that hydrogen uptake occurred from 150°C. At 200°C and 300°C the sample gradually lost about 7.5 wt% (***figure 5.23***).

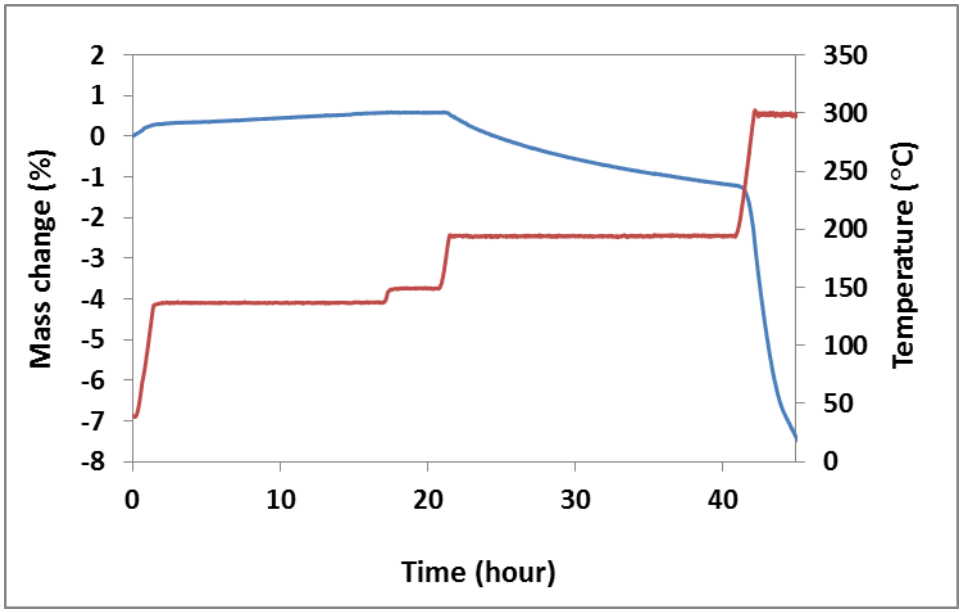

Figure 5.23 *IGA trace of Zn_3N_2 + $LiNH_2$ + 2LiH heated at 100–300 ℃ under 18.5 bar H_2 for 50 hours.*

This decrease was not possible only from hydrogen release (~1.5 wt%) and could be caused by an evolution of ammonia or nitrogen.

The solid products after IGA analysis were then studied by powder X-ray diffraction as shown in ***figure 5.24.*** The products observed were a mixture of LiZnN, LiZn, and Zn. The presence of LiZn and Zn may indicate decomposition of LiZnN under conditions studied. Small amounts of Zn_3N_2, $LiNH_2$, and LiH were also observed, which may indicate incomplete reaction of the starting materials. The large amount of Li_2O probably formed on sample unloading from IGA and should not be present during the measurement.

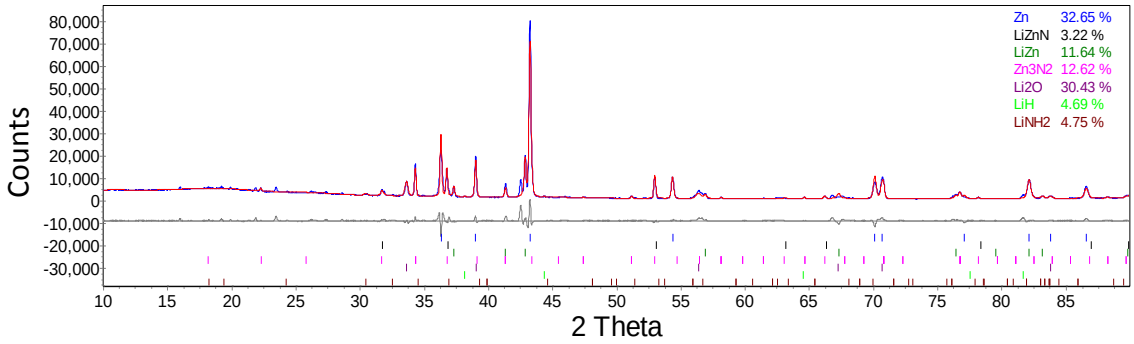

Figure 5.24 *Powder XRD pattern of the products of the mixture of Zn_3N_2 + $LiNH_2$ + 2LiH after heating at 400 ℃ for 48 hours then reheating up to 300 ℃ under 18.5 bar hydrogen in the IGA system, showing observed (blue), Rietveld fit (red) and difference (grey) plots. Peak positions for refined compounds are shown underneath.*

5.10.1.3 Desorption of Zn_3N_2 + $LiNH_2$ + 2LiH to 200 ℃ under hydrogen flow

In order to check whether any mass change appeared at low temperature, a sample of Zn_3N_2 + $LiNH_2$ + 2LiH was tested under 18.5 bar hydrogen from 100°C. A reduction of mass was observed starting at 100°C and after heating up to 200°C for 100 hours more than 2.5 wt% of sample was lost. Desorption under hydrogen flow may suppress

hydrogen release and encourage the release of other gases which could be ammonia or nitrogen.

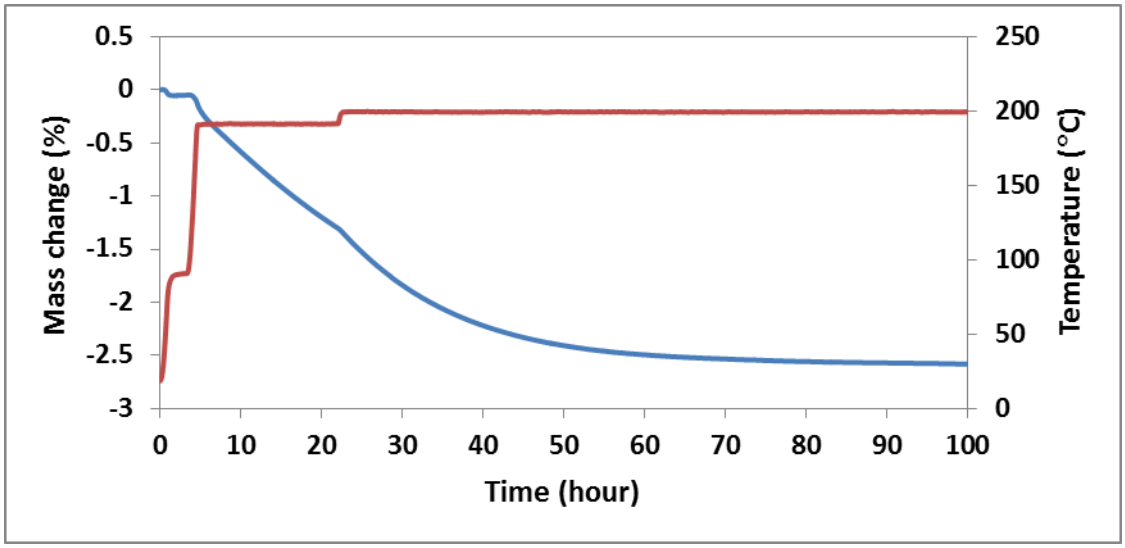

Figure 5.25 *IGA trace of Zn_3N_2 + $LiNH_2$ + 2LiH heated to 200 ℃ under 18.5 bar H_2 for 100 hours.*

After the measurement Zn_3N_2 and LiH starting materials remained in large amounts. $LiNH_2$ was decomposed into Li_2NH. There was no observation of LiZnN. A small amount of Zn was obtained, which may come from the decomposition of LiZnN formed *via* reaction 5.2. However, there was no observation of LiZn among the products which leads to a suggestion that Zn may be formed from the decomposition of Zn_3N_2 or reaction between Zn_3N_2 and LiH.

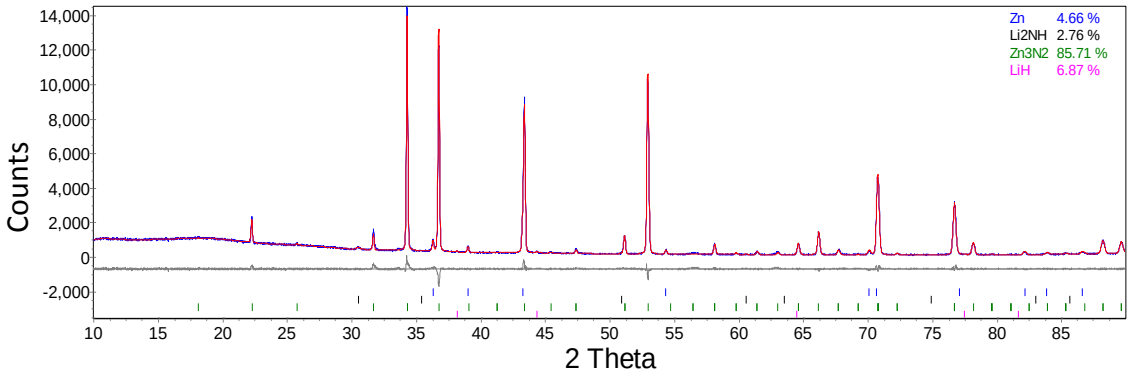

Figure 5.26 *Powder XRD pattern of the products of the reaction of Zn_3N_2 + $LiNH_2$ + 2LiH after IGA measurement under 18.5 bar hydrogen at 200℃ for 100 hours, showing observed (blue), Rietveld fit (red) and difference (grey) plots. Peak positions for refined compounds are shown underneath.*

5.10.1.4 Desorption/absorption of Zn_3N_2 + $LiNH_2$ + 2LiH at 200-220℃ under argon flow

With the purpose of checking whether the flowing hydrogen atmosphere affected desorption/absorption, a sample was run under 18.5 bar argon. After the same time of 100 hours measurement a much smaller reduction of mass occurred and about 1.1 wt% of sample was lost (***figure 5.26***). A drop of ~1.2 wt% is close to the theoretical value of hydrogen release in reaction (5.2). This result confirms that the presence of hydrogen has a significant effect on the desorption of reactions in the IGA.

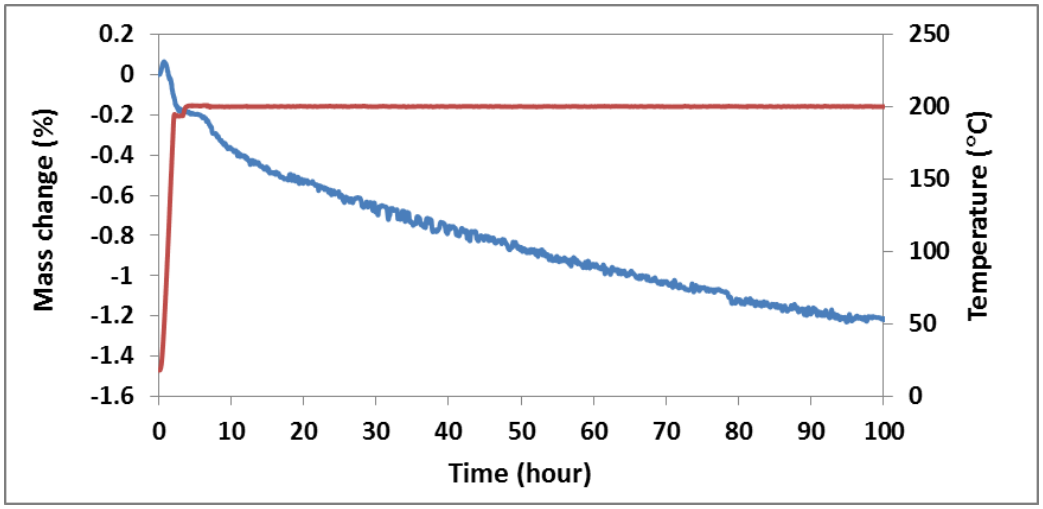

Figure 5.27 *IGA trace for Zn_3N_2 + $LiNH_2$ + 2LiH heated at 200 ℃ under 18.5 bar argon for 100 hours.*

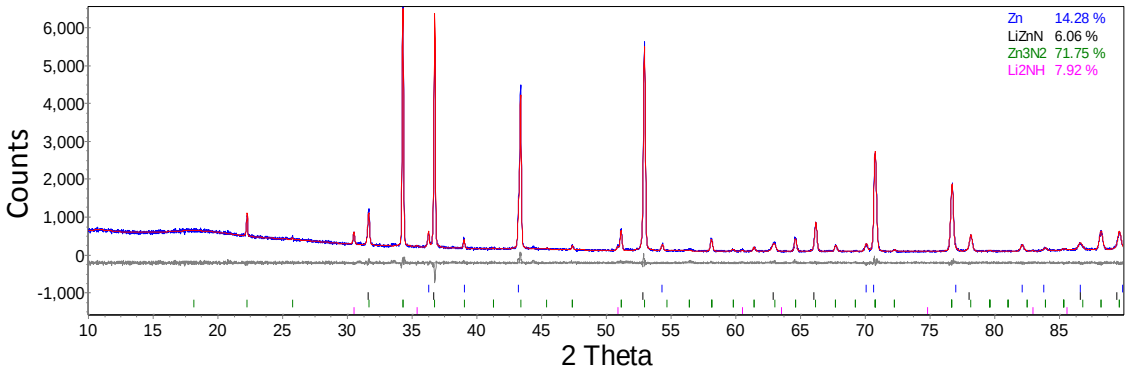

Figure 5.28 *Powder XRD pattern of the products of the reaction of Zn_3N_2 + $LiNH_2$ + 2LiH after IGA measurement under 18.5 bar argon at 200 ℃ for 100 hours, showing observed (blue), Rietveld fit (red) and difference (grey) plots. Peak positions for refined compounds are shown underneath.*

After IGA measurement under 18.5 bar argon at 200°C reaction(s) some Zn was observed and a small amount of LiZnN, which was absent after measurement under hydrogen. Large amounts of Zn_3N_2 remained, and $LiNH_2$ was decomposed into Li_2NH.

There was no observation of LiH in the products which may indicate its complete reaction, though its slight scattering means that it is hard to detect in small amount.

In summary, data obtained from IGA measurements under different conditions show a much greater weight loss under hydrogen than under argon, which was probably due to ammonia or nitrogen loss. No appreciable hydrogen uptake was observed under conditions studied, which may be related to the fact that the weight losses observed were largely due to gases other than hydrogen.

5.10.2 Volumetric measurement (HTP)

With the intention of further investigating the effects of pressure on desorption and absorption of mixtures of Zn_3N_2 and $LiNH_2$ with and without the addition of LiH, samples were heated up to 400°C at pressures up to 90 bar using the HTP system described in Chapter 2.

5.10.2.1 HTP data for Zn_3N_2 + $LiNH_2$ + 2LiH: first desorption at 400℃

A sample of Zn_3N_2, $LiNH_2$ and LiH in a molar ratio of 1:1:2 was studied using the HTP apparatus at 400°C under 90 bar hydrogen. The first desorption at 400°C was completed and the products were then examined by XRD.

A desorption isotherm was performed to ascertain the equilibrium pressure for desorption and the amount of gas desorbed. Desorption data is presented in ***figures 5.29 and 5.31*** and shows that during the first desorption at 400°C about 350 mmol of gases were emitted. As described in **section 2.8**, it is not possible to distinguish if the gas released is H_2, N_2 or NH_3 because this method relates the change of pressure to the

amount of gas uptake or release. However, and any uptake is assumed to be solely due to H_2. The first desorption occurring at low pressure can be associated with a release of hydrogen similar to the result obtained using TPD apparatus. A curve in ***figure 5.30*** was caused by experimental errors due to hot gas in reactor flowing into cold dose volume.

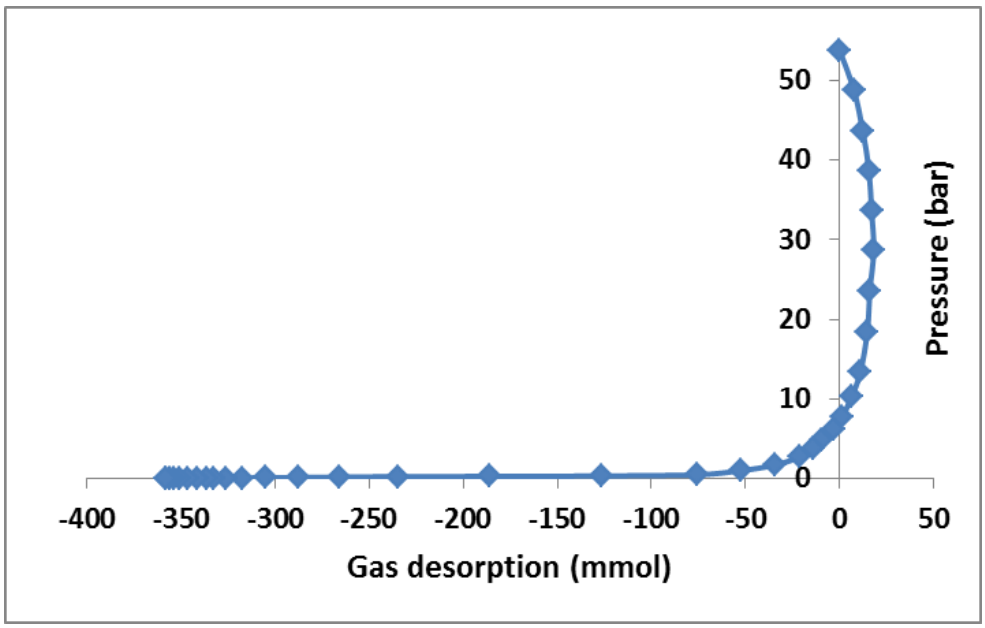

Figure 5.29 *First desorption of reaction between Zn_3N_2 + 3$LiNH_2$ studied using HTP at 400℃.*

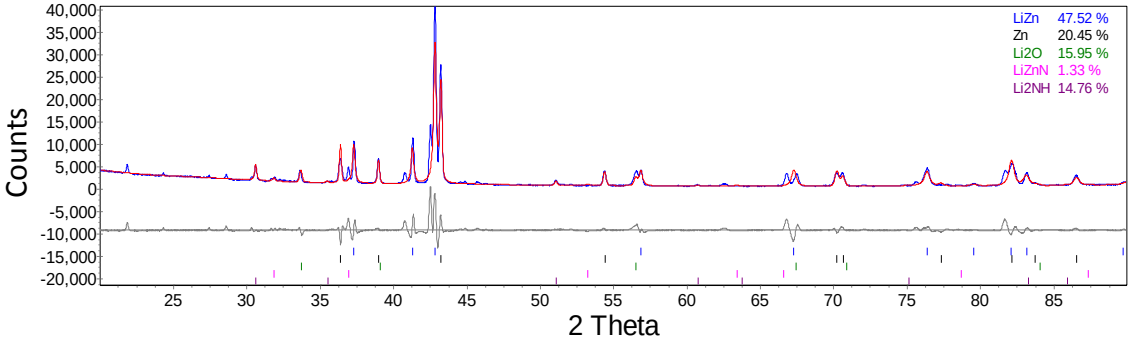

Figure 5.30 *Powder XRD pattern of the products of the reaction of Zn_3N_2 + $LiNH_2$ + 2LiH after the first desorption at 400℃ in the HTP apparatus.*

The reaction products after heating to 400°C under 90 bar hydrogen in the HTP system were a mixture of LiZnN, LiZn, Zn and Li_2NH and Li_2O impurity. No starting materials remained. There were some unidentified peaks which may belong to new compound(s) formed after desorption as known phases including ZnO, LiOH, LiH... were not observed.

5.10.2.2 HTP data for Zn_3N_2 + $LiNH_2$ + 2LiH: first rehydrogenation cycle at 400℃

The first rehydrogenation of the mixture was carried out at 400°C under 90 bar hydrogen in HTP and the results are shown in ***figure 5.31.*** Three separate plateaus were observed suggesting that there might be 3 different reactions occurring: at very low pressure, above 10 bar and around 35 bar.

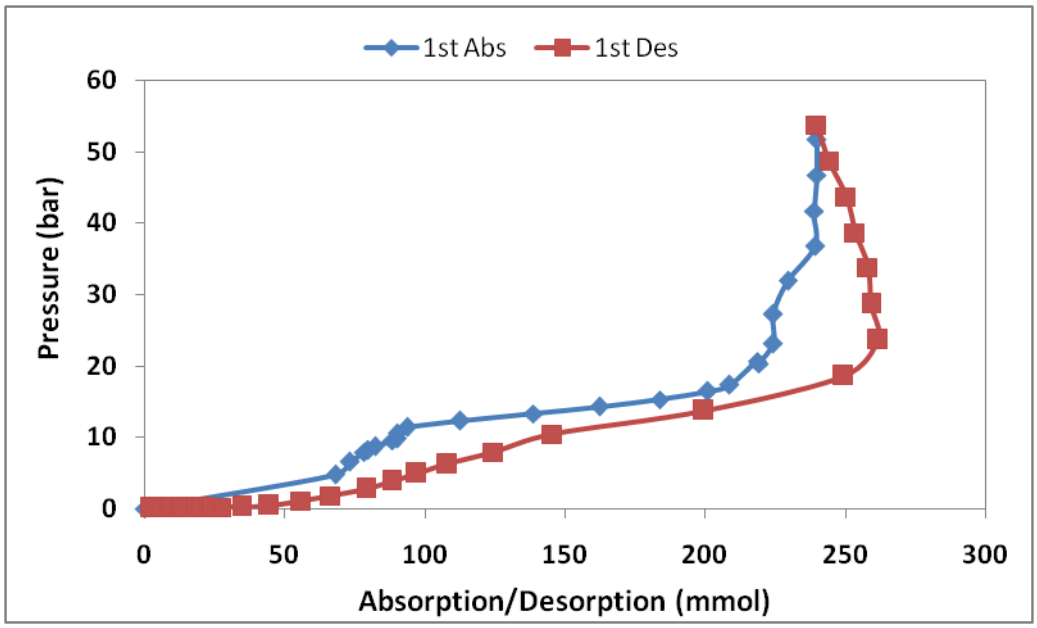

Figure 5.31 *The first desorption/absorption cycle of reaction between* Zn_3N_2 *+* $LiNH_2$ *+ 2LiH studied using the HTP apparatus at 400 ℃ under 90 bar hydrogen.*

The products after the first cycle were then examined by powder XRD. After the first desorption/absorption cycle, the main products were LiZn, a known thermal decomposition product of LiZnN and Li_2NH, a thermal decomposition product of $LiNH_2$. Li_2O impurity was also observed.

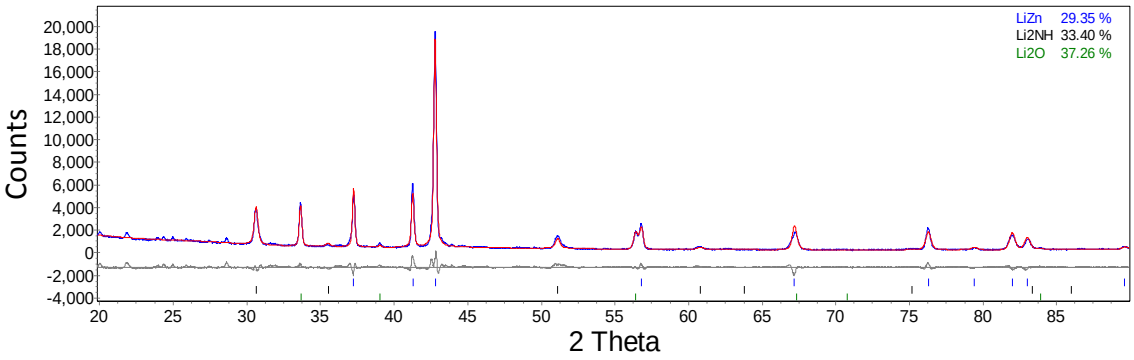

Figure 5.32 *Powder XRD pattern of the products of the reaction of Zn_3N_2 + $LiNH_2$ + 2LiH after the first desorption and absorption cycle in the HTP apparatus.*

5.10.2.3 HTP data for Zn_3N_2 + $LiNH_2$ + 2LiH: 6 rehydrogenation cycles

The reversible properties of the sample were then investigated by running 6 dehydrogenation/rehydrogenation cycles from 400°C to 275°C; the data for the 6 cycles are shown in ***figure 5.33.*** It can be seen that the system was able to take up up to 250 mmol hydrogen but its uptake ability decreased after each cycle. It is proposed that a loss of nitrogen (through desorption of NH_3 or N_2) may be responsible for the observed decline in capacity.

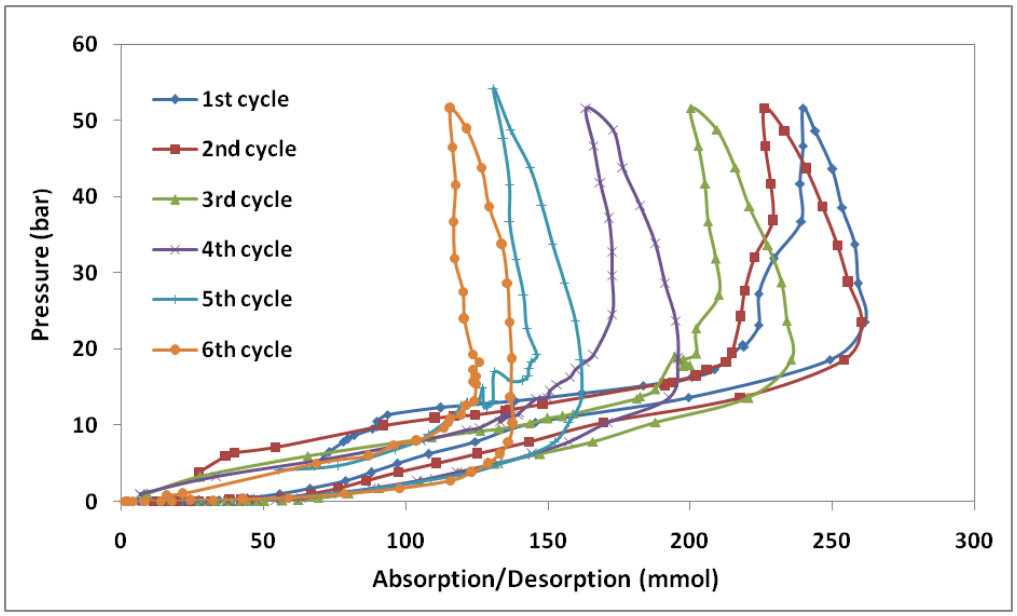

Figure 5.33 *Desorption/absorption of reaction between Zn_3N_2 + $LiNH_2$ + 2LiH studied using HTP at 400 ℃, 375 ℃, 350 ℃, 325 ℃ 300 ℃, and 275 ℃.*

In the products after measurement (shown in ***figure 5.34***), LiZn and Zn were observed, presumably from the decomposition of LiZnN. The presence of these non-hydridable compounds may be a reason for loss of capacity. $LiNH_2$ and LiH were present but Zn_3N_2 was not observed. The large amount of Li_2O may appear during unloading step. There were some small unidentified peaks that do not belong to known compounds containing Li, Zn, O, and H. The presence of $LiNH_2$ and LiH may be formed due to reversibility of this system.

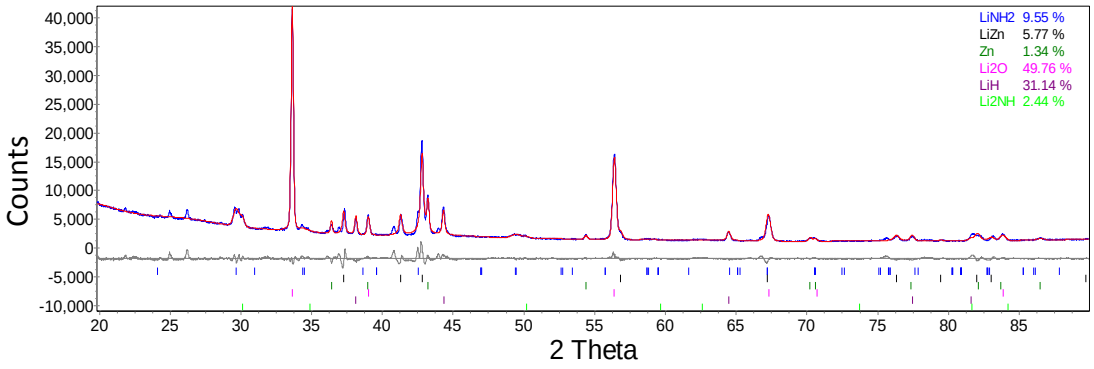

Figure 5.34 *Powder XRD pattern of the products of the reaction of Zn_3N_2 + $LiNH_2$ + 2LiH after cycling in the HTP system under 90 bar argon, showing observed (blue), Rietveld fit (red) and difference (grey) plots. Peak positions for refined compounds are shown underneath.*

In summary, data obtained from the HTP measurements shows that the mixture of Zn_3N_2 + $LiNH_2$ + 2LiH had a reversible hydrogen storage capacity under the conditions studied. There were 3 different desorption plateaus, at low pressure, around 10 bar, and around 35 bar that may relate to 3 different reactions happening during the measurements in HTP. The large mass loss observed in the IGA may include ammonia and or nitrogen, whose loss may be suppressed at higher pressure in the HTP.

5.10.2.4 HTP data for Zn_3N_2 + 3$LiNH_2$ after 6 cycles

For comparison a sample of Zn_3N_2 and $LiNH_2$ in a molar ratio of 1:3 was also studied under the same conditions as the sample in a presence of LiH. This mixture was confirmed to release ammonia and form LiZnN by TPD data, as in reaction (5.1).

Theoretical mass loss would be ~11.6 wt% if the only gas release were ammonia. The theoretical maximum absorption would then be ~2.3 wt% based on reaction (5.4).

A similar procedure to that for the mixture of Zn_3N_2 + $LiNH_2$ + LiH was followed to determine the equilibrium pressure for desorption and the amount of gas desorbed. As shown in ***figure 5.35***, after the first desorption at 400°C about 300 mmol of gases were released, close to that of the sample with the presence of LiH.

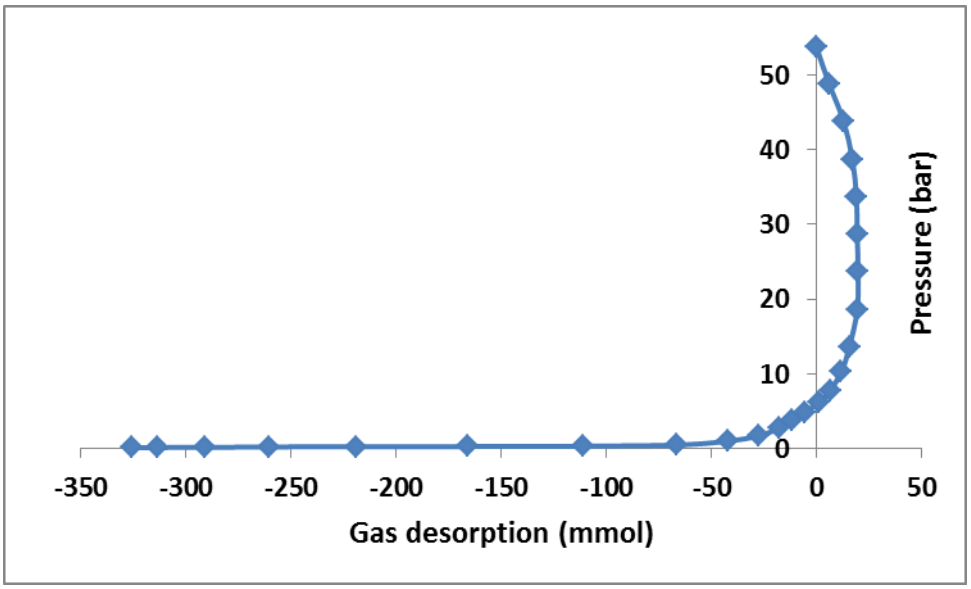

Figure 5.35 *First desorption of the reaction between Zn_3N_2 + 3$LiNH_2$ in the HTP apparatus at 400℃.*

After the first desorption at 400°C the system showed its ability to take up about 300 mmol hydrogen shown in ***figure 5.36***.

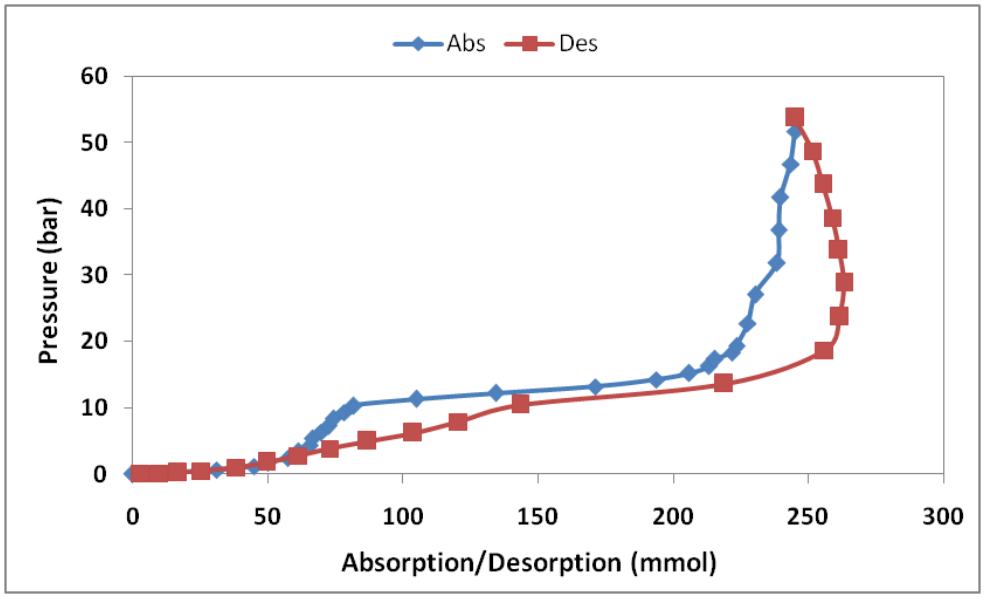

Figure 5.36 *First cycle of reaction between $Zn_3N_2 + 3LiNH_2$ in the HTP apparatus at 400 ℃.*

Similar desorption/absorption was observed after 6 cycles of the mixture of Zn_3N_2 + $3LiNH_2$ (***figure 5.37***). It is suggested that similar reactions to the mixture adding LiH occurred. Therefore this system might release gases then take up hydrogen. However, products obtained after recombination may be changed.

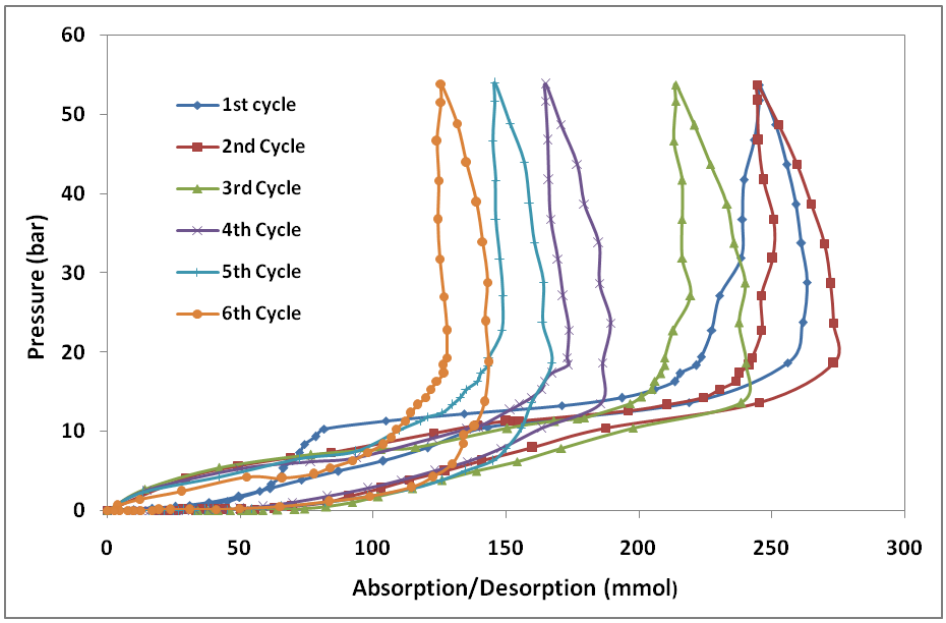

Figure 5.37 *Desorption/absorption cycles of reaction between Zn_3N_2 + 3$LiNH_2$ studied using HTP at 400 ℃, 375 ℃, 350 ℃, 325 ℃, 300 ℃, 275 ℃, and 250 ℃.*

5.11 Mg-doping

Although investigations of the absorption and desorption of hydrogen in the Li–Zn–N system showed some capacity for reversible hydrogen desorption (see above), the role and effectiveness of LiZnN as the dehydrogenated compound remain unclear. For this reason, and those mentioned in chapter 4, we wanted to study whether Mg could be incorporated into LiZnN and might enhance its ability to be hydrogenated. $MgCl_2$ was used to add magnesium into the mixture of Zn_3N_2 and $LiNH_2$.

5.11.1 $Zn_3N_2 + 4LiNH_2 + nMgCl_2$

Samples of $Zn_3N_2 + 4LiNH_2 + nMgCl_2$ (where n = 0.1; 0.15; 0.2; 0.25) were heated up to 490°C and held for 12 hours.

$Zn_3N_2 + 4LiNH_2 + 0.1MgCl_2$

Besides LiZnN, which was the only product in the absence of $MgCl_2$, there were small amounts of LiCl, Zn_3N_2 and MgO. No other Mg-based compound was observed (***figure 5.38***).

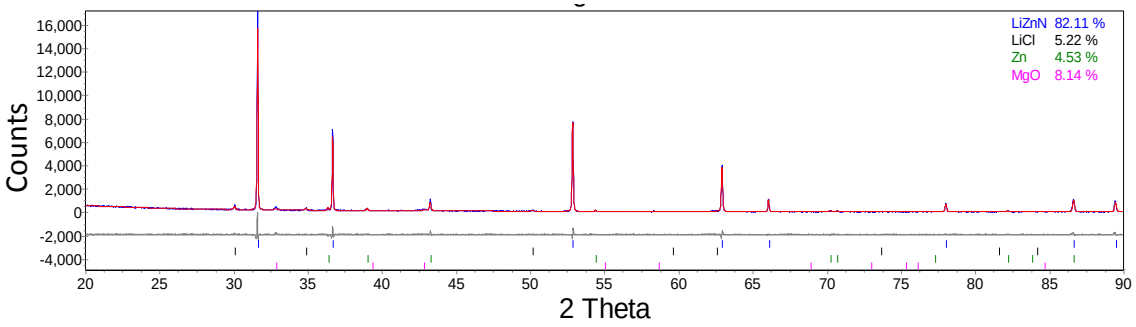

Figure 5.38 *Powder XRD pattern of the products of the reaction of Zn_3N_2 + 4$LiNH_2$ + 0.1$MgCl_2$ at 490℃ for 12 hours showing observed (blue), Rietveld fit (red) and difference (grey) plots. Peak positions for refined compounds are shown underneath.*

Zn_3N_2 + 4$LiNH_2$ + 0.15$MgCl_2$

With 15 mol% of $MgCl_2$, Zn_3N_2 was obtained in the reaction products. The amount of LiCl was higher while that of LiZnN was lower than those from reaction with 0.1$MgCl_2$ (***figure 5.39***). That may be because of the reaction of $LiNH_2$ with $MgCl_2$ to form LiCl leading to not enough $LiNH_2$ to react with Zn_3N_2 to form LiZnN.

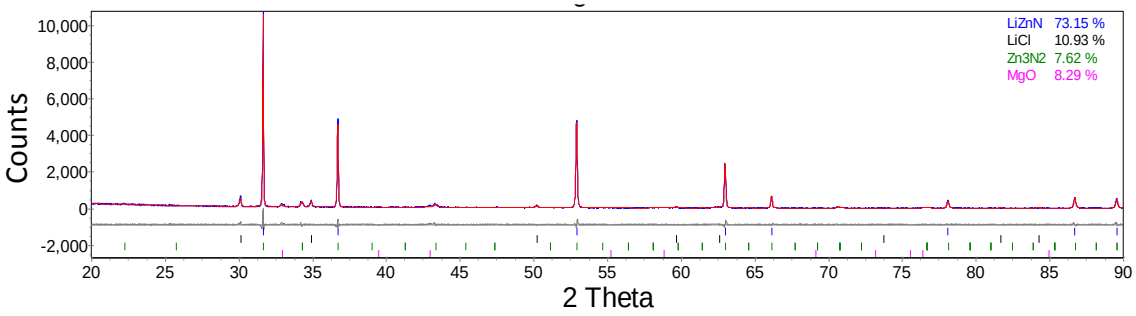

Figure 5.39 *Powder XRD pattern of the products of the reaction of Zn_3N_2 + 4$LiNH_2$ + 0.15$MgCl_2$ at 490℃ for 12 hours showing observed (blue), Rietveld fit (red) and difference (grey) plots. Peak positions for refined compounds are shown underneath.*

The products of reactions using 20% and 25%$MgCl_2$ were similar to those of the reaction using 15 mol% $MgCl_2$. However, amounts of Zn_3N_2 and LiCl are higher.

The lattice parameter of LiZnN obtained from products of reactions $Zn_3N_2 + 4LiNH_2 + n MgCl_2$ at 490°C for 12 hours and the occupancies of atoms in LiZnN were refined and shown in **table 5.3**.

Table 5.3 The lattice parameter of LiZnN and the occupancies of atoms in LiZnN obtained from products of reactions $Zn_3N_2 + 4LiNH_2 + n MgCl_2$.

$MgCl_2$ used	**Lattice parameter of LiZnN (Å)**	**Occupancy**	
		Zn site	**Mg in Zn site**
n = 0	4.89047 (4)		
n = 0.1	4.89084(5)	0.999(29)	0.001(29)
n = 0.2	4.89248(7)	0.998(40)	0.002(40)
n = 0.25	4.89384(8)	0.998(43)	0.002(43)

It can be seen from **table 5.3** that the values of lattice parameter of LiZnN with Mg-doping are larger than that without Mg. There may be a substitution of a small amount of Mg into Zn site. There was no observation of Mg in Zn site.

5.11.2 LiZnN + $n MgCl_2$

To study whether Mg can be doped directly into LiZnN, different amounts of $MgCl_2$ (n = 0.03–0.2) were mixed with pure LiZnN obtained from reaction of Zn_3N_2 and $LiNH_2$,

heated up to 300°C and held for 12 hours. However, no clear evidence of Mg substutition into Zn site was observed.

5.12 Conclusions

In this study, three new preps to produce LiZnN have been carried out. LiZnN was obtained pure after 1 hour reaction at 490°C of Zn_3N_2 and $LiNH_2$ in a molar ratio of 1:4 or after 2 hour reaction at 400°C on addition of LiH, or nearly pure *via* a 12 hour reaction of Zn_3N_2 and Li_3N in a molar ratio of 1:1. The routines were described by reactions (5.1), (5.2) and (5.3) and the lattice parameters for LiZnN were 4.89333(4) Å, 4.89761(5) Å, and 4.89507(5) Å respectively. The crystal structure of synthesized LiZnN was confirmed as known space group of $F\bar{4}3m$. These new methods show some advantages over those reported in literature as they occurred under argon atmosphere, not involve either ammonia gas atmosphere or an electrochemical reaction. Moreover, pure LiZnN can be obtained at lower temperature and after a much shorter reaction time.

Reaction between Zn_3N_2 and $LiNH_2$ release ammonia gas. The addition of LiH led to H_2 being the main gaseous product rather than NH_3. Hydrogen release was observed at low temperature around 180°C and peaked around 330°C.

Neither LiZnN nor Zn_3N_2 were shown to be rehydrogenated alone mixtures of LiZnN and Zn_3N_2, resulting from reaction of Zn_3N_2 and $LiNH_2$ at 500°C, formed $LiNH_2$ after rehydrogenation under 90 bar hydrogen at 300°C for 24 hours.

The cyclability of mixtures of Zn_3N_2 and $LiNH_2$, both in the presence and absence of LiH, was studied using IGA and Sieverts' method measurements. Both mixtures showed their

ability to release gases under low pressure, about 10 bar, and around 35 bar hydrogen. Partly reversible hydrogen absorption and desorption was observed at temperatures above 275°C.

Mg-doping of LiZnN was examined in a hope of enhancing the reversibility of the Li–Zn–N system but was unsucessful.

References

[1] K. Kuriyama, K. Nagasawa, K. Kushida, *J. Crystal Growth*, 2002, 237–239, 2019–2022.

[2] K. Kuriyama, R. Taguchi, K. Kushida, K. Ushiyama, *J. of Crystal Growth*, 1999, , 198/199, 802–805.

[3] V. R. Juza and F. Hund, *Z. Anorg. Allg. Chem.*, 1948, 257, 1–13.

[4] K. Kuriyama, T. Kato and T. Tanaka, *Phys. Rev. B*, 1994, 49, 4511–4513.

[5] K. Kuriyama, R. Taguchi, K. Kushida and K. Ushiyama, *J. Cryst. Growth,* 1999, 802, 198–199**.**

[6] N. Pereira, L. C. Klein, G. G. Amatucci, *J. Electrochem. Soc.*, 2002, 149, A262–A271.

[7] K .Toyoura, T. Goto, K. Hachiya, R. Hagiwara, *J. Electrochem. Soc.*, 2006, 153, G83–G86.

[8] A. E. Carlsson, A. Zunger, D.M. Wood, *Phys. Rev. B*, 1985, 32, 1386–1389.

[9] K. Toyoura, F. Oba, T. Ninomiya, A. Kuwabara and I. Tanaka, *J. Phys. Condens. Matter,* 2007, 19, 046201.

[10] J. Lu, Z. Z. Fang, Y. J. Choi, and H. Y. Sohn, *J. Phys. Chem. C*, 2007, 111, 12129–12134.

L. H. Yu, K. L. Yao, Z. L. Liu, *Physica B*, 2004, 353, 278–286.

Chapter 6: Conclusions

This thesis focused on the hydrogen desorption and reabsorption properties of mixed anion lithium amide and lithium ternary nitride systems, containing transition elements.

6.1 xLiBH$_4$ + yLiNH$_2$ + zCoO

In chapter 3, cobalt (II) oxide was added to mixture of xLiBH$_4$-yLiNH$_2$ to enhance the hydrogen desorption/absorption of the systems. The effects of the CoO catalyst on the hydrogen release and products of these systems have been studied.

The presence of CoO catalyst in LiBH$_4$–2LiNH$_2$–aCoO favoured the formation of the $I4_1/amd$ phase of Li$_3$BN$_2$ over the monoclinic $P2_1/c$ phase. The proportions of the two polymorphs of Li$_3$BN$_2$ were affected by the amount of catalyst with increasing $I4_1/amd$ phase observed with a greater amount of CoO, and transformation from the $I4_1/amd$ to $P2_1/c$ polymorph was observed under 90 bar hydrogen pressure. Temperatures of hydrogen release of xLiBH$_4$–yLiNH$_2$–zCoO systems were up to 100°C lower than those without catalyst, starting from 100°C and peaking around 250°C. In addition, in most CoO-doped samples there was a depression of ammonia evolution which was often below detection limits. The addition of CoO improved hydrogen desorption and may change the mechanism of decomposition of xLiBH$_4$-yLiNH$_2$ systems. However, there was no improvement in rehydrogenation properties of the reaction products.

Ball-milling was found to drastically enhance the amounts of hydrogen release from 3–4 wt% to 10.7 wt%. This may be caused by the smaller particle size of reactants and

greater homogeneity of the samples. Nevertheless, ball-milling did not significantly lower the temperature of hydrogen release.

This study showed that adding CoO into xLiBH$_4$-yLiNH$_2$ mixtures resulted in the release of a large amount (10 wt%) of hydrogen from temperatures as low as 100°C. However, hydrogenation of these systems remains problematic preventing them from being used as reversible hydrogen stores.

It has been reported that incorporation of Li_3BN_2 into carbon nanoscaffolds resulted in some rehydrogenation ability [1]. This may be a way forward to improve the rehydrogenation properties of Li_3BN_2 hence making these systems more likely to be applied for hydrogen storage.

6.2 $ZnCl_2$-based systems

Reactions of $ZnCl_2$ + nLiNH$_2$ at a range of molar ratios and temperatures were investigated and results presented in chapter 4. No stable amide chloride, imide chloride or nitride chloride phases were observed but a mixture of Zn_3N_2 and LiZnN was obtained as products. On addition of LiH into the mixture of $ZnCl_2$ and $LiNH_2$, H_2 instead of NH_3 was the main gaseous product, and was released from a low temperature around 90°C. The reaction products, mixtures of LiZnN and LiCl, showed an ability to be partly rehydrogenated at 300°C to form Li_2NH and zinc metal. When $ZnCl_2$ was replaced by nMgCl$_2$ (n = 0.1–0.5) the lattice parameter of LiZnN obtained in the products was been slightly altereded. However, no improvement in the hydrogenation of this system was observed.

6.3 Chloride-free LiZnN system

In chapter 5, three new routes to synthesize LiZnN were studied as summarized in equations (5.1), (5.2) and (5.3). LiZnN could be produced *via* either the reaction of Zn_3N_2 and $LiNH_2$ in a molar ratio of 1:4 at 490°C for 1 hour, or by heating that mixture in the presence of LiH at 400°C for 2 hours, or *via* the 1:1 reaction of Zn_3N_2 and Li_3N at 500°C for 12 hours. LiZnN synthesized by all three routes had the same space group of $F\bar{4}3m$ with observed lattice parameters of 4.89333(4) Å, 4.89761(5) Å, and 4.89507(5) Å, respectively.

Using these procedures, pure LiZnN can be obtained at lower temperature and after a much shorter reaction than those reported in literature. In addition, these reactions do not involve either ammonia gas atmosphere or an electrochemical reaction.

The main gas released after reaction between Zn_3N_2 and $LiNH_2$ on addition of LiH was H_2, whose release began at low temperature around 180°C and peaked around 330°C.

Neither LiZnN nor Zn_3N_2 alone showed the ability to be rehydrogenated under hydrogen under the conditions used. However, mixtures of LiZnN and Zn_3N_2, resulting from reaction of Zn_3N_2 and $LiNH_2$ at 500°C, could react with hydrogen under 90 bar hydrogen at 300°C to form $LiNH_2$ and zinc metal.

Using IGA and Sieverts method measurements, mixtures of Zn_3N_2 and $LiNH_2$, in both the presence and absence of LiH could release gases under low pressure, about 10 bar, and around 35 bar hydrogen. Partly reversible hydrogen absorption and desorption was observed at temperatures above 275°C.

Mg-doping into LiZnN was also examined in the hope of enhancing the reversibility of this system but was unsucessful.

To follow up the results of this work, unknown phases formed during IGA and HTP measurements could be studied using other techniques such as NMR, neutron diffraction, *etc*. Also, *in situ* characterization could be applied to understand the mechanism of reactions occurring in the hope of improving reversibility in the Li–Zn–N system.

References

[1] H. Wu, W. Zhou, K. Wang, T. J. Udovic, J. J. Rush, T. Yildirim, L. A. Bendersky, A. F. Gross, S. L. Van Atta, J. J Vajo, F. E. Pinkerton and M. S. Meyer, *Nanotechnology*, 2009, 20, 204002.

List of Symbols and Abbreviations

a.u.: arbitrary units

XRD: X-ray diffraction

TPD-MS: Temperature Programmed Desorption with Mass Spectrometry

QPA: Quantitative Phase Analysis

IGA: Gravimetric Analysis

HTP: High Temperature and Pressure Measurement: Volumetric Analysis using Sieverts' method.

SEM: Scanning Electron Microscopy

List of Figures

List of Tables

Appendix of Rietveld refinements

LiBH4+2LiNH2_350C

iters 100000

chi2_convergence_criteria 1e-006

do_errors

'===

r_exp 6.283 r_exp_dash 64.483 r_wp 6.445 r_wp_dash 66.148 r_p 4.748 r_p_dash 76.684 weighted_Durbin_Watson 1.939 gof 1.026

xdd TN212_LiBH4+2LiNH2_350C.raw

'===

range 1

LP_Factor(26.6)

Rp 217.5

Rs 217.5

Slit_Width(!rswidth, 1e-005_LIMIT_MIN_1e-005)

Tube_Tails(!srcwidth, 0.1052947685,!z1, -2.362606686_LIMIT_MIN_-5,!z2, 2.519284648_LIMIT_MIN_1e-005,!fraction, 0.0002805603745_LIMIT_MIN_1e-005)

axial_conv

filament_length 12

sample_length 15

receiving_slit_length 12

primary_soller_angle !soller 4.268541255

secondary_soller_angle =soller; : 4.26854125_0

axial_n_beta 30

lam

ymin_on_ymax 0.001

la =1-area_a2-area_a3-area_a4; : 0.9048_0 lo !wl_a1_never_refine_me 1.540596 lh !lor_a1 0.6361829146

la !area_a2 0.01_LIMIT_MIN_1e-005 lo !wl_a2 1.5433 lh =lor_a1-0.2; : 0.4362_0

la !area_a3 0.009290148992_LIMIT_MIN_1e-005 lo !wl_a3 1.5426 lh =lor_a1-0.2; : 0.4362_0

la !area_a4 0.07591098492 lo !wl_a4 1.5416 lh =lor_a1-0.2; : 0.4362_0

bkg @295.887001`_0.525259674 -342.492424`_0.913733941 162.063757`_0.870437649 -39.8782468`_0.856260433 -6.84148751`_0.798845398 18.9327984`_0.799021397 -9.41027432`_0.781535892 -10.4062902`_0.758124491 17.4086834`_0.767145898 -12.1361607`_0.739673186 0.768679654`_0.745565287 4.09127768`_0.737856531 -5.19020988`_0.716992807  2.85357073`_0.710143259 -1.53306328`_0.704323249 -0.69147998`_0.688546238 1.30656394`_0.698287584 -

0.782231614`_0.676695577 -0.41780789`_0.678968914 0.0663058834`_0.656564669

1.28973416`_0.661907687 -1.88646886`_0.638790572 0.904700865`_0.631771771

0.384503051`_0.609498938 -0.567201557`_0.597869492 0.840182164`_0.564098953 -

1.03510674`_0.546774481  1.01802732`_0.465206144 -0.657884888`_0.39315604

Zero_Error(!ze,-0.01292_0.00204)

'==========

str

phase_name "Li3BN2-P121/c1"

space_group "P121/c1"

a a_Li3BN2_1 5.14336`_0.00128

b b_Li3BN2_1 7.08296`_0.00130

c c_Li3BN2_1 6.77602`_0.00060

al 90.

be 112.956(2)

ga 90.

scale @ 0.0005103260`_0.0000482528

 site Li1   x 0.24995(17)   y 0.48518(12)   z 0.49811(12)   occ Li+1 1. beq beqLi

2.2588`_0.3112

site Li2   x 0.25228(18)   y 0.01212(13)   z 0.37502(13)   occ Li+1 1. beq =beqLi;

site Li3 x 0.74360(16) y 0.20714(11) z 0.31402(12) occ Li+1 1. beq =beqLi;

site B1 x 0.21509(7) y 0.31982(5) z 0.17648(5) occ B 1. beq beqB

4.5219`_0.4324

site N1 x 0.43403(6) y 0.43735(4) z 0.21904(5) occ N 1. beq beqN

1.8618`_0.3413

site N2 x 0.99439(6) y 0.20472(5) z 0.13461(5) occ N 1. beq =beqN;

CS_L(csl_Li3BN2-P121/c1, 319.59732`_989.20344_LIMIT_MIN_0.3)

CS_G(csg_Li3BN2-P121/c1, 196.32116`_339.15426_LIMIT_MIN_0.3)

Strain_L(strl_Li3BN2-P121/c1, 0.00010`_0.29693_LIMIT_MIN_0.0001)

Strain_G(strg_Li3BN2-P121/c1, 0.21196`_0.19711_LIMIT_MIN_0.0001)

r_bragg 1.99578792

weight_percent 61.652_3.412

'==========

str

phase_name "Li3BN2-I41/amd"

space_group "I41/amd"

a a_Li3BN2_2 6.59221`_0.00084

b =a_Li3BN2_2;

c c_Li3BN2_2 10.34763`_0.00194

al 90.

be 90.

ga 90.

scale @ 0.0000699979`_0.0000075218

PV_Peak_Type(@, 0.00010`_1.71308_LIMIT_MIN_0.0001,@,
0.00010`_5.19819_LIMIT_MIN_0.0001,@, 0.00010`_2.14796_LIMIT_MIN_0.0001,@,
0.70286`_1.12944_LIMIT_MIN_0.0001,@, 0.00022`_1.12944_LIMIT_MIN_0.0001,@,
0.33913`_1.12944_LIMIT_MIN_0.0001)

site Li1 x 0 y 0 z 0.1204(7) occ Li+1 1. beq beqLi 1.1337`_0.5231

site Li2 x 0.2707(6) y 0.2707(6) z 0 occ Li+1 1. beq =beqLi;

site B1 x 0 y 0 z 0.3530(6) occ B 1. beq beqB 1.8577`_0.7096

site N1 x 0 y 0.2090(3) z 0.3446(2) occ N 1. beq beqN 1.0016`_0.6271

CS_L(csl_Li3BN2_2, 10000.00000`_1145359.92160_LIMIT_MIN_0.3)

CS_G(csg_Li3BN2_2, 10000.00000`_70743264.08367_LIMIT_MIN_0.3)

Strain_L(strl_Li3BN2_2, 0.04303`_0.36610_LIMIT_MIN_0.0001)

Strain_G(strg_Li3BN2_2, 0.38762`_0.19367)

r_bragg 1.41265651

weight_percent 33.768_3.111

'==========

```
str

phase_name "LiH"

space_group "Fm-3m"

Cubic(@  4.08983`_0.00123)

scale @  0.0004495218`_0.0003404563_LIMIT_MIN_1e-011

PV_Peak_Type(@, 0.00010`_1.71308_LIMIT_MIN_0.0001,@,

0.00010`_5.19819_LIMIT_MIN_0.0001,@, 0.00010`_2.14796_LIMIT_MIN_0.0001,@,

0.70286`_1.12944_LIMIT_MIN_0.0001,@, 0.00022`_1.12944_LIMIT_MIN_0.0001,@,

0.33913`_1.12944_LIMIT_MIN_0.0001)

 site Li1    x 0           y 0           z 0           occ Li+1  1. beq  =beqLi;

site H1     x 0.5         y 0.5         z 0.5         occ H-1   1. beq  beqH  5.5401`_1.6723

CS_L(csl_LiH, 10000.00000`_4846438.35035_LIMIT_MIN_0.3)

CS_G(csg_LiH, 10000.00000`_8255269.04793_LIMIT_MIN_0.3)

Strain_L(strl_LiH, 0.00010`_0.99020_LIMIT_MIN_0.0001)

Strain_G(strg_LiH, 0.00010`_37.80872_LIMIT_MIN_0.0001)

r_bragg  0.860661122

weight_percent  2.471_1.627

'==========================================================================

str
```

Cubic (@ 4.62309`_0.00432)

phase_name "Li2O"

space_group "Fm-3m"

scale @ 0.0000855087`_0.0000665919_LIMIT_MIN_1e-011

PV_Peak_Type(@, 0.00010`_1.71308_LIMIT_MIN_0.0001,@,
0.00010`_5.19819_LIMIT_MIN_0.0001,@, 0.00010`_2.14796_LIMIT_MIN_0.0001,@,
0.70286`_1.12944_LIMIT_MIN_0.0001,@, 0.00022`_1.12944_LIMIT_MIN_0.0001,@,
0.33913`_1.12944_LIMIT_MIN_0.0001)

site Li1 x 0.25 y 0.25 z 0.25 occ Li+1 1. beq =beqLi;

site O2 x 0.5 y 0.5 z 0.5 occ O-2 1. beq beqO
0.0000`_2.2141_LIMIT_MIN_0 min =0;

CS_L(csl_Li2O, 186.38766`_4592.27443_LIMIT_MIN_0.3)

CS_G(csg_Li2O, 10000.00000`_2247008473.59415_LIMIT_MIN_0.3)

Strain_L(strl_Li2O, 0.00010`_3.88853_LIMIT_MIN_0.0001)

Strain_G(strg_Li2O, 0.77125`_2.56830_LIMIT_MIN_0.0001)

r_bragg 0.876904954

weight_percent 2.109_1.723

LiBH4+2LiNH2+0.01CoO_400C

iters 100000

chi2_convergence_criteria 1e-006

do_errors

'==

r_exp 3.729 r_exp_dash 19.308 r_wp 4.212 r_wp_dash 21.808 r_p 3.332 r_p_dash 33.525 weighted_Durbin_Watson 1.599 gof 1.129

xdd TPD46_LiBH4+2LiNH2+0.01CoO_400C_capillary_1h.raw

'==

range 1

LP_Factor(26.6)

Rp 217.5

Rs 217.5

Slit_Width(!rswidth, 1e-005_LIMIT_MIN_1e-005)

Tube_Tails(!srcwidth, 0.1052947685,!z1, -2.362606686_LIMIT_MIN_-5,!z2, 2.519284648_LIMIT_MIN_1e-005,!fraction, 0.0002805603745_LIMIT_MIN_1e-005)

axial_conv

filament_length 12

sample_length 15

receiving_slit_length 12

primary_soller_angle !soller 4.268541255

secondary_soller_angle =soller; : 4.26854125_0

axial_n_beta 30

lam

ymin_on_ymax 0.001

la =1-area_a2-area_a3-area_a4; : 0.9048_0 lo !wl_a1_never_refine_me 1.540596 lh !lor_a1 0.6361829146

la !area_a2 0.01_LIMIT_MIN_1e-005 lo !wl_a2 1.5433 lh =lor_a1-0.2; : 0.4362_0

la !area_a3 0.009290148992_LIMIT_MIN_1e-005 lo !wl_a3 1.5426 lh =lor_a1-0.2; : 0.4362_0

la !area_a4 0.07591098492 lo !wl_a4 1.5416 lh =lor_a1-0.2; : 0.4362_0

bkg @   664.842439`_0.843927236 -196.711995`_1.29322192 56.7848147`_1.20753753 32.4894931`_1.23112131 -45.8778929`_1.04951413  38.4027137`_1.0667385 -9.17772466`_1.053564 -13.0359567`_1.0206229 15.736438`_1.0552781 -6.19396459`_0.989946115 -3.71873741`_0.998740288  4.68394379`_1.03466612 -0.956737629`_0.970488593  6.01483348`_0.969427627 -8.3477674`_0.97386206 9.46239325`_0.931674677 -2.41981593`_0.958131521 -0.179639556`_0.95320189 1.62555358`_0.94234384 -2.95703194`_0.925133251 4.3211818`_0.957512087 0.00777309577`_0.899330021 -3.54931366`_0.917939942  3.06102006`_0.853787816

0.307613339`_0.839850984 -4.5150202`_0.809769848 5.66130774`_0.806359108 -

3.97611341`_0.744354483 -0.788777134`_0.741460323

Zero_Error (!ze,-0.01292_0.00204)

'==

str

phase_name "Li3BN2-P121/c1"

space_group "P121/c1"

a a_Li3BN2_1 5.14314`_0.00161

b b_Li3BN2_1 7.07433`_0.00153

c c_Li3BN2_1 6.78573`_0.00072

al 90.

be 112.956(2)

ga 90.

scale @ 0.0011165114`_0.0000596267

PV_Peak_Type(@, 0.00010`_1.71308_LIMIT_MIN_0.0001,@,

0.00010`_5.19819_LIMIT_MIN_0.0001,@, 0.00010`_2.14796_LIMIT_MIN_0.0001,@,

0.70286`_1.12944_LIMIT_MIN_0.0001,@, 0.00022`_1.12944_LIMIT_MIN_0.0001,@,

0.33913`_1.12944_LIMIT_MIN_0.0001)

site Li1 x 0.24995(17) y 0.48518(12) z 0.49811(12) occ Li+1 1. beq beqLi

2.2588`_0.3112

site Li2 x 0.25228(18) y 0.01212(13) z 0.37502(13) occ Li+1 1. beq =beqLi;

site Li3 x 0.74360(16) y 0.20714(11) z 0.31402(12) occ Li+1 1. beq =beqLi;

site B1 x 0.21509(7) y 0.31982(5) z 0.17648(5) occ B 1. beq beqB

4.5219`_0.4324

site N1 x 0.43403(6) y 0.43735(4) z 0.21904(5) occ N 1. beq beqN

1.8618`_0.3413

site N2 x 0.99439(6) y 0.20472(5) z 0.13461(5) occ N 1. beq =beqN;

CS_L(csl_Li3BN2_1, 482.27882`_35971.10468_LIMIT_MIN_0.3)

CS_G(csg_Li3BN2_1, 555.82265`_19397.15785_LIMIT_MIN_0.3)

Strain_L(strl_Li3BN2_1, 0.07419`_5.01842_LIMIT_MIN_0.0001)

Strain_G(strg_Li3BN2_1, 0.40116`_0.30706)

r_bragg 1.7130672

weight_percent 15.258_0.774

'==========

str

phase_name "Li3BN2-I41/amd"

space_group "I41/amd"

a a_Li3BN2_2 6.59376`_0.00016

b =a_Li3BN2_2;

c c_Li3BN2_2 10.34391`_0.00032

al 90.

be 90.

ga 90.

scale @ 0.0014879501`_0.0000368797

PV_Peak_Type(@, 0.01730`_1.97175_LIMIT_MIN_0.0001,@,

0.00834`_0.49955_LIMIT_MIN_0.0001,@, 0.03174`_1.94993,@,

0.00010`_32.19924_LIMIT_MIN_0.0001,@, 0.34892`_35.83091_LIMIT_MIN_0.0001,@,

0.00010`_40.54240_LIMIT_MIN_0.0001)

site Li1 x 0 y 0 z 0.1204(7) occ Li+1 1. beq =beqLi;

site Li2 x 0.2707(6) y 0.2707(6) z 0 occ Li+1 1. beq =beqLi;

site B1 x 0 y 0 z 0.3530(6) occ B 1. beq =beqB;

site N1 x 0 y 0.2090(3) z 0.3446(2) occ N 1. beq =beqN;

CS_L(csl_Li3BN2_2, 9999.86005`_4629960.77423_LIMIT_MIN_0.3)

CS_G(csg_Li3BN2_2, 9999.88554`_91052682.07131_LIMIT_MIN_0.3)

Strain_L(strl_Li3BN2_2, 0.10347`_1.39510)

Strain_G(strg_Li3BN2_2, 0.43943`_0.19703)

r_bragg 1.49292595

weight_percent 81.752_0.921

'==========

str

Cubic (@ 4.62462`_0.00090)

phase_name "Li2O"

space_group "Fm-3m"

scale @ 0.0007939304`_0.0002016136

PV_Peak_Type(@, 0.00025`_1092.25784_LIMIT_MIN_0.0001,@,

0.00069`_470.67262_LIMIT_MIN_0.0001,@,

0.00024`_1181.56203_LIMIT_MIN_0.0001,@,

0.00010`_17617.82825_LIMIT_MIN_0.0001,@,

0.00010`_12539.21568_LIMIT_MIN_0.0001,@,

0.00010`_20410.17840_LIMIT_MIN_0.0001)

 site Li1   x 0.25   y 0.25   z 0.25   occ Li+1 1. beq =beqLi;

site O2   x 0.5   y 0.5   z 0.5   occ O-2   1.   beq beqO

0.0000`_2.2141_LIMIT_MIN_0 min =0;

CS_L(csl_Li2O, 9999.95141`_16823638.88924_LIMIT_MIN_0.3)

CS_G(csg_Li2O, 29.66748`_32.95915)

Strain_L(strl_Li2O, 0.00010`_4.48614_LIMIT_MIN_0.0001)

Strain_G(strg_Li2O, 0.59756`_1.15022_LIMIT_MIN_0.0001)

r_bragg 0.377943425

weight_percent 2.990_0.600

LiBH4+LiNH2+0.03CoO_400C_TPD47

iters 100000

chi2_convergence_criteria 1e-006

do_errors

'==

r_exp 2.892 r_exp_dash 28.762 r_wp 3.087 r_wp_dash 30.702 r_p 2.433 r_p_dash 50.930 weighted_Durbin_Watson 1.828 gof 1.067

xdd TPD47_capillary.raw

'==

range 1

LP_Factor(26.6)

Rp 217.5

Rs 217.5

Slit_Width(!rswidth, 1e-005_LIMIT_MIN_1e-005)

Tube_Tails(!srcwidth, 0.1052947685,!z1, -2.362606686_LIMIT_MIN_-5,!z2, 2.519284648_LIMIT_MIN_1e-005,!fraction, 0.0002805603745_LIMIT_MIN_1e-005)

axial_conv

filament_length 12

sample_length 15

receiving_slit_length 12

primary_soller_angle !soller 4.268541255

secondary_soller_angle =soller; : 4.26854125_0

 axial_n_beta 30

lam

ymin_on_ymax 0.001

la =1-area_a2-area_a3-area_a4; : 0.9048_0 lo !wl_a1_never_refine_me 1.540596 lh !lor_a1 0.6361829146

la !area_a2 0.01_LIMIT_MIN_1e-005 lo !wl_a2 1.5433 lh =lor_a1-0.2; : 0.4362_0

la !area_a3 0.009290148992_LIMIT_MIN_1e-005 lo !wl_a3 1.5426 lh =lor_a1-0.2; : 0.4362_0

la !area_a4 0.07591098492 lo !wl_a4 1.5416 lh =lor_a1-0.2; : 0.4362_0

bkg @   1158.26459`_1.06172561 -190.556059`_1.65059076 55.8151631`_1.43738261 26.0634504`_1.47531089 -43.1160827`_1.29054815  36.6335135`_1.29041526 -19.8436908`_1.28581778 -8.90438388`_1.26407269 13.362819`_1.30841252 -2.38118208`_1.22393171 -9.90518371`_1.24408194  6.36915373`_1.25521115 -0.820273826`_1.20229223  7.63965641`_1.18615907 -7.97802724`_1.19834226 11.0880783`_1.15090435 -2.63417836`_1.17175107 -0.301565131`_1.19164814 2.10164354`_1.17954328 -1.61948108`_1.16330908 0.454967187`_1.22534272 -

0.425898685`_1.13500089 -4.39606038`_1.12285173 4.45316578`_1.05828844

0.553304712`_1.04258505 -2.78505164`_0.9941203 6.52324861`_1.00523451 -

1.92548398`_0.885549045  2.96191458`_0.951540506

Zero_Error(!ze,-0.01292_0.00204)

'==========

str

phase_name "Li3BN2-I41/amd"

space_group "I41/amd"

a a_Li3BN2_2 6.59191`_0.00022

b =a_Li3BN2_2;

c c_Li3BN2_2 10.34544`_0.00047

al 90.

be 90.

ga 90.

scale @ 0.0009979526`_0.0000440685

PV_Peak_Type(@, 0.02894`_0.95708_LIMIT_MIN_0.0001,@, 0.26002`_0.57415,@,

0.00127`_1.04285_LIMIT_MIN_0.0001,@, 0.00011`_34.90323_LIMIT_MIN_0.0001,@,

1.90254`_16.69524,@, 0.00044`_38.73453_LIMIT_MIN_0.0001)

site Li1 x 0 y 0 z 0.1204(7) occ Li+1 1. beq beqLi 1.1337`_0.5231

site Li2 x 0.2707(6) y 0.2707(6) z 0 occ Li+1 1. beq =beqLi;

site B1 x 0 y 0 z 0.3530(6) occ B 1. beq beqB 1.8577`_0.7096

site N1 x 0 y 0.2090(3) z 0.3446(2) occ N 1. beq beqN 1.0016`_0.6271

CS_L(csl_Li3BN2_2, 10000.00000`_1895550.23720_LIMIT_MIN_0.3)

CS_G(csg_Li3BN2_2, 443.75430`_7174.60828_LIMIT_MIN_0.3)

Strain_L(strl_Li3BN2_2, 0.00010`_0.36086_LIMIT_MIN_0.0001)

Strain_G(strg_Li3BN2_2, 0.41161`_0.14007)

r_bragg 0.903082249

weight_percent 97.811_4.420

'==========

str

Cubic (@ 4.63198`_0.00368)

phase_name "Li2O"

space_group "Fm-3m"

scale @ 0.0007349283`_0.0008626569_LIMIT_MIN_1e-011

PV_Peak_Type(@, 0.00050`_22425.32727_LIMIT_MIN_0.0001,@,

0.00050`_9264.81112_LIMIT_MIN_0.0001,@,

0.00050`_24143.92246_LIMIT_MIN_0.0001,@,

0.00010`_154006.03144_LIMIT_MIN_0.0001,@,

0.00010`_70432.96068_LIMIT_MIN_0.0001,@,

0.00010`_167160.19305_LIMIT_MIN_0.0001)

site Li1 x 0.25 y 0.25 z 0.25 occ Li+1 1. beq =beqLi;

site O2 x 0.5 y 0.5 z 0.5 occ O-2 1. beq beqO

6.7513`_14.7674_LIMIT_MIN_-10

CS_L(csl_Li2O, 10000.00000`_84545751.31258_LIMIT_MIN_0.3)

CS_G(csg_Li2O, 9999.99996`_7339932229.24610_LIMIT_MIN_0.3)

Strain_L(strl_Li2O, 0.00010`_24.11511_LIMIT_MIN_0.0001)

Strain_G(strg_Li2O, 1.73268`_3.76901_LIMIT_MIN_0.0001)

r_bragg 0.373458322

weight_percent 2.189_4.420

LiBH4+LiNH2+0.05CoO_Ball-milled

iters 100000

chi2_convergence_criteria 1e-006

do_errors

'==========

r_exp 2.215 r_exp_dash 25.811 r_wp 2.348 r_wp_dash 27.360 r_p 1.861 r_p_dash 43.353 weighted_Durbin_Watson 1.763 gof 1.060

'==========

xdd BM5_LiBH4+LiNH2+0.05CoO.raw

'==========

range 1

LP_Factor(26.6)

Rp 217.5

Rs 217.5

Slit_Width(!rswidth, 1e-005_LIMIT_MIN_1e-005)

Tube_Tails(!srcwidth, 0.1052947685,!z1, -2.362606686_LIMIT_MIN_-5,!z2, 2.519284648_LIMIT_MIN_1e-005,!fraction, 0.0002805603745_LIMIT_MIN_1e-005)

axial_conv

sample_length 15

receiving_slit_length 12

primary_soller_angle !soller 4.268541255

secondary_soller_angle =soller; : 4.26854125_0

axial_n_beta 30

lam

ymin_on_ymax 0.001

la =1-area_a2-area_a3-area_a4; : 0.9048_0 lo !wl_a1_never_refine_me 1.540596 lh !lor_a1 0.6361829146

la !area_a2 0.01_LIMIT_MIN_1e-005 lo !wl_a2 1.5433 lh =lor_a1-0.2; : 0.4362_0

la !area_a3 0.009290148992_LIMIT_MIN_1e-005 lo !wl_a3 1.5426 lh =lor_a1-0.2; : 0.4362_0

la !area_a4 0.07591098492 lo !wl_a4 1.5416 lh =lor_a1-0.2; : 0.4362_0

bkg @   1979.09071`_0.89350077 -299.78327`_1.46607556 91.2375485`_1.33254674 46.0392164`_1.27592871 -74.7537646`_1.23657127  66.3318403`_1.20276966 -27.0040806`_1.20214065 -6.55477057`_1.19748034 18.1681348`_1.21598944 -10.4377154`_1.19306226 -4.08326557`_1.15579798  7.25414033`_1.1452627 -10.3007966`_1.12375323  16.1659813`_1.09899702 -15.7264208`_1.1231491 15.1701208`_1.09683031 -6.56739372`_1.07961235  3.61154861`_1.07934132 -1.95490682`_1.09795853  2.17282471`_1.08916585 -6.50396602`_1.06974514

13.0868465`_1.03375612 -10.5691713`_1.01818419 7.06170297`_0.995999023

4.10245408`_0.972565158 -2.00653946`_0.975494116 5.37834541`_1.00766074 -

3.00084967`_0.908970358  2.70863259`_0.832437673

 Zero_Error(ze, 0.01276`_0.00102)

'==

'RIETVELD REFINEMENT PHASE - Phase information for Rietveld Refinement

str

Cubic (@ 10.67176`_0.00101)

space_group "I213"

phase_name "Li4(BH4(NH2)3"

scale @ 0.0000592106`_0.0000020314

PV_Peak_Type(@, 0.00089`_104545.95354_LIMIT_MIN_0.0001,@,

0.00089`_43096.10889_LIMIT_MIN_0.0001,@,

0.00089`_112528.85354_LIMIT_MIN_0.0001,@,

0.00010`_89602.82336_LIMIT_MIN_0.0001,@,

0.00010`_47567.01896_LIMIT_MIN_0.0001,@,

0.00010`_98656.18770_LIMIT_MIN_0.0001)

site N1   x 0.2544(7)   y 0   z 0.25   occ N   1.   beq =beqN;

site N2   x 0.7895(3)   y 0   z 0.25   occ N   1.   beq =beqN;

site B1   x 0.0285(3)   y 0.0285(3)   z 0.0285(3)   occ B   1.   beq =beqB;

site Li1 x 0.1068(10) y 0.3775(7) z 0.1587(8) occ Li+1 0.58(1) beq =beqLi;

site Li2 x 0.3755(7) y 0.1493(10) z 0.3311(7) occ Li+1 0.75 beq =beqLi;

site H1 x 0.278(3) y 0.094(3) z 0.233(3) occ H 1. beq =beqH;

site H2 x 0.769(3) y 0.096(2) z 0.258(4) occ H 1. beq =beqH;

site H3 x 0.088(3) y 0.088(3) z 0.088(3) occ H 1. beq =beqH;

site H4 x -0.032(6) y -0.032(7) z 0.088(2) occ H 1. beq =beqH;

CS_L(csl_Li4, 55.93292`_6.00256_LIMIT_MIN_0.3)

'CS_G(csg_Li4, 70.85547_62.62248_LIMIT_MIN_0.3)

' Strain_L(strl_Li4, 0.00010_0.62970_LIMIT_MIN_0.0001)

Strain_G(strg_Li4, 0.40052`_0.09014_LIMIT_MIN_0.0001)

r_bragg 0.450706216

weight_percent 12.112_0.732

'==========

str

a a_LiBH4 7.17603`_0.00188

b b_LiBH4 4.43763`_0.00106

c c_LiBH4 6.79927`_0.00207

scale @ 0.0016290959`_0.0001351792_LIMIT_MIN_1e-011

PV_Peak_Type(@, 0.00089`_104545.95354_LIMIT_MIN_0.0001,@,

0.00089`_43096.10889_LIMIT_MIN_0.0001,@,

0.00089`_112528.85354_LIMIT_MIN_0.0001,@,

0.00010`_89602.82336_LIMIT_MIN_0.0001,@,

0.00010`_47567.01896_LIMIT_MIN_0.0001,@,

0.00010`_98656.18770_LIMIT_MIN_0.0001)

al 90

be 90

ga 90

space_group "Pnma"

phase_name "LiBH4"

site Li1 x 0.1568(4) y 0.25 z 0.1015(6) occ Li+1 1. beq beqLi

7.0964`_0.4820

site B1 x 0.3040(3) y 0.25 z 0.4305(1) occ B 1. beq =beqB;

site H1 x 0.900(1) y 0.25 z 0.956(3) occ H 1. beq =beqH;

site H2 x 0.404(2) y 0.25 z 0.280(2) occ H 1. beq =beqH;

site H3 x 0.172(2) y 0.054(2) z 0.428(1) occ H 1. beq =beqH;

CS_L(csl_LiBH4, 436.64397`_460.55681_LIMIT_MIN_0.3)

' CS_G(csg_LiNBH4, 862.31440_27720.31279_LIMIT_MIN_0.3)

' Strain_L(strl_LiBH4, 0.26704_0.46127_LIMIT_MIN_0.0001)

Strain_G(strg_LiBH4, 0.36346`_0.09397_LIMIT_MIN_0.0001)

r_bragg 0.408911341

weight_percent 8.50_0.858

'--

str

space_group "R-3:H"

phase_name "Li2BNH6"

al 90.0

be 90.0

ga 120.0

a @ 14.48454`_0.00133

b @ 14.48201`_0.00056

c @ 9.22704`_0.00075

scale @ 0.0001610339`_0.0000012842

PV_Peak_Type(@, 0.00089`_104545.95354_LIMIT_MIN_0.0001,@,

0.00089`_43096.10889_LIMIT_MIN_0.0001,@,

0.00089`_112528.85354_LIMIT_MIN_0.0001,@,

0.00010`_89602.82336_LIMIT_MIN_0.0001,@,

0.00010`_47567.01896_LIMIT_MIN_0.0001,@,

0.00010`_98656.18770_LIMIT_MIN_0.0001)

site B x 0.6763(5) y 0.7520(6) z 0.1835(7) occ B 1.0 beq beqB

3.7244`_0.5987

site H1 x 0.7363(11) y 0.8167(11) z 0.2797(14) occ H 1.0 beq beqH

5.5401`_1.6723_LIMIT_MIN_-10

site H2 x 0.7112(13) y 0.7192(13) z 0.0933(15) occ H 1.0 beq =beqH;

site H3 x 0.6457(11) y 0.8057(12) z 0.1036(15) occ H 1.0 beq =beqH;

site H4 x 0.5982(14) y 0.6842(11) z 0.2187(14) occ H 1.0 beq =beqH;

site N x 0.1254(4) y 0.96896(29) z 0.85713(35) occ N 1.0 beq beqN

3.2722`_0.3227

site H5 x 0.1015(17) y 0.9725(20) z 0.7258(19) occ H 1.0 beq =beqH;

site H6 x 0.1431(15) y 0.9211(14) z 0.8288(23) occ H 1.0 beq =beqH;

site Li1 x 0.2903(9) y 0.0608(9) z 0.7816(11) occ Li 1.0 beq =beqLi;

site Li2 x 0.8457(11) y 0.8739(12) z 0.0747(10) occ Li 1.0 beq =beqLi;

CS_L(csl_Li2BNH6, 92.29691`_1.18316)

'CS_G(csg_Li2BNH6, 77.07803_3.65183)

'Strain_L(strl_Li2BNH6, 0.00011_0.02796_LIMIT_MIN_0.0001)

'Strain_G(strl_Li2BNH6, 0.34492_0.01219)

r_bragg 0.355130679

weight_percent 66.349_0.939

'==========

str

a a_LiNH2 5.03919`_0.00120

b =a_LiNH2;

c c_LiNH2 10.24137`_0.00471

al 90.

be 90.

ga 90.

scale @ 0.0004129384`_0.0000173589

PV_Peak_Type(@, 0.00089`_104545.95354_LIMIT_MIN_0.0001,@,

0.00089`_43096.10889_LIMIT_MIN_0.0001,@,

0.00089`_112528.85354_LIMIT_MIN_0.0001,@,

0.00010`_89602.82336_LIMIT_MIN_0.0001,@,

0.00010`_47567.01896_LIMIT_MIN_0.0001,@,

0.00010`_98656.18770_LIMIT_MIN_0.0001)

phase_name LiNH2

space_group "I-4"

```
site Li1    x 0          y 0          z 0          occ Li+1  1.  beq  =beqLi;

site Li2    x 0          y 0.5        z 0.250      occ Li+1  1. beq  =beqLi;

site Li3    x 0          y 0.5        z 0.007      occ Li+1  1.  beq  =beqLi;

site N1     x 0.232      y 0.245      z 0.116      occ N   1.   beq  =beqN;

site H1     x 0.229      y 0.107      z 0.192      occ H   1.  beq =beqH;

site H2     x 0.420      y 0.333      z 0.125      occ H   1.  beq  =beqH;

CS_L(csl_LiNH2, 85.82773`_6.36566_LIMIT_MIN_0.3)

' CS_G(csg_LiNH2, 10000.00000_220514916.37245_LIMIT_MIN_0.3)

' Strain_L(strl_LiNH2, 0.13908_1.11812_LIMIT_MIN_0.0001)

Strain_G(strg_LiNH2, 0.50622_0.08770_LIMIT_MIN_0.0001)

r_bragg  0.261801223

weight_percent  7.760_0.395

'=====================================================

str

a a_CoO   3.01131`_0.00037

b b_CoO =a_CoO;

c c_CoO  4.26419`_0.00104

al 90.
```

be 90.

ga 90.

space_group "I4/mmm"

phase_name "CoO_I4/mmm"

scale @ 0.0028045055`_0.0001214245

PV_Peak_Type(@, 0.00089`_104545.95354_LIMIT_MIN_0.0001,@,

0.00089`_43096.10889_LIMIT_MIN_0.0001,@,

0.00089`_112528.85354_LIMIT_MIN_0.0001,@,

0.00010`_89602.82336_LIMIT_MIN_0.0001,@,

0.00010`_47567.01896_LIMIT_MIN_0.0001,@,

0.00010`_98656.18770_LIMIT_MIN_0.0001)

site Co1 x 0 y 0 z 0 occ Co+2 1. beq beqCo 0.0350`_0.3389

site O1 x 0 y 0 z 0.5 occ O-2 1. beq beqO 1.0284`_0.4360

CS_L(csl_CoO, 221.15435`_311.56605_LIMIT_MIN_0.3)

CS_G(csg_CoO, 68.75586`_16.01473_LIMIT_MIN_0.3)

Strain_L(strl_CoO, 0.23810`_0.15018_LIMIT_MIN_0.0001)

Strain_G(strg_CoO, 0.00010`_254.51755_LIMIT_MIN_0.0001)

r_bragg 0.27360319

weight_percent 4.905_0.259

0.9ZnCl2+0.1MgCl2+3LiNH2_500C_12h

iters 100000

chi2_convergence_criteria 1e-006

do_errors

'==========

r_exp 4.817 r_exp_dash 13.729 r_wp 8.323 r_wp_dash 23.720 r_p 5.799 r_p_dash 29.498 weighted_Durbin_Watson 0.683 gof 1.728

'==========

xdd TN223_0.9ZnCl2+0.1MgCl2+3LiNH2_500C_12h.raw

range 1

LP_Factor(26.6)

Rp 217.5

Rs 217.5

Slit_Width(!rswidth, 1e-005_LIMIT_MIN_1e-005)

Tube_Tails(!srcwidth, 0.1052947685,!z1, -2.362606686_LIMIT_MIN_-5,!z2, 2.519284648_LIMIT_MIN_1e-005,!fraction, 0.0002805603745_LIMIT_MIN_1e-005)

axial_conv

filament_length 12

sample_length 15

receiving_slit_length 12

primary_soller_angle !soller 4.268541255

secondary_soller_angle =soller; : 4.26854125_0

axial_n_beta 30

lam

ymin_on_ymax 0.001

 la =1-area_a2-area_a3-area_a4; : 0.9048_0 lo !wl_a1_never_refine_me 1.540596 lh !lor_a1 0.6361829146

la !area_a2 0.01_LIMIT_MIN_1e-005 lo !wl_a2 1.5433 lh =lor_a1-0.2; : 0.4362_0

la !area_a3 0.009290148992_LIMIT_MIN_1e-005 lo !wl_a3 1.5426 lh =lor_a1-0.2; : 0.4362_0

la !area_a4 0.07591098492 lo !wl_a4 1.5416 lh =lor_a1-0.2; : 0.4362_0

'==========

bkg @ 430.924595`_1.53108264 -413.378159`_1.27134434 244.688739`_2.08034445 2.76450952`_1.45136835 -43.9782472`_1.05891277  61.4898649`_1.18481604 -28.493509`_1.24091114 -12.8211799`_1.03016339 22.164607`_1.40568406 -30.1010083`_1.39275829 1.94858039`_1.05820807  7.39240372`_1.45580095 -15.1580126`_0.966892834  5.18100717`_1.2066312 -8.10647658`_1.10244099 10.1339699`_1.03882443 -12.3824905`_0.983475987  0.58066196`_1.07984606 -5.4297503`_0.939658863 -11.3839799`_1.08993111 0.443532208`_1.08307831 -

7.05342913`_0.894331174 -12.4125867`_1.08385476 0.336975325`_0.890627746 -

7.89384915`_0.944946097 -4.08606062`_0.97117646 0.164515488`_0.809337774 -

7.93334987`_0.853334447 -1.78295762`_0.763465415 0.732234912`_0.774779864 -

0.0577314977`_0.66030307  1.01020702`_0.714437048

  Zero_Error(ze, 0.00638`_0.00060)

'==

'RIETVELD REFINEMENT PHASE - Phase information for Reitveld Refinement

str

phase_name "LiZnN"

space_group F-43m

Cubic(@ 4.89958`_0.00004)

scale @ 0.0017352485`_0.0000951217

MVW(246.863_4.548, 117.6313_0.0050, 47.680_5.540)

site N1   x =0; y =0; z   =0;   occ N   1   min =0; max =1; beq beqN 2.7029`_0.3674

site Li1 x =1/4; y =1/4; z =1/4; occ Li+1 1   min =0; max =1; beq beqLi 0.8539`_0.2051

site Zn1 x =3/4; y =3/4; z =3/4; occ Zn+2 occ_Zn 0.702`_0.0124   min =0; max =1; beq

beqZn 0.0000`_0.4962_LIMIT_MIN_0 min =0;

site Mg x =3/4; y =3/4; z =3/4; occ Mg+2 occ_Mg = 1-occ_Zn; : 0.298`_0.0124   min =0;

max =1; beq beqMg 0.0000`_0.8404_LIMIT_MIN_0 min =0;

CS_L(csl_LiZnN, 257.77889`_40.37121)

CS_G(csg_LiZnN, 490.59705`_374.86699_LIMIT_MIN_0.3)

Strain_L(strl_LiZnN, 0.00010`_0.01568_LIMIT_MIN_0.0001)

Strain_G(strg_LiZnN, 0.21582`_0.00982)

r_bragg 12.1247195

weight_percent 45.964_2.445

'--

str

phase_name "LiCl"

space_group Fm-3m

Cubic(@ 5.14036`_0.00008)

scale @ 0.0015744978`_0.0000154662

site Li1 num_posns 4 x =0; y =0; z =0; occ Li+1 1 beq =beqLi;

site Cl1 num_posns 4 x =1/2; y =1/2; z =1/2; occ Cl-1 1 beq beqCl

0.0000`_0.0760_LIMIT_MIN_0 min =0;

CS_L(csl_LiCl, 195.12812`_33.28497)

CS_G(csg_LiCl, 10000.00000`_4833641.90196_LIMIT_MIN_0.3)

Strain_L(strl_LiCl, 0.00010`_0.02411_LIMIT_MIN_0.0001)

Strain_G(strg_LiCl, 0.24858`_0.01483)

r_bragg 8.48528817

weight_percent 47.234_2.453

'==========

str

Cubic (@ 4.65702`_0.00592)

phase_name "Li2O"

space_group "Fm-3m"

scale @ 0.0012718451`_0.0009827346

site Li1 x 0.25 y 0.25 z 0.25 occ Li+1 1. beq =beqLi;

site O2 x 0.5 y 0.5 z 0.5 occ O-2 1. beq beqO

0.0000`_5.2998_LIMIT_MIN_0 min =0;

CS_L(csl_Li2O, 10000.00000`_35923225.99195_LIMIT_MIN_0.3)

CS_G(csg_Li2O, 85.34376`_19625.96510_LIMIT_MIN_0.3)

Strain_L(strl_Li2O, 0.92225`_10.26576_LIMIT_MIN_0.0001)

Strain_G(strg_Li2O, 5.00000`_5.47129_LIMIT_MAX_5)

r_bragg 0.747417035

weight_percent 2.267_1.888

```
str

phase_name "Zn"

a a_Zn  2.66445`_0.00016

b =a_Zn;

c c_Zn  4.94465`_0.00051

al 90.0

be 90.0

ga 120.0

space_group "P63/mmc"

site Zn1    x =1/3;       y =2/3;       z =1/4;       occ Zn  !occ_Zn1  1 beq  =beqZn;

scale @  0.0004207906`_0.0000340682

MVW( 130.779_0.000, 30.4006_0.0049, 1.583_0.222)

CS_L(csl_Zn, 198.94130`_283.87207_LIMIT_MIN_0.3)

CS_G(csg_Zn, 127.60911`_75.32112_LIMIT_MIN_0.3)

Strain_L(strl_Zn, 0.00010`_0.15912_LIMIT_MIN_0.0001)

Strain_G(strg_Zn, 0.09346`_0.17485_LIMIT_MIN_0.0001)

r_bragg  3.24524955

weight_percent  2.061_0.192
```

str

phase_name "Zn3N2"

space_group Ia-3

Cubic (@ 9.77694`_0.00088)

scale @ 0.0000004938`_0.0000000743

site Zn1 x 0.3975(1) y 0.1498(2) z 0.3759(1) occ Zn+2 1 beq =beqZn;

site N1 x 0.25 y 0.25 z 0.25 occ N 1. beq =beqN;

site N2 x 0.9784(1) y 0 z 0.25 occ N 1. beq =beqN;

CS_L(csl_Zn3N2, 10000.00000`_1143063.24495_LIMIT_MIN_0.3)

CS_G(csg_Zn3N2, 51.86422`_16.21213)

Strain_L(strl_Zn3N2, 0.00010`_0.22995_LIMIT_MIN_0.0001)

Strain_G(strg_Zn3N2, 0.00010`_408.43346_LIMIT_MIN_0.0001)

r_bragg 3.97980281

weight_percent 1.821_0.129

'==========

str

a a_LiZn 2.78158`_0.00077

b =a_LiZn;

c c_LiZn 4.36991`_0.00254

al 90.

be 90.

ga 120.

scale @ 0.0000332783`_0.0000041619

space_group "P63/mmc"

phase_name "LiZn"

site Li1 x 0.3333 y 0.6667 z 0.25 occ Li 0.105 beq =beqLi;

site Zn1 x 0.3333 y 0.6667 z 0.25 occ Zn 0.895 beq =beqZn;

CS_L(csl_LiN, 10000.00000`_3285976.30908_LIMIT_MIN_0.3)

CS_G(csg_LiN, 10000.00000`_9057813.11070_LIMIT_MIN_0.3)

Strain_L(strl_LiN, 0.51645`_0.79939)

Strain_G(strg_LiN, 0.00010`_35.98854_LIMIT_MIN_0.0001)

R_bragg 1.47132224

weight_percent 0.422_0.203